Activity-dependent gene regulation in astroglia-derived induced neurons

Dissertation
Zur Erlangung des Grades
Doktor der Naturwissenschaften

Am Fachbereich Biologie
Der Johannes Gutenberg-Universität Mainz

Nesrin Sharif
geb. am 29.01.1992 in Dortmund

Mainz, 2023

Dekan:
1. Berichterstatter:
2. Berichterstatter:
Tag der mündlichen Prüfung:

Versicherung

für das Gesuch um Zulassung zur Promotion im Fachbereich 10 der Johannes-Gutenberg-Universität Mainz

Hiermit versichere ich gemäß §12, Abs. 2 der Promotionsordnung vom 01.04.2018, dass ich die heute als Dissertation vorgelegte Arbeit selbst angefertigt und alle benutzten Hilfsmittel in der Arbeit angegeben habe. Ich habe oder hatte die jetzt als Dissertation vorgelegte Arbeit nicht als Prüfungsarbeit für eine staatliche oder andere wissenschaftliche Prüfung eingereicht. Ich habe weder die jetzt als Dissertation vorgelegte Arbeit noch Teile einer Abhandlung bei einer anderen Fakultät bzw. einem anderen Fachbereich als Dissertation eingereicht. Für die Anfertigung der vorgelegten Arbeit wurde keine entgeltliche Hilfe Dritter, insbesondere eine Promotionsberatung oder –vermittlung in Anspruch genommen.

Mainz, den	Unterschrift

"Time is short,
my strength is limited,
the office is a horror,
the apartment is noisy,
and if a pleasant, straightforward life
is not possible,
then one must try to wriggle through
by subtle manoeuvres."

- Franz Kafka
letter sent to Felice Bauer in 1912

ACKNOWLEDGEMENTS

Removed due to data protection.

CONTENTS

NOMENCLATURE

Abbreviations & Acronyms

H_2O	distilled water
ANOVA	Analysis of Variance
APV	(2R)-amino-5-phosphonovaleric acid
$Ara-C$	Cytosine-d-arabinofuranoside
bACSF	Buffered artificial cerebrospinal fluid
BCL	Raw Base Call
bHLH	basic Helix-Loop-Helix
BMP	Bone morphogenic protein
bp	base pairs
BSA	Bovine Serum Albumin
CAG	Chicken β - actin gene
CaMK	Ca^{2+}/calmodulin-dependent protein kinase
CCC	Cation-chloride cotransporter
cDNA	complementary DNA
CGE	Caudal ganglionic eminence
CNQX	Cyanquixaline
CNS	Central Nervous System
CREB	Ca^{2+}/cAMP-response element binding protein
Ctrl	Control
d.p.t.	Days post transduction
DAPI	4′,6-diamidino-2-phenylindole
DBD	DNA-binding domain
DEG	Differentially expressed genes
div	Days *in vitro*
DMEM	Dulbecco's Modified Eagle's Medium
DNA	Deoxyribonucleic acid
DRG	Downregulated genes
DsRed	Discosoma red fluorescent protein
E.coli	Escherichia coli
E	Embryonic day
EDTA	Ethylenediaminetetraacetic acid
EGF	Epidermal growth factor
eGFP	Enhanced green fluorescent protein
FACS	Fluorescence-Activated Cell Sorting
FANS	Fluorescence-Activated Nuclei Sorting
FBS	Fetal bovine serum
FDR	False discovery rate
FSC	forward scatter
GABA	γ -Aminobutyric acid
GAPDH	Glyceraldehyde-3-phosphate dehydrogenase
GEM	Gel Bead in Emulsion
GFP	Green fluorescent protein
GRCm38	Genome Reference Consortium Mouse Build 38
GW	Gestational week
H2B	Histone 2B
HBSS	Hank's Balanced Salt Solution
HEK	Human embryonic kidney
HSP	Homeostatic synaptic plasticity
IEG	Immediate-early gene
IPC	Intermediate progenitor cell
IRES	Internal ribosome entry site

kNN	k-nearest neighbor
L − VGCC	L-Type voltage-gated calcium channel
LB	Luria-Bertani
LRG	Late-response gene
LRT	Likelihood-ratio test
MGE	Medial ganglionic eminence
miR/miRNA	micro-RNA
Mm	Mus musculus
MoMLV	Moloney Murine Leukemia Virus
n	Number of biological replicates
NB	Negative binomial
NCBI	National Center for Biotechnology Information
NMDAR	N-methyl-D-aspartate receptor
NPC	Neural progenitor cell
NT − 3	Neurotrophin-3
P/S	Penicillin / Streptomycin
P	Postnatal day
PB	Phosphate buffer
PBS	Phosphate buffer saline
PCA	Principal Component Analysis
PDL	Poly-D-Lysine hydrobromide
PEI	Polyethylenimin
PFA	Paraformaldehyde
PNS	Peripheral nervous system
polyA	Polyadenylation
PV	Parvalbumin
RBP	RNA-binding protein
RFP	Red fluorescent protein
RGC	Radial glia cell
RNA	Ribonucleic acid
ROS	Reactive oxygen species
RT	Room temperature
RV	Retrovirus
sc	single-cell
scRNA − seq	Single cell RNA-sequencing
SD	Standard deviation
SEM	Standard Error of Mean
seq	sequencing
sn	single-nucleus
SSC	side scatter
SST	Somatostatin
STAR	Spliced Transcripts Alignment to a Reference
TARP	Transmembrane AMPAR regulatory protein
TBS	Tris-buffered saline
TF	Transcription factor
TTX	Tetrodotoxin
U	Unit
UMAP	Uniform Manifold Approximation and Projection
UMI	Unique Molecular Identifier
URG	Upregulated genes
v	Version
VSV − G	Vesicular stomatitis virus glycoprotein
WHV	Woodchuck Hepatitis Virus
WPRE	WHV Posttranscriptional Regulatory Element
Wt	Wild type

Gene symbols

Arc	Activity-regulated cytoskeleton-associated protein, Arg3.1 gene id: 23237
Bcl2	B-cell Lymphoma 2 gene id: 12043
BDNF	Brain-derived neurotrophic factor gene id: 12064

$c-Fos$	FBJ osteosarcoma oncogene, Fos gene id: 14281
$Ctip2$	COUP-TF interacting protein 2, Bcl11b gene id: 58208
$Cux1$	Cut-like homeobox 1, CDP, Cux, Cutl1 gene id: 13047
$Cux2$	Cut-like homeobox 2, Cutl2 gene id: 13048
DCX	Doublecortin gene id: 13193
$FGF-2$	Fibroblast growth factor 2 gene id: 14173
$GFAP$	Glial fibrillary acidic protein gene id: 14580
$Iba1$	Ionized calcium-binding adapter molecule 21
$Map2$	Microtubule-associated protein 2, Mtap2 gene id: 17756
$Mef2c$	Myocyte enhancer factor 2C, Mef2 gene id: 17260
$NeuN$	Neuronal nuclei antigen, Rbfox3 gene id: 52897
$NeuroD2$	Neuronal differentiation factor 2, Ndrf, bHLHa1 gene id: 18013
$Neurog2$	Neurogenin 2, Ngn2, Atoh4, Math4a, bHLHa8 gene id: 11924
$Npas4$	Neuronal PAS domain protein 4 gene id: 225872
$Satb2$	Special AT-rich sequence binding protein 2 gene id: 212712
$Tbr1$	T-box brain transcription factor gene id: 21375
$Tbr2$	T-box brain protein 2, Eomes gene id: 13813
$Tcf4$	Transcription factor 4, ME2, TFE, E2-2, ITF2, SEF2, bHLHb19 gene id: 21413
TEF	Thyrotroph embryonic factor gene id: 21685

Units

$°C$	Celcius degree
μg	Microgram
μl	Microliter
A	Ampere
h	Hours
Hz	Hertz
kb	Kilobases (= 1000 base pairs)
min	Minutes
ml	Milliliter
mM	Millimolar
V	Volt

LIST OF FIGURES

LIST OF TABLES

ABSTRACT

The limited regenerative capacity of the adult mammalian brain following neuronal injury has encouraged researchers to explore neuronal replacement strategies to repair neural circuits and to recover compromised behavioural functions. One strategy uses retroviruses that target proliferating glia cells to induce ectopic overexpression of neuronal transcription factors (TFs), leading to glia-to-neuron reprogramming. Although these induced neurons (iNs) have been shown to acquire a neuronal morphology and neuron-specific functional features, it is not known to which extent their molecular phenotype resembles that of endogenous neurons (eNs) and whether they display homeostatic synaptic plasticity, a feature that would allow them to functionally integrate into a pre-existing neuronal network. These two aims were addressed in this work by overexpressing the TF Neurog2 in postnatal cortical glia and coculturing these with cortical eNs that have already established a network *in vitro* to allow integration of newly generated iNs. After a period of two weeks, network activity was either pharmacologically inhibited or left unperturbed and single-nucleus (sn) RNA-sequencing was performed. Interestingly, the subsequent molecular characterization of the iN population pointed to two distinct sources of diversity among the iN population: molecular subtype identities, comprising a broad range of inferred cortical subtypes and distinct developmental stages. To assess if iNs undergo HSP, I investigated the transcriptional dynamics in response to activity inhibition and how these compare to the ones elicited in eNs. While eNs displayed regulation of gene signatures indicative of HSP, iNs displayed downregulation of dendritic and postsynaptic genes that correlated with a reduced morphological complexity following activity inhibition. Interestingly, a set of synapse-related genes that was upregulated by eNs in response to activity inhibition was found to be highly expressed in iNs under control condition. Furthermore, pharmacological network activity disinhibition resulted in minimal c-Fos upregulation in iNs compared to eNs, pointing to limited integration into the network and suggesting that the high basal expression of synaptic genes in iNs may reflect ongoing competition for synaptic input. Immunocytochemical stainings showed that GABAergic, but not glutamatergic synapses decorate iNs. Taken together, these data suggest that iNs are not yet functionally integrated into the network, despite wide expression of synaptic machinery-related genes. Lack of synaptic input may be constraining iN maturation, while their high basal expression of synapse-related genes may indicate an increased competition for synaptic input. In sum, this work provides the first snRNA-seq study comparing the molecular phenotype and activity-dependent transcriptome of glia-derived iNs and cortical eNs, and suggests avenues for refining the iN differentiation process towards a functionally more mature and responsive phenotype.

ZUSAMMENFASSUNG

Die begrenzte Regenerationsfähigkeit des Gehirns erwachsener Säugetiere nach einer neuronalen Verletzung hat Wissenschaftler dazu motiviert, Ersatzstrategien zu entwickeln, welche neuronale Schaltkreise reparieren und beeinträchtigte Verhaltensfunktionen wiederherstellen könnten. Eine Strategie nutzt Retroviren welche proliferierende Gliazellen transduzieren und ektopische Überexpression neuronaler Transkriptionsfaktoren (TFs) induzieren, was zur Umprogrammierung von Gliazellen in Neuronen führt. Obwohl gezeigt wurde, dass diese induzierten Neuronen (iNs) eine neuronale Morphologie und Neuronen-spezifische Funktionsmerkmale erwerben, ist nicht bekannt, inwieweit ihr molekularer Phänotyp dem endogener Neuronen (eNs) ähnelt und ob sie zur homöostatischen synaptischen Plastizität befähigt sind. Dies würde es ihnen ermöglichen, sich funktionell in ein bereits bestehendes neuronales Netzwerk zu integrieren. Diese beiden Ziele wurden in dieser Arbeit angegangen, indem der TF Neurog2 in postnatalen kortikalen Gliazellen überexprimiert und mit kortikalen eNs kokultiviert wurde, die bereits ein Netzwerk *in vitro* aufgebaut haben, um die Integration neu erzeugter iNs zu ermöglichen. Nach einem Zeitraum von zwei Wochen wurde die Netzwerkaktivität entweder pharmakologisch gehemmt oder blieb ungestört und es wurde eine Einzelkern-RNA-Sequenzierung durchgeführt. Interessanterweise wies die anschließende molekulare Charakterisierung der iN-Population auf zwei unterschiedliche Quellen der Diversität in der iN-Population hin: molekulare Subtypidentitäten, die zum einen ein breites Spektrum abgeleiteter kortikaler Subtypen sowie zum anderen unterschiedliche Entwicklungsstadien umfassen. Um zu beurteilen, ob iNs einer HSP unterliegen, habe ich die Transkriptionsdynamik als Reaktion auf die Aktivitätshemmung untersucht und wie diese mit denen vergleichbar ist, die in eNs hervorgerufen werden. Während eNs Regulierung von Gensignaturen zeigten, die auf HSP deutete, zeigten iNs eine Herunterregulierung dendritischer und synaptischer Gene, die mit einer verringerten morphologischen Komplexität nach Aktivitätshemmung korrelierte. Interessanterweise wurde festgestellt, dass eini Set an Synapsen-bezogenen Genen, die durch eNs als Reaktion auf die Aktivitätshemmung hochreguliert wurden, in iNs unter Kontrollbedingungen hoch exprimiert sind. Darüber hinaus führte eine pharmakologische Enthemmung der Netzwerkaktivität zu einer minimalen c-Fos-Hochregulierung in iNs im Vergleich zu eNs, was auf eine begrenzte Integration in das Netzwerk hinweist und darauf hindeutet, dass die hohe Basalexpression synaptischer Gene in iNs möglicherweise einen anhaltenden Wettbewerb um synaptischen Input widerspiegelt. Immunzytochemische Färbungen zeigten, dass GABAerge, aber nicht glutamaterge Synapsen iNs umgeben. Zusammenfassend deuten diese Daten darauf hin, dass iNs trotz der Expression von synaptischen Genen noch nicht funktionell in das Netzwerk integriert sind. Die erhöhte Basalexpression von Synapsen-bezogenen

Genen könnte auf eine verstärkte Konkurrenz um synaptischen Input hinweisen. Zusammenfassend stellt diese Arbeit die erste snRNA-seq-Studie dar, die den molekularen Phänotyp und das aktivitätsabhängige Transkriptom von aus Glia stammenden iNs und kortikalen eNs vergleicht, und schlägt Möglichkeiten zur Verfeinerung des iN-Differenzierungsprozesses hin zu einem funktionell reiferen und reaktionsfähigeren Phänotyp vor.

1

INTRODUCTION

1.1 DEVELOPMENT OF THE MAMMALIAN CEREBRAL CORTEX

> "The development of the vertebrate nervous system is a problem of such complexity that it is sometimes difficult to know where to start."
>
> *W. Maxwell Cowan from Cepko et al., 1998*

The complexity of the brain, or brain-like structure, varies widely across species in the animal kingdom. However, a constant thread throughout this diversity is the remarkable set of functions that this structure fulfills, spanning from the control of fundamental vegetative functions, e.g. breathing, heart rate, and blood pressure, to the orchestration of the body's movements and the construction of sensory experiences, thoughts, emotions, and, most intriguingly, the capacity to learn and remember. While in the human brain these tasks are performed by around 86 billion neurons (Azevedo et al., 2009), the mouse brain, the predominantly used model for mammalian brain research, comprises around 70 million neurons (Herculano-Houzel et al., 2006). Despite the discrepancy in neuronal numbers and overall brain size, core features, such as the general cellular architecture in distinct cortical regions as well as cell type classification, i.e. molecular identities of neurons, are conserved across species (Bakken et al., 2021; Hodge et al., 2019; M. H. Kim et al., 2023), making the mouse model suitable in studying human conditions. Furthermore, the significance of understanding the underlying mechanisms that shape brain development extends beyond understanding normal brain function. It plays an essential role in comprehending conditions like mental disability, schizophrenia, or autism spectrum disorders. Moreover, identifying genes playing key regulatory roles allows recapitulation of the process of neuronal identity acquisition and may open doors to cell replacement therapies and studies of neurodevelopmental disorders.

1.1.1 *Embryonic development of the mammalian brain*

The development of the central nervous system (CNS) begins at the neurulation stage, which takes place around embryonic (E) day 7 after fertilization in the murine embryo (Copp, 2005; La Manno et al., 2021). Early in embryogenesis, the pluripotent epiblast

undergoes gastrulation and develops the three germinal layers, the endoderm, mesoderm and ectoderm. The notochord arises as a tubular invagination of the axial mesoderm between the ectoderm and the endoderm and will serve as the guiding structure for the formation of the nervous system (Purves et al., 2001). The region of the gastrula that eventually will give rise to the nervous system is the ectoderm (Purves et al., 2001). Ectodermal cells constitutively express growth factors belonging to the bone morphogenic protein (BMP) family and lead to the generation of epidermal tissue while suppressing neural fate (Little and Mullins, 2006). The notochord then starts to express BMP antagonists, such as Noggin, Follistatin and Chordin, and triggers the differentiation of a subset of ectodermal cells into the neural ectoderm (McMahon et al., 1998). The forming neural ectoderm thickens into a columnar epithelium that is referred to as the neural plate. During neurulation, the lateral margins of the neural plate fold inward and fuse together, finally forming the neural tube, which eventually gives rise to the CNS (Colas and Schoenwolf, 2001). On an anatomical level, differential cell proliferation along the distinct axes results in the anterior portion of the neural tube undergoing radical morphological changes by bulging out and forming three primary brain vesicles: prosencephalon, mesencephalon and rhombencephalon (see Figure 1.1). As development continues, these three vesicles get further subdivided: out of the prosencephalon, the anterior telencephalon and the caudal diencephalon emerge and eventually form the cerebral hemispheres and the thalamus as well as hypothalamus, respectively 1.1). The midbrain emerges from the mesencephalon and the division of the rhombencephalon into the anterior metencephalon and the posterior myelencephalon give rise to the pons and cerebellum as well as the medulla oblongata, respectively (Gilbert., 2000). During the next days, the brain continues to develop with increasing complexity in cell type diversity, resulting in around 300 distinguishable neuronal subtypes across the entire brain at the time of birth (La Manno et al., 2021).

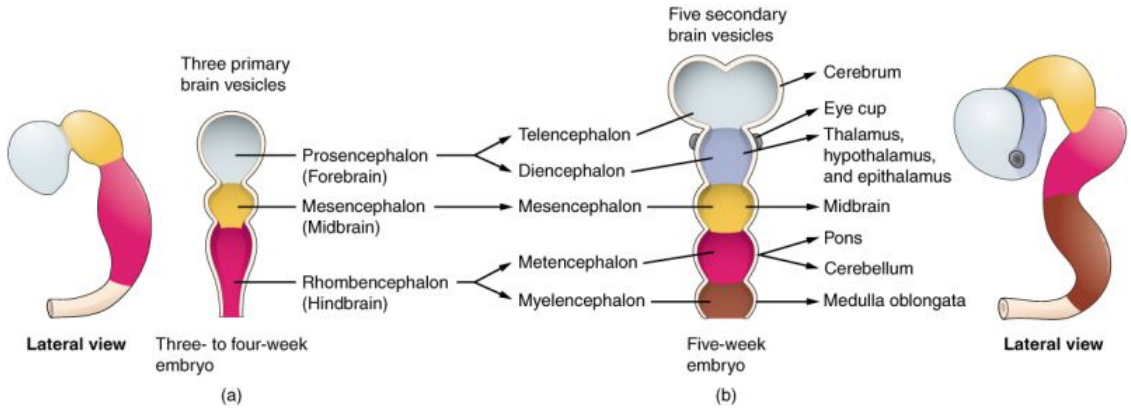

Figure 1.1: **Development of the primary brain vesicles.**
Development of primary and secondary brain vesicles from the neural tube in a three- to five-week-old human embryo highlighting fully developed brain structures resulting from each vesicle. Figure taken from Elshazzly et al., 2022.

1.1.2 *Molecular control of cortical neurogenesis*

During the expansion of the telencephalon, cortical neurogenesis begins with the proliferation of neuroepithelial cells (NECs) that border the ventricle of the telencephalic vesicles (Haines and Mihailoff, 2018; Nieto et al., 2004). NECs are regarded as the very first neural progenitors that proliferate in a symmetric manner to generate a pseudostratified (seemingly multi-layered) neuroepithelium which will eventually give rise to all cortical excitatory neurons (Bonnefont and Vanderhaeghen, 2021). After several rounds of cell division, at around embryonic day 10.5 (E10.5), NECs lose their tight junctions while maintaining apical adherent junctions and transform into radial glial cells (RGC) (see Figure 1.2) (Taverna et al., 2014; Villalba et al., 2021). The generation of the RGC pool marks the onset of cortical neurogenesis and the transformation from NECs into RGCs has been shown to correlate with the emergence of Notch signaling (Gaiano et al., 2000; Martynoga et al., 2012). Notch signaling is activated by the expression of Notch-receptor ligands, e.g. Dll1, which in turn are activated by proneural TFs, such as Ascl1 or Neurog2, during induction of a neuronal differentiation program in neighboring cells (Kageyama et al., 2009). In fact, maintenance of Notch signaling has been shown to be essential in maintaining the neural progenitor pool (Kovach et al., 2013; Martynoga et al., 2012; Shimojo et al., 2008). Similarly, other signaling pathways have been implicated in the maintenance of the proliferating neural progenitor pool as well, including morphogens such as e.g. Wnts, BMP, Sonic Hedgehog and FGF (Bonnefont and Vanderhaeghen, 2021; Martynoga et al., 2012), while others, e.g. neuregulin-I/ErbB signaling has been shown to be essential in suppressing differentiation of RGCs into astrocytes (Martynoga et al., 2012; Sardi et al., 2006; Schmid et al., 2003). In addition, cell intrinsic factors, e.g. fate-determining TFs play a crucial role during the NEC-to-RGC transition. For instance,

the TF Sox1 has been identified to maintain the neuroectodermal commitment of NECs while inhibiting further differentiation, while the subsequent expression of the TF Pax6 has been shown to be causally linked to the differentiation of NECs into RGCs as well as being required to maintain a RGC identity (Götz et al., 1998; Kovach et al., 2013; Suter et al., 2009). Importantly, Pax6 expression in RGCs has been identified as a fundamental intrinsic fate determinant of neuronal fate and its mutation was shown to result in impaired cortical neurogenesis *in vitro* (Heins et al., 2002). Therefore, the formation of the RGC pool is considered to mark the initiation of neurogenesis (Villalba et al., 2021). Interestingly, RGCs resemble morphologically and molecularly NECs and were for a long time merely regarded as scaffold cells with the role of guiding the migration of newly generated neurons towards the appropriate cortical layer due to their unique morphology (Rakic, 2000). Unlike NECs, RGCs remain not only physically attached to the ventricular zone but also extend to the outer basal surface of the developing cortex, serving as a guiding structure for migrating neurons (see Figure 1.2) (Gaspard and Vanderhaeghen, 2011). Importantly, it is now well established that radial glia cells serve as the major pool of neural progenitors throughout the CNS and eventually give rise to all cortical excitatory neurons (Bonnefont and Vanderhaeghen, 2021; Malatesta et al., 2008; Malatesta et al., 2003). RGCs acquire astroglial hallmarks by e.g. expressing multiple glial markers such as GLAST, GFAP, vimentin, S-100β and nestin, while maintaining neuroepithelial characteristics (Martynoga et al., 2012). Moreover, during the transition from the NEC to the RGC state, cells begin to express proneural TFs, most importantly neurogenin-1 and neurogenin-2, which constitute essential TFs in promoting neurogenesis by e.g. counteracting Notch signaling (Bonnefont and Vanderhaeghen, 2021). Early on, RGCs divide symmetrically to maintain an actively proliferating pool of neural progenitors. This is followed by a transition into a phase of asymmetric divisions during which they give rise to a short-lived intermediate progenitor pool, so-called intermediate progenitor cells (IPCs) (Gaspard and Vanderhaeghen, 2011; Hippenmeyer, 2023). In fact, RGCs have been found to either differentiate directly into neurons or indirectly through the IPC stage (Malatesta et al., 2000; Villalba et al., 2021).

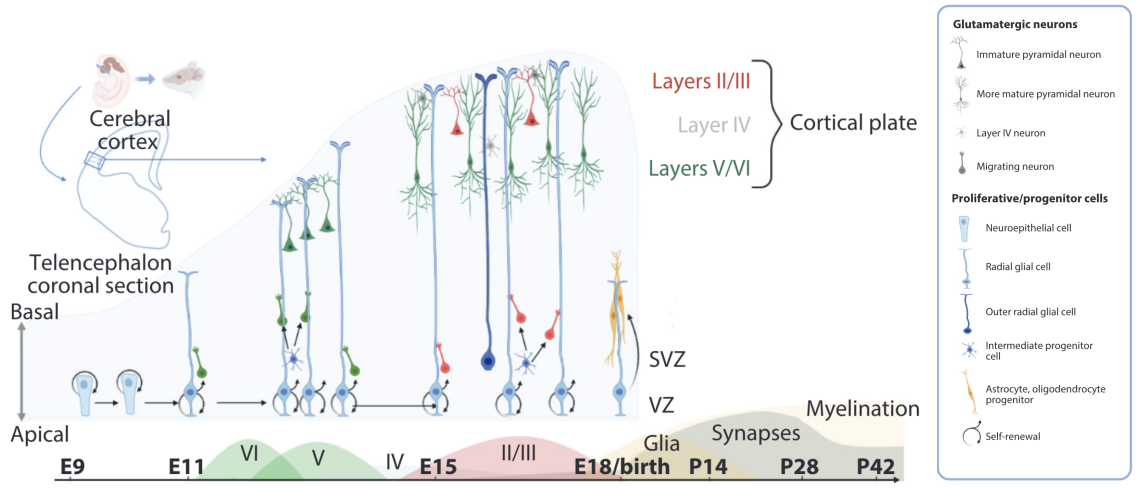

Figure 1.2: **Cortical neurogenesis in the embryonic mouse brain.**
Cortical neurogenesis begins with the proliferation of neuroepithelial cells (NECs). NECs differentiate into radial glia cells (RGCs), which in turn give rise to intermediate progenitor cells (IPCs). IPCs generate the majority of cortical neurons in an 'inside-out' fashion, deep-layer neurons are generated first, followed by the generation of upper-layer neurons. RGCs are used as a scaffold by migrating newborn neurons in order to reach their final position. Figure taken and modified from Libé-Philippot and Vanderhaeghen, 2021.

As cortical neurogenesis advances, the pool of RGCs initially expands by undergoing symmetric divisions and transitions then to neurogenesis via undergoing asymmetric divisions (Hippenmeyer, 2023; Martynoga et al., 2012). RGCs then generate IPCs, which migrate away from the apical surface towards the basal border of the ventricular zone and eventually form the subventricular zone (SVZ) (see Figure 1.2) (Kovach et al., 2013; Villalba et al., 2021). The migration of IPCs into the SVZ is correlated with a progressive loss of Pax6 expression and the upregulation of the T-box transcription factor 2 (Tbr2) expression, which is required for maintaining an IPC identity (Kovach et al., 2013; Molyneaux et al., 2007). After typically one symmetric division, IPCs then give rise to most cortical projection neurons (Anderson and Vanderhaeghen, 2014; Martynoga et al., 2012). Interestingly, the transition from a proliferative state to cell cycle exit with subsequent terminal neuronal differentiation is guided by upregulation of transcriptional repressors, e.g. Bcl6 or Myt1l, of genes related to morphogen signaling pathways that maintain proliferation (Bonnefont et al., 2019; Bonnefont and Vanderhaeghen, 2021; J. Chen et al., 2022; Mall et al., 2017). On a molecular level, it has been shown that upregulation of Bcl6 or Myt1l establishes a neuronal identity through active repression of non-neuronal fates by recruitment of a deacetylase, Sirt1, which induces steady epigenetic repression of target genes (Bonnefont and Vanderhaeghen, 2021). At around E18.5, neurogenesis is completed and the remaining RGCs lose their apical attachment, acquire a multipolar morphology and begin to differentiate predominantly into astro-

cytes and to a lesser extent into oligodendrocytes (Hippenmeyer, 2023; Libé-Philippot and Vanderhaeghen, 2021; Martynoga et al., 2012). On a molecular level, the switch to astrogliogenesis is initiated when developing neurons express Notch ligands that activate Notch signaling in neighboring RGCs, ultimately resulting in demethylation and accessibility of the astrocytic glial fibrillary acidic protein (GFAP) promoter (Kanski et al., 2014; Takouda et al., 2017). Subsequently, further signals from developing neurons result in the activation of the pro-astrocytic Jak/Stat signaling pathway, which further instructs astrogenesis (Kanski et al., 2014; Martynoga et al., 2012). Moreover, the bHLH TF Neuronal PAS domain protein 3 (Npas3) is highly expressed in maturing astrocytes within the entire cortex and has been shown to be crucial in dictating astrocytic functions during development (Y. Li et al., 2022). At postnatal and adult developmental stages, NPCs are only found in two regions within the brain, the subventricular zone (SVZ) of the lateral ventricles and the subgranular zone within the hippocampus (Götz et al., 2016). NPCs continue to generate neurons, which migrate into the olfactory bulb and participate in olfaction (derived from the SVZ), or remain within the hippocampus and contribute to learning behavior and memory formation (Gonçalves et al., 2016; Götz et al., 2016).

1.1.3 *Molecular differentiation trajectories and subtype diversity of cortical neurons*

The cerebral cortex comprises two main neuronal classes. About 80 % of all cortical neurons are excitatory neurons, with the majority referred to as pyramidal neurons which are named after their triangular-shaped soma. The remaining 20 % comprise inhibitory interneurons that are born in the medial and caudal ganglionic eminences of the ventral telencephalon and migrate into the developing cortex (Anderson and Vanderhaeghen, 2014). Interneurons can be divided into four broad neuronal categories depending on the expression of distinct marker proteins, e.g. somatostatin (SST), parvalbumin (PV), vasoactive intestinal peptide (VIP) and reelin expressing interneurons (Wamsley and Fishell, 2017). Depending on their specific pattern of synaptic connectivity with excitatory neurons as well as their molecular profiles, these four classes can be further subdivided into multiple distinct subtypes of interneurons (Scala et al., 2021; Wamsley and Fishell, 2017). Despite their small number within the cortex, interneurons play an essential role in controlling excitation levels by refining circuit activity and therefore contribute not only to the maturation, plasticity and survival of pyramidal neurons but constitute also a relevant variable in the emergence of several neurological diseases (Dehorter et al., 2017; Llorca and Deogracias, 2022). Pyramidal neurons display a high diversity of subtypes and have been identified based on subtype-specific canonical properties regarding their morphology, physiology, or molecular profile (Winnubst and Arber, 2021; Zeng and Sanes, 2017). Intriguingly, recent technological advancement of omics techniques has facilitated a finer characterization of neuronal diversity at the single cell level based on their molecular profiles and achieved a detailed dissection of the neuronal composition of the cerebral cortex at distinct maturation stages (Bragg-Gonzalo et al., 2021; Di Bella et al., 2021; La Manno et al., 2021; Yao, Liu, et al., 2021). These studies have shown that neuronal diversity is significantly higher than previously thought and that neuronal identity seems to be a dynamic state along a continuum rather than discrete states, although distinct groups of neuronal subtypes can still be recognized (Bragg-Gonzalo et al., 2021; Zeng and Sanes, 2017). In fact, due to the enormous neuronal heterogeneity observed at the molecular level, it is currently debated as to how to define discrete neuronal subtypes (Bragg-Gonzalo et al., 2021). Moreover, recent scRNA-seq studies of the mouse brain have revealed the presence of multiple new neuronal subtypes across various brain regions, further expanding the current view of neuronal diversity (Yao, Liu, et al., 2021; Zeisel et al., 2018). Albeit the emerging neuronal diversity of the adult cerebral cortex has been extensively characterized and shown to be remarkably high (Di Bella et al., 2021; Yao, Liu, et al., 2021), the underlying molecular mechanisms have not yet been fully understood. It is however clear that the cortical neuronal diversity emerges to a large extent through an already diverse population of neural progenitors with

heterogenous molecular features (RGCs and IPCs), which, in addition, display distinct temporal competencies to ultimately produce a diverse set of neuronal subtypes (Gaspard and Vanderhaeghen, 2011; Koo et al., 2023; Oberst et al., 2019). Interestingly, studies have shown that the competence of neural progenitors to produce distinct neuronal subtypes differs over time through evolving, stage-specific and tightly-controlled gene regulatory networks (Desai and McConnell, 2000; Di Bella et al., 2021; Koo et al., 2023; Oberst et al., 2019). This ultimately results in the generation of distinct subtypes of pyramidal neurons that follows a typical "inside-out" pattern: deep-layer positioned neurons are generated first by differentiating IPCs, followed by the generation of neurons located in superficial layers, ultimately generating six distinct layers, each with specific gene expression profiles and functional roles (Anderson and Vanderhaeghen, 2014; Molyneaux et al., 2007; Villalba et al., 2021). Neural progenitors increasingly become more restricted in their potential of generating diverse neuronal subtypes, e.g. late-born progenitors could only give rise to UL neurons, while early-born progenitors could generate both, UL and DL neurons (Desai and McConnell, 2000). More recently, heterochronic transplantation experiments showed that while RGCs transplanted into a developmentally younger cortex could achieve the generation of DL neurons, transplanted IPCs into a younger cortex were not able to regain this capability (Oberst et al., 2019). These data provided evidence that neuronal fate commitment is regulated by cell-intrinsic mechanisms and becomes irreversible at the IPC stage (Bonnefont and Vanderhaeghen, 2021; Oberst et al., 2019). IPCs are not pre-committed towards a specific fate but rather gradually develop into distinct neuronal subtypes as scRNA-seq studies have revealed temporal gradients of subtype-determining TF expression (Di Bella et al., 2021; Telley et al., 2019). The differentiation of neurons and the transition from an IPC stage to postmitotic neurons is transcriptionally initiated by downregulation of Tbr2 and upregulation of Tbr1 expression (Englund et al., 2005). Hence, the sequential expression of the TFs Pax6, Tbr2 and Tbr1 during progression from RGCs to IPCs to glutamatergic neurons shows stage-specific expression patterns, which are widely used as molecular markers for identification of distinct differentiation stages (Englund et al., 2005). Expression of Tbr2 and differentiation into IPCs is induced by the TF Neurog2, which together with Pax6 constitutes the main transcriptional activator of cortical neurogenesis (Heins et al., 2002; Nieto et al., 2001; Schuurmans et al., 2004) and hence will be discussed in more detail below. The final laminar position of cortical neurons dictates their connectivity patterns: while neurons within layers II-III (so-called upper-layer (UL) neurons) serve as cortico-cortical neurons by connecting distinct cortical areas within the same, but also with the opposite cortical hemisphere, neurons of layer V-VI (so-called deeper layer (DL) neurons) serve as cortico-fugal neurons by establishing connections with subcortical areas such as the basal ganglia, thalamus or brainstem (Gaspard and Vanderhaeghen, 2011). In contrast, neurons residing in layer

IV mainly receive input from the thalamus and other subcortical regions (Scala et al., 2019). Predictably, layer-specific neurons differ also in their gene expression profiles as well as their electrophysiological properties, e.g. DL neurons are more excitable than UL neurons and display denser synaptical connections among each other which facilitates propagation of excitation (Canavero and Cioni, 2011; Scala et al., 2021). Similar to differentiating progenitors, layer-specific neurons can be molecularly distinguished based on the layer-specific expression of TFs that has been shown to instruct neuronal layer identities and hence serve as molecular markers for distinct cortical identities (Gaspard and Vanderhaeghen, 2011). For instance, expression of the TF Satb2 is only required for the specification of UL neurons residing in layers II/III (Britanova et al., 2008), while Rorβ is required for acquiring a layer IV-specific transcriptional identity (Clark et al., 2020). Moreover, restricted expression of Cux1/2 towards the upper layers (II-IV) has been suggested to drive IPC differentiation from DL towards a UL molecular identity (Nieto et al., 2004). DL neurons are specified by the TF Fezf2 and its target Ctip2, Tbr1 and Sox5 (layer V/VI) as well as Foxp2 (layer VI) (Bragg-Gonzalo et al., 2021; Cánovas et al., 2015; Martynoga et al., 2012). The sequential postmitotic specification of distinct neuronal layer identities at the molecular level is further refined by cross-repressive interactions between the e.g. above-mentioned layer-identity determining TFs (see Figure 1.3). For instance, Tbr1 represses expression of Ctip2 early on in order to allow generation of layer VI neurons, while later on in corticogenesis the UL-specific TF Satb2 represses Ctip2 expression, resulting in generation of UL neurons (see Figure 1.3) (J. Liu et al., 2022; Martynoga et al., 2012; McKenna et al., 2011). On the other hand, Satb2 expression is repressed by Fezf2 in order to allow layer V neuron generation (see Figure 1.3) (McKenna et al., 2015). Recently, the TF Foxg1 was identified as a master regulator of cortical neuronal subtype specification (J. Liu et al., 2022). The study could show that around E14.5, Foxg1 represses Ctip2 and Tbr1, while inducing Satb2 transcription in order to promote the generation of callosal neurons (J. Liu et al., 2022). After E14.5, Foxg1 further specifies neuronal identities of distinct layers by differentially regulating expression levels of Ctip2 and Tbr1 (J. Liu et al., 2022). Similarly, expression of Fezf2 is tightly regulated by Foxg1 (J. Liu et al., 2022). Interestingly, laminar gene expression patterns have been shown to differ significantly across various cortical areas. These variations in gene expression patterns are tightly linked to cortical area-specific functions, such as visual processing or motor control (Bhaduri et al., 2021; Gaspard and Vanderhaeghen, 2011).

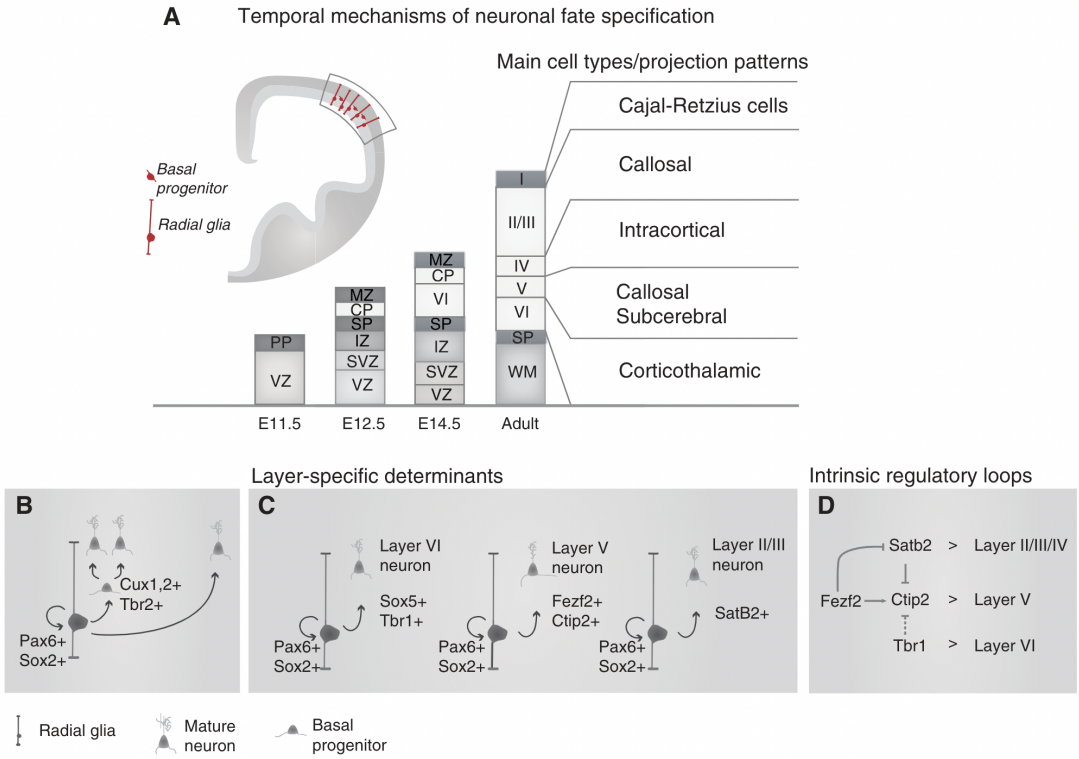

Figure 1.3: **Neuronal subtype-specification in the cerebral cortex.**
Neuronal fate specification is guided by spatial as well as temporal mechanisms. In the presented figure, temporal mechanisms are illustrated. **(A)** Neurogenesis involves the generation of specific neuronal subtypes in a sequential order, emerging from progenitors located in the ventricular zone (VZ) and subventricular zone (SVZ) of the cortex. This results in the cerebral cortex being organized into distinct layers in an 'inside-out' fashion. **(B)** Cortical projection neurons (CP neurons) are primarily generated through an indirect pathway involving intermediate basal progenitors (BPs), but can also emerge directly from differentiating radial glia cells (Pax6+). **(C)** TFs that are responsible for determining the identity of various classes of CPs that make up the distinct layers of the cortex. **(D)** Cross-repressive interactions of layer-specific TFs, either directly (solid lines) or indirectly (dashed lines) repressing TFs responsible for neuronal specification in adjacent layers. The figure was taken from Martynoga et al., 2012.

1.1.4 *The bHLH transcription factor Neurog2: role during corticogenesis*

The regulation of gene expression has long been recognized to be an essential instructive component in building and maintaining distinct organs of an organism (Thanasios and Apavassiliou, 1995). Beyond the role this mechanism plays in the differentiation and maturation of cells, it also enables constitutive tissue- or cell-specific gene expression patterns as well as the adaptive response to internal and external stimuli (Latchman, 1997; Mitsis et al., 2020). Gene expression is mainly regulated by transcription factors (TFs), a heterogeneous group of proteins that possess a DNA-binding domain (DBD). When binding specific DNA sequences, they either promote or repress the recruitment of the RNA polymerase and hence gene transcription (Tong Ihn Lee and Young, 2003). In

general, TFs can be divided into *general* and *specific* TFs. General TFs are ubiquitously expressed across different tissues and are required for basal transcription. By binding to TATA boxes or directly interacting with the RNA-polymerase they are involved in the assembly of the pre-initiation complex during transcription (Sainsbury et al., 2015; Sanders and Mason, 2016). Specific TFs, on the other hand, display cell-type specific expression patterns and mediate or repress the transcription of specific gene sets. Specific TFs can bind to either proximal or distal gene regulatory elements ($>$ 1 kb from the transcription start site), such as e.g. enhancers (Spitz and Furlong, 2012). Based on the structure of their DBD as well as their 3D molecular structure, specific TFs can be further distinguished into 4 main classes and are named according to their distinctive motifs: *(i)* zinc-finger proteins, *(ii)* helix-turn-helix proteins, *(iii)* leucin-zipper proteins and *(iv)* helix-loop-helix proteins (Thanasios and Apavassiliou, 1995). Of particular interest in this thesis is the helix-loop-helix TF class (HLH). Compared to other TF families, HLH TFs were exceptionally well conserved during evolution (Ben-Arie et al., 1996) (see Figure 1.4). Structurally, HLH TFs are composed of a short and a longer amphipathic α-helix that are connected via a loop of variable length (J. C. Hong, 2016) (see Figure 1.4). Typically, the two longer α-helices contain each a basic domain at the N-terminal end and form a functional DNA binding unit that allows interaction with the major groove of acidic DNA while the HLH domain allows dimerization with other TFs (X. Cheng et al., 2019; Georgias et al., 1997) (see Figure 1.4). HLH TFs are therefore generally referred to as basic HLH TFs (bHLH). bHLH TFs bind the DNA at characteristic base sequences 5'-CANNTG-3' (where N can be any nucleotide) called E-boxes that are found at *cis*-regulatory elements of downstream target genes (J. C. Hong, 2016; Tamura et al., 2014). Depending on their expression pattern among distinct tissues, bHLH TFs are subdivided into class I and class II TFs. Class I bHLH TFs are found to be ubiquitously expressed and include TFs such as E12/E47 (Tcf3), Tcf4 and Tcf12, while class II bHLH TFs, comprising TFs such as MyoD, Neurog1 and Ascl1 display tissue-specificity (Dennis et al., 2019; Tamura et al., 2014).

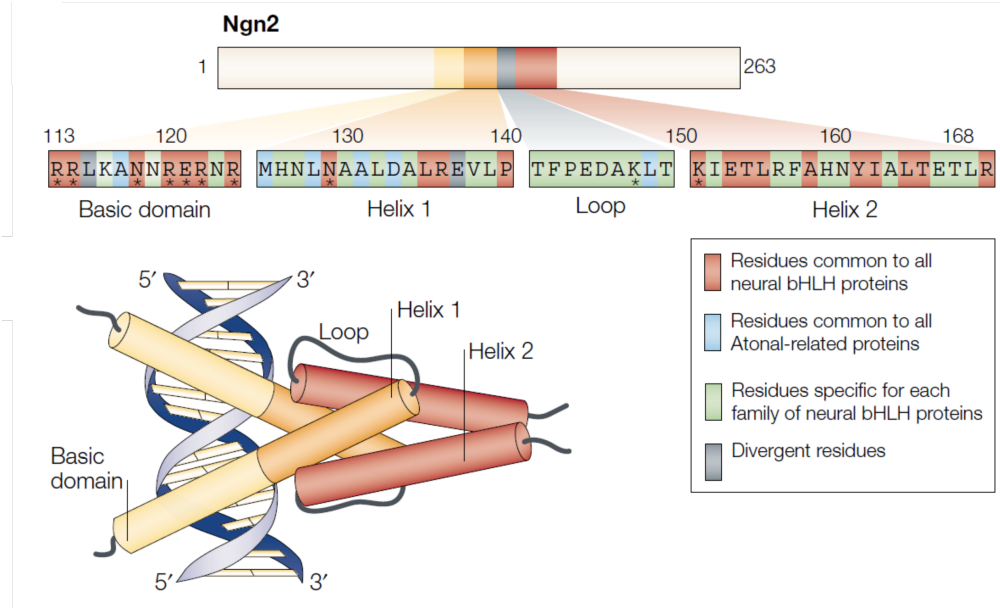

Figure 1.4: **Molecular structure of bHLH TFs.**
(Top) Sequence of the bHLH domain of the vertebrae proneural TF Neurogenin-2 (Ngn2) with color-coded annotation of amino-acid conservation between distinct neural bHLH proteins. The asterisks mark the amino acid residues that form direct contact with DNA. *(Bottom)* Schematic representation of a bHLH TF. The interaction with (acidic) DNA is enabled via a basic DNA-binding domain. The two α-helices, separated by a loop, mediate dimerization of two protein monomers. Figure was modified and taken from Bertrand et al., 2002.

Class II TFs either form homo- or heterodimers with class I TFs in order to initiate transcription (Tamura et al., 2014). bHLH TFs have been shown to be predominantly involved in several developmental processes and a significant subgroup of bHLH TFs exert their function specifically in the developing nervous system (Dennis et al., 2019; Nieto et al., 2001). These neural TFs were historically further subdivided according to their homology to genes found in the nervous system of Drosophila. Among these subgroups are the so-called 'pro-neural' achaete-scute complex and atonal gene families which have been identified to possess a fundamental role as key regulators of neurogenesis as well as in instructing the acquisition of neuronal fate and their subtype identity in a region-specific manner (Baker and Brown, 2018; Bertrand et al., 2002; Dennis et al., 2019; Tomita et al., 2000). In the mammalian nervous system, one achaete-scute like 1 gene (*Ascl1*, or originally also called *Mash1* for mammalian achaete scute homolog-1) has been identified, while several atonal-related bHLH TFs were characterized, among which are members of the Neurogenin (Neurog1-3), NeuroD (NeuroD1, NeuroD2, NeuroD4 and NeuroD6), Olig (Olig1-3) and Atonal (Atoh1) TF families (Dennis et al., 2019; Guillemot et al., 1993). With a few exceptions (e.g. Olig2), proneural TFs usually act as transcriptional activators by inducing a cascade of pan-neuronal genes (Bertrand et al., 2002; Hulme et al., 2022). As proneural TFs, their expression promotes cell-cycle

exit and induces neuronal commitment in IPCs (Bertrand et al., 2002). Two proneural TFs are particularly well characterized due to their fundamental role during cortical development: Ascl1 and Neurog2 (Aydin et al., 2019; Dennis et al., 2019). At the beginning of neurogenesis, Neurog2 is expressed in cortical progenitors of the ventricular zone in the dorsal telencephalon and has been identified as a key regulator of corticogenesis (Dennis et al., 2019; Hulme et al., 2022). Interestingly, while e.g. Neurog1 expression declines already at around E15.5 (Dennis et al., 2019), Neurog2 is detected during the entire period of neurogenesis from E10.5 to E17, despite significant changes in expression levels (Dennis et al., 2019; Gohlke et al., 2008). Moreover, despite Neurog1 and Neurog2 having been shown to display in part overlapping functional roles during development, only Neurog2 mutant animals display defects in cerebral cortex development (Hulme et al., 2022; Nieto et al., 2001). IPCs of the dorsal telencephalon express Neurog1/2, where their expression determines a glutamatergic neuronal fate in the forebrain (Di Bella et al., 2021; Gohlke et al., 2008). Similarly, NPCs of the ventral telencephalon express Ascl1 and differentiate into GABAergic neurons, which in part, migrate into and populate the cerebral cortex at later stages (Gohlke et al., 2008). Differentiation into glutamatergic or GABAergic neurons via Neurog2 or Ascl1 expression, respectively, has recently been shown to be mediated by their binding onto largely non-overlapping sets of genomic sites (Aydin et al., 2019). Interestingly, the study could show that the distinct binding pattern of the two proneural TFs is not a consequence of intrinsic differences, but instead due to the presence of distinct E-box sequences at their respective target gene sites (Aydin et al., 2019). Moreover, the study showed that despite largely distinct binding onto genomic sites, Ascl1 and Neurog2 influence accessibility as well as activity of a few common downstream TFs (e.g. Brn2, Ebf2, Onecut2), resulting in neuron-specific transcriptomic profiles with around 80% of similarity in gene expression profiles after 48 hours of proneural activation (Aydin et al., 2019). Interestingly, Neurog2 prevents an alternative GABAergic fate by inhibiting Ascl1 expression (Kovach et al., 2013; Schuurmans et al., 2004). Cellular identity is established by finely regulated molecular processes involving TFs, CREs as well as accessible chromatin (Noack et al., 2022). Intriguingly, a recent study could show that Neurog2 is able to directly regulate enhancer activity and by binding to both, enhancer and promoter regions of its target genes, can induce a significantly stronger expression (Noack et al., 2022). Moreover, Neurog2 was shown to induce DNA demethylation as well as chromatin accessibility at its target gene binding sites, therefore facilitating (epi)genomic remodeling, supporting its previously presumed role as a pioneer factor (Bocchi et al., 2022; Noack et al., 2022). The upstream TF Pax6 directly induces Neurog2 expression through binding to its enhancer element, and Neurog2 in turn inhibits Pax6 expression in order to allow IPC differentiation into neurons (Hulme et al., 2022). Via a transient high expression profile, Neurog2 induces cell-cycle exit

of IPCs via direct repression of a group of cell cycle regulators of the G1/S phases (Lacomme et al., 2012). Subsequently, Neurog2 induces expression of downstream TFs that are necessary for differentiation and specification of cortical neurons, such as Tbr1 or NeuroDs as well as terminal differentiation markers such as Myt1l (J. Chen et al., 2022; Hulme et al., 2022; Imayoshi and Kageyama, 2014; Muhr and Hagey, 2021). Depending on the cellular context or distinct post-translational modifications, Neurog2 can drive diverse molecular processes that are independent of its proneural activity. For instance, Neurog2 expression by molecularly distinct NPC populations has been shown to drive differentiation into either motor, dopaminergic or sensory neurons of the PNS (Hulme et al., 2022), by e.g. phosphorylation of the two conserved serine residues S231 and S234 on Neurog2 leading to the specification of a motor neuron identity (Hulme et al., 2022; Ma et al., 2008). Moreover, low levels of BMP in the context of Neurog2 expression drive the specification of sensory neurons, while high levels of BMP result in the acquisition of an autonomic neuronal identity in the PNS (Hulme et al., 2022; Lo et al., 2002), whereas Ascl1 directs an autonomic neuronal identity acquisition at both low and high levels of BMP (Lo et al., 2002). In cortical NPCs, phosphorylation on the tyrosine residue 241 of Neurog2 leads to the specification of their dendritic morphology as well as their radial migration behavior, a process that is essential for the formation of the layered cortex (Hand et al., 2005; Hulme et al., 2022). This is achieved by regulation of neuronal polarity as well as initiating the development of a leading process by Neurog2 (Imayoshi and Kageyama, 2014). Moreover, neuronal migration is inhibited by RhoA and Neurog2 was found to inhibit RhoA activity as well as inducing expression of the GTPase Rnd2, an inhibitor of RhoA signaling (Imayoshi and Kageyama, 2014). This process was shown to be independent of its proneural activity and therefore suggests that Neurog2 specifies multiple neuronal features. Furthermore, Neurog2 expression has been suggested to not only specify a regional (cortical) or a specific neurotransmitter (glutamatergic) identity but also to impose a laminar, DL identity (Schuurmans et al., 2004). Intriguingly, UL cortical neurons have been shown to develop independently of Neurog2 expression (Schuurmans et al., 2004). During late corticogenesis, Neurog2 function is diminished via its phosphorylation by the kinase GSK3 (S. Li et al., 2012). Overall, the pioneer activity as well as extensive (pro-neural) functions of Neurog2 during corticogenesis are strengthened by its comprehensive use in cellular reprogramming approaches into induced neurons (iNs), which will be further discussed in the next chapter.

1.2 CELLULAR REPROGRAMMING

> "In adult centers the nerve paths are something fixed, ended, immutable. Everything may die, nothing may be regenerated. It is key for the science of the future to change, if possible, this decree."
>
> *Santiago Ramón y Cajal*
> *1928*

ALREADY 30 YEARS after Santiago Cajal, founder of modern neuroscience, issued his decree on neuronal regeneration in 1928, scientists had come to the realization that, unlike previously thought, the cellular commitment to a certain identity is not irreversibly fixed and, in effect, this finding opened doors to unprecedented opportunities to generate cell types of choice for regenerative purposes. It was John Gurdon who provided the foundation when he transferred a nucleus from a differentiated intestinal cell of a tadpole into an irradiated frog's egg (Gurdon, 1962). Strikingly, the outcome was a vital frog who reached the adult stage which provided an elegant demonstration that despite having reached terminal differentiation, the nucleus still harbors the potential to give rise to a morphologically and functionally vital organism (Gurdon, 1962). This groundbreaking work was followed by another fundamental study approximately 40 years later: in 2006, Kazutoshi Takahashi and Shinya Yamanaka demonstrated that fibroblasts can be converted into pluripotent stem cells (hence referred to as *induced* pluripotent stem cells) by instruction through no more than four TFs (*Oct3/4, Sox2, c-Myc, Klf4*) (Takahashi and Yamanaka, 2006). Finally, in 2012, John Gurdon and Shinya Yamanaka received the Nobel Prize for laying the foundation for a newly emerging scientific field: cellular reprogramming.

1.2.1 *Direct neuronal reprogramming*

Since then, scientists have shown that cell identity can be reprogrammed via many distinct means. While ectopic expression of lineage-determining TFs represents the most widely used approach for converting one cell type into another and will be the focus of this chapter, other means such as small molecules that interfere with crucial signaling pathways, microRNAs or epigenetic regulators have also shown to possess the ability to access the necessary genetic information to induce a switch in cellular identity (Bocchi et al., 2022; K. P. Kim et al., 2020; J. Xu et al., 2015). Ectopic expression of as few as a single TF has been shown to successfully lead to the conversion into diverse cell types, such as cardiomyocytes (Ieda et al., 2010), β-cells of the pancreas (Q. Zhou et al., 2008), as well as neurons (Heinrich et al., 2010; Heins et al., 2002; Vierbuchen et al., 2010). These

TFs have been selected due to their necessary functions in specifying distinct cell types during development, i.e. their ability to access silent chromatin, and specifically target cell-type specific enhancer clusters, and initiate gene transcription leading to a change in cell identity that can extend beyond lineage restrictions (Mircea and Semrau, 2021). The selection of the initial cell type for reprogramming purposes is another crucial factor that likely affects the efficiency of the process, as it is influenced by distinct chromatin accessibility and epigenetic characteristics that may reflect distinct developmental origins (Vignoles et al., 2019). Interestingly, despite the use of pioneer TFs, their pioneer activity has been shown to be likely context-dependent, i.e. binding to inaccessible binding sites was shown to differ between distinct starting cell types, as a recent study showed in the case of Ascl1 (Aydin et al., 2019). Within the brain, various types of glial cells, i.e. NG2 glia, astroglia or microglia, demonstrated the ability to reprogram into neurons by ectopic expression of TFs (Heinrich et al., 2014; Tai et al., 2021). Astroglial cells, in particular, have emerged as an attractive cell type for neuronal reprogramming purposes. This is due to the fact that NSCs share astroglial properties, suggesting that astrocytes may possess the necessary genetic predisposition to facilitate neuronal fate conversion (Vignoles et al., 2019), Additionally, they are ubiquitously distributed and have the capacity to self-renew through proliferation following neuronal injury or death. As described in the previous chapter, neurons and astrocytes are both sequentially generated from RGCs and hence share a common developmental origin. This may explain a higher reprogramming competence towards excitatory neurons compared to other glial types, while for instance, NG2 glia may more easily reprogram into inhibitory neurons possibly due to their common developmental origin in the ganglionic eminences (Vignoles et al., 2019). Along this line, glia-to-neuron reprogramming was already successfully demonstrated in multiple regions within the CNS, e.g. cerebral cortex (Heinrich et al., 2010), the striatum (Zhang et al., 2022), hippocampus (Lentini et al., 2021), spinal cord (X. Chen and Li, 2022) as well as in the retina (Lahne et al., 2020). Noteworthy, although both reactive astrocytes *in vivo* as well as cultured astrocytes *in vitro* are proliferative, this state is not an obligatory condition for neuronal reprogramming (Gascón et al., 2016; Heinrich et al., 2010; Vignoles et al., 2019). However, it is suggested that the proliferative state impacts the chromatin landscape and facilitates reprogramming (Vignoles et al., 2019). This is supported by observations from *in vitro* studies, in which it was shown that with increased culturing time, astroglia displayed a progressive decrease in their proliferative capacity as well as in their capacity to undergo reprogramming. This decline is likely due to reduced accessibility of neuron-specific target sites (Masserdotti et al., 2015). The first TF that showed the ability to convert cortical glia cells into excitatory neurons *in vitro* was Pax6 (Heins et al., 2002), however, it was quickly disused as its downstream target, Neurog2, was shown to be significantly more efficient in driving

neuronal reprogramming (Berninger et al., 2007; Heinrich et al., 2010; Heins et al., 2002). Notably, Neurog2 instructs cortical astroglia towards glutamatergic neurons with the ability to form functional synapses (Heinrich et al., 2010; Heinrich et al., 2012). Interestingly, the pro-neural TF Ascl1, in turn, directs cortical glia towards a GABAergic neuronal identity, which embryonically emerges from the ventral telencephalon (Blum et al., 2011; Heinrich et al., 2010). Therefore, proneural TFs are able to impose class-specific neuronal identities independent of the regional identity of the glial population (Heinrich et al., 2010). Nonetheless, it remains to be assessed to which extent the regional origin of glia impacts the reprogramming process, as recent studies could show that traces of original identities persist following reprogramming and may impact maturation or functionality (Chouchane et al., 2017; Herrero-Navarro et al., 2021; Kempf et al., 2021). Interestingly, overexpressing the same TFs in different starting cell types or local environments, both *in vitro* and *in vivo*, resulted in variable outcomes in terms of efficiency as well as neuronal specification (Vignoles et al., 2019). This is illustrated by the successful induction of neuronal conversion of striatal astrocytes using Sox2, while neuronal reprogramming of cortical glia could only be achieved following injury (Heinrich et al., 2014; Niu et al., 2015; Vignoles et al., 2019). Similarly, the TF Neurog2 successfully converted striatal glia into neurons but failed to achieve a comparable efficiency within the cerebral cortex (Grande et al., 2013; Vignoles et al., 2019). The available results therefore prompted scientists in the field to further investigate whether different non-neurogenic brain regions possess distinct competencies for reprogramming purposes (Vignoles et al., 2019). Moreover, the molecular identity of iNs generated within distinct brain regions but via the same TF was shown to differ (Vignoles et al., 2019). For instance, Neurog2-iNs displayed a glutamatergic phenotype within the cortex following stab wound injury but displayed features of striatal projection neurons when reprogrammed within the striatum (Gascón et al., 2016; Grande et al., 2013; Vignoles et al., 2019). Although it has become clear that the reprogramming process is influenced by the starting cell type as well as by the local environment, such observations raise the question of how subtype specification is achieved and which role pro-neural TFs effectively play during cellular reprogramming, a crucial aspect, especially for cell-based replacement therapies (Bocchi et al., 2022). A recent study examined the timing and molecular makeup of NPCs and their neuronal progeny in the developing cortex. The study revealed that NPCs generate unique molecular profiles in a sequential manner, leading to diverse populations of neurons. These profiles are further shaped by signals from the environment that occur later in development (Telley et al., 2019). Therefore, while TFs play a crucial role in driving neuronal conversion, the specification of specific subtypes seems to be heavily influenced by both the innate reprogramming abilities of the source cells as well as external environmental cues. In order to advance neuronal

reprogramming towards an effective clinical strategy for cell-based regenerative medicine, there is a need to pinpoint specific instructive factors that can be used to more effectively control and direct the development of desired neuronal identities (Vignoles et al., 2019). To promote the acquisition of subtype identity, one could link the expression of proneural TFs, such as Neurog2, with other TFs. For instance, combined expression of Neurog2 and Nurr1 in astrocytes *in vivo* led to the generation of glutamatergic neurons with a specific layer identity and typical axonal projections to their intended target regions (Mattugini et al., 2019). Intriguingly, albeit multiple studies could obtain both unspecified as well as subtype-specific iNs through TF-mediated reprogramming, it is still not fully understood to which extent iNs molecularly resemble their endogenous counterpart (Amamoto and Arlotta, 2014). Moreover, it remains unclear to which extent iNs in fact need to resemble endogenous neurons in order to be able to restore lost function (Bocchi et al., 2022). Recently, it was shown that overexpression of Ascl1 and Dlx2 in hippocampal glia resulted in induced interneurons which could modulate circuit activity in an epileptic mouse model and reduce chronic seizure activity (Lentini et al., 2021). Intriguingly, the TFs induced a wide range of distinct interneuron subtypes, as identified by protein marker expression, however, a comprehensive characterization and comparison of their molecular identity as well as functional properties to matching interneuron subtypes was not performed (Lentini et al., 2021). Moreover, distinct brain regions may also possess distinct levels of plasticity that allow maturing induced neurons to functionally integrate (Turnley et al., 2014). Via cell transplantation studies of embryonic neurons into the adult neocortex, it could however be shown that maturing neurons can functionally integrate into the local environment, suggesting that the cerebral cortex may be also permissive for iN integration, given the acquisition of an adequate molecular identity (Falkner et al., 2016; Grade et al., 2022; Thomas et al., 2022). Importantly, multiple obstacles during glia-to-neuron reprogramming have yet to be overcome for successful clinical applications. For instance, one major hurdle is the restricted viability of iNs that has been, at least in part, attributed to differences in the metabolic state between astroglia and neurons (Bocchi et al., 2022; Gascón et al., 2016). Astroglia mainly rely on anaerobic glycolysis, while neurons depend on oxidative metabolism (Gascón et al., 2016). However, attempting to switch to neuronal oxidative metabolism during reprogramming may disturb the balance of redox homeostasis and generate reactive oxygen species (ROS), which can interfere with the reprogramming process. Indeed, a previous study has demonstrated that the presence of ROS, which induces ferroptosis, is a significant factor that hinders both the reprogramming process and the survival of iNs (Gascón et al., 2016). Through ectopic expression of anti-apoptotic genes along the reprogramming factor, such as Bcl2, which also counteracts ferroptosis, the authors could achieve an improved survival rate (Gascón et al., 2016). However, despite the achieved improvement, cell death remains a major

challenge at later time points and impairs the long-term survival of iNs (Amamoto and Arlotta, 2014; Turnley et al., 2014). The limited maturation that iNs could achieve so far presents a second hurdle to successful reprogramming, which may be compromised by limitations in their survival (Nehme et al., 2018). Nonetheless, the reason could also be attributed to an insufficient repression of the molecular identity of the starting cell, leading to cell-intrinsic homeostatic disturbances. For instance, when the first neurons were generated from fibroblasts *in vitro*, the reprogramming factors included Ascl1, Brn2 and Myt1l, a transcriptional repressor (Vierbuchen et al., 2010). The significance of Myt1l lies in suppressing genes that are typically expressed in non-neuronal cells (such as fibroblasts), Notch-related genes (like Hes1), proliferation effectors (such as Jak/Stat and Shh), and regulators of various non-neuronal processes, therefore enhancing the maturation of iNs (Mall et al., 2017; Vierbuchen et al., 2010). Moreover, a recent study could show that Myt1l expression facilitates neuronal maturation by repressing neuronal genes that are known to be specifically expressed during earlier developmental stages (J. Chen et al., 2022). On the other hand, insufficient access to target sites may also result in an incomplete reprogramming process. For instance, impaired Neurog2 binding to its target sites was shown to occur due to REST binding, which is known to suppress neuronal genes (Masserdotti et al., 2015). Correspondingly, the deletion of REST in astrocytes significantly increased Neurog2-mediated reprogramming efficiency due to gained accessibility to crucial downstream targets, such as NeuroD4 (Masserdotti et al., 2015). Therefore, overcoming repressive marks at essential neuronal gene loci represents a vital hurdle that needs to be addressed for optimized astrocyte-to-neuron conversion. Moreover, it is essential to understand the degree of alteration in the epigenetic profile needed to resemble that of a neuron, as well as to determine whether the reprogramming factors activate the neurogenic program while completely suppressing the original cellular identities, or if iN cells maintain some molecular "memories" of their original cell type (N. Yang et al., 2011). Finally, there are still uncertainties about whether subtype-specific iNs can be functionally integrated into the brain, in particular into pathological networks, when considering potential cell-replacement applications (Bocchi et al., 2022; Vignoles et al., 2019). Hence, a significant objective to achieve in the field will be to generate iNs that can effectively restore lost synaptic transmission and positively modulate the activity of pathological networks in which they are embedded, ultimately leading to correction of neurological deficits and functional recovery (Lentini et al., 2021; Tai et al., 2021; Vignoles et al., 2019).

1.3 NEURONAL ACTIVITY-DEPENDENT GENE REGULATION

The ability of neurons to respond to electrical signals with an adaptive regulation of gene transcription constitutes a *conditio sine qua non* for their maturation, survival, neuron-to-neuron communication and functional role within the entire circuit (Benito and Barco, 2015; West and Greenberg, 2011). Moreover, activity-dependent regulation of gene transcription allows the translation of transient synaptic activity into long-lasting neuronal circuit plasticity that effectively mediates cognitive functions such as learning or memory formation (S. M. Cohen et al., 2016). In addition, regulation of gene expression in neurons constitutes a clinically relevant aspect, as mutations in key regulators of activity-dependent transcription as well as an activity-dependent transcriptional dysregulation have been identified as early hallmarks of several congenital as well as degenerative neurological disorders (Ebert and Greenberg, 2013; España et al., 2010; Flavell and Greenberg, 2008; Roussos et al., 2016; Seredenina and Luthi-Carter, 2012).

1.3.1 *Activity-transcription coupling mechanism*

The activation of gene expression programs following synaptic activity resembles the cellular response program to various external stimuli, such as growth factors or mitogens (Leslie and Nedivi, 2011). In order to convert transient extracellular information, e.g. distinct temporal firing patterns of neurons, into persisting information in the brain, it is necessary to trigger long-lasting adaptations of neuronal structure and function (Tyssowski et al., 2018a). Such activity-dependent processes are initiated at the synapses: activation of membrane receptors initiates an intracellular signaling cascade towards the nucleus, leading to a bi-phasic transcriptional response (Leslie and Nedivi, 2011). The initial phase involves immediate early genes (IEGs), which are rapid-response genes that do not require protein synthesis for their expression. A large number of IEGs encode for TFs that trigger a secondary phase of the activity-dependent transcriptional program, leading to the expression of so-called delayed early genes, comprising downstream TFs and so-called 'effector molecules', that stably modify neuronal function, allowing adaptation to the specific stimulus (Leslie and Nedivi, 2011).

Initiation of gene expression following synaptic signaling

Following neurotransmitter reception, several ligand- and voltage-gated calcium channels in the postsynaptic neuron set in motion a calcium flux across the plasma membrane, leading to an elevation of intracellular calcium concentration. Such a rise in intracellular calcium concentration constitutes a fundamental component of signaling pathways that ultimately lead to functional consequences such as activity-dependent neuronal survival

and synaptic plasticity mechanisms (Bito et al., 1997; West et al., 2001). Two main receptor classes have been identified that allow calcium influx and hence participate in activity-dependent gene transcription: *N*-methyl-D-aspartate (NMDA)-type glutamate receptors (NMDAR) as well as L-type voltage-gated calcium channels (L-VGCC) (West and Greenberg, 2011). Interestingly, not only distinct temporal firing patterns but also e.g. the specific entry points of calcium have been associated with the activation of distinct downstream intracellular signaling pathways that result in the upregulation of confined subsets of activity-dependent gene programs (Bading et al., 1993; Tyssowski et al., 2018a). Intracellularly, calcium-binding proteins, of which the most prominent representative is calmodulin, bind to calcium in response to elevated levels. This interaction initiates a change in conformation and allows calmodulin to translocate to the nucleus and mostly activate kinases of the calcium-calmodulin-dependent protein kinases (CaMK) pathways (Madabhushi and Kim, 2018). CaMKs, especially CaMKII and CaMKIV, are well established as key regulators of neuronal activity-dependent calcium signaling, however, other signaling pathways have been shown to be involved in activity-dependent induction of gene expression as well. For instance, in response to strong neuronal activation, calmodulin may also activate the Ras/mitogen-activated protein kinases (MAPK) pathway, which in turn can then phosphorylate downstream TFs and transcriptional coregulators (Benito and Barco, 2015; Madabhushi and Kim, 2018; West and Greenberg, 2011). Moreover, calmodulin has been shown to activate the phosphatase calcineurin in response to neuronal activation in order to target a notable set of TFs that will be discussed further below (Madabhushi and Kim, 2018; West and Greenberg, 2011). These signaling pathways eventually converge on a set of constitutively expressed TFs that will be activated via phosphorylation and, consequently, orchestrate the initial transcriptional response via IEG induction following synaptic stimulation. The calcium/cAMP-response element binding protein (CREB), the serum response factor (SRF), myocyte enhancer factor 2 (Mef2) or MeCP2 are among the well-characterized key transcriptional regulators activated by CaMKs (Bito et al., 1997; Clapham, 2007). Due to their constitutive expression, the activation of these TFs relies on their capacity to integrate and discriminate signals from various calcium-dependent pathways in order to subsequently undergo post-translational modifications, like phosphorylation, resulting in their activation and subsequent IEG induction (Yap and Greenberg, 2018). Interestingly, different kinases mediate the phosphorylation of different TFs. For example, while MeCP2 is phosphorylated by CaMKII, but not by CamKIV in response to activity, several distinct CaMKs were shown to drive the phosphorylation of CREB (Buchthal et al., 2012; G. Y. Wu et al., 2001). This suggests not only a possible focal point of distinct signaling cascades and highlights the well-established importance of CREB for neuronal functioning but also emphasizes the dynamic complexity of information processing that

leads to highly specific induction of gene expression programs in response to distinct activity patterns. Once activated, these (constitutively expressed) TFs initiate expression of numerous IEGs, such as Fos, Npas4 or Egr1, which lead to the expression of a myriad of effector molecules that have just recently been confirmed via genome-wide analysis (Hrvatin et al., 2018; Spiegel et al., 2014). These TFs directly modulate various aspects of synaptic connectivity and functionality by initiating local changes at the synapses. These changes include e.g. increased surface expression or internalization of glutamate receptors, local mRNA translation as well as post-translational modifications of synapse-related proteins, allowing neurons to effectively respond to external stimuli (Flavell and Greenberg, 2008; Yap and Greenberg, 2018). Once induced, IEG expression is rapidly suppressed. Recently, it has been suggested that the nucleosome remodeling and deacetylase complex (NuRD) plays a significant role in this process by inducing changes in the histone composition that leads to suppression of activity-induced transcription (Y. Yang et al., 2016; Yap and Greenberg, 2018). Despite their rapid shutoff, IEGs result in long-term 'information storage' by inducing stable changes to synaptic connectivity (Yap and Greenberg, 2018). Moreover, neuronal activity itself was shown to induce an epigenetic 'memory' by modifications of cytosine methylations across activity-inducible gene sites, such as Bdnf or Arc, resulting in a persistent change of the neuronal gene expression profile (Bird, 2002; Lubin et al., 2008; Yap and Greenberg, 2018). Intriguingly, an increased extent of cytosine methylation could be detected during critical periods of cortical development and displayed a neuronal subtype-specific pattern (Luo et al., 2017). Activity-dependent gene regulation constitutes therefore not only a crucial mediator of synaptic plasticity in the adult brain that establishes long-lasting, experience-dependent adaptations within neuronal circuits, but it also shapes neuronal development and circuit assembly in the developing brain (Abe, 2008; E. J. Hong et al., 2008).

Immediate early genes: pioneer signals for long-term adaptations of neuronal function

In 1984, Greenberg and Ziff discovered the stimulus-specific induction of the IEG c-Fos and were the first to describe that cells have the ability to respond to their environment through gene transcription taking place within minutes following stimulation (Greenberg and Ziff Edward B, 1984; Yap and Greenberg, 2018). IEGs are characterized by a low basal expression level and a rapid, protein-synthesis-independent transcriptional upregulation (Leslie and Nedivi, 2011; Yap and Greenberg, 2018). Many IEGs, such as c-Fos, Npas4, BDNF, Narp, Homer1a, Arc, and Cpg2 induce circuit plasticity via various modifications at the synapse (Leslie and Nedivi, 2011). Neuronal activity-dependent transcription is therefore finely regulated in order to maintain stable circuit activity while enabling transcriptional responses of activated neurons. Low basal expression levels of IEGs in the absence of neuronal activity is maintained by the bHLH TF Arnt2, which recruits the

NCoR2 repressor complex in order to suppress activity-sensitive regulatory elements of target genes (Sharma et al., 2019). Conversely, during increased synaptic excitation, Arnt2 forms a heterodimer with the neuron-specific and selectively activity-inducible bHLH-PAS TF Npas4 instead and induces activity-sensitive regulatory elements, resulting in gene transcription (Sharma et al., 2019; Sun et al., 2016). Today, the IEG c-Fos continues to be widely used as a canonical IEG for identifying recently activated neurons (Jaeger et al., 2018; Lacar et al., 2016). Following translation, c-Fos translocates to the nucleus and forms a dimer with the IEG and TF Jun (Malik et al., 2014). Recent genome-wide studies focused on TF binding sites have shown that the Fos/Jun heterodimer (also called AP-1 complex) then initiates transcription of late-response genes (LRGs) by primarily binding to enhancer elements of target genes and therefore drives cell-type specific activity-dependent gene expression (Malik et al., 2014). Interestingly, the TFs Fosb, Fosl1, Fosl2 as well as Junb and Jund are other potential components of the AP-1 complex that can replace Fos or Jun, respectively, albeit neither their functional roles nor the degree of redundancy in the constitution of AP-1 is understood yet (Yap and Greenberg, 2018). A vast number of LRGs have been classified as 'effector molecules' that fulfill a variety of functions such as promoting dendritic growth, facilitating spine maturation and contributing to synapse assembly in order to regulate the balance of neuronal excitation and inhibition, hence affecting circuit activity and neuronal plasticity (Yap and Greenberg, 2018). Moreover, recent technological advancements enabled the detection of the genome-wide activity-dependent gene program in response to diverse stimulations and identified several hundreds of genes, that have yet to be functionally characterized (Hrvatin et al., 2018; Schaukowitch et al., 2017; Spiegel et al., 2014). To add further complexity, dissecting the functional roles of specific TFs or gene programs induced by selective IEGs via gene knockouts has been complicated due to high functional redundancies of activity-dependent TFs (Yap and Greenberg, 2018).

Cell-type specific activity-dependent transcriptome

Early studies focusing on the AP-1 complex have provided the first evidence of the cell-type specificity of activity-dependent gene transcription by highlighting that AP-1 binds to selective enhancer sequences instead of, as previously thought, to gene target promoters (Eferl and Wagner, 2003). Intriguingly, while extracellular stimuli activate the AP-1 complex in a high number of diverse cell types, AP-1 was shown to interact with lineage-determining TFs, and by recruiting the BAF complex, induces nucleosome remodeling in order to establish a cell-type specific accessible chromatin landscape of enhancer sequences, albeit the mechanisms by which enhancer sites in distinct cell types are selected are not yet understood (Malik et al., 2014; Vierbuchen et al., 2017). Intriguingly, motif analyses of TFs interacting with AP-1 in neuronal subtypes revealed

the presence of the bHLH sequence (Vierbuchen et al., 2017). In sum, these findings suggest that AP-1 drives the targeted selection of a cell-type specific enhancer collection and hence may determine the specificity of stimulus-dependent gene expression in the respective cell type (Yap and Greenberg, 2018). Recently, an increasing number of studies have provided evidence that the activity-dependent transcriptome is highly neuronal subtype-specific, both *in vitro* (Spiegel et al., 2014) as well as *in vivo* (Mardinly et al., 2016). Interestingly, *in vitro* work has shown that, albeit shortly after stimulation of excitatory as well as inhibitory neurons, both populations display largely similar sets of IEGs; however, prolonged time following stimulation shows expression of distinct gene programs (Spiegel et al., 2014). *In vivo* work additionally uncovered that sensory experience induces a gene program in VIP-expressing interneurons of the visual cortex that is detected neither in excitatory neurons nor, more interestingly, in other interneuron subtypes, such as SST- or PV-expressing interneurons and further supports the finding of neuronal subtype-specific transcriptional responsiveness to activity (Mardinly et al., 2016). More recent *in vivo* work provided a more comprehensive understanding of the diversity of activity-dependent transcription by performing scRNA-sequencing of the whole visual cortex following light stimulation (Hrvatin et al., 2018). The authors identified 30 molecularly distinct cell types and could attribute stimulus-specific transcriptional responses to each of them (Hrvatin et al., 2018). Moreover, excitatory neurons of distinct cortical layers displayed heterogeneous transcriptional programs. Finally, these studies revealed stimulation-specific transcriptional dynamics in non-neuronal cells, e.g. astrocytes, microglia as well as oligodendrocytes (Hrvatin et al., 2018; Spiegel et al., 2014), which could further impact neuronal function and circuitry via stimulus-specific secretion of neurotrophins. The characterization of cell-type-specific activity-dependent gene programs has significant implications not only for the functional diversity of neuronal subtypes and understanding of dysregulated cortical function due to developmental disorders but also leads to the question of the mechanisms by which this diversity of transcriptional responses is established. The TF and IEG Npas4 has been shown to play a critical role in inducing neuronal subtype-specific gene programs in response to activity modulations. Intriguingly, while Npas4 expression is induced in both, excitatory as well as inhibitory neurons, following stimulation, it induces distinct gene programs of LRGs in these neuronal populations (Spiegel et al., 2014; Sun et al., 2016). Moreover, the authors could show that while these LRGs facilitate synaptic inhibition onto excitatory neurons, they, in turn, facilitate excitation onto inhibitory neurons and hence contribute to subtype-specific synaptic activity that may aim for homeostatic circuit activity (Spiegel et al., 2014; Sun et al., 2016).

1.4 SYNAPTIC PLASTICITY

The term synaptic plasticity specifically describes the activity-dependent adaptation of the strength and transmission efficacy of individual synapses or at the network level (Citri and Malenka, 2007). Two parameters regulate synaptic efficacy: the probability of action potential-dependent exocytosis of synaptic vesicles and hence neurotransmitter release from the presynaptic neuron and the density of available postsynaptic receptors for binding the neurotransmitter at the postsynaptic neuron (Lisman et al., 2012; Vitureira and Goda, 2013). When occurring at different time scales, changes to these two parameters can induce distinct forms of synaptic plasticity (Abbott and Nelson, 2000; Lisman et al., 2012; Vitureira and Goda, 2013). In fact, multiple distinct forms of synaptic plasticity mechanisms have been identified to contribute to the dynamic and adaptive regulation of neuronal circuit connectivity and function (Citri and Malenka, 2007). These mechanisms have been directly linked to cognitive functions such as learning or memory formation (Kandel, 2001). In general, one can distinguish two broad types of plasticity mechanisms that play an essential role in adjusting synaptic strength: Hebbian and non-Hebbian mechanisms (Fox and Stryker, 2017).

1.4.1 *Hebbian synaptic plasticity*

Hebbian plasticity is an extensively studied neuronal mechanism that has been identified as the main coupling between neurophysiology and cognitive processes or memory formation (Langille and Brown, 2018). Hebbian plasticity is synapse-specific and naturally rapidly induced. Adjustment of synaptic strength is restricted to already active synapses and therefore referred to as input-specific (Vitureira and Goda, 2013). Induction of this mechanism requires correlated action potential firing of the pre- as well as postsynaptic neuron resulting in a corresponding long-term change in synaptic strength that may last hours to months (Vitureira and Goda, 2013). Synapse efficiency can be either strengthened, resulting in long-term potentiation (LTP), or reduced, hence leading to long-term depression (LTD) (Lüscher and Malenka, 2012). At most types of synapses, these changes are mediated by the activation of NMDARs, therefore, both pre- and postsynaptic neurons are required to be simultaneously active; the postsynaptic neuron is required to be depolarized in order to remove the Mg^{2+} block of NMDARs while simultaneously being stimulated (*"Neurons that fire together, wire together."*- Donald Hebb, 1949) (Henley and Wilkinson, 2013; Lüscher and Malenka, 2012). Subsequently, the immense amount of calcium influx through NMDARs activates intracellular signaling pathways that lead to long-term alterations of synaptic efficacy via rapid recruitment of additional AMPAR into the postsynaptic membrane (Lüscher and Malenka, 2012).

Predictably, alterations in synaptic strength are correlated with structural plasticity, which ultimately results in long-term modification of the circuitry (Nägerl et al., 2004; Vitureira and Goda, 2013). For instance, synaptic efficacy has been shown to correlate with spine head size (Engert and Bonhoeffer, 1999; Matsuzaki et al., 2004; Vitureira and Goda, 2013). Moreover, modulation of the actin cytoskeleton dynamics can initiate cytoarchitectural changes leading to the formation of new synapses (Matsuzaki et al., 2004), processes that require the synthesis of new proteins. The fact that synapses in close proximity can independently be either strengthened (LTP) or weakened (LTD) constitutes a distinctive characteristic of Hebbian plasticity (Bliss and Cooke, 2011; Dudek and Bear, 1992). Most importantly, Hebbian plasticity is generally considered as a 'positive feedback' mechanism (Fox and Stryker, 2017): once synapses are potentiated or depressed, it becomes either easier or more demanding (*'sliding threshold'*) to undergo excitation. Ultimately, this may lead to synapses with either maximal (LTP) or minimal (LTD) strengths that produce an unstable and inflexible neuronal network (Fox and Stryker, 2017; G. G. Turrigiano, 1999; Vitureira and Goda, 2013). Yet, the brain seems to possess the tools that allow the flexibility needed to undergo learning or memory formation while employing stabilizing mechanisms that maintain overall network function. How is this achieved?

1.4.2 *Homeostatic synaptic plasticity*

> "[...] somehow the unstable stuff of which we are composed has learned the trick of maintaining stability."
>
> *Walter Cannon, The Wisdom of the Body, 1932*

Not even 20 years after the first experimental evidence of Hebbian plasticity, studies have been focusing on understanding the constraint mechanisms at play (LeMasson et al., 1993). Indeed, early studies reported that cultured cortical neurons display the ability to regulate their intrinsic excitability in response to changing synaptic input in order to maintain stable firing frequencies (G. Turrigiano et al., 1994). When subjected to 48 hours of activity inhibition, neurons displayed a striking increase in mEPSC amplitudes after removal of inhibitors (see Figure 1.5) (G. G. Turrigiano et al., 1998). This effect was observed bidirectionally: when subjected to blockage of GABA-mediated network inhibition, excitatory firing rates initially increased, but decreased back to control levels within 48 hours (G. G. Turrigiano et al., 1998). Since then, multiple studies described such 'negative feedback' mechanisms that counteract excessive excitation or inhibition and maintain the stability of network activity by adjusting overall synaptic strengths (G. W. Davis, 2006; Fox and Stryker, 2017; Pozo and Goda, 2010; G. G. Turrigiano, 2008). Such

stabilizing mechanisms have been collectively termed homeostatic synaptic plasticity (HSP) (Heir and Stellwagen, 2020; G. Turrigiano, 2012). HSP usually affects the neuronal network on a global level but has also been described to occur on single neurons (Vitureira and Goda, 2013). In both cases, HSP leads to equal 'scaling' of all synapses and can therefore preserve relative differences in synaptic strengths that e.g. may have resulted from Hebbian plasticity (Galanis and Vlachos, 2020; Vitureira and Goda, 2013). Although the connection between Hebbian and HSP has been extensively described (Galanis and Vlachos, 2020; Vitureira and Goda, 2013), the underlying molecular mechanisms and distinct forms of HSP have been mostly studied independent of Hebbian plasticity (G. G. Turrigiano, 2008; Vitureira and Goda, 2013). A characteristic of HSP is the duration of activity modulation that is required for the homeostatic process to kick in. First, a minimum of several hours of altered activity levels are necessary to induce HSP, and second, the compensatory cellular changes require again several hours in order to occur in a cumulative fashion (G. G. Turrigiano and Nelson, 2004). These slow dynamics have been described as essential to the process of maintaining network stability: if HSP occurred more rapidly, it may interfere with Hebbian plasticity dynamics or even alter activity fluctuations that are necessary for information transmission (G. G. Turrigiano and Nelson, 2004).

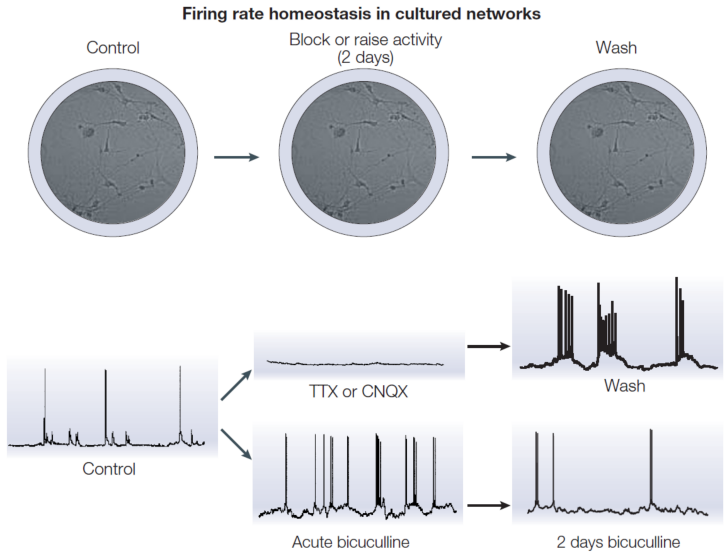

Figure 1.5: **Cultured cortical neurons display firing rate homeostasis following activity manipulation.** Cortical neuronal cultures are composed of excitatory pyramidal and inhibitory interneurons. Neurons develop spontaneous activity *in vitro* that can be pharmacologically manipulated. For instance, inhibition of activity by the sodium channel blocker TTX or the AMPAR inhibitor CNQX results in a compensatory increase in firing frequency. Conversely, blockage of GABA-mediated network inhibition by Bicuculline application results in an immediate increase in activity that settles back to control levels within a short time. Figure taken from G. G. Turrigiano and Nelson, 2004.

Intriguingly, the precise mechanisms that induce HSP as well as the intracellular signalling pathways underlying the scaling processes could not yet be deciphered, mostly due to the prolonged time scales in which the process is induced (G. G. Turrigiano and Nelson, 2004). Therefore, it remains unclear whether e.g. the induction of HSP requires pre- as well as postsynaptic changes in activity or if it is a cell-autonomous process. HSP has also been described *in vivo*, where manipulations of cortical activity are achieved by e.g. intraocular injection of TTX or through visual deprivation, such as dark-rearing or retinal lesions. These manipulations have been widely shown to result in increased mEPSC amplitudes, spine sizes and recruitment of AMPAR in excitatory synapses in the visual cortex (Keck et al., 2013; H. K. Lee and Kirkwood, 2019; Pozo and Goda, 2010; Rodriguez et al., 2019; Sanderson et al., 2018; Whitt et al., 2014). However, differences in the mechanisms of induced HSP have been described depending on the manipulations performed (Pozo and Goda, 2010). Intriguingly, contrasting results regarding compensatory plasticity have been described when altering cortical activity. For instance, studies employing eyelid suture did not result in a compensatory increase of network activity in the visual cortex, suggesting that the same circuit may employ distinct HSP mechanisms in order to compensate for sensory deprivation (H. K. Lee and Kirkwood, 2019; Maffei and Turrigiano, 2008; Tien and Kerschensteiner, 2018). These observations were backed up by similarly conflicting observations in other systems, such as the barrel cortex (Bender et al., 2006; Chung et al., 2017; Inquimbert et al., 2012; H. K. Lee and Kirkwood, 2019; Yu et al., 2012). It has therefore been suggested that such different observations reflect differences in the intensity of activity changes that were induced via distinct sensory deprivations (H. K. Lee and Kirkwood, 2019). Assessing HSP *in vivo* may be particularly challenging, not only due to the high diversity of input activity patterns on the investigated neuronal network but also due to the high degree of interconnectivity between neuronal subnetworks (H. K. Lee and Kirkwood, 2019). Moreover, how these modifications at the synapse level translate into changes in higher-order network structure is not yet fully understood. Given the little consistency between observations regarding HSP mechanisms derived from available *in vivo* studies, it has therefore been suggested that 'input-specific' HSP mechanisms may fit the *in vivo* context better rather than a global scaling mechanism (H. K. Lee and Kirkwood, 2019). Additional work is required in order to clarify the nature of the events triggering plasticity mechanisms as well as dictating influences within defined (cortical) subnetworks following activity alterations. Nonetheless, alterations in HSP responses have been detected in neurological disorders, such as Alzheimer's disease or autism disorder (Heavner et al., 2021; Jang and Chung, 2016). In Alzheimer's disease, accumulation of β-amyloid was shown to increase intrinsic excitability, leading to sustained synaptic downscaling which ultimately counteracts LTP mechanisms and manifests itself clinically

in memory impairments (Jang and Chung, 2016). Moreover, HSP mechanisms are indispensable for the proper development of maturing cortical circuits (G. G. Turrigiano and Nelson, 2004; Wen and Turrigiano, 2021). Developing neuronal circuits require a high level of synaptic plasticity as they undergo constant changes in their connectivity, albeit it is not yet understood which precise plasticity mechanisms are at play during distinct phases of circuit development.

Molecular mechanisms mediating homeostatic synaptic plasticity

Although Hebbian and HSP have been studied so far independently of each other, several studies suggest that they may share similar molecular mechanisms to functionally modulate the same set of effector proteins at the synapse (Fernandes and Carvalho, 2016). In fact, multiple molecules that are known to mediate Hebbian plasticity were also shown to be crucial players in the regulation of HSP (Arendt et al., 2013; Fernandes and Carvalho, 2016; Pozo and Goda, 2010). Following alterations in network activity levels, neurons are able to induce compensatory mechanisms that allow homeostatic control of either presynaptic neurotransmitter release, postsynaptic neurotransmitter receptor expression, or their intrinsic excitability (Fernandes and Carvalho, 2016; G. G. Turrigiano, 2017). Which precise mechanism is initiated has been shown to be dependent on the developmental stage and subtype (Wen and Turrigiano, 2021). For instance, neuronal intrinsic excitability can be adjusted to altered activity levels in order to increase neuronal sensitivity to existing activity levels. This process depends on the developmentally-regulated expression of voltage-gated ion channels (e.g. Na^+, K^+ and Ca^{2+}) and results in adjusted firing frequency in response to changed network activity levels (Fernandes and Carvalho, 2016). Although HSP mechanisms occur in both inhibitory as well as excitatory neurons, it has been so far best studied in the latter neuronal population (Kilman et al., 2002; Rannals and Kapur, 2011). In excitatory neurons, it is expressed via bidirectional alterations of glutamate receptors in order to maintain firing rates within a functional range, leading to a homeostatic regulation of synaptic strength and therefore generally referred to as synaptic scaling (G. G. Turrigiano, 2017). HSP comprises two main scaling processes that allow neurons to adjust their synaptic strength to persistently change network activity levels (G. G. Turrigiano, 2017). On the one hand, synaptic downscaling reduces synaptic efficacy in response to increased network activity, while synaptic upscaling increases synaptic efficacy in response to decreased network activity (G. G. Turrigiano, 2017). The most commonly employed approach to induce and study these two forms of HSP *in vitro* is the pharmacological induction of increased global synaptic activity or its inhibition in neuronal cultures, either via application of the $GABA_A$-receptor antagonist bicuculline or sodium channel blocker TTX, respectively (see Figure 1.5) (G. G. Turrigiano, 2008; Vitureira and Goda, 2013). As

discussed above, the resulting effect at excitatory synapses is a global 'scaling' process that enables a compensatory decrease or increase in firing rates. Intracellular calcium levels have been shown to serve as the main signal for changed activity levels. For instance, reduced calcium influx and subsequently reduced activation of CaMKIV were shown to induce synaptic scaling via transcriptional upregulation (Ibata et al., 2008). It is now well established that scaling processes, which occur in a cumulative manner, require transcriptional regulation (E. B. Han and Stevens, 2009; Ibata et al., 2008) as well as protein synthesis even during early stages (Dörrbaum et al., 2020; Pozo and Goda, 2010). At the molecular level, synaptic scaling is predominantly driven by activity-dependent adjustments of the number and properties of postsynaptic AMPAR (Heavner et al., 2021; G. Turrigiano, 2011). AMPARs belong to the glutamate receptor (GluR) family of ligand-gated ion channels and consist of four subunits (GluA1-4) and mediate the majority of excitatory transmission, hence constituting a central molecular complex underlying synaptic plasticity (Bissen et al., 2019; Henley and Wilkinson, 2013). Synaptic downscaling is achieved by internalization of AMPARs, while upscaling is mediated via increased AMPAR surface expression (Jeans et al., 2017; G. Turrigiano, 2012; G. G. Turrigiano, 2017). Interestingly, multiple distinct molecules are involved in the regulation of AMPAR trafficking to or from the synapse in order to promote synaptic scaling in the appropriate direction. In fact, maintaining a basal synaptic strength while enabling plasticity requires an intricate regulation of constant receptor trafficking that is achieved by scaffold as well as cell-adhesion molecules, soluble factors as well as transcriptional or translational regulators (Fernandes and Carvalho, 2016). Members of the AMPAR-associated regulatory protein family (TARPs) play an essential role in this process. For instance, it was shown that the TARP Stargazin directly interacts with the postsynaptic scaffold protein PSD-95 following phosphorylation in order to increase AMPAR stability at the postsynaptic density (PSD) (Bats et al., 2013; Payne, 2008). The importance of stargazin was further demonstrated by a study that over-expressed a phosphomutant version of the protein, which resulted in the complete abolishment of synaptic upscaling following neuronal inhibition (Louros et al., 2014). Other postsynaptic proteins, such as the glutamate receptor-interacting protein (GRIP) GRIP1 and the protein interacting with C kinase (PICK1) directly interact with the GluA2 subunit of AMPARs (Jaafari et al., 2012). GRIP1 has been shown to be necessary in promoting AMPAR insertion into the membrane following neuronal silencing, while not participating in AMPAR internalization following increased activity (Bissen et al., 2019). Interestingly, PICK1 on the other hand is a crucial mediator of AMPAR endocytosis during LTD (Bissen et al., 2019). Intriguingly, activity inhibition results in reduced PICK1 expression and, using a PICK1 knock-out mouse model, it could be shown that while it is a relevant component for synaptic upscaling, the protein is not involved in the downscaling process despite its suitable role (Anggono

et al., 2011). In turn, clathrin-mediated endocytosis of AMPARs during downscaling has been shown to be mediated by Eph receptors (Bissen et al., 2019). Another protein that plays a significant role in AMPAR trafficking is the protein Arc (*Activity-regulated, cytoskeleton-associated protein*), which encodes a protein that belongs to the group of IEGs and is therefore induced following increased neuronal activity and quickly accumulates at synapses (Penrod et al., 2019). It displays the closest homology to α-spectrin and is known as a master regulator of synaptic function as well as plasticity (Béïque et al., 2011; Leung et al., 2019; Penrod et al., 2019). Interestingly, Arc was shown to directly interact with the endocytosis machinery in order to promote AMPAR internalization in an activity-dependent manner (Shepherd and Bear, 2011). Changes in the number of AMPAR at the synapse effectively result in altered AMPAR-mediated mEPSCs (Goel et al., 2011; O'Brien et al., 1998). The significance of Arc in synaptic upscaling could be demonstrated in an *in vivo* study, in which visual stimulation following a period of visual deprivation induced significant upscaling assessed via increased mEPCs amplitudes in L2/3 pyramidal neurons, concomitant with the upregulation of Arc in the visual cortex (Gao et al., 2010). Intriguingly, when using an Arc knock-out mouse, the same experimental paradigm did not result in increased mEPSCs amplitudes, highlighting the critical role of Arc for HSP (Gao et al., 2010). Moreover, AMPAR subunit composition has been shown to impact neuronal activity levels. For instance, pharmacological induction of synaptic scaling processes both *in vitro* as well as *in vivo* has been shown to be mediated via selective increase in GluA1-containing AMPAR at the PSD, possibly due to their increased Ca^{2+}-permeability facilitating upscaling of mEPSC amplitudes (Cull-Candy et al., 2006; Goel et al., 2011). Finally, other forms of modulating AMPAR function involve for instance the modification of accessible AMPAR binding sites by expansion or retraction of the postsynaptic density (PSD) (G. G. Turrigiano, 2017). Albeit a vast number of relevant molecular players in synaptic scaling have been already characterized, mostly by single gene knock-out studies, recent genome- and proteome-wide studies are beginning to reveal the full set of molecules that are involved in HSP processes that will allow a better understanding of the underlying mechanisms (Dörrbaum et al., 2020; Jaeger et al., 2018; Schaukowitch et al., 2017). Future experiments will be needed in order to address the interplay and interdependency between Hebbian and HSP.

2

AIM OF THE STUDY

After embryonic development, the cerebral cortex loses its ability to generate new neurons, giving it no possibility of replacing neurons lost to injury or degenerative processes. Consequently, cell-based replacement therapies offer an opportunity to generate neurons from other cellular sources. One approach focuses on direct cellular reprogramming through the expression of specific transcription factors in order to convert specialized cells, such as astroglia, into neurons. Astroglia present an excellent source for neuronal reprogramming since they are found throughout the brain, respond to neuronal injury and can self-renew their population. Moreover, due to their close lineage proximity to neurons, multiple previous studies showed success in generating functional excitatory neurons. However, whether induced neurons acquire the ability to undergo network activity-dependent gene regulation is yet unclear. This project aims to assess the authenticity of astroglia-derived induced glutamatergic neurons by comparing them to endogenous cortical neurons at a molecular level, with a focus on their ability to undergo activity-dependent gene regulation. This information is crucial in understanding how successfully induced neurons integrate into a neuronal network and eventually take over lost function.

To achieve this, the project was divided into the following main objectives:

- Characterize and compare the molecular profiles of astroglia-derived induced neurons and endogenous neurons using single-cell RNA-sequencing analysis.
- Assess the activity-dependent transcriptional responsiveness of induced neurons and compare it to that of endogenous neurons following pharmacological network activity modulation.

3

METHODS

3.1 ANIMALS

All experimental procedures were performed in compliance with governmental and ethical specifications provided by our institution. Wild-type C57BL/6J timed-pregnant females (Janvier labs, Le Genest-Saint-Isle, France) were used for experiments requiring embryonic (E) mouse primary cultures. For primary astrocyte cultures, wild-type C57BL/6J postnatal (P) 5-7 littermates were used from own breedings. Mice were maintained in a 12-hour light/dark cycle and food and water were available *ad libitum*.

3.2 CELL CULTURE

3.2.1 *Embryonic cortical neuronal culture*

Primary neurons were grown on PDL/laminin-coated surfaces. One day prior to culture preparation, the coating of the growth surface was initiated, to ensure the successful adhesion of freshly seeded neurons. The surface of either glass coverslips or tissue culture plates was first coated with Poly-D-Lysine (PDL) (coating solution I, see Table 4) and incubated overnight at 37°C. The next day, the coating solution was aspirated and wells were washed three times with dH_2O. The surfaces were then coated with Laminin (coating solution II, see Table 4) and plates were incubated for 4 hours at 37°C. Laminin constitutes a main component of the extracellular matrix (*source:* Engelbreth-Holm-Swarm murine sarcoma basement membrane) that has been shown to significantly improve the attachment of primary cells onto glass coverslips. The synthetic polymer PDL serves mainly as a link between Laminin molecules and the glass or plastic surface. Right before the seeding of cells, the coating solution II was aspirated and the wells were washed three times with H_2O. Dissociated neuronal cultures were prepared from cortices of 14.5-day-old embryonic wild-type C57BL/6J mice (E14.5). At this stage, neurogenesis is already ongoing (E10.5 through E18.5), with deep-layer neurons being present and an ongoing transition towards the production of mid- and upper-layer neurons. Briefly, a timed pregnant female mouse was deeply anesthetized by Isofluran-Piramal and sacrificed by cervical dislocation. The abdominal cavity was opened and the uterus, containing the embryos, was removed and placed into a 10 cm dish containing ice-cold

1x Hanks' Balanced Salt Solution (HBSS). After careful removal of the embryos from the placenta and the amniotic sac, they were placed into ice-cold 1x HBSS. The following steps were performed under a laminar flow hood using a dissection stereo microscope. First, the embryo's head skin layers and soft skull tissue were removed so that the brain could be extracted from the skull and placed into a new dish with ice-cold 1x HBSS. The two hemispheres of each brain were separated along the longitudinal fissure and the meninges were carefully peeled away from each hemisphere. Ventral (ganglionic eminences) and medial structures were removed from each hemisphere. The cleaned cortices were collected in a 15 ml tube containing ice-cold HBSS. The solution was then aspirated and the tissue was resuspended in 0.05 % Trypsin-EDTA solution (see Table 4) with the addition of DNase I and incubated for 15 min at 37°C. Following incubation, the trypsin was blocked by adding Dulbecco's Modified Eagle's Medium (DMEM) containing 10 % FBS and the suspension was centrifuged for 5 min at 120 g. The solution was aspirated and the tissue pellet was resuspended in 1 ml of neuronal maintenance medium with careful mechanical dissociation until a single-cell solution was obtained. Cell concentration was assessed by preparing a 1:1 solution of the cell suspension mixed with Trypan Blue and subsequent manual counting using a hemocytometer. The cell suspension was then diluted in an appropriate volume of neuronal maintenance medium and plated into coated tissue culture plates with a density of approximately 550 cells / mm^2. Cells were maintained in an incubator at 37 °C with humidified air containing 5% CO_2. Five days after the culture preparation, cells were treated with 500 nM of the mitotic inhibitor cytosine-d-arabinofuranoside (AraC) in order to purify the neuronal culture from proliferating cell types. From then on, every second day, one-fifth of the medium volume was replaced with fresh neuronal maintenance medium (see Table 4).

3.2.2 *Postnatal cortical astrocyte culture*

A thorough protocol on how to prepare and maintain the astrocyte cultures for reprogramming purposes has been adapted from a previously published protocol (Heinrich et al., 2011, Sharif et al., 2021).
Postnatal cortical astrocytes were isolated and expanded from cortices of P5 to P7 days-old C57Bl6/J mice. In brief, mice were decapitated and the brains were removed from their skull and transferred into ice-cold 1x HBSS. The following steps were performed under a laminar flow hood using a dissection stereo microscope. First, the brain regions caudal to the forebrain were removed by a cut at the level of the transverse fissure. Next, the most anterior part of the forebrain was removed by a coronal cut at the level of the optic chiasm. The two hemispheres were separated along the longitudinal fissure and hippocampal, diencephalic and midbrain structures were removed. Next, meninges

were removed and cortices were thoroughly cleaned from developing white matter. The cortical structures were then collected in 1x HBSS. Under a sterile laminar flow hood, the cortices were mechanically dissociated using a glass Pasteur pipette. The homogenized tissue was centrifuged at 120 g for 5 min at RT. The supernatant was carefully removed and cells were resuspended in astrocyte medium (see Table 4). Cells were maintained in T25 flasks and expanded for 5-7 days in an incubator at 37 °C with humidified air containing 5 % CO_2.

Passage of expanded astrocytes

Astrocytes were passaged when they reached 70-80% confluence, usually 5 to 7 days after culture preparation. One day prior to passaging, glass coverslips were distributed onto 24-multiwell plates and incubated in coating solution I for 4 hours at 37 °C after which the coating solution was aspirated and coverslips were washed 3x with 1x PBS and left to dry overnight. For passaging, astrocytes were first washed with 1x PBS and incubated in trypsin solution for 5 min at 37 °C. Trypsin was then inhibited by adding astrocyte medium (see Table 4). The cell suspension was collected and centrifuged at 120 g for 5 min at RT. The obtained cell pellet was thoroughly resuspended in 1 ml of astrocyte medium. Cell concentration was assessed by preparing a 1:1 solution of the cell suspension mixed with Trypan Blue and counted using a hemocytometer. The cell suspension was then diluted in the appropriate volume of astrocyte medium and plated into coated 24-multiwell tissue culture plates. Into each well, 5 x 10^4 to 8 x 10^4 cells were seeded. Cells were maintained in an incubator at 37 °C with humidified air containing 5% CO_2.

3.2.3 *A coculture system of induced and endogenous neuronal cells*

In this work, an *in vitro* co-culture system was established that allows investigating the integration of induced neurons into a mature endogenous neuronal network as well as a comparative analysis of their physiological responses to network activity manipulations. To this end, astrocytes were transduced 24 hours before the co-culture setup. The next day, astrocytes were washed with 1x PBS and trypsinized for 5 min at 37°. After detachment of the cells, trypsin was inhibited via the addition of astrocyte medium, the cell suspension was then collected and centrifuged at 120 g for 5 min. The supernatant was aspirated and astrocytes were resuspended in neuronal maintenance medium. The number of cells in the cell suspension was determined using a hemocytometer and 25.000 cells were plated onto 100.000 neurons per coverslip (ratio 1:4). Cells were maintained in an incubator at 37 °C with humidified air containing 5% CO_2. Every second day, one-fifth of

the medium volume was replaced with fresh medium which was supplemented with 20 ng/ml Neurotrophin-3 (NT-3) and 10 ng/ml Brain-derived neurotrophic factor (BDNF) every 4^{th} day.

3.2.4 *Astrocyte-to-neuron conversion through retroviral gene delivery*

In order to reprogram cultured astrocytes into neurons, retrovirus-based delivery of the TF Neurog2 with following ectopic overexpression in astrocytes was employed throughout this project as the main reprogramming scheme. Astrocytes were transduced with retroviruses 4 hours after passaging onto coverslips. For the co-culture system, cells were transduced 24 hours before passage. Retroviral vectors are widely used tools for efficient and stable gene insertion into the genome of target cell populations. Interestingly, the insertion of transgenes into the host genome occurs in a predictable way. For example, retroviral vectors based on the Moloney Murine Leukemia virus (MoMLV), display a preferential selection of their target sites in the host genome, with a strong bias towards transcription start sites (TSS) and other transcription regulatory elements (X. Wu et al., 2003). The stable integration of the transgene into the host genome results in a persistent expression. A crucial aspect to consider when using retroviruses as gene delivery tools is their selective transduction of cells undergoing mitosis, enabled by the temporarily fragmented nuclear membrane, which allows access to the nuclear genome.

3.2.5 *Production of retroviral vectors*

The retroviral vectors used for astrocyte-to-neuron reprogramming allowed for the exogenous overexpression of the TF Neurog2 and the anti-apoptotic protein Bcl2 together with either DsRed or H2B-GFP downstream of an internal ribosomal entry site (IRES) under the control of a CAG promoter.
In this study, replication-defective retroviral vectors that are based on the Moloney Murine Leukemia viruses (MoMLV) were used for cell transduction and gene delivery. In fact, MoMLV-based retroviral vectors were amongst the first vectors to be engineered for the purpose of serving as gene delivery tools (Mann et al., 1983). For the production of replication-defective MoMLV-based vectors, a monoclonal cell line from a batch of 293GPG cells was used (Ory et al., 1996). This cell line possesses the benefit of stable, constitutive expression of the vesicular stomatitis virus glycoprotein (VSV-G) by inducible expression. The VSV-G protein constitutes a viral peplomer protein that plays a critical role in viral entry into the host cell. However, as a class III fusion protein, constitutive expression of VSV-G is ultimately toxic for most cells. Therefore, the expression of VSV-G in this cell line is controlled via a tetracycline-repressed (tetO) promotor.

1F8 cells were expanded in growth medium (see Table 4) by passaging them every second day in a ratio of 1:2 in order to maintain an exponential growth phase at all times and were maintained in incubators at 37 °C with humidified air containing 5% CO_2. The day before transfection, cells were passaged and plated into plating medium (see Table 4), which contains half of the Tetracycline concentration as in the growth medium in order to gradually enable the cells to express the VSV-G with minimal induction of cellular stress. For transfection, 25 µg of the desired plasmid per plate and polyethyleneimine (PEI) were diluted in Opti-MEM with a 3:1 mass ratio of PEI to DNA and incubated for 20 min at RT. After incubation, the mix was added dropwise to the cells. The medium was changed after 12-14 h to packaging medium with full absence of tetracycline.
Viral particles were harvested after 3 days, then every 2nd day, with a total of 3-4 viral harvests. To this end, the supernatant was collected and centrifuged for 15 min at 3000 rpm at RT. The supernatant, cleared from cell debris, was then filtered using a 0.45 µm PVDF filter and centrifuged for 2 hr at 15000 x g at 4°C. The supernatant was aspirated and the viral pellet resuspended with 100 µl of TBS-5 (see Table 4) and kept on ice at 4°C until the 2nd viral harvest. Viral particles of the 1st and 2nd harvest were merged, while the 3rd harvest was kept separate.
The viral harvest was titrated using HEK293 cells. In brief, cells were passaged and plated at a density of 10.000 to 15.000 cells per well into a 24-multiwell plate. After 24 hours, two coverslips were fixed in order to determine the total number of cells at the time of transduction. The remaining cells were transduced with 1 µl of virus per well and fixed after 24 hours. After performing an immunocytochemical staining for the fluorescence protein encoded by the produced virus, the infected cells were counted. The total cell number was assessed through the addition of the nuclear marker DAPI. The titer (transducing units per ml (TU/ml)) was then calculated as following:

$$TU/ml = \frac{P \cdot N \cdot 1000}{100 \cdot V}$$

where:
P is the percentage of infected cells
N is the total number of cells
V is the total volume of the virus

3.3 IMMUNOCYTOCHEMISTRY

Adherent cell cultures on glass coverslips were washed with 1x PBS, fixed in 4% PFA for 15 min at RT, and then washed once more with 1x PBS. Cells were then permeabilized and blocked by incubation in blocking solution (see Table 4) for 30 min at RT in order

to prevent unspecific antibody binding. Next, cells were incubated in blocking solution containing primary antibodies (see Table 5) for 1 hour at RT. After three washes with 1x PBS, cells were incubated in blocking solution containing secondary antibodies (see Table 6) for another hour at RT. Lastly, nuclei were labelled by incubation in blocking solution containing 4',6'-Diamidino -2-phenylindole dihydrochloride (DAPI) for 5 min at RT. After three final washes with 1x PBS, cells were mounted onto glass slides using Aqua-Poly/Mount. Mounted coverslips were stored at 4 °C. For immunocytochemical stainings performed with multiple primary antibodies from the same species, the Zenon Labeling Kit (see Table 13) was used according to the manufacturer's instructions. Full lists of all used primary and secondary antibodies are provided in table 5 and table 6.

3.4 MICROSCOPY

Immunofluorescence images were acquired using an upright Axio Imager.M2 epifluorescent microscope equipped with an ApoTome.2 system (Zeiss GmbH). Images were acquired with the 20x dry objective (NA 0.5) or the 40x dry objective (NA 0.75) in ApoTome mode. Serial Z-stacks of 15-20 µm with interval steps of 1.25 µm (using the 20x objective) or 0.25 µm (using the 40x objective) were taken through the whole depth of the sample. For analysis, 5-10 images were acquired of each coverslip by blinded location finding. Images of a particular experiment were all acquired with the same settings.

3.5 FLUORESCENCE IMAGE ANALYSIS AND QUANTIFICATION

Images were processed and analyzed using ImageJ (see Table 14). Maximum intensity projections were generated for all images and were split into distinct channels to be individually thresholded, using the same threshold for a certain channel across all images of a single experiment. For selective quantification of protein immunocytofluorescence (ICF) intensities in neuronal somata, the NeuN signal was used to delineate the region of interest, which was used to measure expression levels of e.g. IEGs. Measured fluorescence intensities were normalized to a mean background intensity measurement. In order to reconstruct and analyze neuronal morphology based on fluorescent reporter labeling, a maximum intensity projection was first generated. Sholl analysis was then performed using the ImageJ plugin Simple Neurite Tracer. After marking the center of each neuronal soma and tracing individual processes of a chosen neuron, a grid of concentric circles (5 µm diameter) centered at the soma centroid was overlaid and the number of dendritic intersections with the circles was counted. Morphological complexity was further conducted by counting primary branches, i.e. processes that directly emerge from the neuronal soma.

3.6 LIVE-CELL IMAGING OF CALCIUM DYNAMICS

Cells were incubated in 3 µM Fluo4-AM and 0.1 % pluronic acid reconstituted in HBSS for 60 min at 37°C. After incubation, cells were washed three times with HBSS and live-cell imaging was performed within the next 30 min. A coverslip was placed into a Zeiss Axio Imager 2 epifluorescent microscope and was perfused with buffered artificial cerebrospinal fluid (bACSF) (see Table 3) with a rate of 1 ml/min and was maintained at 32°C. Recordings were performed with a 20x objective (NA 0.5). For image acquisition, the camera setting was set to 8-bit. An excitation wavelength of 480 nm was chosen, as specified by the manufacturer's instructions (494 nm). The emission from the calcium indicator dye Fluo-4 was measured at 525 nm (523 nm) and indicated a rise in cytoplasmic calcium levels. For imaging fluorophore signal, the eGFP ET filter set (F46-002) was used. For the detection of the DsRed signal from transduced cells, the Cy3 ET filter set (F46-004) was used. Obtained traces of calcium dynamics were plotted as fold changes over the background level. The latter was obtained by calculating the 10^{th} percentile of all intensity levels belonging to a given trace. The traces were visualized using Prism 8 (see Table 14).

3.7 PHARMACOLOGY

During this work, neuronal activity was pharmacologically modulated in order to assess activity-dependent transcriptional changes in induced and endogenous neurons within the co-culture setting. For KCl stimulation experiments, cultures were treated with 1 µM Tetrodotoxin (TTX) and 100 µM (2R)-amino-5-phosphonovaleric acid (APV) overnight. The next day, neurons were either maintained under this condition or were subjected to membrane depolarization by addition of KCl to a final concentration of 55 mM by replacing $\frac{1}{3}$ of the neuronal medium with KCl depolarization buffer (see Table 4). After 3 hours of stimulation, cells were fixed with 4% PFA. For induction of homeostatic plasticity, neurons were subjected to chronic activity suppression for 48 hours with administration of 0.5 µM TTX, 50 µM APV and 20 µM cyanquixaline (CNQX) every 24 hours. Subsequently, cells were either fixed for immunocytochemical staining or the nuclei were isolated for downstream analysis of transcriptional changes. The drugs used in this study are well-established chemical tools used to study excitable cells. TTX has been used since the discovery of its selective inhibition of voltage-gated sodium channels in the 1960s for the inhibition of neuronal action potential firing (NARAHASHI et al., 1964). CNQX is a competitive AMPA receptor antagonist and results in the inhibition of synaptic transmission at excitatory synapses. APV is a NMDA receptor antagonist.

3.8 MOLECULAR BIOLOGY

3.8.1 *Agarose gel electrophoresis*

In general, 1-2% agarose gels were prepared by dissolving agarose in 1 x TAE by heating in the microwave. Once the solution cooled down to approximately 60°C, ethidium bromide was added into the gel solution at a concentration of 0.5 µg/ml. The solution was poured into the agarose gel casting tray to solidify. Each sample was supplemented with Gel Loading Dye (6x) and was then loaded into the gel pockets. During each run, a DNA ladder (100 bp or 1 kb) was loaded in order to assess the sizes of DNA fragments. The gel electrophoresis was run at 100 Volt (V) for 30-45 min. The concentration of agarose used was conditional on the sizes of DNA fragments to be visualized.

3.8.2 *Oligonucleotide design*

Oligonucleotide primers used for RT-qPCR were designed using the Primer3 software (https://primer3.ut.ee/). The genomic sequence of interest was identified by using the *Mus musculus* coding sequence provided by the National Center for Biotechnology Information (NCBI). The amplified product size range was set to be 60 - 200 bp. The size of the selected primer ranged from 20 to 24 bp. The primer melting temperature (T_M) was set between 58 °C and 62 °C. Oligonucleotide primers used to amplify a DNA sequence within a plasmid for cloning purposes were designed by selecting the first 20-22 bp (forward primer) or 20-22 bp of the complementary sequence at the 3′ end (reverse primer) of the sequence of interest. If needed, a recognition site for a restriction enzyme was added to the 5′ end (forward primer) or to the 3′ end (reverse primer). An additional 6 nucleotides (TAAGTA) were added to the 5′ end of each primer in order to facilitate enzymatic digestion near the end of the sequence.

3.8.3 *LR recombination*

For transferring a gene of interest (GOI) from an entry clone into a destination clone, LR recombination using the Gateway™ LR Clonase™ II Enzyme Mix (see Table 12) was performed according to the provided instructions. First, the GOI was inserted in between the recombination sites attL1 and attL2 (L - left) sites of an entry clone via enzymatic digestion (see Table 12 for a full list of all used restriction enzymes) and subsequent ligation. To produce the final expression clone, the GOI is recombined into a destination clone containing the two recombination sites attR1 and attR2 (R - right). These two sites flank the gene ccdB which encodes for a toxic protein to *E. coli* bacteria and serves as

a negative selector during the cloning process. The LR recombination reaction leads to a specific and highly efficient reaction between the attL1 and attR1 as well as the attL2 and attR2 sites, inserting the GOI into the destination vector and removing the ccdB gene. The recombination reaction is terminated by addition of 2 µg Proteinase K and incubation of the reaction at 37° C for 10 min. The clone of interest is transformed and selected via the destination clone-specific antibiotic resistance, while bacteria containing unrecombined plasmids are negatively selected due to ccdB expression.

3.8.4 *Enzymatic digestion of plasmid DNA*

Plasmids were digested using restriction endonucleases (see Table 12). Restriction endonucleases cut double-stranded DNA at enzyme-specific recognition sites and leave either blunt ends or, in case of an asymmetric cut, single-stranded overhang ends behind. Two DNA fragments with compatible overhang ends can then be ligated in the next step. An enzymatic digestion of DNA was set up as following:

Component	Amount
Plasmid DNA	1 µg
NEB Reaction buffer (10x)	1x
NEB restriction endonuclease	1 U
Nuclease-free Water	to 20 µl

The reaction was incubated at an enzyme-specific temperature (specified by the manufacturer) for 2 hours. If needed, the restriction enzymes were subsequently inactivated by incubation at 65° or 80° for 20 min. Next, the digested vector DNA, but not the digested insert DNA, was dephosphorylated at the 5'-end in order to prevent re-circularization. Dephosphorylation was performed within the digestion reaction mix and was set up as following:

Component	Amount
Plasmid DNA	1 pmol of DNA ends
Antarctic Phosphatase Reaction Buffer (10X)	1x
Antarctic Phosphatase	5 U
Nuclease-free Water	to 30 µl

The reaction was incubated at 37°C for 30 min. The enzyme was then heat-inactivated by incubation at 80°C for 2 min. The digestion efficiency was assessed by agarose gel electrophoresis. The DNA fragments of interest were cut out and purified from the agarose using the MinElute Reaction Cleanup Kit (see Table 13).

3.8.5 *Ligation of DNA fragments*

Two DNA fragments with compatible, cohesive ends were joined together by a ligase via the formation of a new phosphodiester bond. For the ligation reaction, 50-100 ng of the vector DNA fragment was used, with a vector : insert molar ratio of 1:3. A reaction without insert was set up as a control and was transformed in order to assess the likelihood of re-circularization of the vector DNA fragment. The ligation reaction was set up as following:

Component	Amount
Vector DNA	100 ng
Insert DNA	x
T4 DNA Ligase Buffer (10x)	1x
T4 DNA Ligase	1 µl
Nuclease-free Water	to 20 µl

The reaction mix was incubated at 16°C overnight. The enzyme was then heat-inactivated by incubation at 65°C for 10 min and the reaction was chilled on ice until the transformation took place.

3.8.6 *Transformation*

The transformation was performed by adding 5 µl of a ligation or LR recombination reaction to 50 µl of chemically-competent *E. coli* Top10 cells. The competent cells and DNA mixture was incubated for 20 min on ice followed by a heat shock at 42° for 1 min. The tubes were incubated on ice for 2-5 min before adding 150 µl of LB medium and incubating the cells at 37° and 400 rpm for 45 min to 1 hour. After this pre-growth step, the transformed bacteria were plated on agar plates containing 100 µg/µl of the antibiotic against which a resistance gene is present in the uptaken plasmid and incubated at 37°C overnight.

3.8.7 *Plasmid preparation*

Following bacterial transformation, colonies were screened for the correct plasmid. To this end, 10 - 20 colonies were picked and inoculated in 2 ml of LB medium for 12-16 hours (high copy plasmid) or 18-20 hours (low copy plasmid). The plasmid DNA was recovered by using the NucleoSpin®Plasmid EasyPure kit (see Table 13). The plasmid DNA was then enzymatically digested in order to confirm the approximate DNA sequence and organization of features. Once confirmed, the colony containing the correct

plasmid was inoculated again in order to produce a small-scale plasmid preparation (MiniPrep) for further cloning steps or a large-scale plasmid preparation (MaxiPrep) for harvesting sufficient DNA for retroviral vector production. The cloned features of a plasmid construct were then confirmed via Sanger sequencing. The kits used for a MiniPrep or a MaxiPrep are listed in table 13.

3.8.8 *Sanger DNA sequencing*

The sequence of newly cloned plasmid elements was confirmed by Sanger sequencing prior to retroviral vector production. For sequencing, 30-100 ng/µl of the DNA and 10 µM of each sequencing primer were diluted in 20 µl of DEPC water and were sent to Eurofins Genomics, Ebersberg (http://www.eurofinsgenomics.com). The sequencing results were obtained as .fasta files. The assessment and alignment of the sequenced nucleotide sequences to the reference sequence was performed by using SnapGene Viewer V5 (see Table 14). The primers used for sequencing are listed in Table 11.

3.8.9 *Plasmid cloning strategies*

The cloning of the plasmids listed in table 9 was performed according to the steps described above. The aim was to construct a plasmid that allows the expression of Neurog2 and Bcl-2 together with an enhanced green fluorescent protein (eGFP)-histone 2B (H2B) fusion reporter. The H2B-eGFP fusion protein incorporates into the nucleosome and allows nuclear visualization and facilitates fluorescence-based sorting of isolated nuclei compared to more highly diffusible fluorescent reporters. The plasmid containing the H2B-eGFP sequence was a kind gift from Dr. Rumpel (AG Prof. Simon Rumpel, Institute of Physiology, Mainz). The plasmid was digested with *KpnI* and *HindIII* in order to recover the H2B-eGFP sequence. The plasmid CAG-Ngn2-IRES-DsRedExpress2 was digested with *BstXI* and *NotI* in order to remove the fluorescent reporter DsRedExpress2 and replace it with H2B-eGFP in the next steps. After purification of the vector and insert sequences, they were ligated and the plasmid CAG-Ngn2-IRES-H2B-eGFP was obtained (see Figure 3.1 top). The Ngn2 sequence was then excised via digestion with *BamHI* and the plasmid CAG-IRES-H2B-eGFP was obtained (see Figure 3.1 middle). For the addition of the H2B-eGFP sequence into the plasmid containing the Ngn2 and Bcl-2 sequences, both of these plasmids were digested with *HindIII* and *HpaI*. The vector and insert fragments were then ligated and the construct CAG-Ngn2-T2A-Bcl2-IRES-H2B-eGFP was obtained (see Figure 3.1 bottom).

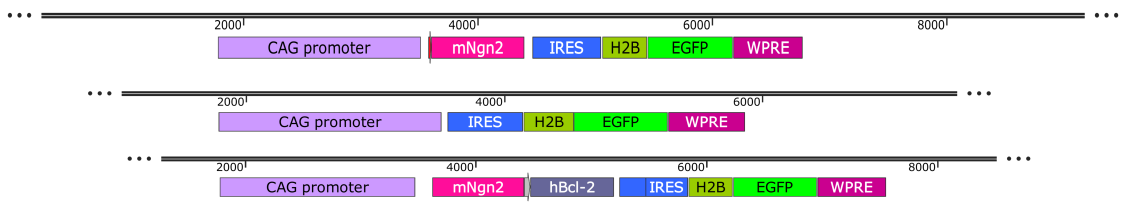

Figure 3.1: Schematic of cloned plasmids for retroviral delivery of reprogramming factors. *Top.* The construct comprises the mouse Neurog2 (mNgn2) coding sequence followed by an internal ribosomal entry site (IRES) and the histone H2B-eGFP (H2B-eGFP) fluorescent reporter. The total size of the construct is 9449 bp. *Middle.* The construct was used as a control vector and does not comprise any reprogramming factor. The total size of the construct is 8539 bp. *Bottom.* The construct comprises the mNgn2 sequence followed by a human Bcl-2 (hBcl-2) sequence. The total size of the construct is 10229 bp.

3.8.10 *Extraction of RNA*

For performing RT-qPCR, total RNA of cultured cells was isolated from cells using TRIzol reagent according to the provided instructions. Total RNA from nuclei purified by Fluorescence-Activated Nuclei Sorting (FANS) was extracted by using the RNeasy Micro Kit (see Table 13) according to the provided instructions. An on-column DNase I treatment was included in the steps. For homogenization of nuclei lysates, the QIAshredder columns were used (see Table 13). The amount of extracted RNA was estimated by measuring its optical density (OD) according to the Lambert-Beer law using a BioPhotometer. The purity of RNA was determined by calculating the ratio of absorption at 260 nm (absorption maximum of proteins) and 280 nm (absorption maximum of nucleic acids). RNA with an OD260/OD280 ratio of 2.0 is generally considered pure, therefore all RNA samples with an OD260/OD280 ratio of < 1.8 were discarded from further processing. At all times, at least two to three biological replicates, each with two technical replicates, were processed. RNA samples were stored in RNase-free H_2O at -80° until cDNA preparation by reverse transcription.

3.8.11 *Real-time quantitative PCR*

cDNA was synthesized from extracted RNA by using the High-Capacity cDNA Reverse Transcription kit according to the provided instructions (see Table 13). Each reaction was carried out on 700 ng of RNA. The final cDNA sample was then diluted 1:10 in RNase-free H_2O. Real-time quantitative PCR (RT-qPCR) was performed on a StepOnePlus Real-Time PCR-System (Applied Biosystems) with the thermal cycling conditions listed in table 1. This method allows the quantitative assessment of expression levels of selected genes in RNA samples from distinct experimental conditions. The technique is based on the

detection of the quantity of double-stranded DNA by measuring the fluorescence of SYBR Green after each cycle. SYBR Green allows real-time monitoring of DNA amplification by intercalation into double-stranded DNA and emitting a fluorescence signal with each cycle. The intensity of the fluorescence signal after each cycle directly correlates with the amount of double-stranded DNA and therefore allows quantification. The cycle threshold (c_T) for each DNA amplification curve is defined as the number of required cycles for the fluorescence signal to intersect the threshold level, i.e. surpassing the background fluorescence signal. For quantitative analysis, the c_T value for each target gene was then normalized to the c_T value of a chosen housekeeping gene.

Table 1: RT-qPCR program

	Step	Temperature	Duration	Cycle
qPCR amplification	Initial denaturation	95°C	600 sec	1x
	Denaturation	95°C	15 sec	40x
	Annealing/Elongation	60°C	60 sec	
Melting curve	Denaturation	95°C	15 sec	1x
	Annealing	60°C	60 sec	
	Heating	95°C	15 sec	
	Storage	4°C	∞	

3.9 ISOLATION OF NUCLEI

All steps of the nuclei isolation procedure were performed on ice or at 4°C. All solutions and equipment were pre-cooled on ice. Cells were carefully washed once with ice-cold PBS. The PBS was aspirated and nuclei isolation buffer (NI buffer, see Table 4) was added to each well. With a wide-bore pipette tip, the cell suspension mix was gently pipetted until the cells were completely suspended. The lysed cell suspension was kept for 5 min on ice before nuclei wash buffer (see Table 4) was added to each well, reaching a dilution of the NI buffer of 1 to 4. The lysed cell suspension was then collected and centrifuged at 500 g for 10 minutes. The supernatant was carefully removed without disrupting the nuclei pellet. Using a regular-bore pipette tip, 1 ml of nuclei wash buffer was added and the solution was pipetted approximately 5 times. Two further washing steps with nuclei wash buffer were performed, during which nuclei were centrifuged at 500 g for 10 min each. The nuclei pellet was then resuspended in nuclei wash buffer and filtered using 40 µm Flowmi Tip Strainers. The final nuclei suspension was diluted in an appropriate volume to achieve a target concentration of 1000 nuclei/µl after determining nuclei

concentration through counting using Trypan blue along with a hemocytometer. Nuclei quality was assessed via visualization with a Microscope (40x Magnification / Brightfield). The nuclei quality was considered good when the suspension was found mostly clump- and debris-free and individual nuclei displayed well-resolved rims, indicating an intact nuclear membrane.

3.10 FLUORESCENCE-ACTIVATED NUCLEI SORTING

Nuclei from virally transduced cells were enriched by selecting for enhanced GFP (eGFP) expression via Fluorescence-Activated Nuclei Sorting (FANS). FANS was performed on a BD FACSAria™ SORP sorter (BD Biosciences) using the BD FACSDiva™ Software. A nozzle size of 70 µm was consistently used for all nuclei sorts. Four gating steps were performed for each sorting: First, nuclei were distinguished based on their forward (FSC) and side scatter (SSC) properties, which allow an assessment of the size and granularity of the nuclei, respectively. After gating around the population of interest, the second gating step comprised doublet discrimination based on FSC area (FSC-A) and height (FSC-H). Third, the DAPI+ population was gated on to isolate nuclei from debris. DAPI fluorescence was detected by using a 405 nm laser with a 450/50 nm filter. The last step distinguished nuclei populations based on eGFP fluorescence, which was detected by a 488 nm laser with a 530/30 nm filter. Backgating was performed at every step to confirm the gating strategy. Representative scatter plots showing the gating strategy are visualized in figure 3.2. Data were analyzed using the FlowJo software (see Table 14).

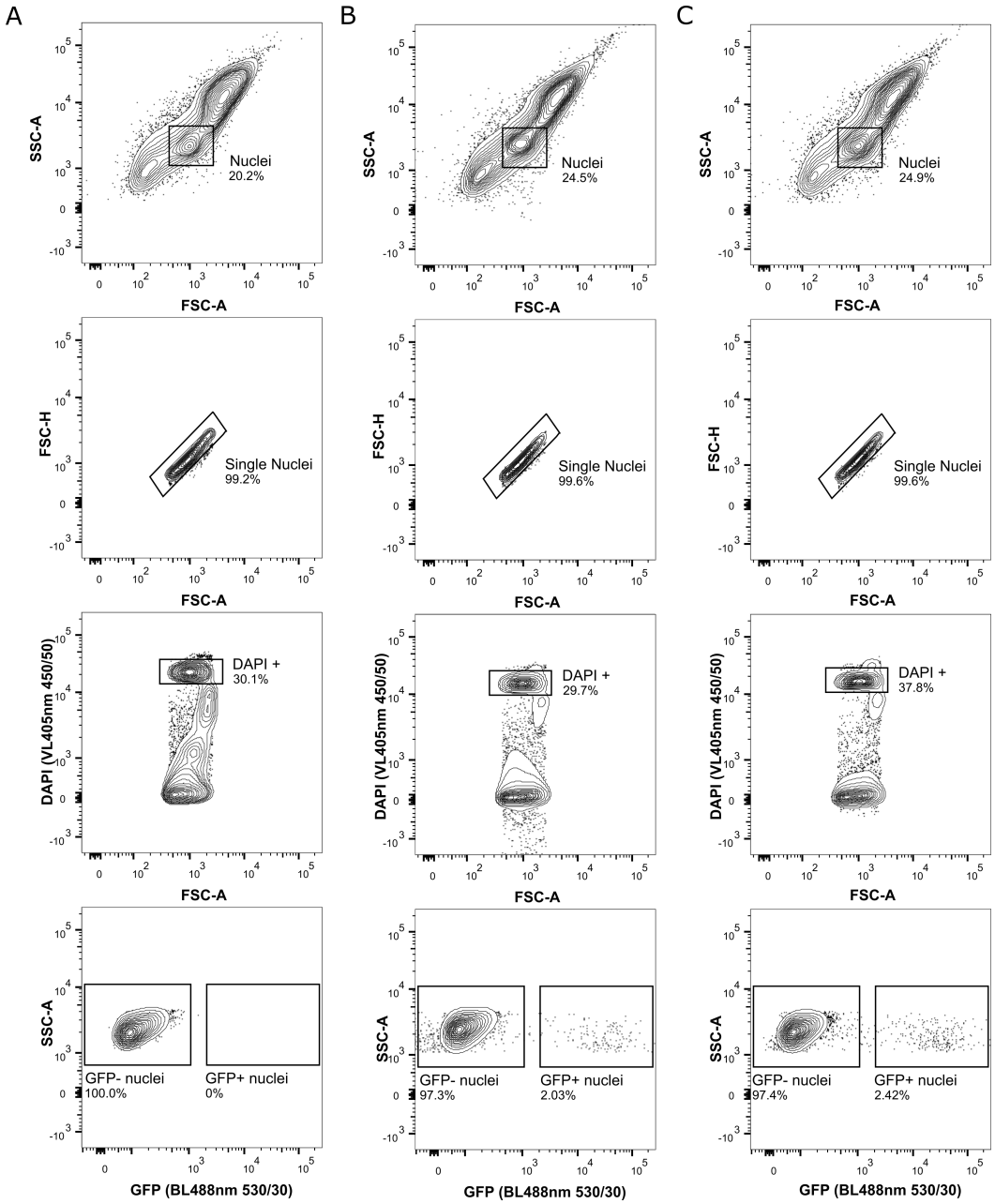

Figure 3.2: Purification of H2B-GFP containing nuclei from *in vitro* transduced cells via FANS. Depicted are the four gating steps for the negative control (A.), untreated sample (B.), and inhibited sample (C.). A nozzle size of 70 was consistently used for all sorts.

3.11 SINGLE-NUCLEUS RNA-SEQUENCING

3.11.1 *Droplet-based snRNA-sequencing*

The generation of Gel Bead in Emulsions (GEMs) and barcoding, cDNA amplification, library construction and snRNA-sequencing were performed by the TRON gGmbH (Translational Oncology at the University Medical Center of the Johannes-Gutenberg University, Mainz). For snRNA-seq library preparation from the above-mentioned FANS-purified single-nuclei suspensions, Chromium Next GEM Single-Cell 3' Reagent Kits v3.1 were applied on all samples according to manufacturer instructions. The RNA-seq poly(A) libraries were generated using poly(dT) primers. Quality control of the 10x libraries was carried out on a BioAnalyzer and a Qubit Fluorometer. Libraries were sequenced using the Illumina Novaseq^{TM} 6000 Sequencing System (S1).

3.12 COMPUTATIONAL ANALYSIS OF SINGLE-NUCLEUS TRANSCRIPTOMICS DATA

3.12.1 *Pre-processing*

The raw base call (BCL) files generated by the Illumina sequencer were processed using the 10x CellRanger v4.0 pipeline. BCL files of each flowcell directory were demultiplexed into a FastQ file using the *cellranger mkfastq* function. For read alignment, barcode and UMI counting, a reference transcriptome from the Genome Reference Consortium Mouse Build 38 (GRCm38) was generated in which each gene transcript locus is registered as an exon. As the snRNA-seq pipeline captures both unspliced pre-mRNA containing exons and introns as well as mature mRNA that represent only the exonic regions of a given gene and the CellRanger pipeline only counts reads that are aligned to exons, registering each transcript locus as an exon ensures reading and counting of all existing reads. The applied version of CellRanger used the Spliced Transcripts Alignment to a Reference (STAR) version 2.5.1b algorithm in order to align reads to the genome. Only uniquely mapped reads were retained for UMI counting. The Woodchuck Hepatitis Virus (WHV) Posttranscriptional Regulatory Element (WPRE) sequence element (Higashimoto et al., 2007) was added to the reference transcriptome in order to attempt identifying transduced nuclei based on WPRE transcripts, which may enable omitting FANS in future experiments. However, WPRE-mapping reads could not be detected in any cell (data not shown). After UMI counting and cell identification, a feature-barcode matrix was generated for downstream analysis. The above-described steps were performed using the *cellranger count* and *aggr* functions. In the following chapters, each nuclear transcriptome is referred to as a "cell".

3.12.2 *Analysis of the snRNA-seq dataset*

The SCANPY (v.1.6.0) toolkit was used to further process the snRNA-seq dataset and perform the initial data analysis (Wolf et al., 2018). Quality control (QC) was performed by excluding cells with less than 200 and more than 8000 detected genes as well as cells with mitochondrial transcript proportion higher than 3% (see Figure 3.3 A). Moreover, all genes detected in less than 3 cells were excluded from the dataset. These QC steps resulted in the removal of 23 cells and 11670 genes from the gene expression matrix (see Figure 3.3). In order to allow comparisons of counts between cells, normalization for library size differences was performed by rescaling transcript counts to 10^4 reads per cell and performing a log transformation. Highly expressed genes (*Dpp10, Lrp1b, Lingo2, Ptprd, Kcnip4, Chl1, Grm7, Dlg2, Kcnq3, Lsamp, Cmss1, Gm2418, AY036118, Nrxn1, Malat1, 1700054A03Rik, Tsix, Pcdh11x, Frmpd4*) were excluded from the computation of the normalization factor per cell as they can strongly impact the normalized values of all other genes. Next, highly variable genes were identified and a reduced dimensional representation was computed using principal component analysis (PCA). As shown in Figure 3.3 D, a high fraction of the variance in the dataset is described by the first 10 PCs. Therefore, a k-nearest neighbor (kNN) graph of the dataset was computed using the first 10 PCs with the size of local neighborhood set to 15. The graph was then embedded into 2-dimensional space using the non-linear Uniform Manifold Approximation and Projection (UMAP) algorithm (McInnes et al., 2018). The leiden algorithm was applied to perform unsupervised clustering of cells, which resulted in 11 distinct clusters (resolution = 0.5).

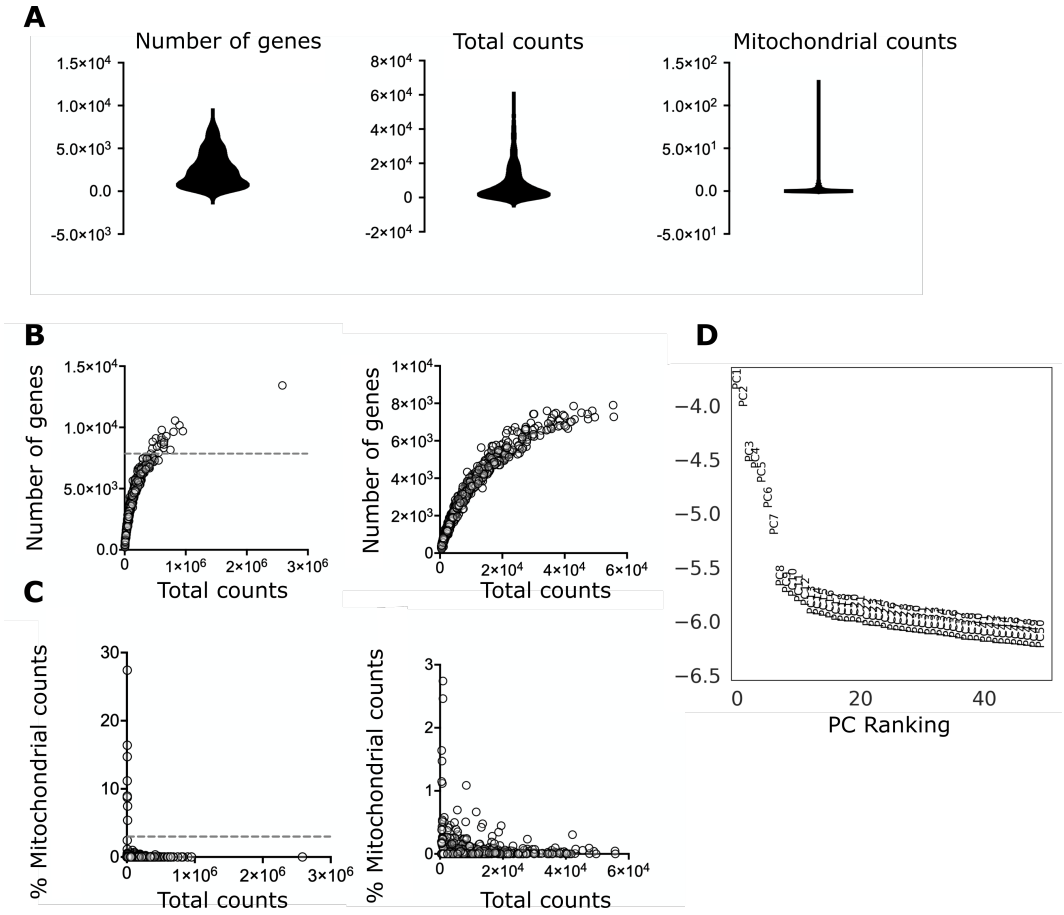

Figure 3.3: **Quality control of Single-nucleus RNA-sequencing dataset.**
A. Violin plots visualizing the distribution of the total number of genes (*left*), total counts (*middle*) and total number of mitochondrial genes (*right*) per cell. **B.** Plots depicting the relationship between number of genes and total counts per cell before (*left*) and after (*right*) filtering. **C.** Plots depicting the relationship between the percentage of mitochondrial genes and total counts per cell before (*left*) and after (*right*) filtering. Dashed lines in B. and C. depict the filtering threshold. **D.** PC variance ratio plot depicting a ranking of the first 50 PCs based on the percentage of variance that each PC accounts for.

3.12.3 *Single-cell projection onto reference transcriptome datasets*

In order to comprehensively identify cellular identities within the obtained dataset, three independent mouse reference scRNA-seq datasets were retrieved as references: the developing mouse brain (La Manno et al., 2021), the adolescent mouse nervous system atlas, which includes both the central nervous system (CNS) and peripheral nervous system (PNS) (Zeisel et al., 2018) and the adult mouse (Yao, Liu, et al., 2021). Projection of individual cells of the query dataset onto the reference datasets was performed in RStudio using scmap (see Table 15). Of each dataset, the top 100 most variable features across annotated clusters were selected and were used to assess the similarity of cells

from the query dataset to cells of each reference (see Table 16). The *scmap-cluster* function was used to simultaneously compute three similarity scores (Pearson and Spearman correlations, cosine similarity) between cells in the query dataset and the centroid values for each annotated cluster from the three references. For assigning an identity of the reference clusters onto a query cell, the requirement that at least two of the similarity scores are in agreement regarding cell type, and that at least one score be > 0.5 was set. Projections were visualized via a Sankey plot.

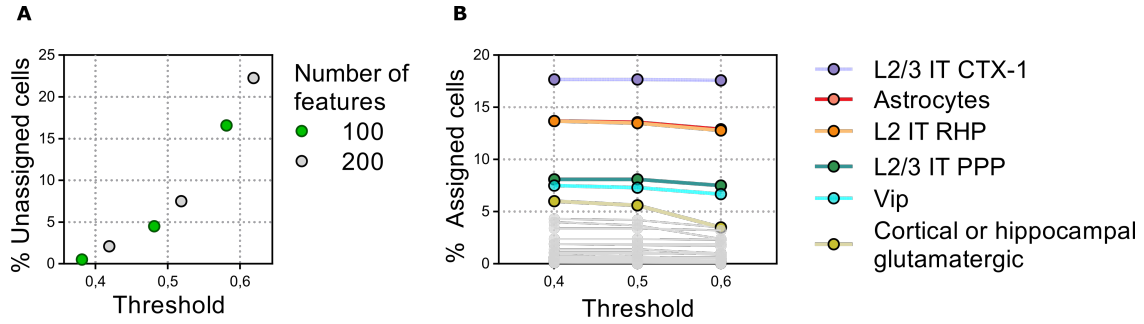

Figure 3.4: Definition of projection parameters.
A. The query dataset was projected onto the three reference datasets from which each either 100 or 200 most variable features across cell clusters were selected. The percentage of unassigned cells after the projection of the query dataset is plotted against the applied similarity thresholds. **B.** The percentage of assigned cells is plotted against the applied similarity thresholds in order to assess potential changes in the cell populations accounting for more than 5% of the total cell population through threshold manipulation.

3.12.4 *Differential gene expression analysis*

One of the most commonly applied analyses on transcriptomic datasets is the quantitative analysis of differentially expressed genes (DEG) across distinct experimental conditions. The scRNA-seq dataset consists of count-based gene reads and DEG analysis is highly dependent on the accuracy of gene expression profiles (transcript abundance), yet, performing this analysis on sc-RNAseq datasets has been shown to be challenging as the data is inherently noisy and sparse as a result of its zero-inflation as well as its high degree of sample heterogeneity (H. Chen et al., 2019). Interestingly, although tools that have been designed for DEG analysis in scRNA-seq datasets address these dataset characteristics (Kharchenko et al., 2014), several studies have shown that bulk RNA-seq DEG analysis tools perform better in terms of accuracy in DEG detection and a lower rate of false positive DEGs (Soneson & Robinson, 2018; T. Wang et al., 2019). Moreover, tools designed for bulk RNA-seq datasets have been adapted to model scRNA-seq datasets more accurately and have been shown to outperform scRNA-

seq DEG analysis tools (Risso et al., 2018; Van den Berge et al., 2018). Hence, two commonly employed tools, EdgeR (Robinson et al., 2010) and DESeq2 (Love et al., 2014), combined with the modification introduced by the ZINB-WaVE package (Risso et al., 2018), have been shown to be best suited for DEG analysis in scRNA-seq datasets (Luecken & Theis, 2019). In the following study, the DESeq2 package combined with the ZINB-WaVE package (see Table 15) was used in order to assess DEG between experimental groups using the zero-inflation weighting approach. The implemented workflow for the analysis of the obtained snRNA-seq data has been followed according to the guidelines provided (https://github.com/mikelove/zinbwave-deseq2). For the detection of differentially expressed genes, the analysis included all neurons of an experimental group, instead of layer-specific types, in order to increase statistical power. As a statistical test, the likelihood-ratio test (LRT) was applied to assess significance. Genes were called differentially expressed with a false discovery rate (FDR) cutoff of 0.05 and a fold change (FC) > 1.25.

3.12.5 *Gene Ontology Enrichment Analysis*

Gene Ontology (GO) enrichment analysis of DEGs was performed using ShinyGo 0.76 (http://bioinformatics.sdstate.edu/go/). The FDR cutoff was set to 0.05 and the minimum number of genes within a pathway was set to 5. Synapse-specific GO term analysis was performed using the SynGO portal (https://www.syngoportal.org). Significantly enriched ontologies were visualized using Prism 8 (see Table 14).

3.12.6 *Inference of gene regulatory networks*

Gene regulatory networks were inferred using pySCENIC (Aibar et al., 2017). As a first step, the pySCENIC pipeline assesses coexpression between TFs via a predefined list of TFs and potential target genes based on the raw gene expression matrix. Next, the algorithm identifies genes in which the TFs' binding motif is significantly enriched and generates regulons that contain only direct target genes and which are defined by the name of the regulator (TF). Finally, the tool scores the activity of each regulon in each cell. Due to the stochastic nature of the algorithm, the same input expression matrix can lead to slightly variable output regulons for repeated runs. The pipeline was therefore run 10 times. Regulons that were obtained in at least 80% of all runs were retained for further analysis. The regulon composition was refined by retaining target genes of a given TF only when found in at least 60% of the regulons for the given TF across the 8-10 runs. Activity scores of each regulon per cell was obtained by averaging the values across all runs for a given regulon.

3.13 STATISTICAL ANALYSIS

Each experiment was performed on at least three independent biological replicates with at least two technical replicates each. Statistical analysis was performed in SPSS and GraphPad Prism 8. Initially, each data set was tested for a Gaussian distribution assessed by the Shapiro-Wilk normality test. Datasets were considered approximately normally distributed with $p > 0.05$, otherwise not. For normally distributed data, the parametric two-tailed Student's t-test with Welch's correction was used when comparing two groups. For the comparison of three or more groups, a one-way analysis of variance (ANOVA) was performed on the data. If data did not display a normal distribution, the non-parametric Mann-Whitney U test was applied when comparing two groups and the Kruskal-Wallis test was applied for comparing three or more groups. Differentially expressed genes between experimental conditions were identified using the LRT in DESeq2, otherwise, pairwise Wilcoxon rank sum tests between groups of cells were performed, with the application of the Benjamini-Hochberg correction of the FDR. For every statistical test, the rate of Type-I errors was controlled for by setting the α-level to 0.05, therefore:

not significant (n.s.):	$p > 0.05$
*:	$p < 0.05$
**:	$p < 0.01$
***:	$p < 0.001$

Data are expressed as mean $\pm$ standard error of the mean (SEM). Graphical representations of results were obtained through either GraphPad Prism 8, ggplot2 (RStudio) or matplotlib (Python) functions (see Table 15).

3.14 DATA AND CODE DEPOSITION

Analysis scripts as well as the raw and processed sequencing data generated within the scope of this thesis work are securely stored in the long-term archive of the data center (Zentrum für Datenverarbeitung - ZDV) at the JGU. Data analysis files that are currently not present in the archive are stored on a hard drive present in the lab and will eventually be made publicly available. Upon publication, snRNA-seq raw data generated during this study, as well as the scripts written and employed for data processing and analysis, will be deposited and made publicly available through a dedicated online repository (e.g. Gene Expression Omnibus - NCBI, GitHub, respectively).

4

MATERIALS

4.1 BIOLOGICAL MATERIAL

Table 2: Biological Material

Cells	Source
E.coli Dh5α Competent Cells	Invitrogen
One Shot^{TM} TOP10 Chemically Competent *E.coli* Cells	Invitrogen C4040-10

4.2 BUFFERS AND SOLUTIONS

4.2.1 *General buffers, media and solutions*

Table 3: General buffers, media and solutions

Solution	Composition	Diluted in	pH
1x PBS	137 mM NaCl 100 mM Na_2HPO_4 18 mM KH_2PO_4 2.7 mM KCl	milliQ H_2O	7.4
TBS-5	1 M Tris-HCl 5 M NaCl 1 M KCl 1 M $MgCl_2$	milliQ H_2O	7.8
1x TAE	40 mM Tris free base 1 mM Disodium EDTA 20 mM Glacial Acetic Acid	ddH_2O	8.6

Continued on next page

Table 3 – continued from previous page

Solution	Composition	Diluted in	pH
0.4 M PB	117 mM Na_2HPO_4 x 12 H_2O 128 mM NaH_2PO_4 x 2 H_2O	milliQ H_2O	7.4
LB medium	10 g/l Tryptone 5 g/l Yeast extract 10 g/l NaCl	milliQ H_2O	7.5
LB Agar	10 g/l Tryptone 5 g/l Yeast extract 10 g/l NaCl 15 g/l Agar	milliQ H_2O	7.5
4 % PFA	4 % (w/v) PFA 0.4 M Phosphate Buffer	milliQ H_2O	-
Blocking solution	1 % (v/v) BSA 1 % (v/v) Triton X-100	0.1 M PB	-
bASCF	125 mM NaCl 25 mM $NaHCO_3$ 25 mM D-Glucose 2.5 mM KCl 1.25 mM NaH_2PO_4 1 mM $MgCl_2$ 2 mM $CaCl_2$ 10 mM HEPES	milliQ H_2O	-
Intracellular solution	125 mM K-Gluconate 5 mM NaCl 10 mM HEPES 10 mM EGTA 2 mM $MgCl_2$ 2 mM ATP	milliQ H_2O	7.4

4.2.2 *Cell culture media*

Table 4: Cell culture media

Medium	Composition	Diluted in	pH
Astrocyte medium	10 % (v/v) FBS 5 % (v/v) Horse serum 1x Penicillin/Streptomycin 1x GlutaMax 1x B27 supplement	DMEM/F12	-
Neuronal medium	1x Penicillin/Streptomycin 1x GlutaMax 1x B27 supplement	Neurobasal Medium	-
Growth medium	1x Glutamine 10 % (v/v) FBS 2 µg/ml Puromycin 0.3 mg/ml G418 Sulfate 2 µg/ml Tetracycline	DMEM/F12	-
Plating medium	1x Glutamine 10 % (v/v) FBS 1x NEAA 1x Na-Pyruvate 0.5 µg/ml Tetracycline	DMEM	-
Transfection medium	375 µl PEI 125 µg DNA	Opti-MEM	-
Packaging medium	10 % (v/v) FBS 1x Glutamine 1x NEAA 1x Na-Pyruvate	DMEM	-

Continued on next page

Table 4 – continued from previous page

Medium	Composition	Diluted in	pH
Nuclear Isolation Buffer (NIB)	10 mM Tris-HCl 10 mM NaCl 3 mM $MgCl_2$ 0.1% Nonidet^{TM} P40 Substitute	nuclease-free H_2O	7.4
KCl Depolarization buffer	170 mM KCl 2 mM $CaCl_2$ 1 mM $MgCl_2$ 10 mM HEPES	dest. H_2O	7.4
Nuclear wash buffer	1 % (v/v) BSA 0.2 U/µl RNase Inhibitor	1x PBS	-
Coating solution I	20 µg/ml Poly-D-Lysine	dest. H_2O	-
Coating solution II	3 µg/ml Laminin	dest. H_2O	-

4.3 ANTIBODIES

4.3.1 *Primary Antibodies*

Table 5: Primary Antibodies

Antigen	Host	Dilution	Source
β III-tubulin	Mouse	1:500	Sigma (T8660)
Doublecortin	Guinea pig	1:400	Millipore (AB2253)
GFP	Chicken	1:500	AvesLab (GFP-1020)
GFAP	Rabbit	1:500	Dako (Z0334-29-2)
GLAST	Rabbit	1:500	Frontier Inst. (AB_2571715)
Iba1	Rabbit	1:400	Wako (019-19741)
Ki67	Rabbit	1:500	Abcam (ab16667)
GABA	Guinea pig	1:500	Abcam (ab174139
Ctip2	Rat	1:500	Abcam (ab18465)
Cux2	Rabbit	1:500	Abcam (ab216588)
Tbr1	Chicken	1:500	Millipore (AB2261)
Tbr1	Rabbit	1:500	Abcam (ab31940)
Tbr2	Rabbit	1:500	abcam (ab23345)
Nestin	Mouse	1:500	Covance (PRB-315C)
NeuN	Mouse	1:500	Millipore (MAB377)
NeuN	Chicken	1:500	Synaptic Systems (266 006)
c-Fos	Rabbit	1:400	Santa Cruz (sc-52)
Arc	Guinea pig	1:400	Synaptic Systems (156 004)
Npas4	Rabbit	1:500	LSBio (LS-C356222)
Satb2	Guinea pig	1:500	Synaptic Systems (327 004)
Sox10	Goat	1:500	Santa Cruz (sc-17342)
PSD-95	Rabbit	1:500	Synaptic Systems (124 003)
RFP	Rabbit	1:500	Biomol (600-401-379)
MAP-2	Mouse	1:500	Leinco Technologies (M119)
vGlut1	Rabbit	1:500	Synaptic Systems (135 302)

4.3.2 *Secondary Antibodies*

Table 6: Secondary Antibodies

Fluorescence	Species	Dilution	Source
Alexa 488	Donkey α-chicken	1:1000	Jackson Immunoresearch (703-545-155)
Alexa 488	Donkey α-Mouse	1:1000	Invitrogen (A21202)
Cy3	Donkey α-Rabbit	1:1000	Dianova (711-165-152)
Cy3	Donkey α-Goat	1:1000	Dianova (705-165-147)
Cy3	Goat α-Mouse	1:1000	Dianova (115-165-166)
Cy5	Donkey α-Goat	1:1000	Dianova (705-155-147)
Cy5	Goat α-Rabbit	1:1000	Dianova (115-115-144)

4.4 REAGENTS

Table 7: Reagents

Reagent	Source	Identifier
1 kb ladder	New England Biolabs	N3232S
100 bp ladder	New England Biolabs	N3231S
10% Pluronic^{TM} F-127	ThermoFisher	P3000MP
Aqua-Poly/Mount	Polysciences Inc.	18606-20
Antarctic Phosphatase Reaction Buffer (10X)	New England Biolabs	B0289S
B27 Supplement	Life Technologies	17504-044
BDNF	PeproTech	450-02-10UG
Blue S'Green qPCR 2x Mix	Biozym	331416
DMEM-F12	Gibco	21331-020
dNTP Mix	New England Biolabs	N0447S
DMEM	Gibco	21969-035
Epidermal Growth Fator	PeproTech	AF-100-15-1mg
Fast Green FCF	Sigma-Aldrich	F7252
Fibroblast Growth Factor-2	PeproTech	100-18B-100µg
Gel Loading Dye, Purple (6X)	New England Biolabs	B7024S
HBSS (10x)	Gibco	14025092
Neurobasal Medium	Invitrogen	21103049

Continued on next page

Table 7 – continued from previous page

Reagent	Source	Identifier
Non-Essential Amino Acids	Gibco	1140-035
Neurotrophin-3	StemCell	78074
OptiMEM™	Gibco	31985-047
Oregon Green™ 488 BAPTA-1, AM	Invitrogen	O6807
PBS, pH 7.2 (10x)	Gibco	70013-016

4.5 CHEMICALS

Table 8: Chemicals

Chemical	Source	Identifier
2-Propanol	Sigma-Aldrich	I9516-500ML
Agar	Merck	1119251000
Agarose	Lonza	98200-100
Ampicillin Sodium Salt	AppliChem	4G017739
APV	Tocris	0106
Biocytin	Sigma-Aldrich	B4261E
Bovine Serum Albumin (BSA)	Sigma-Aldrich	A9418-50g
Calcium Chloride dihydrate	VWR	437053L
CNQX	Tocris	1045
DAPI	Sigma-Aldrich	D9542
Ethanol absolute	Sigma-Aldrich	34923
Ethidium bromide	Sigma-Aldrich	46065
Fast Green FCF	Sigma-Aldrich	F7252
Fetal Bovine Serum (FBS)	Invitrogen	10270-106
Forskolin	Merck	F6886
G5418 sulphate	InVivoGen	Ant-gn-5
D-Glucose	Sigma-Aldrich	G8270-1KG
Glycerol 99%	Sigma-Aldrich	G5516-500ML
Glycine	Merck	56-40-6
HEPES 1M	Sigma-Aldrich	H0877-100ML
Horse serum	Invitrogen	16050-130
Kanamycin sulfate	Sigma-Aldrich	60615-5g

Continued on next page

Table 8 – continued from previous page

Chemical	Source	Identifier
Laminin	Sigma-Aldrich	L2020-1MG
L-GlutaMax	Invitrogen	35050-0380
L-Glutamine	Gibco	25030081
Magnesium chloride anhydrous	Sigma-Aldrich	M8266
Non-Essential Amino Acids	Gibco	1140-035
Nonident^{TM} P40 Substitute	Sigma-Aldrich	74385-1L
Paraformaldehyde	Merck	8.18715.1000
Sodium chloride	VWR	0241-1KG
UltraPure^{TM} Tris	Invitrogen	15567-027
Potassium chloride	Sigma-Aldrich	60129-250G
Tryptone	Sigma-Aldrich	T7293

4.6 RECOMBINANT DNA

Table 9: Plasmids

Plasmid	Source
RV-CAG-mNgn2-T2A-hBcl2-IRES-DsRed	Berninger Lab
RV-CAG-mNgn2-IRES-DsRedExpress2	Berninger Lab
RV-CAG-mNgn2-IRES-H2B-eGFP	Personally cloned
RV-CAG-IRES-H2B-eGFP	Personally cloned
RV-CAG-mNng2-T2A-hBcl2-IRES-H2B-eGFP	Personally cloned
RV-CAG-IRES-DsRedExpress2	Berninger Lab
RV-CAG-IRES-GFP	Berninger Lab
pAAV-hSyn-H2B-eGFP	Gift from the Rumpel Lab

4.7 OLIGONUCLEOTIDES

4.7.1 *Primers for RT-qPCR*

Table 10: Real-time quantitative PCR primers

Primer	Forward Sequence (5′ - 3′)	Reverse Sequence (5′ - 3′)
Cacnb2	CGGACTTTAGCCTCCTCAACTT	TGATCACCTTGAGAACCCTGTG
GAPDH	TTCACCACCATGGAGAAGG	CACACCCATCACAAACATGG
Casp3	CAGCCAACCTCAGAGAGACATT	AATCACACACACAAAGCTGCTC
Grik1	GGATATTGCCTGGATCTGCTGA	TCCACTCCCCTTTGTCATTCTG
Nav2	TTCAGACAGTGTTCTCGGCTAC	CCCTTTGACGGTCACCAAGATA
Opa1	CAAAGGAAAGGAACACGACGAC	ATACTCTCCTCCTTCACAGCCT
Rpl19	CTCGTTGCCGGAAAAACA	TCATCCAGGTCACCTTCTCA
Synpr	CTGCAACAGGTGACCTTTGAAG	GGAGTAGAGAAAGGCGAACACA
Vav3	CTGCTGCGATACCTTTGGAATG	TACTTTCTTCAGTGGGGAACGG
Kcnn2	AACAATTCTAACAACCTGGCGC	AGCCGATGTTCTGGTTCTTCTT
Neurod2	ACAAACAGACACAGAGCTTCCA	CACATCCCCTCCCACCAAAATA
Stat3	ACACTGACTGATGAAGAGCTGG	CTGCAGCTCCTCCAGTTTCTTA
Nr4a1	ATTGACAACATCCTGGCCTTCT	CGATCAGTGATGAGGACCAGAG
Lrig1	GGAGTACAGCGTCACTAACACA	TGAGAGGAGAGGTAGCTTGGAA
Sox4	ACAACGCCGAGATCTCCAAG	TCCTGGATGAACGGAATCTTGT
Camk4	GGTGGAGAAAGATGCAGGTGTA	AGCTTCTCCTCTGAATCCCTCT
Homer2	GTCCTCTCACCTTACCCTACCT	CGCAGTAAATCATCAGCCTTGG

4.7.2 *Primers for Sanger DNA sequencing*

Table 11: Primers used for Sanger DNA sequencing

Primer	Sequence (5′-3′)	Target
CAG_FW	CGTGTGACCGGCGGCTCTA	CAG, 3′-end
IRES_FW	CGATGATAATATGGCCACAACC	IRES, 3′-end
IRES_RV	CACCGGCCTTATTCCAAGC	IRES, 5′-end
WPRE_RV	CCAGTCAATCTTTCACAA	WPRE, 5′-end

4.8 ENZYMES

Table 12: Enzymes

Enzyme	Source
Antarctic Phosphatase	New England Biolabs
DNase I (RNase-free)	StemCell Technologies
Gateway™ LR Clonase™ II Enzyme Mix	Invitrogen
KAPA HiFi DNA Polymerase	Roche
OneTaq DNA Polymerase	New England Biolabs
T4 DNA Ligase	New England Biolabs
XhoI	New England Biolabs
EcoRI-HF	New England Biolabs
BamHI	New England Biolabs
BstXI	New England Biolabs
PspXI	New England Biolabs
KpnI-HF	New England Biolabs
HindIII	New England Biolabs
DraIII-HF	New England Biolabs
HpaI	New England Biolabs
NotI	New England Biolabs

4.9 COMMERCIAL KITS

Table 13: Commercial Kits

Kit	Source	Identifier
High-Capacity cDNA Reverse Transcription Kit	ThermoFisher	4368813
RNeasy®Micro Kit	Qiagen	74004
PureLink HiPure Plasmid Maxiprep kit	Invitrogen	K2100-07
MinElute Reaction Cleanup Kit	Qiagen	28204
KAPA HiFi PCR Kit	Roche	KR0368
Zenon Rabbit IgG Labeling Kit AF488	ThermoFisher	Z25302
NucleoSpin®Gel and PCR Clean-up	Macherey-Nagel	740609.50
NucleoSpin®Plasmid EasyPure	Macherey-Nagel	740727.250
QIAshredder	Qiagen	79654

4.10 SOFTWARES

Table 14: Softwares

Software	Source
ImageJ	National Institute of Health
ZEN	Carl Zeiss Microscopy
GraphPad Prism 8	GraphPad
ApE (A Plasmid Editor) v3.0.8	M. W. Davis and Jorgensen, 2022
pClamp10	Molecular Devices
Origin 7.5 V5	OriginLab
FlowJo	BD Biosciences
SPSS Statistics 23 V5 R	IBM
SnapGene Viewer V5	GSL Biotech LLC

4.11 ALGORITHMS

Table 15: Algorithms used in R and Python

Package	Version	Reference
DESeq2	1.30.1	Love et al., 2014
scmap	1.12.0	Kiselev et al., 2018
Seurat	4.0.2	Stuart et al., 2019
ZINB-WaVE	1.12.0	Van den Berge et al., 2018
apeglm	3.14	Zhu et al., 2019
pySCENIC	0.11.2	Aibar et al., 2017
Scanpy	1.6.0	Wolf et al., 2018
glmGamPoi	1.4.0	Ahlmann-Eltze and Huber, 2021

5

RESULTS

The bHLH TF Neurog2 is well characterized for its fundamental role in neuronal development in mammals (Lacomme et al., 2012; Wilkinson et al., 2013). As a master regulator, it inhibits the commitment towards a gliogenic fate while inducing a neurogenic lineage commitment (Morrison, 2001). In line with its function during neuronal development, it has been shown to drive direct reprogramming of diverse somatic cells into neurons. The approach has proven eminently effective: induced neurons (iNs) have been shown to develop to a stage in which they spontaneously generate action potentials and form synapses with surrounding neurons (Berninger et al., 2007; Blum et al., 2011; Heinrich et al., 2010). However, it is not yet understood to which extent iNs display an excitation-transcription coupling mechanism and are able to respond with transcriptional changes to distinct activity modulations known to induce neuronal plasticity mechanisms. In addition, it remains unclear whether iNs acquire a complete synaptic machinery as well as a neuron-specific ion channel composition that dictates their intrinsic excitability. Moreover, functional integration, assessed by means of excitation-transcription coupling in response to synaptic activity modulation, of excitatory iNs into a network of mature cortical neurons has been so far not yet shown. At the same time, iNs have been consistently shown not to survive for extended periods in neuronal networks and it remains unclear whether this may be reflecting an incomplete acquisition of the necessary molecular components driving synaptic integration, or whether it may be due to external factors deriving from the environment. In this study, a co-culture system was utilized in which astroglial cultures were transduced with retroviruses encoding for the reprogramming factor Neurog2 and subsequently plated onto a more mature cortical neuronal culture. This system was designed in order to mimic in a simplified *in vitro* setting the context of *in vivo* reprogramming in which iNs would be embedded into a preexisting network. Here, iNs go through their developmental trajectory within a more mature environment, while being under the influence of the same activity patterns as endogenous neurons and, ideally, should respond to these influences as the logic of the network demands. Activity-dependent transcriptional changes elicited in endogenous neurons were therefore taken as a reference in order to assess the *bona fides* of changes detected in iNs.

5.1 EXPERIMENTAL DESIGN USED TO ASSESS ACTIVITY-DEPENDENT TRANSCRIPTIONAL REGULATION IN INDUCED NEURONS

5.1.1 *Establishment of a mature neuronal network as the framework for studying activity-dependent gene regulation*

In order to be able to directly compare endogenous neurons (eNs) and astroglia-derived induced neurons (iNs), a coculture system was established in which retrovirally transduced astroglia were embedded into a pre-existing cortical network and subsequently reprogrammed into maturing iNs following ectopic expression of the TF Neurog2. Cortical cultures were prepared from embryonic mice at developmental day 14.5, during which stage cortical neurons of deeper layers of the cerebral cortex have been generated and upper layer neurons are currently expanding (Di Bella et al., 2021). To characterize the system, cortical neurons were initially independently characterized after 14 *div* by assessing the percentage of neurons versus astroglia among all plated cells. Immunocytochemical labeling of NeuN- and GFAP-expressing cells displayed a predominant presence of neuronal cells (NeuN: 91.22 ± 1.59 %; GFAP: 6.22 ± 1.22 %), with little presence of astroglia (see Figure 5.1 B). To ensure that retroviral targeting is restricted to postnatal astroglia when the coculture was prepared, the proportion of proliferating cells derived from the embryonic cortex was assessed by Ki67 immunolabeling. Immunocytochemical labeling of Ki67-expressing cells displayed no proliferating cells (Ki67: 0.00 ± 0.00 %, (see Figure 5.1 B and C *top panel*).

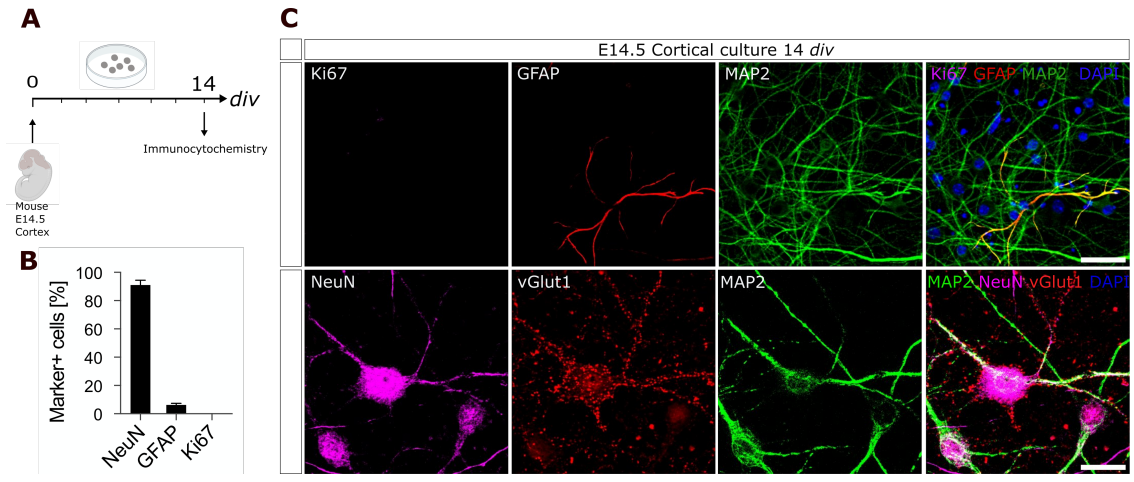

Figure 5.1: **Characterization of E14-cortex derived neuronal cultures.**
(A) Experimental timeline. **(B)** Immunocytochemical analysis of neuronal and astroglial-specific marker-expression after 14 *div*. The majority of cells express NeuN and only a minor fraction of cells express GFAP. No proliferating (i.e. Ki67-expressing) cells were detected. **(C)** Immunocytochemistry labeling of neuronal (MAP2) and astrocytic (GFAP) marker as well as Ki67 (*top panel*). Neuronal somata and dendrites were decorated with presynaptic terminals containing vesicular glutamate transporters (vGlut1) at 14 *div* (*lower panel*). Scale bar, 40 µm.

The prepared cortical neurons express the vesicular glutamate transporter 1 (vGlut1) from 14 *div* on, indicating the presence of glutamatergic synapses in culture (see Figure 5.1 C *lower panel*). To evaluate neuronal activity, which will be pharmacologically modulated in subsequent experiments, Ca^{2+}-imaging was performed. At 14 *div*, neurons displayed a synchronized activity pattern (see Figure 5.2 A). Upon addition of transduced astrocytes, the activity pattern was assessed after 7 days of coculture and displayed a sustained synchronized activity pattern (see Figure 5.2 B).

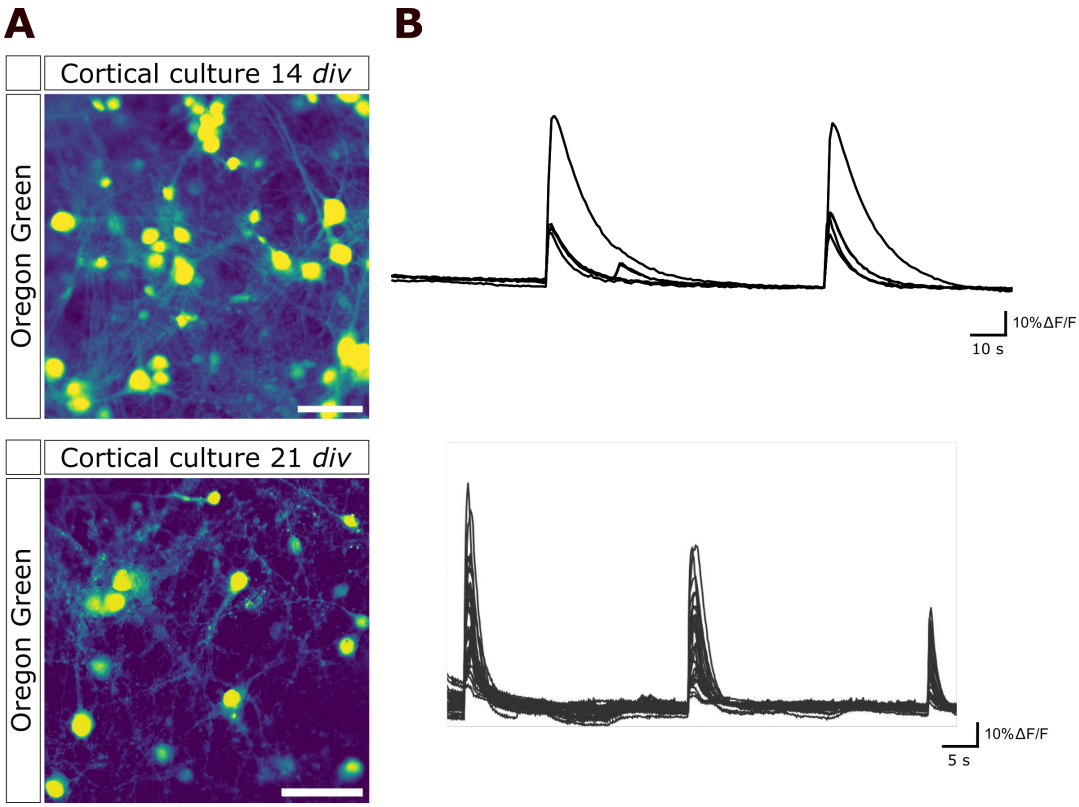

Figure 5.2: **Calcium dynamics of cortical neurons display synchronization after 2 weeks *in vitro*.** **(A)** Imaging of calcium dynamics in 14 *div* old neurons was performed and rhythmic activity was detected. Traces from 10 neurons are shown. **(B)** Calcium imaging from 21 *div* old neurons cocultured with Neurog2-transduced astrocytes at 14 *div*. Synchronized rhythmic activity was sustained. Representative traces from 25 neurons are shown.

In order to further characterize neuronal subtype identities in the culture, immunocytochemical analysis of layer-specific markers was performed. At 14 *div* only weak expression of cortical layer-specific markers could be detected (data not shown); therefore, expression was assessed at 28 *div*. The majority of neurons express the upper layer

(UL)-specific TF Satb2 (70.25 ± 5.72 %), while only 26.29 ± 7.06 % were found to express Cux2 (see Figure 5.3 A). A minor fraction of neurons expresses deeper-layer (DL) markers such as Ctip2 (30.44 ± 2.98 %) or Foxp2 (19.30 ± 8.61 %) (see Figure 5.3 A). In agreement with previous studies, cultured cortical neurons from the E14.5 cortex display mostly UL subtype-identity and display a stable activity pattern *in vitro*.

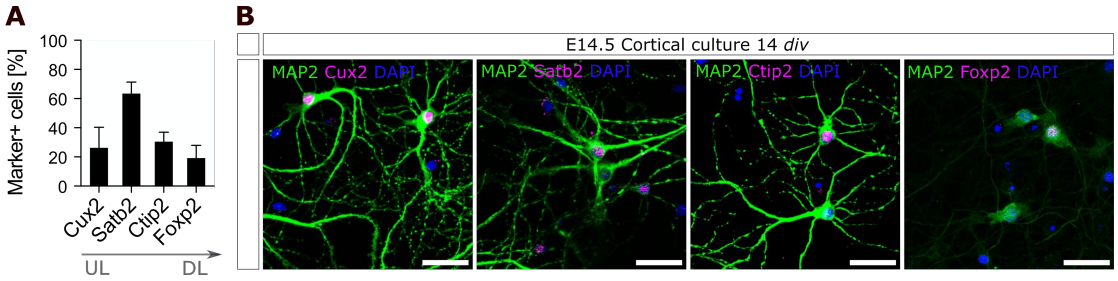

Figure 5.3: **Characterization of cortical layer-specific neuronal identities.**
(A) Immunocytochemical analysis of layer-specific marker expression in neurons after 28 days of maturation. **(B)** Immunocytochemical labeling of layer-specific marker expression in neuronal cultures. Scale bar, 40 µm.

5.1.2 *Characterization of the astroglia-to-neuron conversion process within a neuronal network in vitro*

The reprogramming of astroglia cells into iNs via the ectopic overexpression of neurogenic TFs represents a well-established tool *in vitro* (Berninger et al., 2007; Heinrich et al., 2011; Vignoles et al., 2019). Therefore, astroglial cultures were prepared as previously described (Heinrich et al., 2011) with minor modifications (Sharif et al., 2021). The first set of analyses examined the cellular composition within the glial culture in order to understand the heterogeneity within the initially targeted cell population. For this, cortical glial cultures were prepared from postnatal mice (P4-6) and expanded in culture for 5-7 days and subsequently fixed for immunocytochemical labeling of distinct cell type-specific marker proteins. The majority of cells (80.61 ± 4.49 %) expressed the astrocyte-specific marker glial fibrillary acidic protein (GFAP) (see Figure 5.4 A). In addition, smaller percentages of Iba1-expressing microglia (11.23 ± 3.67 %) or Sox10-expressing oligodendroglia (7.62 ± 1.55 %) were detected (see Figure 5.4 A). Notably, the percentage of neuronal precursor cells (neuroblasts) was assessed and found to be minimal, indicating almost complete absence in the culture (1.89 ± 0.68 %) (see Figure 5.4 A). These results demonstrate a predominant presence of astroglial cells in the culture, which is in line with previous studies relying on this system (Gascón et al., 2016; Heinrich et al., 2010; Masserdotti et al., 2015).

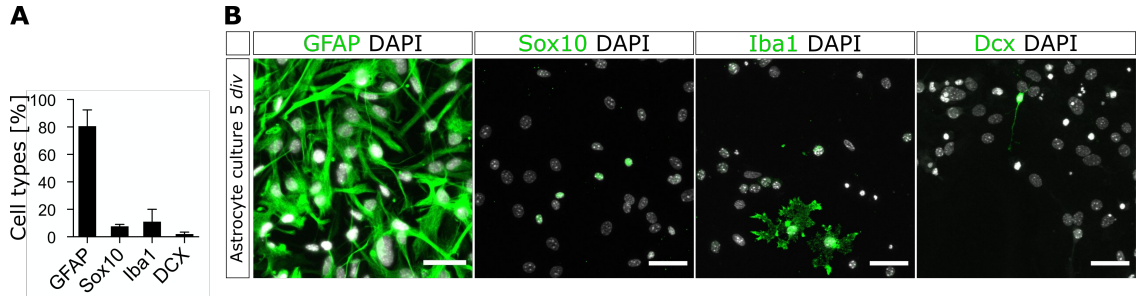

Figure 5.4: **Cellular composition of glial cultures prepared from the postnatal cortex.**
(A) Immunocytochemical analysis of cell type-specific marker expression in distinct glial cells after 5 days of expansion. **(B)** Immunocytochemical stainings of cell type-specific marker proteins. Scale bar, 40 µm.

Diverse glial populations in the culture may display proliferative capacity and hence can be targeted by retroviral transduction. Differences in the ability of distinct glial cells to undergo reprogramming in response to Neurog2 overexpression may affect the estimation of the reprogramming efficiency. Furthermore, heterogeneity within the targeted glial population may result in a heterogeneous iN population. Therefore, the next analysis focused on assessing the proportion of proliferating cells among astrocytes and non-astrocytic cells. As retroviral vectors will target only proliferating cells, the aim was to confirm that the highest proportion of proliferating cells are indeed astrocytes within the culture. In order to assess potential dynamics in proliferative capacity and identify the best time point during which the highest number of proliferating astrocytes can be harvested, two time points were chosen for the analysis. Cells were either fixed after 5 or 7 days in culture and an immunocytochemical labeling of the proliferation marker Ki67 was performed together with the astrocytic marker GFAP. After 5 *div*, 38.06 ± 6.33 % of all cells are found to be proliferating, out of which 72.61 % were GFAP-expressing astrocytes (see Figure 5.5 A). Intriguingly, while there was no significant difference in the percentage of total proliferating cells after two more days (7 *div*: 27.28 ± 9.55 %, (*p-value* 0.4078, unpaired Student's t-test with Welch's correction, n=3 exp. per. cond.), the proportion of proliferating astrocytes decreases to 63.51 % after 7 *div* compared to 72.61 % at 5 *div* (see Figure 5.5 A). The proliferating fraction within the astrocyte population was therefore assessed and found to be significantly decreased after 7 *div* compared to 5 *div* (5 *div*: 52.35 ± 8.151 %; 7 *div*: 21.24 ± 6.09 %, *p-value* 0.0418, unpaired Student's t-test with Welch's correction, n=3 exp. per. cond.) (see Figure 5.5 B). These data demonstrate that albeit astroglia represent the majority of proliferating cells within this system, GFAP-negative cells were found to be proliferating as well, therefore suggesting that non-astroglial cells may be targeted by retroviruses. Moreover, the astrocytic population displays a significant decrease in proliferation rate between 5

and 7 *div*, for which reason the passage and transduction were consistently performed after 5 days of expansion in all experiments.

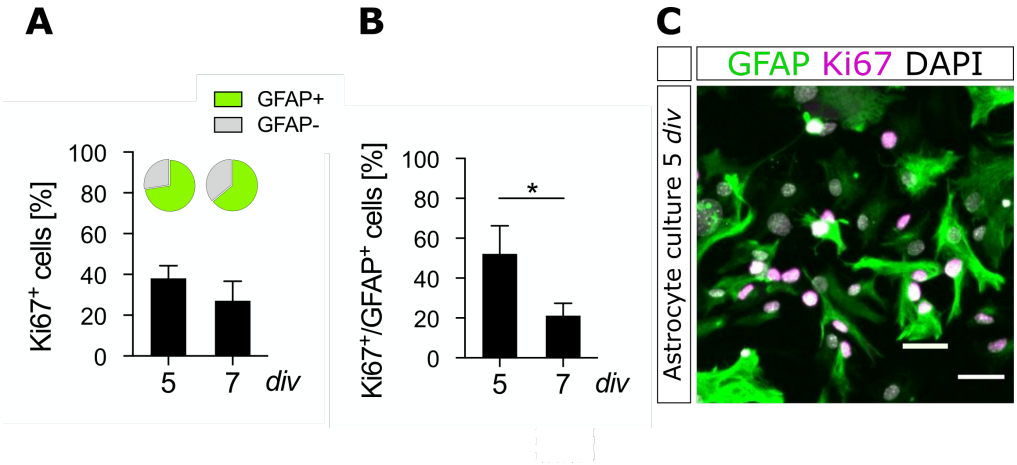

Figure 5.5: **Assessment of proliferation rate in glial culture.**
(A) Immunocytochemical analysis of proliferating (Ki67-expressing) glial cells at 5 and 7 *div* and the proportion of GFAP-expressing astrocytes among proliferating cells visualized as pie charts. **(B)** Immunocytochemical analysis of proliferating astrocytes at 5 and 7 *div* **(C)** Immunocytochemical staining of proliferating (Ki67-expressing) astrocytes (GFAP-expression). Scale bar, 40 µm.

Next, astroglia were passaged after 5 *div* of expansion and transduced with a control vector (CAG-IRES-GFP/-DsRED) in suspension. Cells were then plated onto 14 *div* old cortical neurons and subsequently fixed after 48 hours in order to determine the proportions of distinct cell types targeted by the retroviral vectors. The majority of transduced cells comprised astrocytes (54.69 $\pm$ 2.97 %), however, smaller proportions of microglia (19.76 $\pm$ 4.82 %) as well as oligodendroglia (19.64 $\pm$ 1.07 %) were consistently targeted as well (see Figure 5.6 A). Importantly, DCX, a marker that is transiently expressed in neuroblasts and immature neurons, could not be detected in retrovirally transduced cells (0.00 $\pm$ 0.00 %). These data demonstrate that culturing and transducing glial cells under the mentioned conditions does not lead to retroviral targeting of immediate neurogenic progenitors. Moreover, these data suggest that reprogramming may occur from glial populations other than astroglia, albeit their relative abundance in the culture suggests a minor contribution to the iN population.

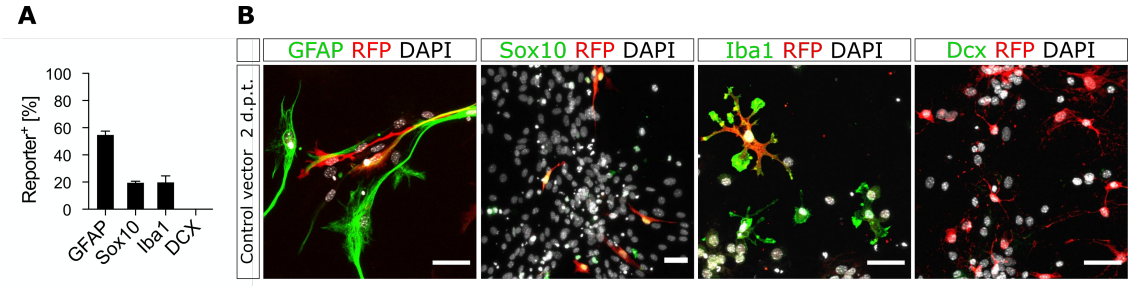

Figure 5.6: **Cell type composition among transduced glial cells assessed in coculture.**
(A) Immunocytochemical analysis of cell type-specific marker expression was performed 48 hours after coculturing retrovirally transduced cells into the neuronal culture. Marker expression was assessed among the transduced population. **(B)** Immunocytochemical staining of cell-type specific marker proteins expressed by transduced cells. After coculturing transduced glial cells with neurons, no neuroblasts were detected among the transduced population. Scale bar, 40 µm.

5.1.3 *Reprogramming of iNs within a cortical network in vitro*

Ectopic expression of Neurog2 in astroglia has been shown to result in the direct reprogramming into excitatory glutamatergic neurons *in vitro* (Berninger et al., 2007; Blum et al., 2011; Heinrich et al., 2010). In this study, the reprogramming process was performed and validated within the co-culture system. Therefore, astroglia were transduced with retroviral vectors encoding for the TF Neurog2 (CAG-Neurog2-IRES-DsRED) after 5 days of expansion and following 12-24 hours passaged and added onto the 14 *div* neuronal culture. A control vector comprising the same plasmid backbone but lacking the Neurog2 gene was used. The reprogramming efficiency was first assessed after 3 days post-transduction (d.p.t.) by performing immunocytochemical analysis of neuron-specific protein expression in transduced cells. Among the Neurog2-transduced cells, 61.5 $\pm$ 7.65 % were found to express the immature neuronal marker doublecortin (DCX), while almost no cells of the control condition displayed DCX expression (0.92 $\pm$ 0.84 %) (see Figure 5.7 A).

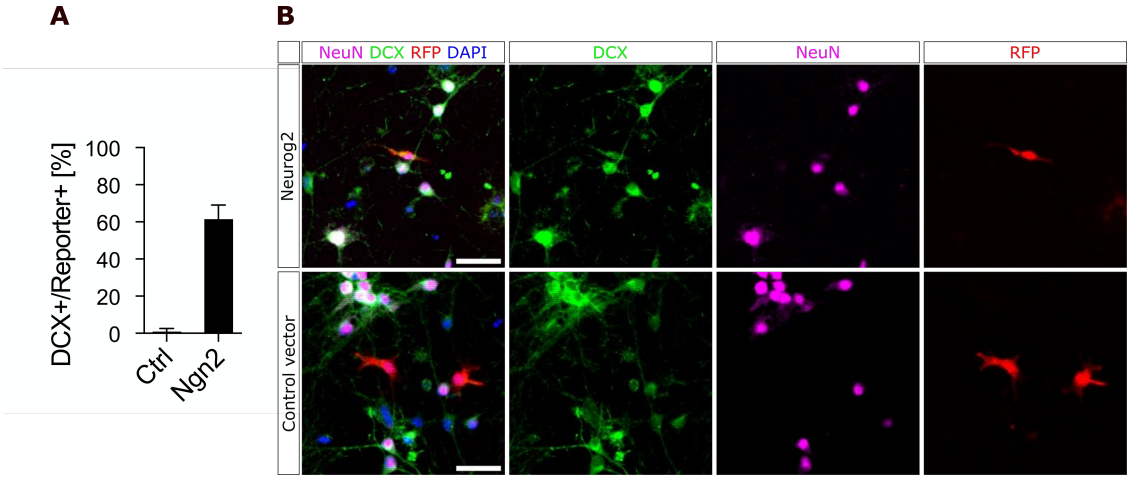

Figure 5.7: **Neurog2-induced reprogramming of glial cells in coculture.**
(A) Expression of neuronal marker DCX in Neurog2- and control-transduced cells. DCX signal is also visible in (untransduced) endogenous neurons. **(B)** Immunocytochemical stainings of neuron-specific marker in transduced cells. At 3 dpt, iNs express the immature neuronal marker DCX but display no expression of NeuN. Scale bar, 40 µm.

Although transduced cells reprogram into iNs within the coculture environment, the proportion of iNs among the transduced cell population was consistently and significantly decreasing between 7 (59.02 ± 5.99%) and 14 d.p.t. (11.60 ± 1.93%) (*p-value* 0.0103, Student's t-test with Welch's correction). This was shown by a decrease in the percentage of NeuN-expressing cells among the transduced population in the absence of proliferation of transduced cells (see Figure 5.9). NeuN-expressing cells were at all times absent in the control transduced cell populations (7 d.p.t.: 1.15 ± 0.46%; 14 d.p.t.: 0.12 ± 0.17%; 21 d.p.t.: 0.00 ± 0.00%). These data suggest that iNs face challenges in surviving in this experimental setting, similar to previous studies studying iNs in a different *in vitro* model (Gascón et al., 2016). In order to promote iN survival, several molecules, which were previously shown to enhance iN survival and maturation, were tested in this setting; e.g. Forskolin or α-tocopherol treatment (Gascón et al., 2016). While Forskolin treatment from d.p.t. 5 did not show any improvement of iN survival, treatment with α-tocopherol resulted in non-viable cocultures several days after treatment as observed by brightfield microscopy (data not shown). While previous studies showed an enhanced iN survival, the survival could not be improved in coculture. Therefore, astroglia cells were transduced with retroviruses encoding for Neurog2 and the anti-apoptotic and anti-ferroptotic factor Bcl-2, which has been previously shown by work in the lab to promote the survival and maturation of Neurog2-induced iNs (Gascón et al., 2016). Overexpression of Neurog2-Bcl2 resulted in iNs which displayed expression of immature neuronal markers DCX or βIII-tubulin at 3-4 d.p.t. along with expression of Tbr2 (see Figure 5.8).

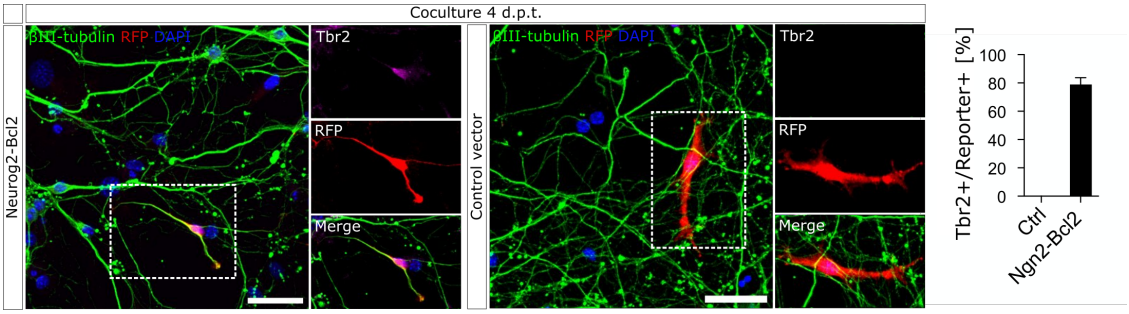

Figure 5.8: **Induced neurons express Tbr2 - a marker specific to the neurogenic process generating glutamatergic PNs.**
Immunocytochemical staining of cocultured neurons against βIII-tubulin and Tbr2 shows expression in iNs at 4 d.p.t. Expression of these neuronal markers are absent in control transduced cells. Scale bar, 40 µm.

Indeed, transducing astroglia with a construct encoding for both Neurog2 and Bcl-2 (CAG-Neurog2-T2A-Bcl2-IRES tagged with -H2B-GFP or -DsRed) resulted in initially similar reprograming efficiency to Neurog2-only transduced cells at 7 d.p.t. (Neurog2: 59.02 ± 5.99%; Neurog2-Bcl2: 59.11 ± 4.80%), but greatly improved survival of iNs as assessed at 14 d.p.t. (Neurog2: 11.60 ± 1.93%; Neurog2-Bcl2: 54.54 ± 10.04%, see Figure 5.9).

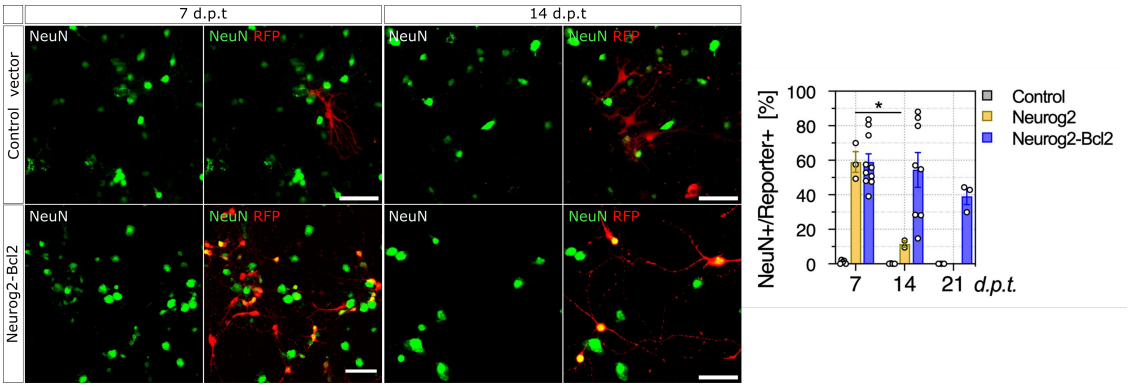

Figure 5.9: **Survival of induced neurons beyond one week in coculture requires Bcl-2.**
Immunocytochemical staining of cocultured neurons against the neuronal marker NeuN and the fluorescent reporter RFP at 7 and 14 d.p.t. and quantification of NeuN-expressing cells among all RFP-positive cells (*right*). Coexpression of Bcl2 leads to an extended viability of iNs in coculture with eNs compared to Neurog2-only expression. No NeuN-expressing cells were detected in control transduced cells. Scale bar, 40 µm.

Expression of DCX is maintained for 7-10 days but displays decreasing expression intensities while NeuN expression is upregulated, suggesting that constitutive overexpression of Neurog2 does not affect the maturation process. Moreover, these Neurog2-Bcl2-iNs mature into morphologically complex neurons within approximately 2 weeks in coculture. An increase in morphological complexity was assessed by quantification of the

primary dendritic branch number across two time points (see Figure 5.10 A). Moreover, an increase in nuclear size (measured based on the DAPI signal as a landmark) was used as a further indication of (morphological) maturation. The observed increase in nuclear size at distinct time points was further compared to age-matched cortical neurons. Albeit variability was observed at each time point in both neuronal populations, possibly reflecting distinct neuronal types or maturation trajectories, mean nuclear area was similar between iNs and age-matched eNs at all time points (see Figure 5.10 B). This may suggest a time-matched developmental trajectory in iNs and eNs as opposed to a potentially prolonged maturation period of iNs.

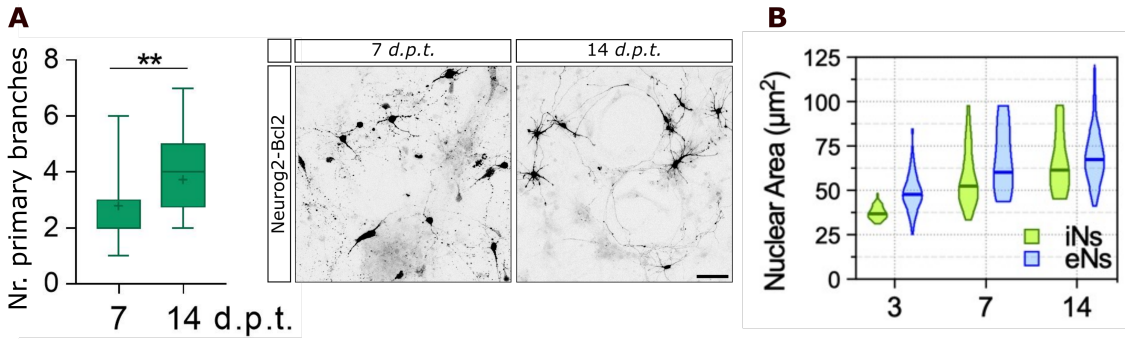

Figure 5.10: **Features of iN morphological maturation in coculture.**
(A) Number of primary branches extending from the neuronal soma were counted at 7 and 14 dpt and was significantly increased (n[cells]=74 (7 dpt) and 34 (14 dpt) from 3-4 biological replicates). Overall morphological complexity was visibly increasing as assessed by dendrite length. Representative images visualizing iNs based on reporter signal. **(B)** Nuclei size of iNs and age-matched eNs were measured based on DAPI (3 dpt/div) or NeuN signal. Scale bar, 40 µm.

At 14 dpt, Ca^{2+}-imaging was performed in coculture in order to assess the iN activity pattern. Unlike the strictly synchronized burst firing observed in eNs, iNs mostly display asynchronous neuronal firing, however, with intermittent participation in cortical burst firing (see Figure 5.11). Hence, the available data suggest that iN seem to participate in cortical burst firing and, based on synchronized calcium traces, are synaptically connected with eNs (see Figure 5.11).

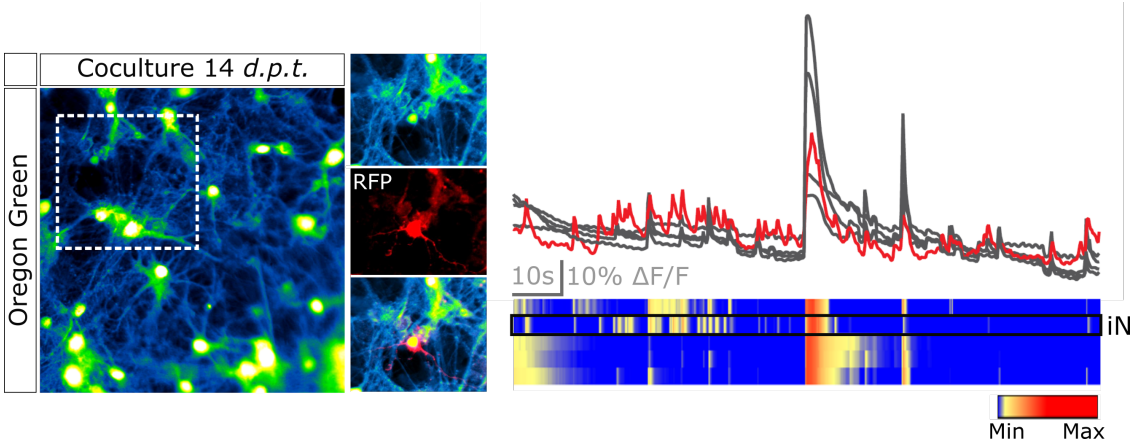

Figure 5.11: **Calcium dynamics of iNs suggest functional connectivity with eNs.**
Imaging of Ca^{2+}-dynamics in iNs was performed after 2 weeks of coculture. Partly synchronous firing of iNs and eNs suggests connectivity.Astrocytic calcium waves were filtered out.

I aimed to maintain the coculture for a longer period in order to obtain more mature iNs. However, although the proportion of NeuN-expressing cells among all transduced cells did not significantly change between 14 and 21 d.p.t. (39.10 ± 4.57% at 21 d.p.t., see Figure 5.9), iN density significantly decreased (density at 14 d.p.t.: 46.80 ± 4.81, 21 d.p.t.: 19.25 ± 3.71; *p*-value = 0.004; see Figure 5.12 *right*), concomitant with an observed loss of iN viability as assessed by observed dendritic beading (see Figure 5.12 *left*). Notably, the viability of eNs as assessed by changes in density as well as morphological parameters, was not compromised up to 6 weeks *in vitro*. Therefore, all further experiments were consistently performed at 14 dpt.

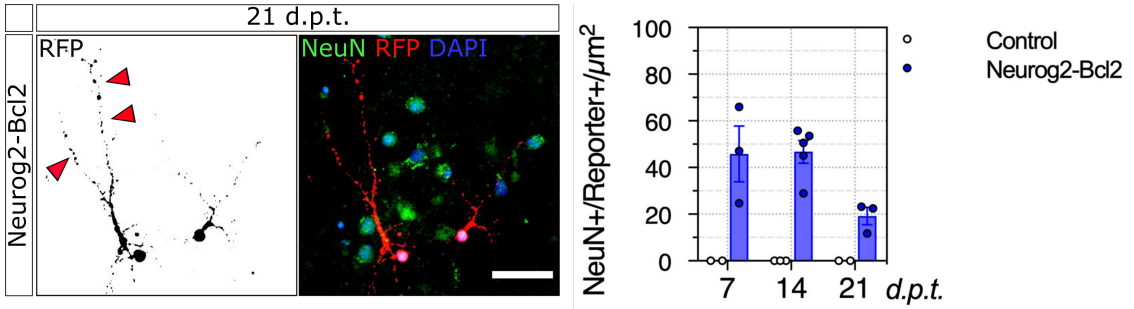

Figure 5.12: **Reduced viability of induced neurons after 3 weeks in coculture.**
Immunocytochemical staining of induced neurons at 21 d.p.t. show dendritic beading (*left*). Density of NeuN-expressing transduced cells assessed across distinct time points in coculture shows a drop between 14 and 21 dpt (*right*). Scale bar, 40 µm.

Interestingly, iNs displayed a high variability of morphological phenotypes as well as evident heterogeneity in the expression of the maturation-associated marker MAP-2 at 14 d.p.t., suggesting the presence of iNs at distinct stages of maturation (see Figure 5.13).

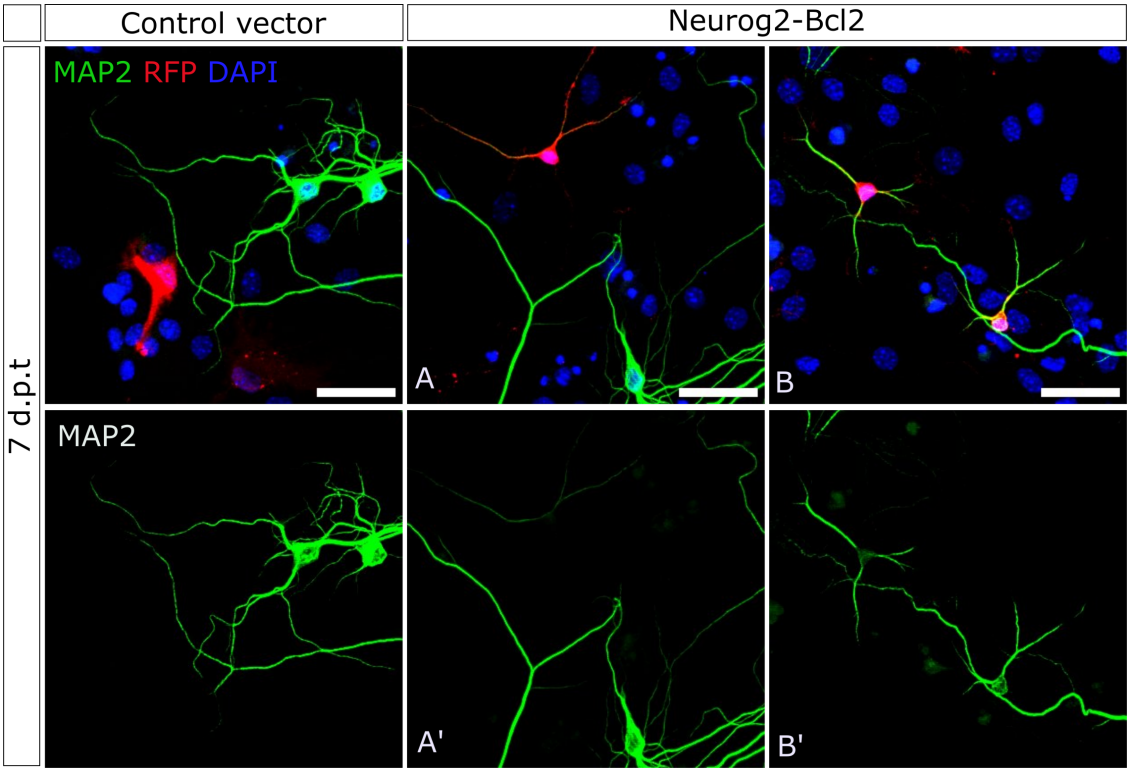

Figure 5.13: **Heterogenous MAP-2 expression levels in induced neurons.**
Immunocytochemical staining of MAP-2 in control transduced (left) and Neurog2-Bcl2 transduced (right) cells. Scale bar, 40 µm.

In sum, these data show that Neurog2-Bcl2 overexpression in glial cells cocultured with mature eNs results in the generation of iNs that display relatively mature neuronal features. However, further maturation seems compromised due to limited long-term survival, as most iNs did not display a viable phenotype beyond approximately 2 weeks in coculture.

5.2 ACTIVITY-DEPENDENT GENE REGULATION IN INDUCED NEURONS

5.2.1 *iNs display IEG upregulation in response to L-VGCC activation*

Previous studies have shown that iNs reprogrammed from astroglia acquire the ability to fire action potentials and form functional synapses (Blum et al., 2011; Heinrich et al., 2010). However, it has not yet been addressed whether iNs would participate in the activation that a specific stimulation exerts on the neuronal network and whether this activation is reflected in meaningful gene regulation that resembles the one elicited in endogenous neurons (eNs). To investigate neuronal activity-induced changes in gene expression, cocultured induced and endogenous neurons were subjected to elevated levels of potassium chloride (KCl). This stimulation paradigm relies on membrane depolarization through activation of L-VGCC and subsequent calcium influx, which leads to the induction of a specific set of canonical TFs which, in turn, initiate subsequent gene regulation specific to the triggering stimulus intensity and duration (Brigidi et al., 2019; S. Cohen and Greenberg, 2008). Membrane depolarization by elevated KCl levels is hence a well-established approach used to study the effect of increased synaptic excitation on gene expression changes that ultimately contribute to neuronal plasticity (Krukoff, 2003; Murphy et al., 1991). Moreover, calcium influx through L-VGCC has been shown to be the key mediating event driving c-Fos expression (Madabhushi and Kim, 2018). IEG expression and *de-novo* protein synthesis are induced within minutes after stimulation and constitute an essential component for long-lasting synaptic plasticity (Brigidi et al., 2019). Here, the activity-dependent regulation of prototypical IEGs was assessed via immunofluorescence staining and analysis of corresponding protein levels. In order to selectively assess the L-VGCC-mediated rise in IEG protein expression following activation, effects mediated via NMDARs and non-NMDARs were eliminated by treating cells overnight with APV (NMDAR antagonist) and CNQX (AMPAR/kainate receptor antagonist), respectively, and silenced via application of TTX (sodium channel inhibitor). Membrane depolarization was induced by treating cells for 3 hours with 55 mM KCl and subsequently fixed and immunocytochemical staining was performed for protein expression of the IEG *c-Fos* along the neuronal marker NeuN or MAP2. Both neuronal populations, eNs and iNs, display a robust and significant increase in c-Fos protein expression following KCl stimulation (eNs: 1.85 ± 0.05, iNs: 2.35 ± 0.17, FC increase $\pm$ SEM, in both cases $p\text{-}value < 0.0001$, Student's t-test with Welch's correction, see Figure 5.14). Interestingly, c-Fos upregulation is stronger in iNs than eNs, and the proportion of iNs that increase c-Fos expression at least 1.5-fold compared to control levels was found to be higher than the percentage of eNs (71.43 % compared to 50.56 % in iNs and eNs, respectively), suggesting a facilitated depolarization of iNs compared to eNs, possibly due to a higher intrinsic excitability.

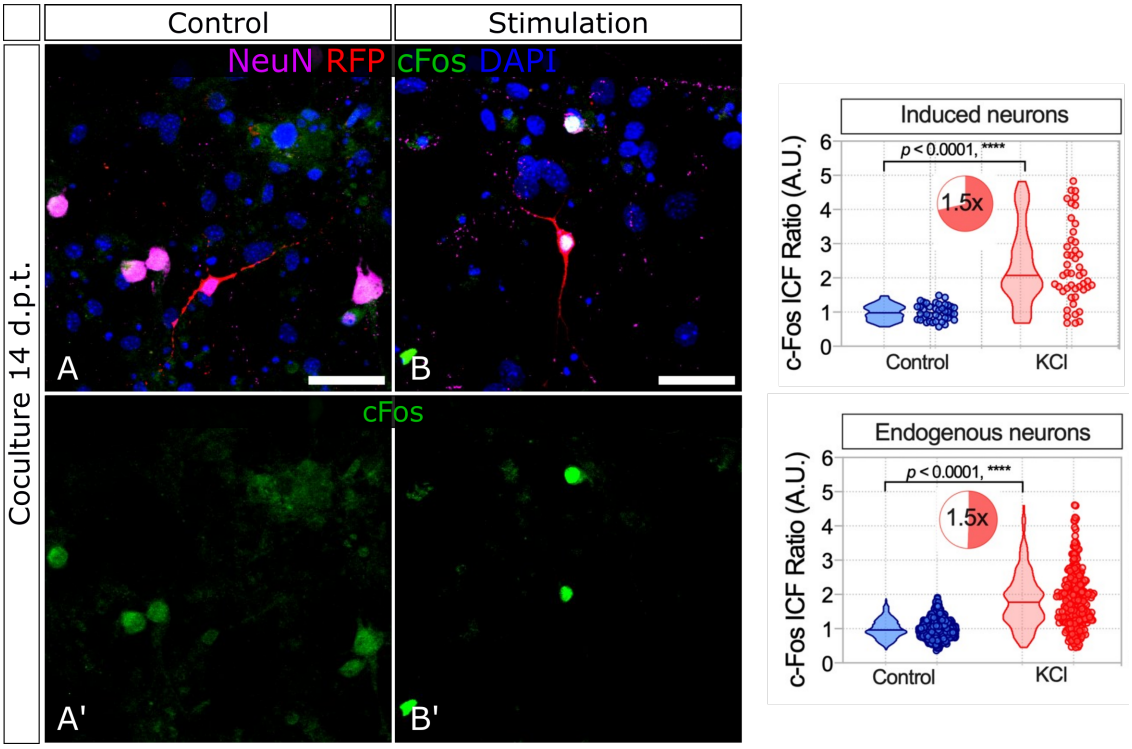

Figure 5.14: **c-Fos upregulation in response to elevated KCl in induced and endogenous neurons.** c-Fos upregulation in induced and endogenous neurons following high KCl treatment was evaluated based on immunocytochemistry stainings (*left*). c-Fos protein expression intensities in stimulated neurons were normalized to the control group. (*right*). Scale bar, 40 µm.

Second, activity-dependent regulation of the 'effector' IEG Arc was assessed. In contrast to c-Fos, Arc is not a TF but a cytoskeleton-associated protein (Chung et al., 2017). Its mRNA as well as protein is usually enriched at dendritic sites that display active synapses and have been shown to mediate synaptic plasticity (Dynes and Steward, 2007; Lyford et al., 1995). Similarly to c-Fos, Arc was strongly upregulated in iNs (2.17 ± 0.15 FC increase, $p\text{-value} < 0.0001$, Student's t-test with Welch's correction) following KCl depolarization (see Figure 5.15). Similarly, Arc upregulation was observed in eNs (2.08 ± 0.07 FC increase, $p\text{-value} < 0.0001$, Student's t-test with Welch's correction). Similar proportions of neurons were found to increase Arc expression at least 1.5-fold compared to control levels (59.7 % and 53.1 % in iNs and eNs, respectively). Intriguingly, while Arc expression following KCl treatment was detected in somatic as well as dendritic regions in eNs, Arc expression in iNs was restricted to the somatic area (see Figure 5.15).

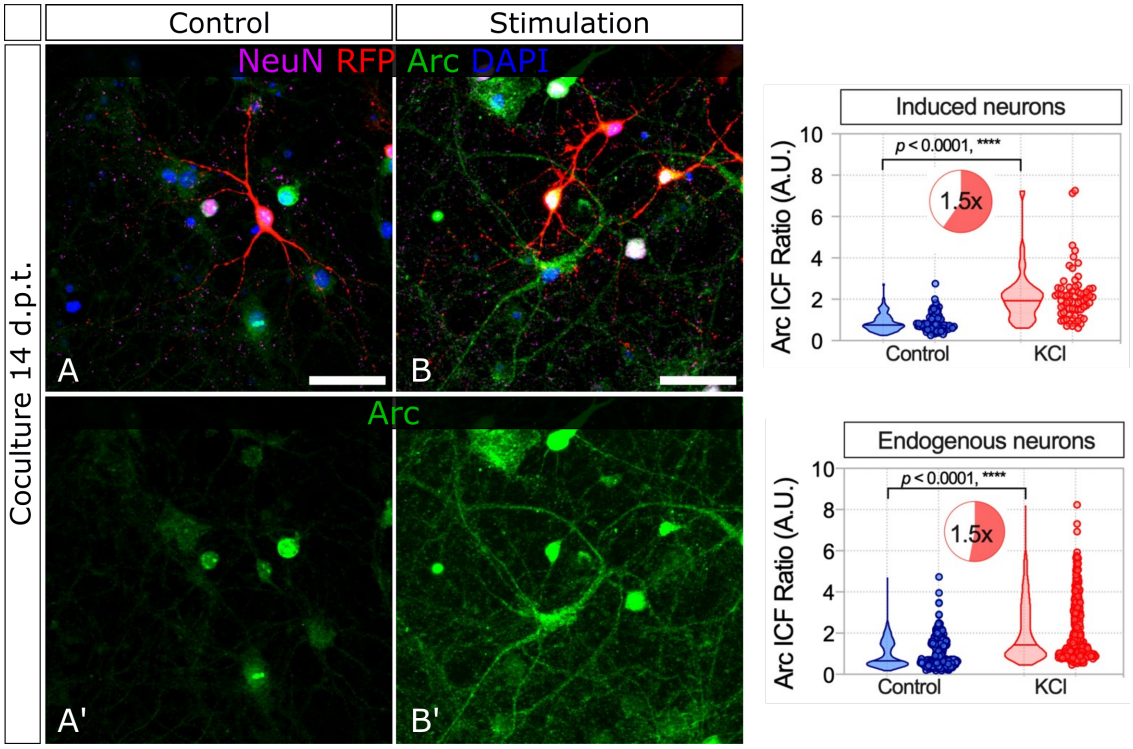

Figure 5.15: **Arc upregulation in response to elevated KCl in induced and endogenous neurons.** Arc upregulation in induced and endogenous neurons following high KCl treatment was evaluated based on immunocytochemistry stainings (*left*). Arc protein expression intensities in stimulated neurons were normalized to the control group. (*right*). Scale bar, 40 µm.

In summary, these data demonstrate that iNs, which matured in a cortical neuronal network, express prototypical activity-dependent IEGs and respond robustly to KCl-induced depolarization by upregulation of these genes.

5.3 DISSECTION OF CELL TYPE HETEROGENEITY BY SNRNA-SEQ

Based on the findings that iNs possess the ability to upregulate IEGs in response to depolarization and participate in network activity dynamics, the next focus was to assess whether they display the ability to undergo genome-wide transcriptional modulations in response to a change in network activity level which would reflect synaptic integration into the network. Moreover, transcriptional profiling of neurons was carried out with the aim of dissecting differences in neuronal identity and maturation stages between iNs and eNs. Specifically, transcript levels of neuron-defining features that dictate electrical excitability or synaptic properties were compared across the neuronal populations. In order to explore genome-wide activity-regulated gene transcription, co-cultured iNs and eNs were maintained for 12 days under normal conditions and subsequently either exposed for 48 hours to the glutamate receptor antagonists CNQX and APV and the sodium channel inhibitor TTX (inhibited population) or maintained under control condition (with medium changes performed according to the treatment, excluding inhibitors) (see Figure 5.16). Previous work has shown that the combination of these receptor antagonists robustly depresses excitatory activity and synaptic transmission *in vitro* and induces synaptic upscaling via an increase in postsynaptic sensitivity to glutamate, mainly driven via the upregulation of AMPARs (Deeg and Aizenman, 2011; Gonzalez-Islas et al., 2018; O'Brien et al., 1998; H. L. Wang et al., 2011). After activity inhibition, nuclei were isolated and subsequently sorted based on the histone H2B-eGFP reporter using FANS (see Figure 3.2). Samples from 3 biological replicates with 2 technical replicates of each condition were then pooled and handed to the TRON GmbH for downstream processing and snRNA-seq using the 10x Chromium v3.1 protocol. For detection of neuronal activity-regulated gene transcription, snRNA-seq has been shown to yield more accurate results compared to scRNA-seq as the sample preparation protocol does not require any enzymatic digestion that can lead to aberrant transcription overlapping with gene expression profiles known to be induced during acute activity stimulation protocols and which may confound downstream analysis (Lacar et al., 2016).

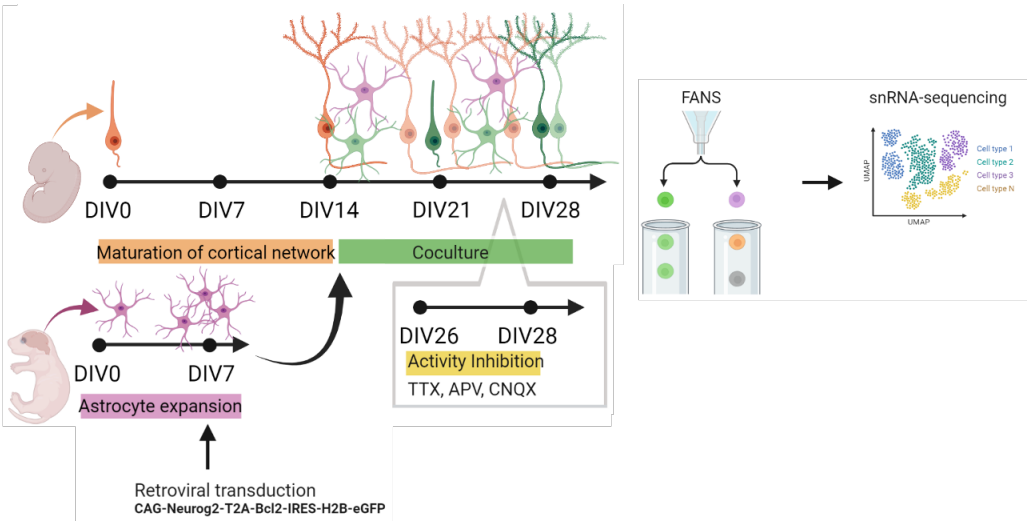

Figure 5.16: **Schematic depicting the snRNA-seq experimental design.**
Cortical neurons were prepared from E14 cortices and matured for 14 *div*. In parallel, astroglia cultures were prepared from the postnatal cortex and expanded for 5 days before being transduced and passaged into the neuronal culture. Induced neurons mature for further 2 weeks in coculture. At 12 dpt, network activity was pharmacologically inhibited by the application of CNQX, APV, and TTX. 48 hours later, nuclei were isolated, FAN sorted and sequenced using the 10x Chromium. The figure was assembled using BioRender.

Following preprocessing and QC steps (see Figure 3.3), the final dataset comprised a total of 1029 cells with a total detection of 20615 genes (see Figure 5.17). Exploring the composition of the samples within the snRNA-seq dataset revealed that of the 1029 cells, 260 cells (25.27 % of the total cell population) were containing the H2B-eGFP reporter, hereinafter referred to as the "transduced" population, while the remaining 769 cells (74.73 % of the total cell population) are hereinafter referred to as the "endogenous" population (5.17 A). Among the endogenous population, 297 of the cells are derived from the activity-inhibited population (38.62 % of the endogenous cell population), while among the transduced cells, 158 (60.76 % of the transduced cell population) cells are derived from the activity inhibition group (5.17 B). While there were around 1.5 times more cells retrieved in the active endogenous population, 1.5 times more cells of the inactive transduced population were recovered (see Figure 5.17 B). Interestingly, transduced and endogenous cells are mostly found in distinct clusters within the UMAP embedding. The first aim in analyzing the dataset was to obtain a comprehensive understanding of the cellular heterogeneity within the culture system. Obtaining an accurate identification of each cell type or state was considered a critical prerequisite to examining activity-induced gene transcription, in particular due to cell-type specific transcriptional responses to changes in activity levels (Gray and Spiegel, 2019). In order to assign a biological label to each cell type, initially canonical cell-type specific marker genes were used to characterize the cellular composition, similar to other single-cell

transcriptomic studies (Lin et al., 2021a). Neurons were identified based on NeuN (Rbfox3) expression and comprised the majority of endogenous, and importantly, of transduced cells (see Figure 5.17 C). The expression pattern of vGlut1 (Slc17a7) was visualized on the UMAP in order to estimate the portion of mature glutamatergic neurons. The majority of endogenous cells are expressing vGlut1, however, low expression was found among the transduced population, suggesting distinct developmental stages between the two neuronal populations. Moreover, among both sample types, expression of Gad1/2 was detectable (see Figure 5.17 C).

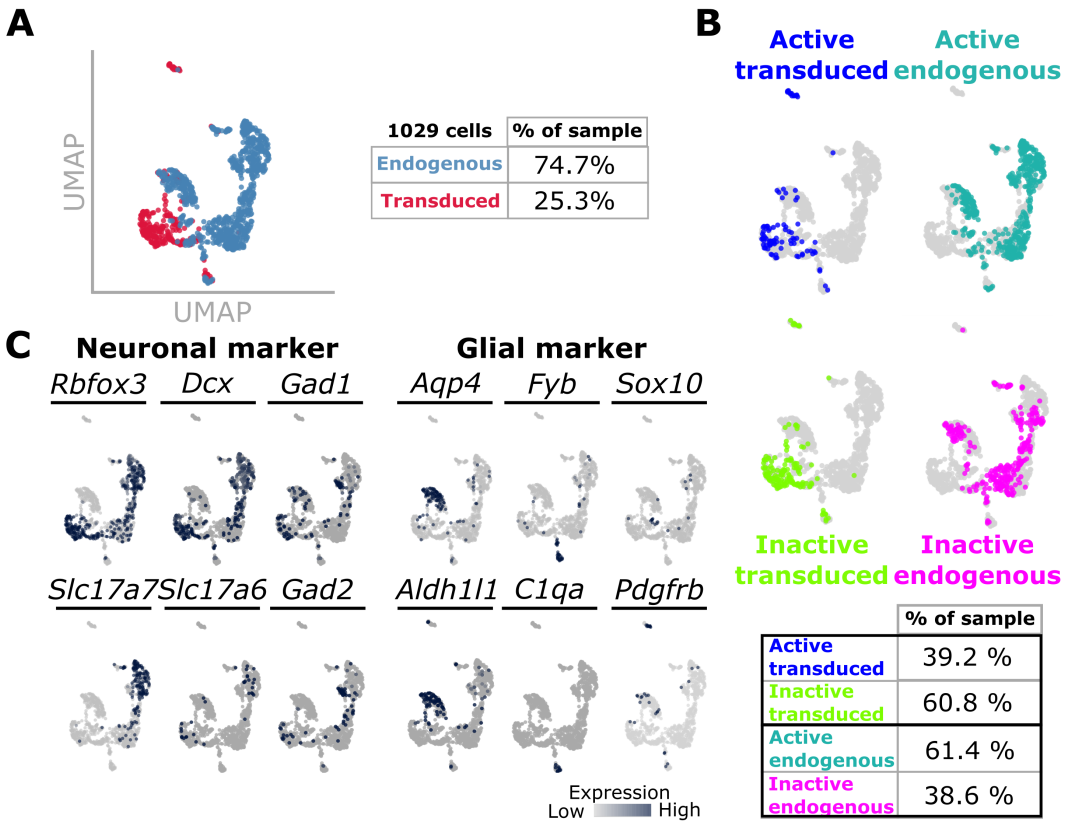

Figure 5.17: **Cell type composition within the coculture system identified single-nucleus RNA-sequencing.** A total of 1029 cells were retrieved from the snRNA-seq experiment and are visualized using UMAP embedding. Cells are colored by cell source **(A)** or sample treatment **(B)**. Distribution of sample types on the UMAP plot and percentages identified by snRNA-seq. **(C)** Expression profiles of canonical neuron- and glial-specific marker genes are visualized on individual UMAP plots.

Other cell types, such as astroglia and microglia, identified based on the expression of glial marker Aquaporin-4 (Aqp4) and Aldh1l1 or Fyb and C1qa, respectively, were both abundant and displayed each a coherent cluster within the UMAP. Smaller cell numbers are found for Sox10 and Pdgfrb expressing cells that do not form an independent cluster

within the dataset but are scattered throughout the UMAP embedding (see Figure 5.17 C). Finally, the UMAP embedding reveals that cells are organized primarily by major cell classes, while the transduced population, albeit being abundantly NeuN-positive, is segregated from the endogenous neuronal population. The identification of cellular identity based on the expression of predefined canonical cell type-specific markers is a widely used approach when annotating cellular identities in transcriptomic datasets. Such cell type markers are usually either well-established markers known from the literature or can be retrieved from available databases. Cells that display a characteristic expression pattern of such marker genes are then annotated accordingly. However, the use of such cell type-specific markers does not allow a clear resolution of cell type heterogeneity within the dataset, especially crucial when reprogramming cells towards a neuronal identity that has yet to be defined in detail. Better approaches in identifying and annotating cellular identities of individual cells have been recently established and rely on the use of reference single-cell datasets and function via a "guilt-by-association" approach (Clarke et al., 2021). Gene expression profiles of cells of the dataset to be annotated (so-called 'query dataset') are compared to gene expression signatures of defined cell types of a reference dataset and, if cells are sufficiently similar, the identity of the reference cell gets assigned onto the query cell. This has the advantage that the identities of individual cells are assessed independently of neighborhood, consequently minimizing the odds of overlooking relevant differences between distinct cells of the same cluster within the query dataset. Moreover, this approach facilitates the identification of novel cell types by reducing the chance of misassignment. However, this approach is only meaningful when reference datasets of high quality are chosen. In this work, scmap (Kiselev et al., 2018) was used as a tool to assess the transcriptional identities of cells, especially with regard to the transduced population. Moreover, a developmental axis was incorporated by mapping the query dataset simultaneously to three reference datasets from distinct developmental stages of the murine brain. The embryonic dataset comprises an extensive *per diem* single-cell profiling of the whole mouse brain spanning from E7 to E18 (La Manno et al., 2021). The 'adolescent dataset' was obtained by performing comprehensive single-cell profiling of the central and peripheral nervous system of P12 to P30 mice (Zeisel et al., 2018), while the 'adult dataset' covers the whole isocortex and hippocampal formation from P50 to P120 (Yao, van Velthoven, et al., 2021). Although individual cells are projected onto the reference datasets, the tool requires that the query cells have been clustered as well. Therefore, an unsupervised leiden clustering was performed and a total of 12 independent clusters were obtained and are visualized in figure 5.18 B. Moreover, the 100 most variable genes across the subpopulations of each reference dataset were selected for projections (see Table 16). Three similarity scores between the signatures of query cells and cells of the reference datasets were then

calculated (cosine similarity, Spearman and Pearson correlations) and, if criteria were fulfilled (see Methods chapter), cell type identities were assigned onto matching query cells. In total, 51 distinct cell identities were distinguished based on this approach and are listed in table 17 for complete inspection. Cells belonging to similar broad cell type categories (astrocytes, oligodendrocytes, blood-, vascular-, immune- and barrier (BVIB) cells, GABAergic neurons, glutamatergic neurons) were then manually pooled. The Sankey diagrams in figure 5.18 C visualize the proportion of cells from each leiden cluster assigned an identity that was summarized in 6 broad categories (*left Sankey plot*) and the proportion of cells that got assigned an identity based on one of the three reference datasets (*right Sankey plot*).

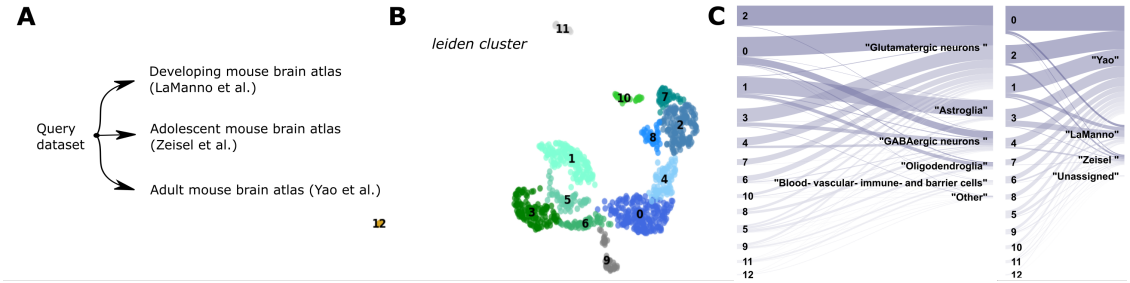

Figure 5.18: **Projection of single cells onto reference datasets confirms the presence of distinct cellular populations.**
(A) The query dataset was projected simultaneously onto three developmentally distinct reference datasets. **(B)** UMAP embedding with cells colored by leiden cluster. Unsupervised leiden clustering was performed with a resolution of 0.4 **(C)** Sankey plots visualizing the mapping of query cells from projecting from leiden clusters into summarized cell groups.

The compositions of cell types across transduced and untransduced cells was then examined independently (see Figure 5.19). As predicted, most of the cells in both groups are glutamatergic neurons (62.18 % and 56.2 % among untransduced and transduced, respectively) and a minor proportion of GABAergic neurons was detected as well (14.54 % and 14.34 % among untransduced and transduced, respectively, see Figure 5.19 A and B). Astrocytes (transduced: 13.95 %, untransduced: 14.67 %), BVIB (transduced: 8.14 %, untransduced: 1.35 %) and oligodendroglia cells (transduced: 2.71 %, untransduced: 6.46 %) were all found among both transduced and non-transduced cells. Only a very small fraction of all cells could not be assigned an identity and is labeled as "Other" (transduced: 4.65 %, untransduced: 0.81 %). The cell classes distributed mostly similarly across the four experimental conditions, with only BVIB cells being present more prominently among the transduced cell populations (see Figure 5.19 C). Moreover, pharmacological activity modulation did not result in distinct sample composition regarding distinct cell classes (see Figure 5.19 D).

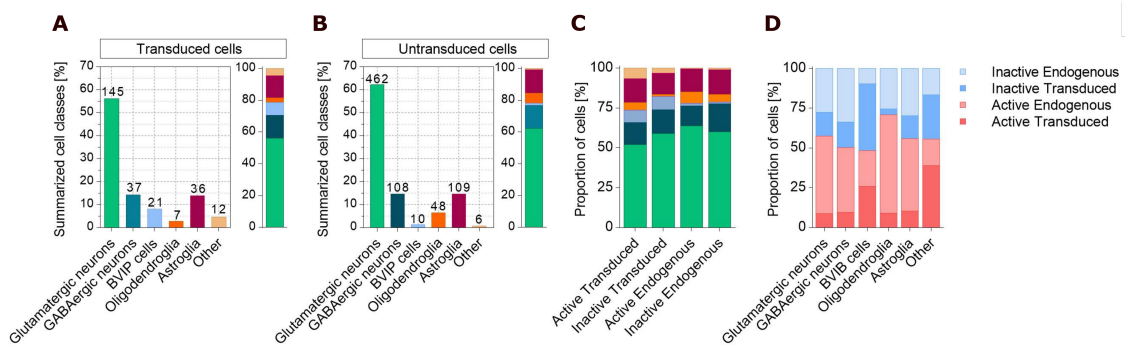

Figure 5.19: **Characterization of sample compositions across experimental conditions.**
(A) Distribution of cell classes among transduced and endogenous **(B)** cells. The numbers above the bar plots indicate total cell numbers. **(C)** Proportion of cells belonging to distinct cell classes in each experimental condition. **(D)** Distribution of experimental conditions across the distinct cell classes.

The quality of the assignment of identities and clustering into major cell type groups was assessed via three means. First, the expression pattern of canonical cell type-specific markers across the 6 main groups was assessed. As figure 5.20 A shows, cell-type specific genes were mostly enriched within distinct groups. Genes such as Fyb, Tgfbr1, and Gad1/2 display an exclusive expression in specific cell types (Immune-related cells and GABAergic neurons, respectively), however, most marker genes, although displaying strong enrichment for distinct cell classes, are expressed at various levels across multiple groups. For example, Sox6 expression is detected in oligodendrocytes and GABAergic neurons, but also in astrocytes. Therefore, and as a second approach, gene signatures that are group-specific were identified via a Wilcoxon rank-sum test, and the top 10 most highly expressed genes of each group were plotted onto a reference dataset that was not used for assignment of cell identities but spans the cell type diversity of the cerebral cortex (Di Bella et al., 2021). The expression of group-specific genes across annotated cell types of the reference dataset is visualized in figure 5.20 C. The matrix plot displays the almost exclusive expression pattern of cell cluster-specific genes in cell types belonging to the corresponding cell class. As a third validation method, Pearson correlation between the 6 cell classes was calculated based on the first 50 PCA components and visualized in a matrix plot in figure 5.20 B. In line with the other two approaches, distinct clusters show little correlation with other cell type clusters (see Figure 5.20 C). In conclusion, these data show that the approach of cell projection onto reference datasets comprising three distinct developmental stages accurately captured cell type diversity.

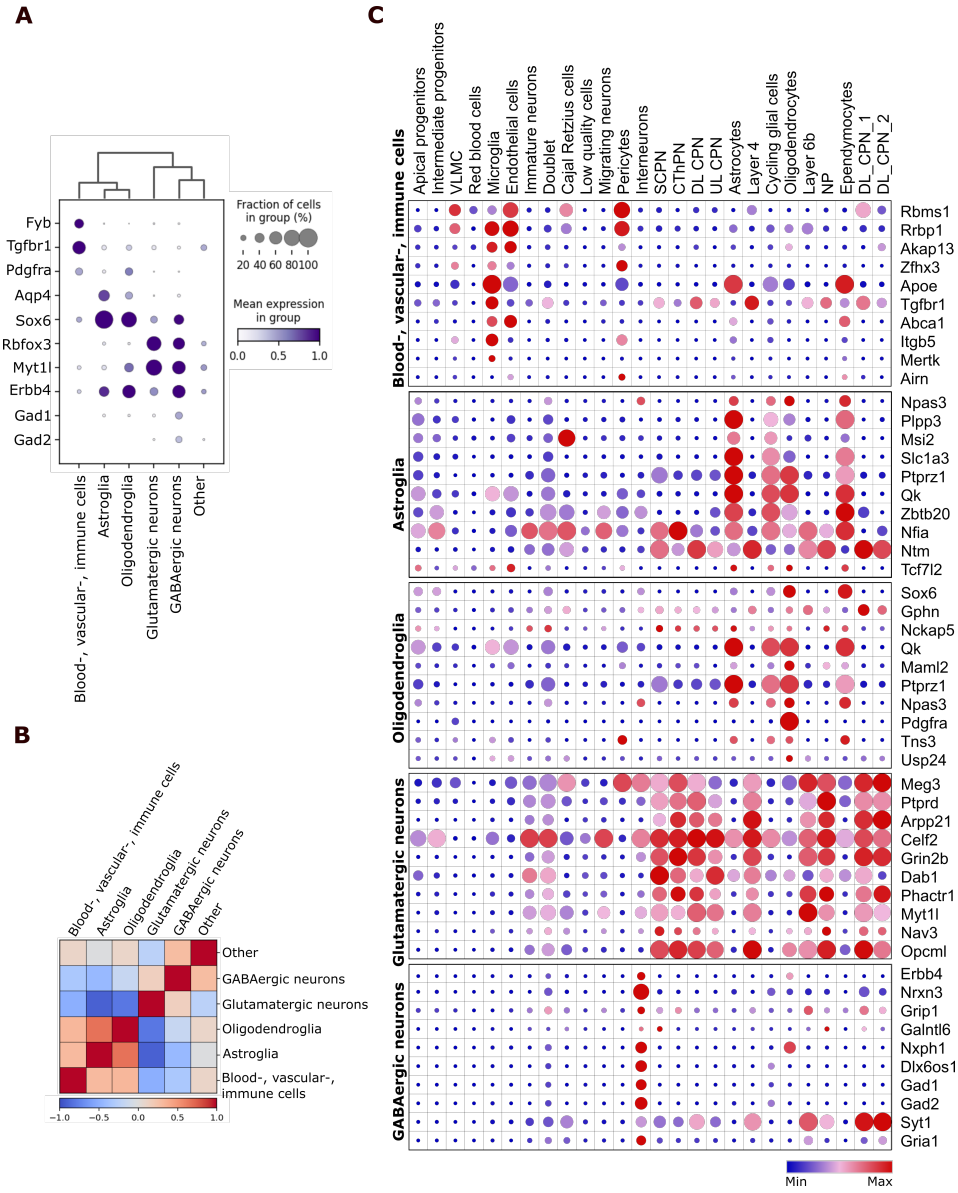

Figure 5.20: **Validation of cell type identification.**
(A) Expression of well-established cell-type specific genes in summarized cell type groups verifies that each group contains **(B)** Correlation matrix of summarized groups verifies that each cluster contains minimal to no contamination with other cell types **(C)** Wilcoxon rank-sum test with Benjamini-Hochberg correction was performed on all cell type clusters and the top 10 genes specifically expressed in each cluster were plotted onto the Di Bella et al., 2021 dataset. The expression pattern verifies that genes expressed in each cluster display cell-class specificity. (Abbreviations: *VLMC* - vascular and leptomeningeal cells, *SCPN* - sub cerebral projection neuron, *CThPN* - corticothalamic projection neuron, *DL CPN* - deep layer cortical projection neuron, *UL CPN* - upper layer cortical projection neuron)

5.3.1 *Transcriptomic characterization of neuronal subtype heterogeneity within the iN population*

A central issue regarding iN populations obtained from various starting cell populations has often been the extent of acquired heterogeneity of neuronal subtypes (Lin et al., 2021a). In this study, projection of iNs onto three reference atlases comprising cortical and hippocampal neurons of distinct maturation stages was performed in order to identify the closest similarity to a neuronal subtype. As shown in Figure 5.19, the majority of cells comprised glutamatergic and GABAergic neurons, therefore, a subset of the snRNA-seq dataset was created that comprised only those cells annotated as neuronal cells. From here on, 'induced neuron' describes a cell that was found among the transduced population (referred to as 'induced'), displayed Rbfox3 expression and projected onto a neuronal cell type derived from any of the three references. Other neuron-specific markers, such as *Myt1l, Mapt, Dcx*, are largely expressed among both neuronal populations (see Figure 5.21 D). The neuronal dataset comprised a total of 752 cells with a total of 20615 detected genes. Out of these, 182 cells were iNs (24.20 % of the total neuronal population), from which 115 cells were derived from the inhibited cell population (63.18 % of all iNs).

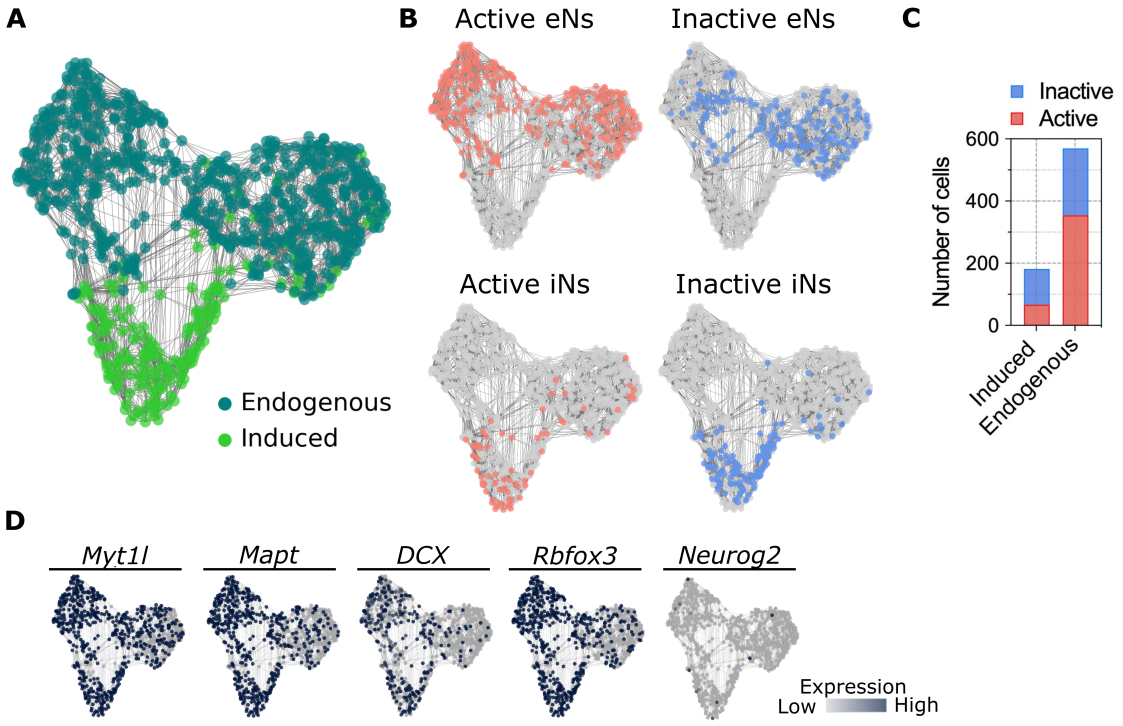

Figure 5.21: **UMAP embedding of induced and endogenous neurons.**
(A) UMAP embedding of endogenous and induced neurons. **(B)** UMAP plots visualizing each neuronal population from both experimental conditions. **(C)** Stacked bar plot showing the numbers of neurons per experimental condition. **(D)** Neuron-specific marker expression visualized on individual UMAP plots.

Among the endogenous neurons, 216 cells were derived from the inhibited cell population (37.89 % of all eNs) and the remaining 354 from the active population (see Figure 5.21 C). The results obtained from the projections onto the reference datasets were then examined in detail for neuronal identities (see Figure 5.22). Among eNs, the fraction of detected glutamatergic neurons lies at around 80 %, while GABAergic neurons constitute around 20 %, therefore reflecting the ratio found *in vivo* (Sahara et al., 2012). In line with layer-specific cortical subtype characterization of eNs (see Figure 5.3), the majority of eNs (Active eNs: 57.06 %, Inactive eNs: 60.65 %) displayed highest transcriptional similarity to superficial projection neurons (*L2 IT RHP, L2/3 IT CTX-1* and *L2/3 IT PPP* derived from the Yao, Liu, et al., 2021 dataset, see Figure 5.22 *bottom*). A smaller subset (Active eNs: 15.54 %, Inactive eNs: 10.65 %) of deep-layer projection neurons was identified (*L4/5 IT CTX, L5 NP and IT CTX, L6b CTX* derived from the Yao, Liu, et al., 2021 dataset). Few eNs projected onto immature neuronal types that could not be clearly identified as cortical neurons (5.22 *bottom middle*). Moreover, distinct subtypes of inhibitory interneurons (Active eNs: 16.67 %, Inactive eNs: 22.69 %) could be detected among eNs, with the majority of them being VIP- or Pvalb-expressing interneurons.

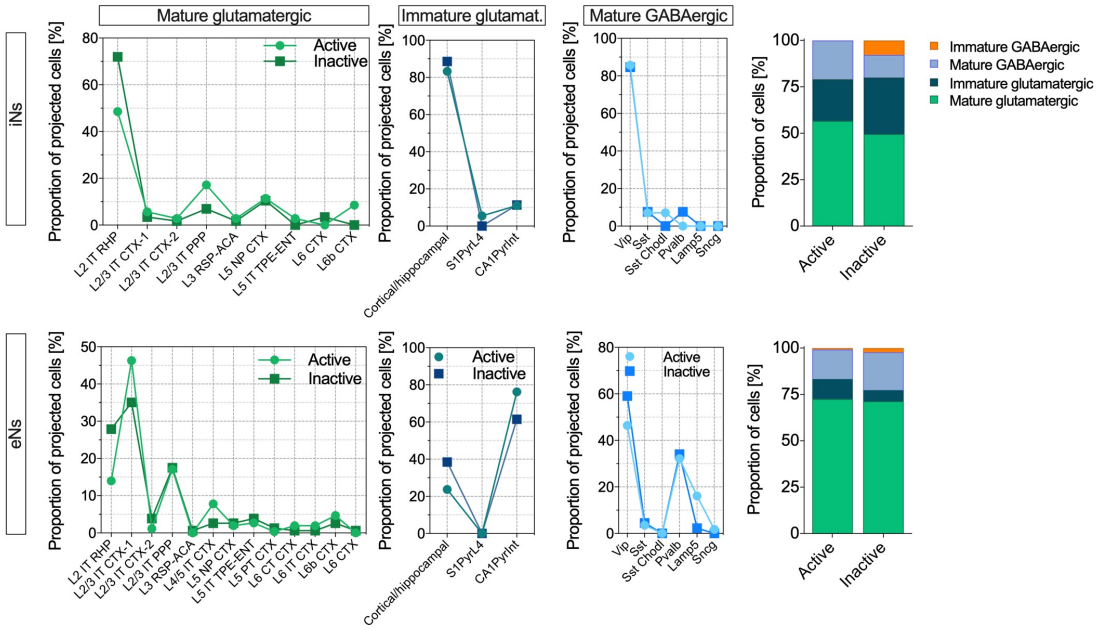

Figure 5.22: **Characterization of neuronal projections onto reference datasets.**
Induced (*top panel*) and endogenous (*bottom panel*) neurons were projected onto distinct neuronal subtypes across the three reference datasets. Stacked bar graphs display the proportions of distinct neuronal classes across the experimental conditions. Abbreviations: *IT - Intrathalamic, RHP - retrohippocampal, PPP - post-pre-parasubiculum, RSP - retrosplenial, ACA - anterior cingulate.*

Within the iN population, the projections revealed a surprisingly similar layer-specific neuronal diversity (see Figure 5.22 *top*). The mapping revealed the closest transcriptional similarity between almost half of the population (Active iNs: 40.29 %, Inactive iNs: 42.61 %) and superficial projection neurons (*L2 IT RHP* and *L2/3 IT CTX* derived from the Yao, Liu, et al., 2021 dataset). In line with this, transcripts of the upper-layer neuronal marker Cux1 and Cux2 were detected in iNs (48.35 % Cux1, 25.82 % Cux2, see Figure 5.21), despite not being among the features used to compute similarity (see Table 16). The upper-layer neuronal marker Satb2 was instead sparsely detected among iNs (8.24 %). In addition, the expression of the upper-layer markers Satb2 and Cux2 was validated by immunocytochemical staining (see Figure 5.23). A smaller fraction of iNs (Active iNs: 11.94 %, Inactive iNs: 6.96 %) displayed transcriptional similarity to deeper-layer projection neurons, and similarly, the deeper-layer cortical marker Ctip2 and Foxp2 were expressed in iNs and validated by immunocytochemistry (see Figure 5.23).

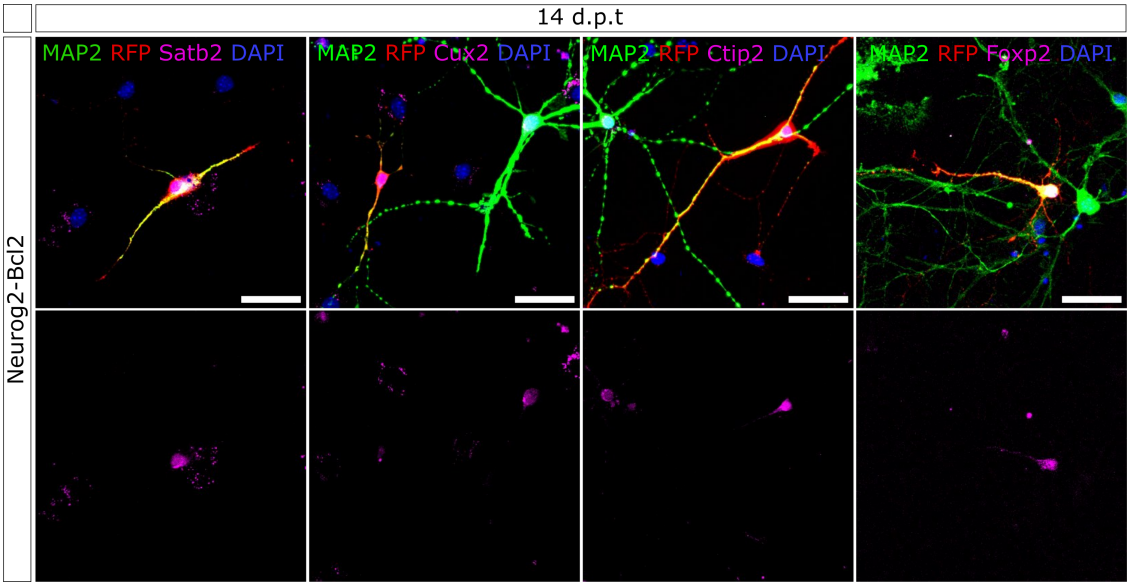

Figure 5.23: **Cortical layer-specific marker expression in induced neurons.**
Immunocytochemical stainings were performed in cocultured neurons in order to assess layer-specific marker expression in iNs. The top panel displays the merged image, bottom panel shows the expression of the layer-specific marker only. Scale bar, 40 µm.

Intriguingly, the projections revealed an unexpected subdivision of the iN population whose transcriptomes displayed similarity to either glutamatergic or GABAergic neurons (see Figure 5.22). iNs annotated as 'GABAergic' projected mostly onto mature GABAergic neurons (Active iNs: 20.89 %, Inactive iNs: 12.17 %) and a smaller percentage of immature GABAergic neurons (Active iNs: 0.0 %, Inactive: 7.83 %). Given the role Neurog2 plays during fate specification, this was rather unexpected. Therefore, a Wilcoxon-rank sum test was performed between iNs annotated as GABAergic neurons based on mapping

versus the remaining neuronal population in order to identify the cluster-specific genes for this population (p-values were adjusted using the Benjamini-Hochberg correction, FDR < 0.05). The top 20 genes of the obtained set of genes were then plotted onto a distinct reference dataset comprising similar diversity of neuronal types (S. Cheng et al., 2022). Most of these genes expressed specifically in iNs annotated as 'GABAergic neurons' indeed displayed higher transcript levels in GABAergic neurons compared to glutamatergic neurons (see Figure 5.24). Only a few genes were found to be higher expressed in glutamatergic neurons compared to GABAergic neurons (*Tenm4*, *Smad4* and *Mtcl1*). Moreover, the expression level does not seem to be dependent on distinct developmental stages of either neuronal type (see Figure 5.24).

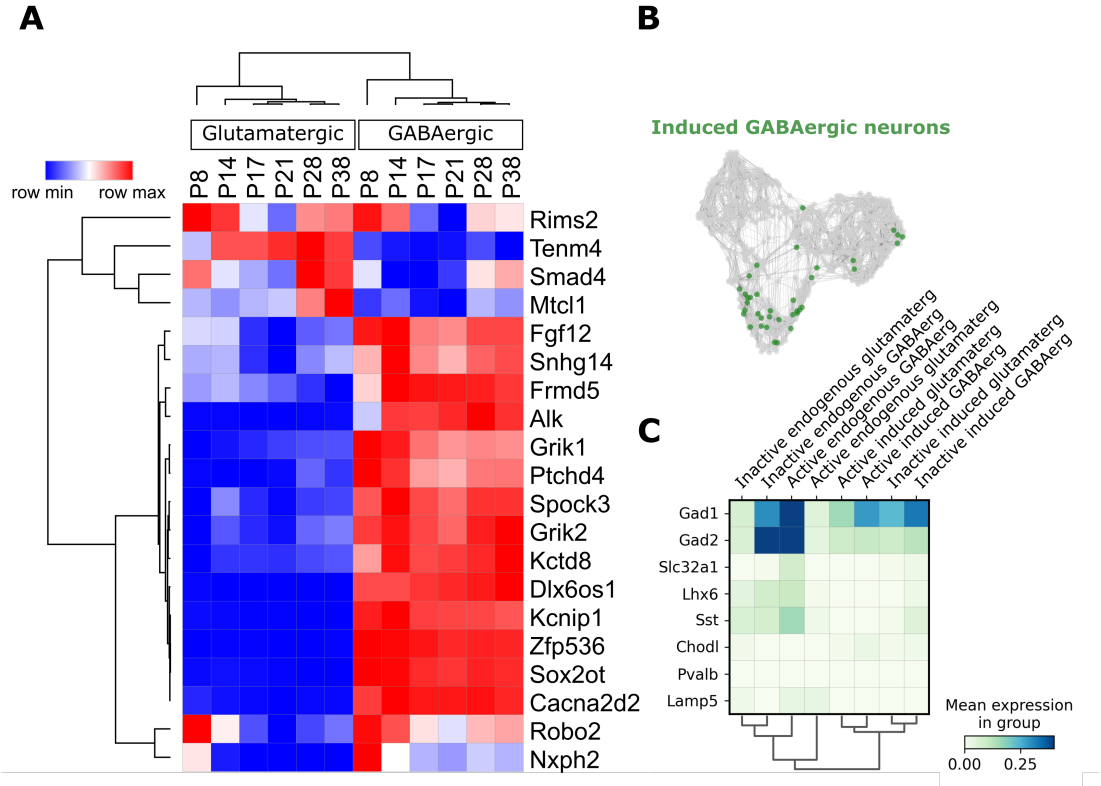

Figure 5.24: **Validation of GABAergic neuronal cluster-specific genes.**
(A) Genes expressed specifically in GABAergic neurons among the iNs were identified by performing a Wilcoxon rank sum test. The top 20 cluster-specific genes were then plotted onto the S. Cheng et al., 2022 dataset available at www.singlecell.broadinstitute.org and expression profiles were compared between glutamatergic and GABAergic neurons in order to assess specificity. Moreover, developmental regulation of expression levels within the two neuronal populations was visualized. **(B)** UMAP plot visualizing induced neurons annotated with GABAergic identity. **(C)** GABAergic marker expression in neuronal populations.

The majority of these iNs exhibited further sub-specification, e.g. VIP-expressing interneurons (see Figure 5.22). These data suggest that a fraction of the iN population

obtained a GABAergic transcriptional identity, displaying the expression of GABAergic-specific signature genes. However, it should be noted that iNs did not exhibit immunoreactivity for the inhibitory neurotransmitter GABA at this stage (data not shown). Interneuron-specific marker proteins, such as cholecystokinin or vGAT could also not be detected by immunocytochemistry staining (data not shown). However, a very scarce number of parvalbumin-expressing iNs could be detected (see Figure 5.25), hence supporting the transcriptomic observation that indeed, Neurog2-induced reprogramming results, in small proportion, in interneuron-like cells.

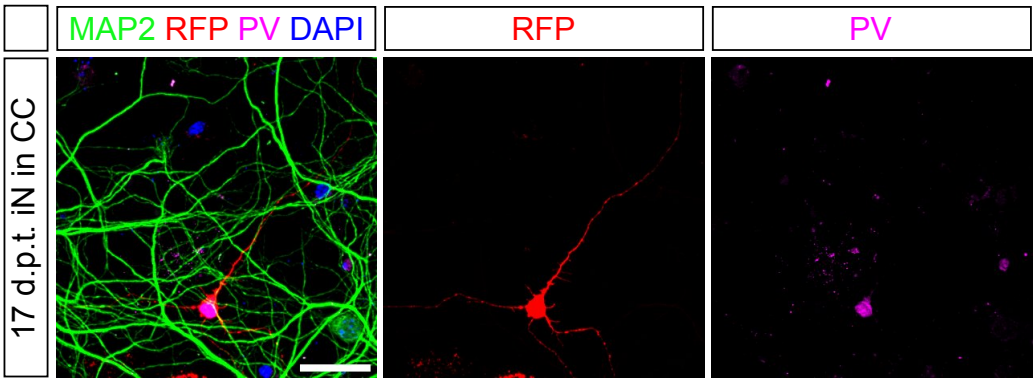

Figure 5.25: **Parvalbumin expression in induced neurons.**
Immunocytochemical staining showing that cocultured induced neurons express the interneuron-specific marker parvalbumin (PV) at 17 dpt. Scale bar, 40 µm.

Lastly, a subpopulation of iNs could not be assigned a layer-specific identity and displayed higher similarity with immature neurons that were annotated by the original study as "cortical or hippocampal neurons" (Active iNs: 25.37 %, Inactive iNs: 30.44 %). Therefore, iN heterogeneity was assessed from a developmental perspective by inspecting the distribution of projections across the three developmentally distinct reference datasets. Surprisingly, two distinct maturation stages could be identified based on distinct projection routes: 35.14 % of all iNs displayed the highest similarity with developing embryonic neurons, while 64.86 % of iNs displayed the highest similarity with adult cortical neurons (see Figure 5.26 A). In comparison, eNs almost exclusively displayed the highest similarity with adult cortical neurons (89.65 % of eNs projected onto the Yao, Liu, et al., 2021 dataset, with only 3.33 % and 7.02 % of eNs projecting onto the La Manno et al., 2021 and Zeisel et al., 2018 datasets, respectively (see Figure 5.26 A *right*). The enrichment towards a certain developmental stage of iNs was not confounded by the experimental condition (see Figure 5.26 B). Similarly, the enrichment of iN subsets towards a distinct developmental stage was not driven by the experimental condition (see Figure 5.26 C).

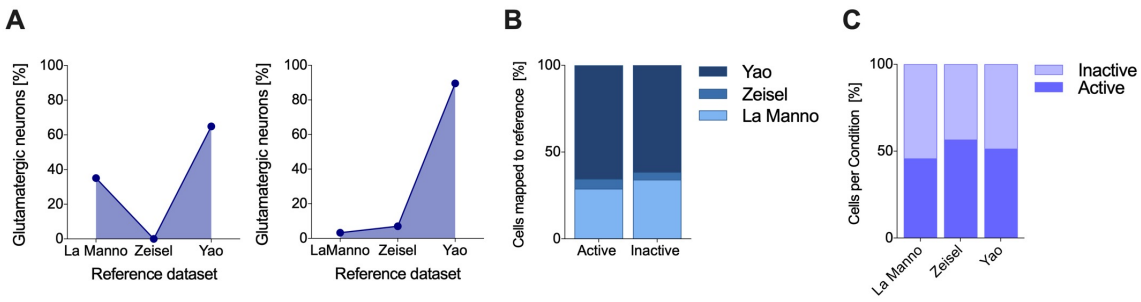

Figure 5.26: **Induced neurons display two distinct maturation stages.**
(A) Proportions of glutamatergic neurons among induced (*left*) and endogenous (*right*) neurons of distinct developmental stages assessed by projections onto neurons of distinct reference datasets. **(B)** Stacked bar plot diagram visualizes that there is no difference in proportions of active and inactive glutamatergic induced neurons projected onto each reference dataset and that the projections are constant across experimental condition (**C**).

Collectively, these data show that iNs acquire heterogeneous transcriptional identities *in vitro* that, in part, display similarities to distinct layer-specific cortical pyramidal neurons and suggest that ectopic expression of Neurog2 is either not sufficient in specifying a defined neuronal identity or not restrictive in instructing cortical layer-specific neuronal identities. Moreover, while eNs display a homogenous projection onto mature neuronal subtypes, iNs display two distinct maturation stages: approximately half of the iN population shows highest similarity to immature glutamatergic neurons, while the other half shows strong similarity with diverse layer-specific glutamatergic neurons (see Figures 5.22 and 5.26).

5.3.2 *Transcriptomic similarity between iNs and eNs*

In the upcoming results sections, I will compare the transcriptional identities of iNs and eNs and examine their responses to activity manipulation. As part of this analysis, I will present and discuss individual genes when I show their expression profiles. This approach will help understand the significance of these genes and provide a clear context for why they were selected for examination. The subsequent discussion chapter will then provide a more extensive discussion of the findings and their broader implications.

Here, the transcriptional profiles of iN cells were compared to endogenous neurons. Previous work could provide fundamental insights into transcriptomic changes occurring during Neurog2-mediated reprogramming at early time points (Masserdotti et al., 2015). More recent work, although using a different experimental system (human iPSCs), investigated the molecular identity of Neurog2-induced iNs at later time points during the differentiation trajectory and compared their transcriptomic signature to endogenous neurons (Lin et al., 2021a). In the work presented herein, I used the obtained single-nucleus

dataset to assess the extent to which the iN transcriptome differs from the astroglial transcriptome and, more importantly, how closely it resembles the eN transcriptome at 14 dpt. For this, transcriptomes were compared between the respective populations (Astrocytes vs eNs, Astrocytes vs iNs, iNs vs eNs). Between the three populations, 5056 genes were commonly detected in at least 3% of the cells of each population. Both neuronal populations, iNs and eNs, shared a common set of 886 genes (excluding genes that are also shared with astrocytes) (see Figure 5.27 A). Interestingly, each neuronal population displayed a set of exclusively expressed genes: 409 genes were uniquely detected in iNs and 878 genes were uniquely detected in eNs (see Figure 5.27 A). In order to derive further insights into the functional role of these genes, enrichment analysis for gene ontologies (GO term analysis) was performed. Based on available annotation databases, this analysis reveals in which biological processes a given gene has already been described in the literature. Interestingly, genes exclusively detected in iNs enriched for GO terms associated with biological processes such as 'cell activation', 'immune response' and 'regulation of immune system processes', consistent with the retroviral transduction and the potentially ongoing connected cellular processes in these cells (see Figure 5.27 B). Conversely, the 878 genes exclusively detected in eNs enriched for GO terms associated with 'synaptic signaling' and 'ion transport' (see Figure 5.27 B). Interestingly, the set of 886 commonly expressed genes between iNs and eNs enriched for GO terms associated with 'synaptic signaling', 'neuron development' as well as 'regulation of synaptic plasticity' (see Figure 5.27 B).

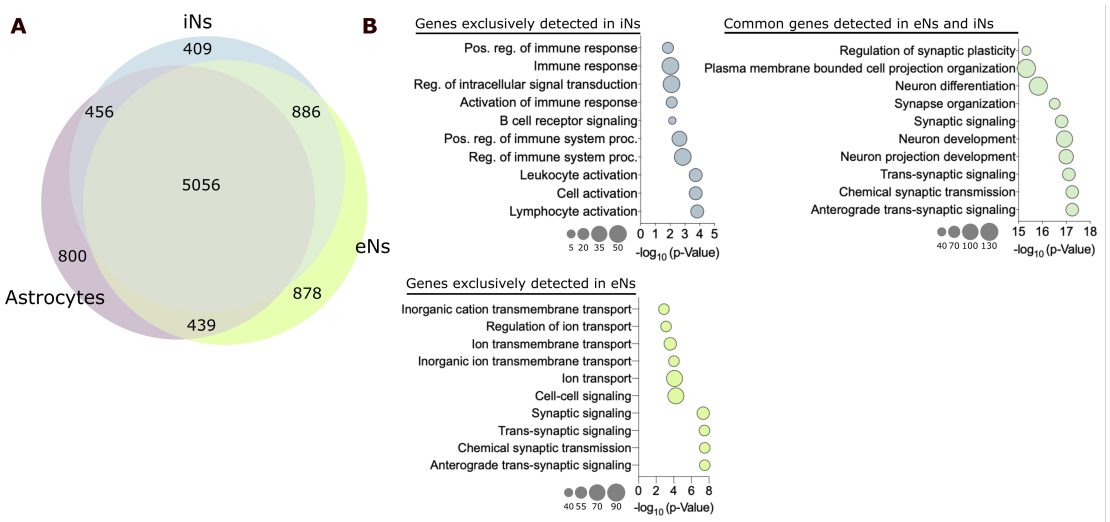

Figure 5.27: **Transcriptomic similarity between astrocytes, induced and endogenous neurons.** **(A)** Venn diagram visualizing the overlap of total detected genes between astrocytes, induced and endogenous neurons. **(B)** GO term analysis of genes exclusively detected in iNs (*top left*) or eNs (*bottom left*) reveals distinct functional roles of gene sets. GO term analysis of commonly detected genes in iNs and eNs (*top right*) shows synaptic signaling-related terms.

Genes expressed by both neuronal populations and that enriched for functionally relevant GO terms (see above) may suggest that iNs have acquired a comprehensive transcriptional program that resembles the one found in eNs. However, multiple genes displayed strong differences in expression levels between eNs and iNs. For instance, shared genes that enriched for the GO term "Regulation of synaptic plasticity" (see Figure 5.27) seem to be higher expressed in eNs compared to iNs (e.g. *Adcy1*, *Plk2*, *Camk2a*, *Syt7*, *Slc1a1*, *Snap25*, *Neto1* and others; see Figure 5.28), further supporting differences in maturation stages or potential functional diversity.

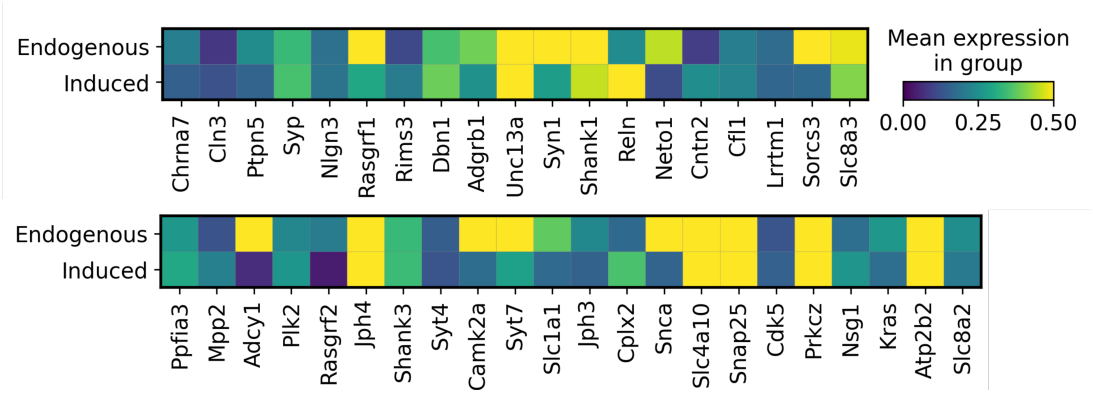

Figure 5.28: **Regulation of synaptic plasticity-related genes display distinct expression levels between iNs and eNs.**
Matrixplot showing differences in gene expression levels between iNs (*Induced*) and eNs (*Endogenous*) in genes related to the regulation of synaptic plasticity as assessed via GO term analysis.

Moreover, genes that were specifically expressed in astrocytes associated with GO terms related to glial function and myelination (data not shown), suggesting that iNs not only express pan-neuronal genes but also display no expression of astrocyte-specific genes (e.g. *Npas3*, *Plpp3*, *Msi2*, *Slc1a3*, *Ptprz1*, *Qk*, *Zbtb20*, *Nfia*, *Ntm*, *Tcf7l2*; see Figure 5.29).

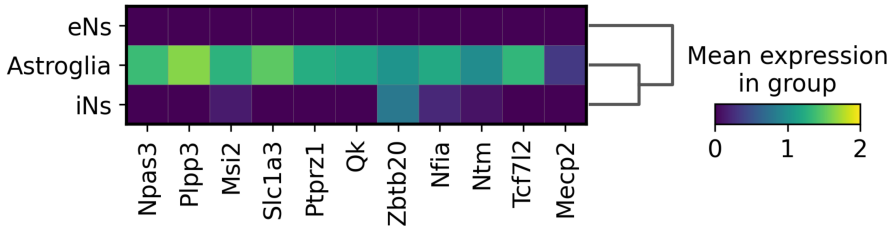

Figure 5.29: **Expression of astrocyte-specific genes is absent in induced neurons.**
Matrixplot visualizing the expression of astrocyte-specific genes in induced and endogenous neurons as well as astrocytes under control conditions. MeCP2 was added to the list in order to compare its expression levels between the astrocytic and neuronal populations.

Assessing the transcriptional similarity of iNs to eNs is of interest as it can facilitate understanding the degree of neuronal identity acquisition. Therefore, the above comparison was complemented with a DEG analysis between the active, glutamatergic iNs and eNs (both control conditions) using DESeq2 in order to identify significant differences in transcriptional phenotypes (LRT with adj. p-value < 0.05 and FC > 1.25). The analysis was performed with the aim of identifying genes strongly expressed in eNs but not in iNs, and vice versa, which would allow the identification of differences in neuronal type, maturity, or indications of incomplete reprogramming. The analysis identified 341 genes that were significantly more highly expressed in eNs, while 852 genes were significantly higher expressed in iNs (see Figure 5.31 A and Tables 18 and 19). Interestingly, genes that were higher expressed in eNs were enriched for GO terms associated with biological processes such as 'synapse organization', 'synaptic signaling' and 'regulation of trans-synaptic signaling', suggesting that albeit these gene transcripts were detected in iNs the significant difference in expression levels suggests distinct functional phenotypes between the two populations (see Figure 5.31 B). Interestingly, genes associated with mature cortical layer-specific identities, such as *Satb2*, *Cux1/2*, *Ctip2*, *Foxp2*, were not expressed at distinct levels. However, despite the detection of similar transcript levels of such marker genes, maturation stages seem to diverge at least in part as assessed by projections onto reference datasets (see Figure 5.26), highlighting the importance of relying on genome-wide sequencing data for comprehensive characterization. On the other hand, iNs display stronger expression of neuronal genes, such as *Rbfox3* (*Neuronal Nuclei - NeuN*), *Dcx*, *Ncam1* or *Mapt* (see Figure 5.31 C). The pre-mRNA alternative splicing regulator Rbfox3 is well known for its role in promoting neuronal differentiation during brain development (H. Y. Wang et al., 2015). Combined with a detection of higher expression of immature neuronal markers such as *Dcx* and *Ncam1* this further suggests the idea that iNs may still be undergoing a differentiation program. Moreover, iNs express significantly higher levels of the histone demethylases *Kdm5a* and *Kdm5b*. Kong et al., 2018 recently showed that *Kdm5a* overexpression leads to a reduction in transcriptional activity of the GFAP promoter and that it is required for repressing astrocytogenesis in neural progenitors (Kong et al., 2018). The iN-URG were screened for known Neurog2 target genes, such as *Tbr2*, *Nhlh1*, *Elav4*, *Zfp238* or members of the Notch signaling pathway, such as *Dll1*, *Hes5 and Mfng* (Gohlke et al., 2008) (see Figure 5.30). However, none of these genes were found among the iN-URG, suggesting that the current maturation stage exceeds the time window in which these genes are upregulated. In fact, downregulation of Tbr2 expression indicates the progression from an IPC to a postmitotic neuron during development (Englund et al., 2005), therefore suggesting subsequent gene regulatory processes despite constitutive Neurog2 expression. Microarray analysis following 24 hours of Neurog2 induction in astroglia has previously identified further

target genes, such as *Atoh8*, *Hes6*, *Insm1*, *Prox1*, *NeuroD4*, *Sox11*, *Trnp1*, *Cnr1*, *NeurodD1*, *Phf6* and *Sfrp1* (Masserdotti et al., 2015). Almost none of these genes were detected in iNs at 14 *dpt* (see Figure 5.30). Only *Prox1* and *Sox11* were found to be highly expressed in iNs compared to eNs and were found among the significantly DEG (see below, Figure 5.31).

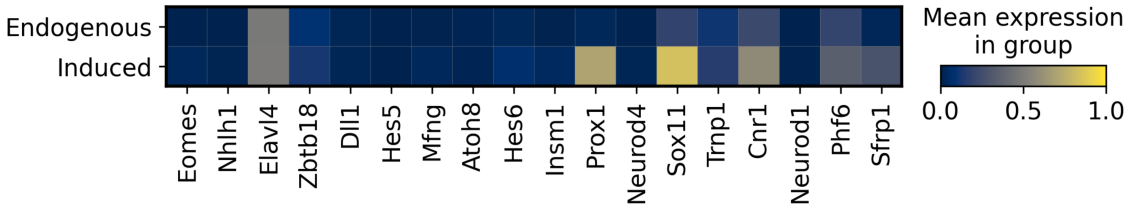

Figure 5.30: **Expression of Neurog2-target genes in endogenous and induced neurons.** Matrixplot visualizing the expression of known direct target genes of the TF Neurog2 in endogenous and induced neurons under control conditions.

In addition, *Sox4* was found to be highly expressed in iNs. The TFs Sox4/11 have been shown to be critical regulators for the establishment of pan-neuronal features during neuronal maturation (Bergsland et al., 2006; C. Chen et al., 2015). Moreover, Sox4 is known to interact with Neurog2 in order to activate the expression of neurogenic genes (Bocchi et al., 2022; C. Chen et al., 2015; Mu et al., 2012). In fact, knockdown of Sox4 expression in Neurog2-reprogrammed fibroblasts was shown to almost abolish reprogramming (Bocchi et al., 2022; Smith et al., 2016). Remarkably, iNs highly express FoxO3, a TF that has been shown to inhibit Ascl1 transcriptional activity as well as limiting the accumulation of ROS (McLaughlin and Broihier, 2018).

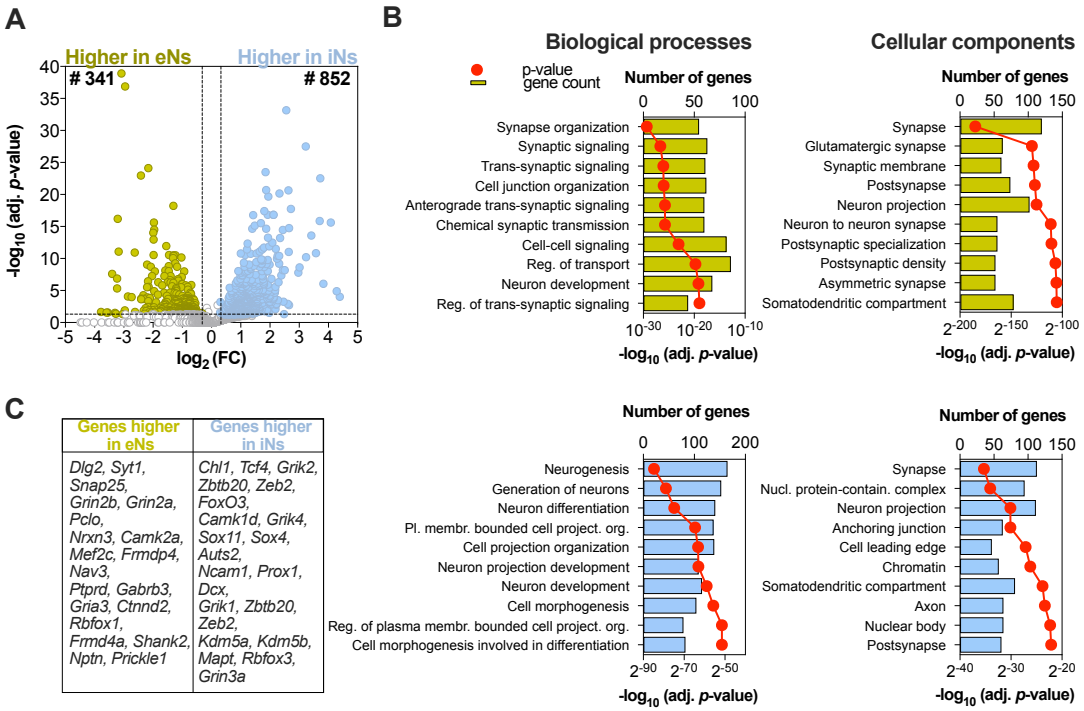

Figure 5.31: **Shared neuronal genes display distinct expression levels between iNs and eNs.** **(A)** Box plots showing differences in gene expression levels between iNs (*top*) and eNs (*bottom*) in genes relating to the regulation of synaptic plasticity. **(B)** GO term enrichments for biological processes (*left*) and cellular components (*right*) of genes upregulated in eNs (*top*) and iNs (*bottom*). The length of the bar plots displays the number of genes and the dot plot visualizes the p-value. **(C)** Selected set of genes highly expressed in eNs and iNs.

Assessing expression levels of known regulators of synaptic plasticity may reveal whether iNs possess the ability to undergo such processes. As delineated in the introduction, two TFs have established roles in regulating neuronal plasticity mechanisms: MeCP2 and Mef2c. Interestingly, MeCP2 was not found to be differentially expressed between iNs and eNs and was detected in both neuronal populations at lower levels than in astrocytes (see Figure 5.29). As MeCP2 represents a transcriptional regulator with diverse roles in controlling neuronal function and can function as an activator or repressor depending on cofactors, the expression of its numerous cofactors was assessed in order to infer more information about potential downstream effects (Chahrour et al., 2008). Interestingly, the two cofactors of MeCP2, Smc3 and Ncor1, which are involved in the assembly of a transcriptional repressor complex (Lyst et al., 2013), are significantly more highly expressed in iNs compared to eNs (see Table 19). As a repressor, MeCP2 is known to inhibit Mef2c expression (Chahrour et al., 2008). In line with this, Mef2c was found to be significantly lower expressed in iNs compared to eNs (see Figure 5.31 C). These findings suggest that MeCP2 may be active in different modes of regulation

(activator/repressor) between iNs and eNs. Expression levels of other molecules relevant for plasticity mechanisms, such as Creb1, PKA, Crem and CPEB were not found to be differently expressed between eNs and iNs (see Table 18 and 19). On a related note, the calcium-regulated TF Nfatc3 which, upon activation by calcineurin, regulates the expression of target genes that are involved in neuronal survival, synaptic plasticity and axon growth (Vihma et al., 2016), was found to be highly expressed by iNs. Next, expression levels of genes related to synapse assembly and function were compared across both neuronal populations. Besides the essential role of structural components of synapses, the most fundamental molecular components that determine excitability, synaptic transmission and plasticity are neurotransmitter receptors and ion channels. Moreover, kinases and phosphatases have been shown to be central players in synaptic plasticity (Desch et al., 2021). Importantly, several of these molecular components of the synaptic machinery are developmentally regulated in order to shape distinct plasticity behaviors according to the needs of the evolving circuit (Lohmann and Kessels, 2014). As to date, no comprehensive molecular profiling of synaptic machinery-related genes or proteins exists for Neurog2-derived iNs at any developmental stage that may help assess the extent of neuronal phenotype acquisition. Crucial for the nature of synaptic transmission and of great interest for translational purposes is the expression of the desired neurotransmitter receptor in iNs. Therefore, genes related to glutamate receptor signaling were assessed and were all found to be expressed by iNs (*Gria1-3*, *Grin1*, *Grin2a*, *Grin2b* and *Grin3a*). However, 50 % of these genes, mostly NMDAR subunits, were expressed at significantly lower levels than in eNs (*Gria3*, *Grin2a*, *Grin2b*, *Grin3a* subunits; see Figure 5.32). Intriguingly, AMPAR subunits Gria1 and Gria2, both relevant players during HSP, were expressed at similar levels between iNs and eNs. Synaptic strength of glutamatergic neurons is not only controlled by the number and composition of postsynaptic AMPAR but is also heavily dependent on functional modulation via transmembrane AMPAR regulatory proteins (TARPs), which regulate trafficking and function and play a major role in synaptic plasticity mechanisms (Bissen et al., 2019). A comparison of expression levels showed no significant difference between eNs and iNs except for *Dlg1*. I then compared expression levels of pre- and postsynaptic-specific genes. Interestingly, genes coding for proteins associated with the postsynaptic density were not displaying a significant difference in levels (e.g. *Dlg4*, *Dap3*, *Homer1-3*, *Shank1* and *Shisa6*). Only *Lrrc7*, coding for a protein that interacts with NMDAR as well as Camk2a (Chong et al., 2019), was found differentially expressed (see Figure 5.32). Interestingly, deletion of Lrrc7 has been shown to reduce expression levels of postsynaptic NMDAR subunits (Chong et al., 2019). Among the presynapse-related genes, several synaptic vesicle-associated genes were expressed at significantly lower levels in iNs compared to eNs (*Snap25*, *Syt1*, *Syt7*, *Sv2a*, *Sv2b*), potentially reflecting the fact that iNs are less active

and require less synaptic vesicle-associated proteins. Finally, cell adhesion-related genes such as *Neurexin1/2* and *Nptn* were found significantly less expressed in iNs, however, the majority of the assessed cell adhesion-related genes were expressed at similar levels.

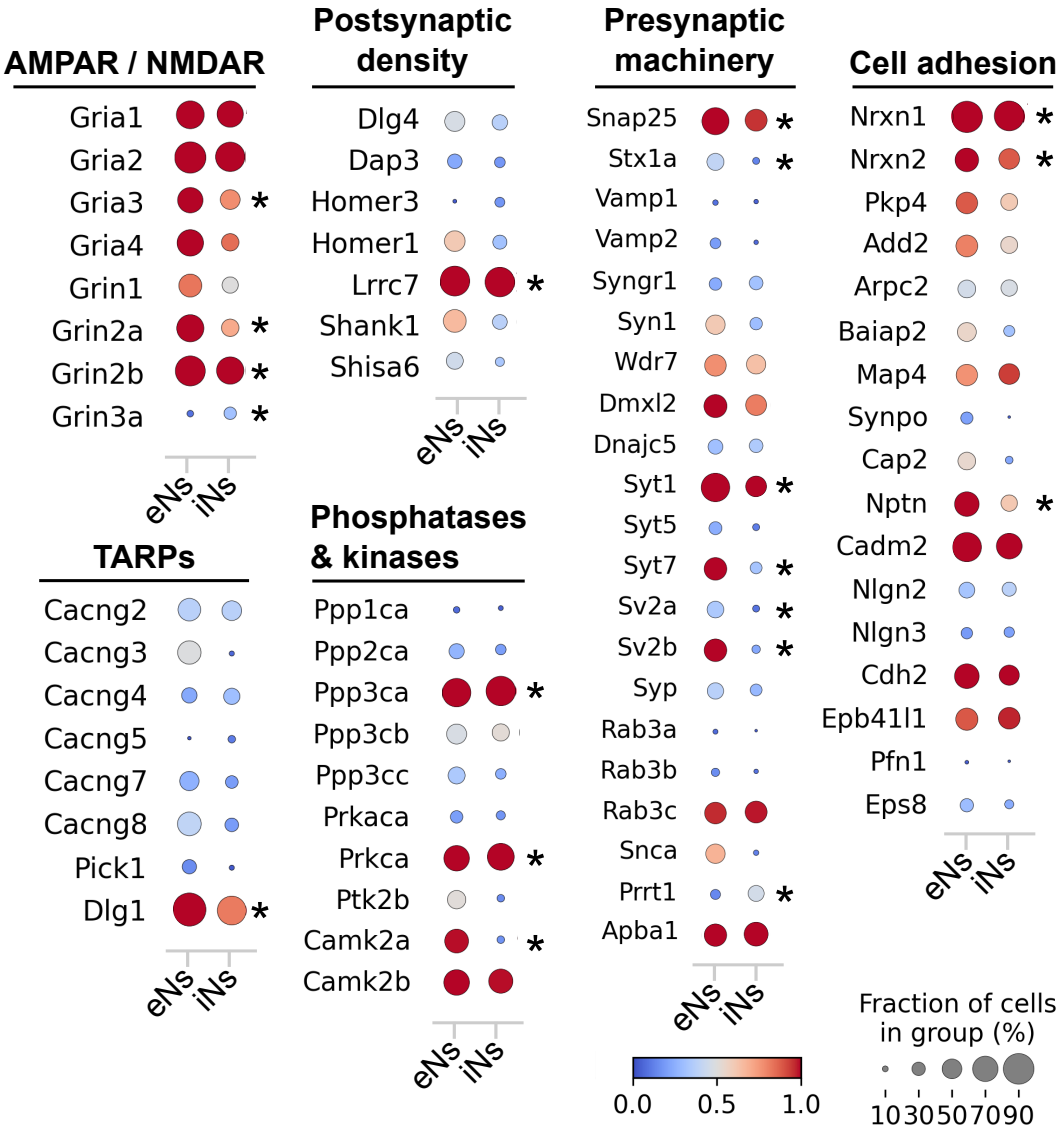

Figure 5.32: **Expression of genes related to synapse formation and function in induced and endogenous neurons.**
Distinct dot plots visualizing the expression level of different synapse-related gene families. Genes marked with an asterisk (*) were found to be significantly differentially expressed between active iNs and eNs (see Differential gene expression analysis in Figure 5.31). Abbreviations: *PSD* - postsynaptic density, *TARP* - transmembrane AMPAR regulatory proteins.

Genes relating to the synaptic machinery could display differential expression between the identified mature and immature iN population and would support the idea of two

functionally distinguishable subpopulations at a given time point. However, when assessing expression levels at this population scale, multiple genes displayed a mosaic-like expression profile, possibly due to neuronal heterogeneity or resulting from typical high drop-out rates in snRNA-seq data influenced by the size of the population. In sum, most synaptic machinery-related genes are expressed by iNs at comparable levels to eNs. Genes that have been shown to directly correlate with neuronal maturation (e.g. *Camk2a, SNAP25* or NMDAR subunits) are expressed at lower levels in iNs than in eNs (Bayer et al., 1999). The GO term as well as differential gene expression analysis further support the results from the previous projections onto reference datasets, that the iN population is developmentally heterogenous but confirm that iNs generally display a transcriptomic phenotype that is immature compared to the surrounding eNs. Moreover, the analysis unravels the transcriptional state of iNs after 14 days of maturation and identifies that some Neurog2-target genes remain highly expressed (see Figure 5.30). Furthermore, iNs display a global transcriptional program that resembles the one found in eNs to a large extent, including multiple gene transcripts directly relating to neuronal differentiation as well as synaptic assembly and transmission. However, iNs display lower expression of several synaptic machinery-related genes than detected in mature eNs. Consequently, this observation raises the question of whether the difference in transcriptional state reflects distinct underlying gene regulatory networks in iNs and eNs. Therefore, pySCENIC, a regulatory network inference tool, was used in order to identify TFs and their putative target genes in distinct neuronal populations (see Table 15) and score their activity. The list of putative target genes was then trimmed to contain only putative direct-binding target genes based on cis-regulatory motif analysis (Aibar et al., 2017). The resulting data contains cell type-specific regulons, e.g. a list of TFs with their respective putative direct targets. Furthermore, pySCENIC scores the 'activity' of each regulon in individual cells and provides a regulon specificity score (RSS) that shows whether a certain regulon displays cell type specificity. Analysis of iNs and eNs revealed 49 and 37 regulons, respectively (see Figure 5.33 A). In both populations, regulon sizes were diverse and spanned from 300 to less than 10 target genes. The majority of regulons displayed specificity towards eNs or iNs, respectively. However, 19 regulons were found to be shared, hence the overlap in their respective target genes was compared (see Figure 5.33 B). Interestingly, although these 19 TFs were predicted to control transcription in both iNs and eNs, they were inferred to modulate largely non-overlapping sets of genes (see Figure 5.33 B). This suggests that similar TFs target distinct gene sets between iNs and eNs and possibly reflect differences in identities and maturation stages or result from distinct accessibilities of all target genes in iNs.

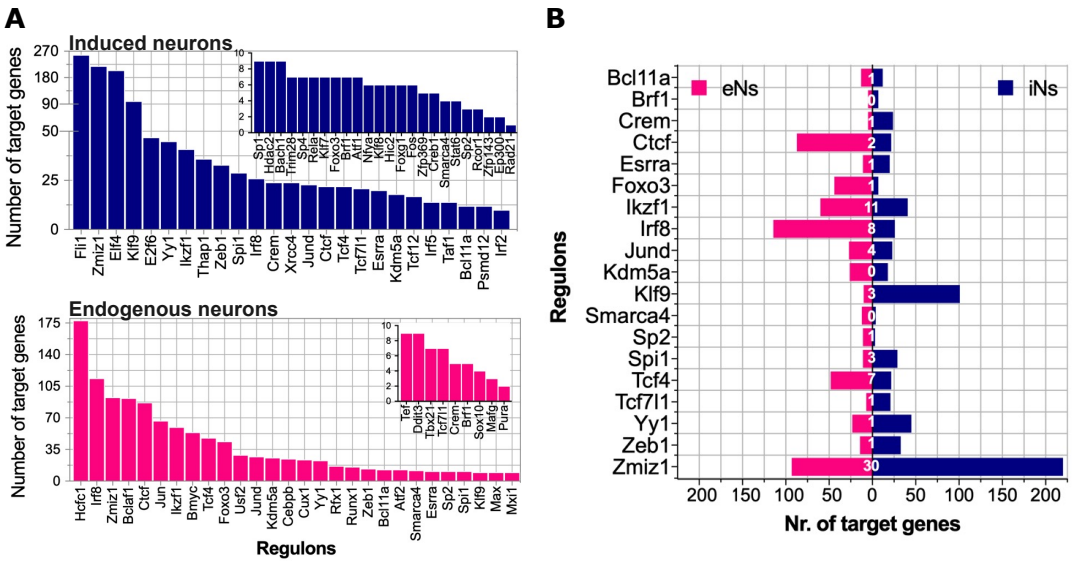

Figure 5.33: **Regulon size and composition overlap between iNs and eNs.**
(A) Regulons detected in iNs and eNs (top and bottom, respectively) were inferred from snRNA-seq data. 49 regulons were detected in iNs, among which 24 regulons were composed of less than 10 target genes (insert histogram). In eNs, 37 regulons were retrieved, out of which 9 regulons were containing less than 10 target genes. **(B)** In iNs and eNs, 19 shared TFs were found and the overlap of target genes per regulon between iNs and eNs was assessed (white number).

5.4 iNs and eNs regulate distinct gene programs in response to activity inhibition

5.4.1 *Regulation of synaptic plasticity-related genes suggests homeostatic upscaling in response to pharmacologically-induced activity inhibition in eNs*

Previous studies demonstrated that 24-48 hours of activity inhibition elicited increased miniature excitatory postsynaptic current (mEPSC) amplitudes and induced synaptic upscaling in cultured cortical or hippocampal neurons (Dörrbaum et al., 2020; K. Y. Lee et al., 2015; Schaukowitch et al., 2017; G. G. Turrigiano et al., 1998; G. Turrigiano et al., 1994). Despite being established that transcriptional regulation is essential for synaptic upscaling (Ibata et al., 2008), the molecular basis of the underlying intrinsic transcriptional program has just recently begun to be explored (Schaukowitch et al., 2017; Valakh et al., 2021). In this study, neurons were either treated with the sodium channel blocker (hence action potential blocker) TTX and the glutamate receptor inhibitors CNQX and APV in order to decrease neuronal network activity and induce homeostatic upscaling (Inhibited / Inactive) or were maintained under basal conditions (Control / Active). I verified that activity inhibition for 48 hours did not impact neuronal density in both populations (see Figure 5.34).

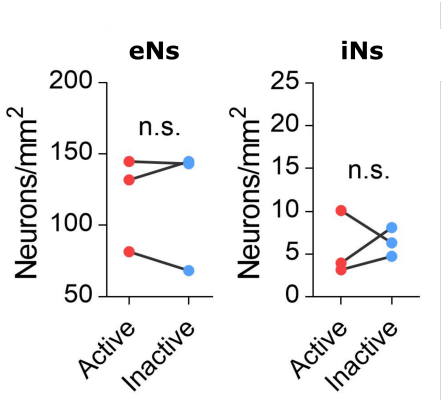

Figure 5.34: **Effect of 48 hr pharmacological activity inhibition on neuronal density at 28 *div*.** Cocultures were treated with the glutamate receptor inhibitors CNQX and APV as well as the sodium channel inhibitor TTX for 48 hours. Density was assessed by counting the number of NeuN-expressing neurons among DAPI or RFP and normalized by area.

Differentially expressed genes (DEG) in all endogenous glutamatergic neurons were identified using the LRT (see Methods chapter) and a total of 785 genes (9.6 % of all genes) were found to be upregulated and 601 genes (7.4 % of all genes) downregulated in response to activity inhibition in eNs (false discovery rate (FDR) of < 0.05, fold change (FC) cutoff at 1.25, adj. p-value < 0.05). In comparison, 79 (1.5 % of all genes) and 160 (3.1 % of all genes) genes were found to be up- and downregulated in iNs, respectively (see Figure 5.35). When comparing the overlap of regulated genes between eNs and iNs, surprisingly only 13 genes were found to be commonly upregulated and 36 genes commonly downregulated (see Figure 5.35). The regulation into opposite directions was assessed and 10 genes were found to be upregulated by eNs but downregulated by iNs (*Zfhx2*, *Prkg1*, *Prkag2*, *Peak1*, *Larp4*, *Grik1*, *Galnt13*, *Cntnap2*, *Chl1*, *Cblb*) while only two genes were downregulated by eNs but upregulated by iNs (*Prpf4b*, *Cacna1a*). The small proportion of shared regulated genes between eNs and iNs suggests an unfolding of largely distinct transcriptional programs in response to activity inhibition in iNs and eNs. Therefore, induced transcriptional responses in both neuronal populations were investigated separately.

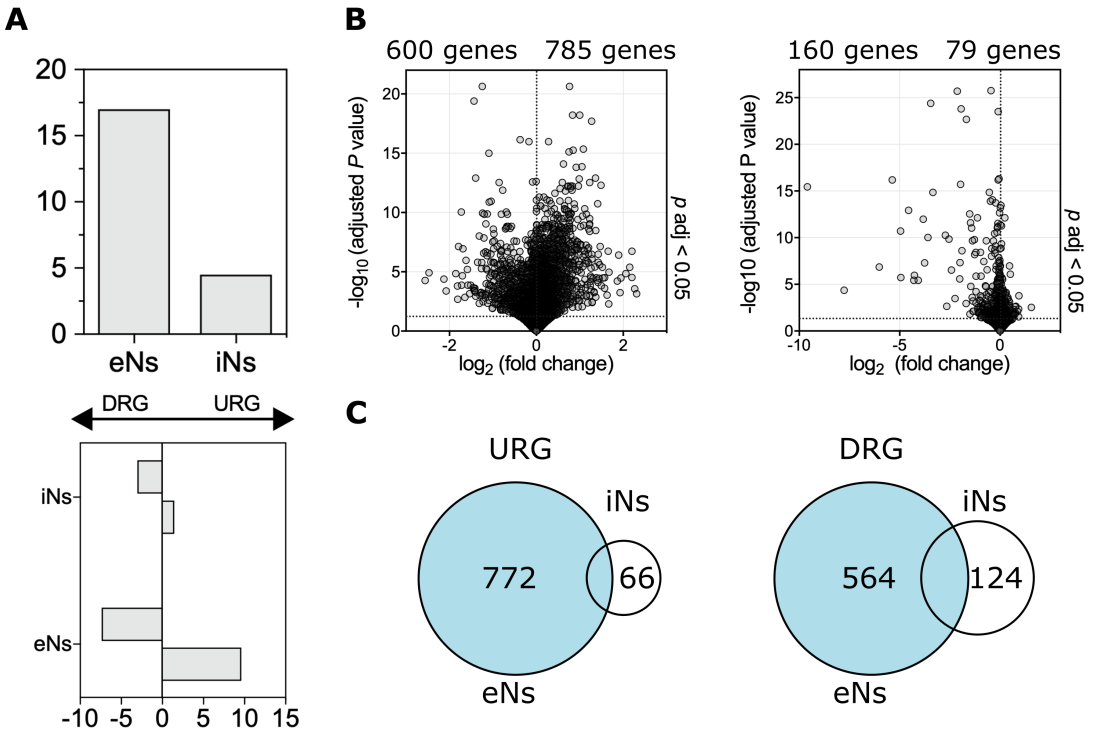

Figure 5.35: **iNs and eNs regulate distinct gene programs in response to activity inhibition.** **(A)** Percentage of total differentially expressed genes (DEG) (*top*) and up- as well as downregulated gene sets (*bottom*) in induced (iNs) and endogenous neurons (eNs), respectively. **(B)** Volcano plots visualizing total numbers of DEG in eNs and iNs. **(C)** Venn diagrams showing the overlap in shared up- and downregulated genes between iNs and eNs.

In line with observations from previous studies, the intrinsic mechanism of synaptic upscaling would suggest a one-directional regulation of gene transcription. However, the analysis of eN-specific DRG suggests a functional relevance of bidirectional transcriptional regulation in response to activity inhibition. Within the upregulated gene (URG) program, several members of the cadherin gene family were identified (*Cdh19*, *Cdh9*, *Cdh13*, *Pcdh9*) as well as genes implicated in cytoskeletal rearrangement (*Map7*, *Map4k4*, *Map2k2*, *Map2k6*) and axon guidance (*Cntn2*, *Epha5*, *Unc5c*, *Arpc1a*, *Sipa1l3*), suggesting structural adaptations in response to activity inhibition (see Table 20). Genes associated with cytoskeletal dynamics were also found among the DRG set (*Synpo*, *Sipa1l1*, *Lgi1*, *Nrxn3*, *Cdh10*) (see Table 21). Most prominently, genes associated with the presynaptic fusion machinery that releases neurotransmitters into the synaptic cleft were widely upregulated (*Syt1*, *Syt14*, *Syt17*, *Syn1*, *Syn2*, *Syn3*, *Synpr*, *Synpo2*, *Synj2bp*, *Dnajc1*, *Sv2c*, *Snap47*, *Snca*, *Sncb*), suggesting an acquired ability to sustain increased presynaptic neurotransmitter release rate in response to reduced network activity. Consistent with the concept of synaptic upscaling and the established increase of AMPAR surface expression, GluA1 was found to be significantly upregulated, while GluA2 was found to be downregulated

(see Figure 5.36 B). Moreover, several other postsynapse-related genes were found to be significantly upregulated (*Camk2a*, *Nos1*, *Grik1*, *Grik2*, *Psd*, *Ptk*, *Plk2*, *Neto1*, *Neto2*, *Ncam1*, *Cacna1e*, *Cacnb2*, *Cacng2*, *Cacng4*, *Cacng8*, *Map2k2*, *Map2k6*, *Atp1a3*). Moreover, consistent with previous studies (Schaukowitch et al., 2017; Valakh et al., 2021), the expression of the TF Tef was found significantly upregulated. A recent study identified the PAR bZIP TFs Tef and Hlf as TFs required for the proper tuning of the homeostatic upscaling process and preventing an exaggerated upregulation of excitatory synaptic transmission (Valakh et al., 2021), consistent with earlier studies demonstrating an epileptic phenotype in knock-out mice of these PAR bZIP TFs (Gachon et al., 2004; Rambousek et al., 2020). Moreover, the histone demethylases Kdm6a, Kdm6b and Kdm5c were upregulated in response to activity inhibition, suggesting that chromatin-related processes play a role in HSP (see Table 20). In fact, a previous study linked Kdm5c expression to the regulation of activity-dependent enhancers in maturing neurons (Scandaglia et al., 2017). In addition, the polycomb chromatin reader L3mbtl1 has been recently shown to be regulated by neuronal activity and constitutes an essential player in regulating synaptic downscaling in response to neuronal activity (Mao et al., 2018). In line with the above-mentioned observations, here, L3mbtl1, as well as L3mbtl4, were found to be downregulated in response to activity inhibition. In order to obtain further insight into the biological relevance of these DEG sets, enrichment analysis for gene ontologies was performed. Interestingly, the GO term analysis for the URG set revealed enrichments for biological processes related to chemical synaptic transmission, trans-synaptic signaling, and neuron projection development (see Figure 5.36 *top left*). Moreover, the GO term analysis exclusively enriched for the cellular components 'synapse' and 'axon' (see Figure 5.36 *top right*). Interestingly, also downregulated genes displayed enrichment for biological processes related to 'synapse organization' and 'synaptic signaling' (see Figure 5.36 *bottom left*) and enrichment for similar cellular components (see Figure 5.36 *bottom right*).

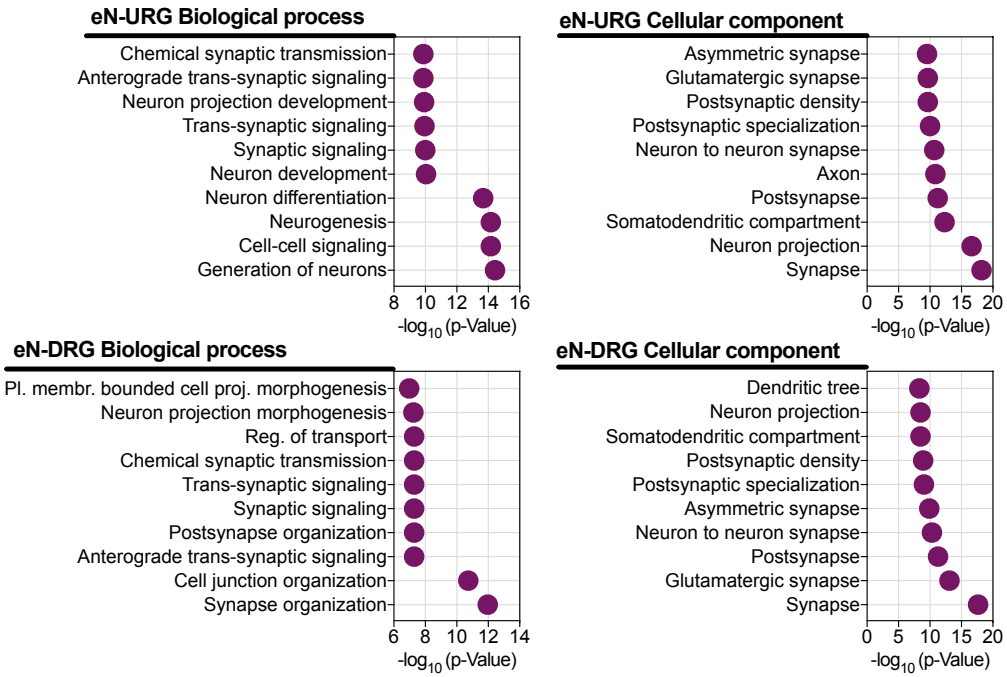

Figure 5.36: **Activity inhibition induces synaptic signaling related gene program in eNs.** Dotplots for the top ten GO terms for URG (n = 785; *top*) and DRG (n = 600; *bottom*) enriching for biological processes (*left*) and cellular components (*right*).

Since general GO term databases contain only limited representations of synapse-related processes and structural components, a recently assembled, synapse-specific ontology was used in order to comprehensively characterize synapse-related genes (Koopmans et al., 2019). This revealed that eN display significant regulation of pre- as well as postsynaptic-related genes (see Figure 5.37 *top*). Moreover, while synaptic metabolism does not seem to be significantly affected, significant enrichment is detected in ontology terms such as 'synapse organization' and 'synaptic signaling' (see Figure 5.37 *bottom*).

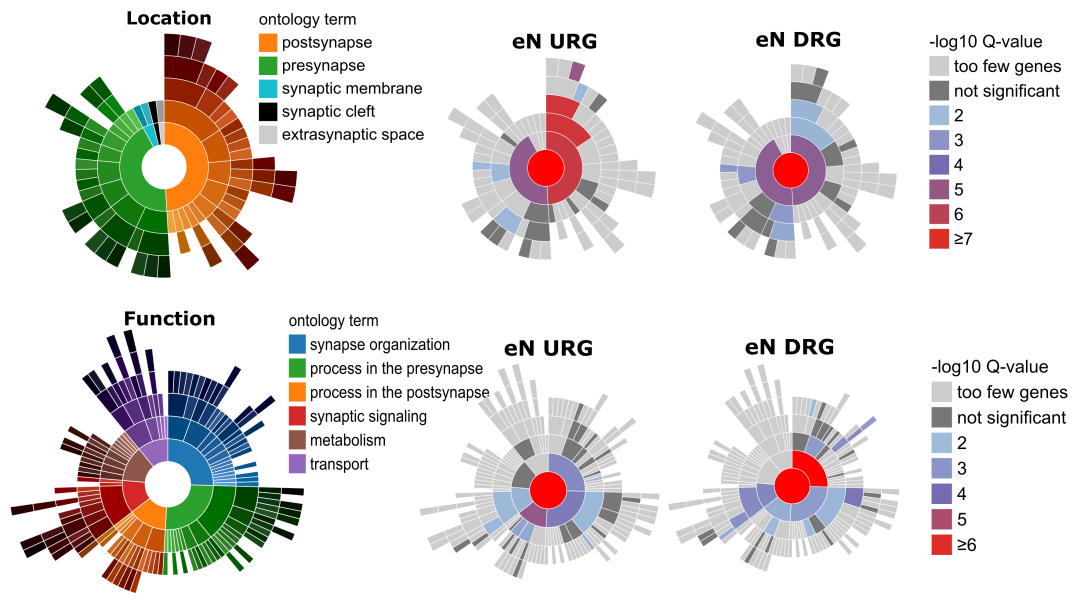

Figure 5.37: **eN-regulated genes show strong enrichment for synaptic genes.** Synapse-specific GO term analysis on eN-URG and DRG sets results in overrepresented terms relating to synaptic location *(top)* and function *(bottom)*. eNs regulate pre- as well as postsynaptic genes in response to activity inhibition, which are involved in synaptic organization and signaling.

Among the DEG, 12 candidate genes (DRG: *Synpr, Homer2, Camk4, Kcnn2, Nr4a1;* URG: *Stat3, Neurod2, Vav3, Grik1, Sox4, Cacnb2, Lrig1*) were selected for further validation via qRT-PCR analysis and the respective changes observed in the genome-wide data were confirmed (see Figure 5.36 C). Previous studies have identified a crucial role of the above-mentioned genes in synaptic scaling, more specifically synaptic upscaling. For instance, N-cadherin (Chd2) has been shown to be an essential molecule during homeostatic synaptic plasticity as it is involved in the regulation of synaptic expression of AMPARs (Fernandes and Carvalho, 2016; Thalhammer and Cingolani, 2014). Notably, N-cadherin binds to β-catenin, which contains an armadillo repeat domain that allows binding of the Tcf4/LEF TFs (Thalhammer and Cingolani, 2014; Wisniewska, 2013). The TF Tcf4 has been shown to be required for plasticity mechanisms (Kennedy et al., 2016) and was found to be among the upregulated genes in activity-deprived eNs (see Figure 5.36 B). Interestingly, expression of CamkIV was shown to be regulated by Tcf4/LEF (Arrázola et al., 2009), however, CamkIV was found among the DRG. Moreover, modulation of AMPAR number at the synapse by the transmembrane AMPAR regulatory proteins (TARPs) Cacng2, Cacng4, and Cacng8 is well established and has been shown to play a crucial role in homeostatic plasticity (Isaac et al., 2007; A. G. Lee et al., 2016). For instance, overexpression of Cacng2 was shown to result in an exclusive increase in AMPAR-

mediated EPSCs (Payne, 2008). Finally, six genes among the DRG were identified (*Auts2*, *Cntnap2*, *Smg6*, *Rbfox1*, *Upf2*, *Bbs4*) that have been shown to be implicated in autism spectrum disorders and ten genes (*Nrg1*, *Pde4b*, *Vegfa*, *Qk*, *Cdh13*, *Erbb4*, *Gabrb2*, *Gria1*, *Ranbp9*, *Tcf4*) that are known to be risk genes for schizophrenia (Boulenouar et al., 2022; Wittmann and Häberle, 2018).

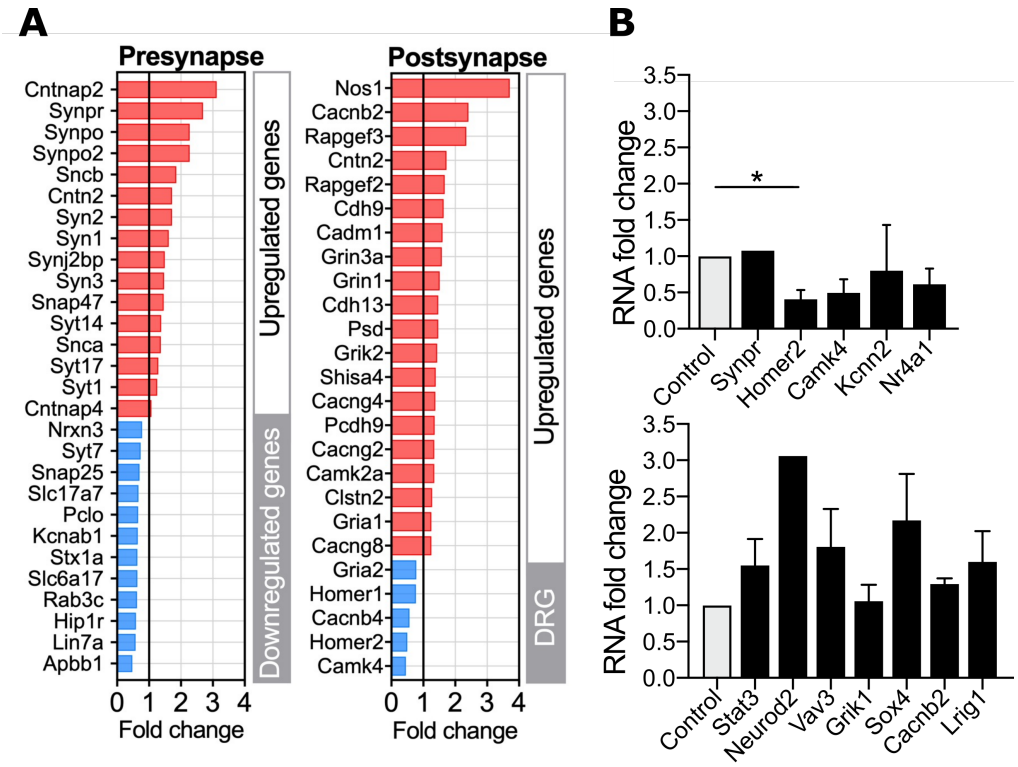

Figure 5.38: **Differentially regulated genes relating to pre- and postsynapse in endogenous neurons in response to activity inhibition.**
(A) Fold change values of differentially regulated genes relating to presynaptic (*left*) and postsynaptic (*right*) proteins are visualized. Upregulated genes are visualized in red and downregulated genes are in blue. Bar length is determined by the fold change increase/decrease in expression in inactive eNs compared to active eNs. **(B)** qRT-PCR analysis of selected downregulated (*top*) and upregulated (*bottom*) genes.

5.4.2 *Identification of transcription factors regulated in response to activity inhibition as putative modulators of synaptic upscaling*

Neuronal activity-dependent responses are mediated to a significant extent by TFs, which regulate the expression of a multitude of genes related to plasticity and development. Despite intense work on HSP, only few TFs and downstream molecular pathways that instruct the induction of homeostatic scaling processes have been identified so far

(Huang et al., 2022; Kennedy et al., 2016; Valakh et al., 2021). This work shows that activity suppression of cortical neurons *in vitro* leads to the induction of a large set of TFs, apart from genes directly related to structural and functional synaptic remodeling, which possibly play a role in governing the compensatory increase in synaptic function and neuronal excitability. In line with this, several of the detected TFs have already been linked to essential regulating roles during homeostatic synaptic scaling, such as Tcf4, Tef, Foxo3 (here found to be upregulated) and L3mbtl4, L3mbtl1 or Nr4a1 (here found to be downregulated) (see Figure 5.39). For instance, the TF Tef, which was found to be upregulated in inhibited eNs, has recently been shown to be upregulated during homeostatic synaptic upscaling and functions to restrain the scaling process (Valakh et al., n.d.). While knockout of Tef resulted in an excessive homeostatic response, basal network activity remained unaffected, suggesting a restraining function of Tef in this specific context (Valakh et al., n.d.). Moreover, the polycomb chromatin reader L3mbtl1 has been recently shown to be regulated by neuronal activity and constitutes an essential player in regulating synaptic downscaling in response to neuronal activity (Mao et al., 2018). In line with the above-mentioned observations, here, L3mbtl1, as well as L3mbtl4, were found to be downregulated in response to activity inhibition. Expression of the TF Nr4a1 is regulated by key regulators of synaptic function, e.g. NMDAR, CREB and MEF2, and is therefore directly involved in synaptic plasticity mechanisms (Y. Chen et al., 2014). Moreover, a recent study showed that Nr4a1 directly regulates the expression of synaptic organizer molecules in an activity-dependent manner in inhibitory interneurons of the forebrain (Huang et al., 2022). Lastly, the upregulated bHLH TF Tcf4 represents an interesting candidate: it is expressed in the developing as well as adult CNS and has therefore been linked to neurodevelopmental as well as plasticity processes (Wittmann and Häberle, 2018). In fact, loss of function results in the neurodevelopmental disorder Pitt-Hopkins syndrome which is associated with intellectual disability and an autistic phenotype (Crux et al., 2018). Several studies have suggested its role in synaptic plasticity: by using a mouse model with an inducible functional knockout in cortical as well as hippocampal neurons, the authors showed that loss of Tcf4 leads to a reduction in dendritic spine numbers with perturbed morphology as well as reduced spiking via disinhibition of hyperpolarizing ion channels (Crux et al., 2018; Wittmann and Häberle, 2018). Here, Tcf4, as well as two of its known downstream targets, *Nrxn1* and *Cntnap2* (Kennedy et al., 2016), are upregulated in response to activity inhibition. Beyond the above-mentioned TF which have established roles in plasticity, this work provides a large list of TFs that may represent novel transcriptional regulators of synaptic scaling. For instance, Atf2 or Jun have not yet been implicated specifically in HSP mechanisms but are known and relevant TFs in transmitting extracellular signals to the nucleus in an activity-dependent manner (Ahlgren et al., 2014; West and Greenberg, 2011). An interesting candidate for a

potentially significant role in regulating HSP mechanisms is the strongly upregulated TF NeuroD2. NeuroD2 is a class II bHLH TF that is known to interact with Tcf4 (Crux et al., 2018) and is implicated in the regulation of neuronal differentiation during brain development (Kennedy et al., 2016; Runge et al., 2021) by repressing the REST complex (Ravanpay et al., 2010). Interestingly, while expression of its paralog gene NeuroD1 eventually terminates around birth, expression of NeuroD2 persists until adulthood (Runge et al., 2021), suggesting a role in mature neuronal physiology. Moreover, NeuroD2 has been identified as an activity-dependent TF and shown to mediate synaptic innervation as well as intrinsic excitability of cortical pyramidal neurons (Y. C. Chen et al., 2016). Here, NeuroD2 was detected among the upregulated TFs and verified by qRT-PCR (see Figure 5.38 B). Given its known function, this observation suggests a strong implication in homeostatic synaptic plasticity processes.

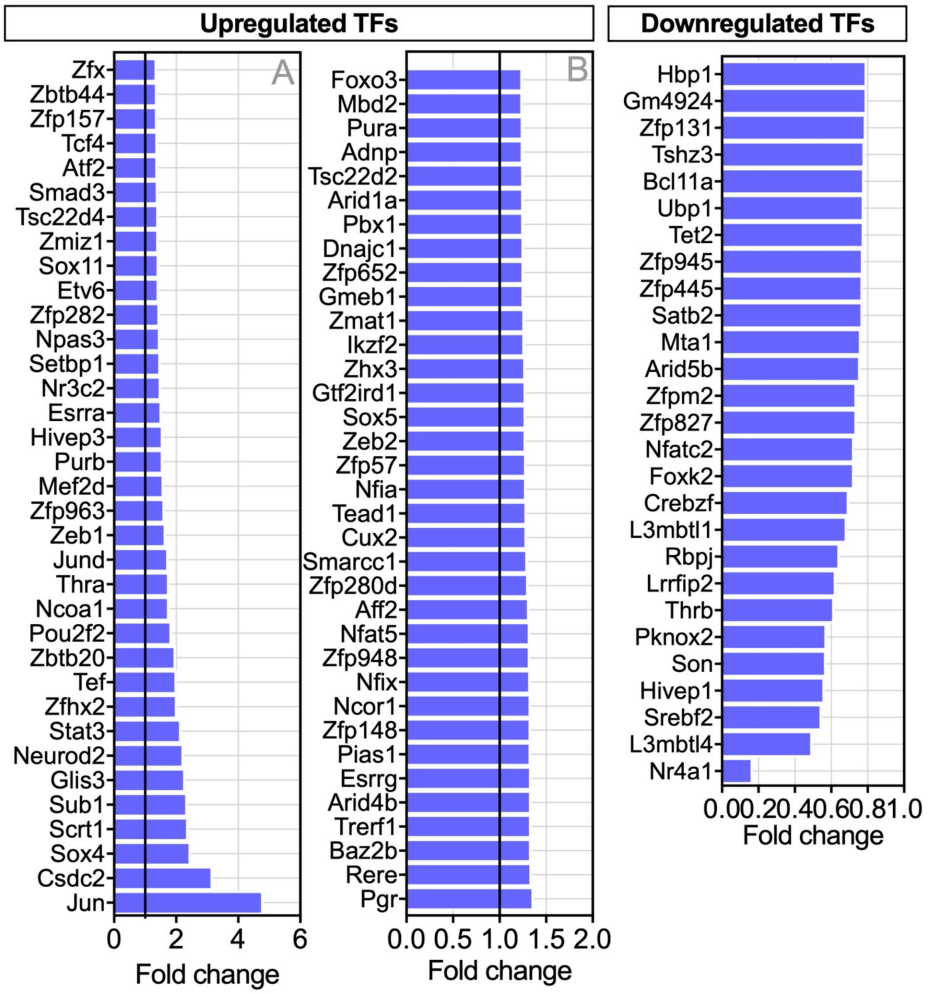

Figure 5.39: **Regulation of TF expression in response to activity suppression in endogenous neurons.** Differential gene expression analysis identified a set of upregulated (*left*) and downregulated (*right*) transcription factors in eNs.

5.4.3 *Downregulation of postsynapse-specific genes in induced neurons following activity inhibition*

In the previous chapter, the applied pharmacological treatment was validated in eNs as it indeed induced a plethora of known synaptic plasticity-related genes that are implicated in homeostatic upscaling following activity inhibition. The next focus was to assess whether iNs display the ability to regulate their transcriptome in response to network activity modulation and whether the extent of the regulation resembles eN-induced changes. DEG were initially assessed using the same thresholds as for eNs (FDR of < 0.05, FC cutoff at 1.25, adj. p-value < 0.05). Surprisingly, the DEG analysis revealed only 79 upregulated genes and 160 downregulated genes by iNs in response to activity inhibition (see Figure 5.35 A and B). Between the transcriptional responses elicited in eNs and iNs, only 13 genes (*Atrx*, *Bod1l*, *Caln1*, *Ddx*, *Fam214a*, *Hivep3*, *Hook2*, *Kcnq1ot1*, *Map7*, *Metap1d*, *Phc2*, *Polr2a* and *Pou2f2*) were found to be commonly upregulated and 36 genes (*9630014M24Rik*, *Agrn*, *Cadps2*, *Cdk8*, *Cmss1*, *Ctnna3*, *Ddx17*, *Ddx39b*, *Fgf1*, *Gm11867*, *Gm15594*, *Gm20275*, *Gm26749*, *Gm26917*, *Gm37240*, *Gm50368*, *Gphn*, *Hnrnpa3*, *Hsd17b12*, *Lysmd4*, *Macrod1*, *Mir124a-1hg*, *Nrbp2*, *Oxr1*, *Parp8*, *Pmpca*, *Ppm1l*, *Rps6ka3*, *Rsrp1*, *Shc3*, *Slc24a5*, *Sorbs2os*, *Srsf5*, *Thrb*, *Tsix* and *Ube3a*) commonly downregulated (see Figure 5.35 C). The regulation into opposite directions was assessed and 10 genes were found to be upregulated by eNs but downregulated by iNs (*Zfhx2*, *Prkg1*, *Prkag2*, *Peak1*, *Larp4*, *Grik1*, *Galnt13*, *Cntnap2*, *Chl1*, *Cblb*) while only two genes were downregulated by eNs but upregulated by iNs (*Prpf4b*, *Cacna1a*). The small proportion of shared regulated genes between eNs and iNs suggests a regulation of distinct transcriptional programs in response to activity inhibition. In order to assess whether the discrepancy may be due to distinct strengths of gene regulation that may be masked by the stringent criteria for the fold change cut-off value (FC > 1.25), the threshold was lowered for iN regulated genes (FC > 1.07). Surprisingly, this analysis resulted in the detection of 306 downregulated and 227 upregulated genes from which only 44 and 30 genes overlapped with the eN-regulated gene sets, respectively (FC > 1.07, p-value 0.05). The proportion of overlapping genes hence decreased from 16.46 to 13.22 % for URG (FC > 1.25 vs 1.07 in iNs) and from 22.5 to 14.38 % for DRG (FC 1.25 $>$ vs 1.07 in iNs), suggesting that indeed the regulated gene sets by iNs and eNs are distinct and likely relate to distinct functional responses. To exclude the possibility that the comparative analysis of DEG between eNs and iNs in response to activity inhibition may have been confounded by discrepancies in neuronal developmental stages, a previously performed study on transcriptional regulation in response to activity inhibition in 14 *div* cortical neurons was used to compare DEG with those induced by iNs (Schaukowitch et al., 2017). Surprisingly, only 4 (*Fam171a1*, *Shc3*, *Thrb*, *Zfhx2*) and 2 (*Polr2a*, *Fbxl20*) genes were found to be commonly

up- and downregulated, respectively. Although the small overlap of DEGs could be attributed to different technologies used to assess transcriptomic regulations, 24.7 % and 19.9 % of the genes shown to be up- and downregulated in 14 *div* cortical neurons overlapped with DEG detected in (28 *div*) eNs, respectively (data not shown). This further confirms that iNs and eNs initiate distinct transcriptional regulation in response to activity inhibition. Moreover, the observed deviation does not seem to be explained by the maturation differences observed between iNs and eNs. Strikingly, iNs display a more prominent downregulation of genes rather than an upregulation in response to activity inhibition (see Figure 5.35). Interestingly, iN-downregulated genes, also comprise a bigger proportion of DEG compared to upregulated genes (see Figure 5.35). When exploring iN-upregulated genes, no obvious and coherent functional category could be identified. Moreover, GO term analysis of iN-upregulated genes did not show any functional enrichment while iN-downregulated genes showed significant enrichment for cellular components related to 'synapse', e.g. 'postsynapse', 'glutamatergic synapse' or 'dendrite' (see Figure 5.40), and this observation was maintained when loosening the FC cutoff threshold (FC 1.25 > vs 1.07). Crucially, while eNs display regulation of the AMPAR subunits *Gria1* and *Gria2*, indicative of mature synaptic connections, iNs display downregulation of the AMPAR subunit *Gria4* in response to activity inhibition. Expression of *Gria4* as well as *Gria4*-dependent plasticity mechanisms have been linked to immature, developing synapses (Huupponen et al., 2016; Luchkina et al., 2014). In fact, cortical neurons temporarily express the AMPAR subunit *Gria4* during critical periods, e.g. time windows of increased formation of synaptic connectivity (Huupponen et al., 2016; Luchkina et al., 2014). In addition, previous studies could show that *Gria4* expression is not only sufficient in driving LTP (Luchkina et al., 2014) in immature neurons, but also critical for establishing sensitivity to activity-dependent changes in intrinsic excitability and glutamatergic transmission (Huupponen et al., 2016). At earlier developmental stages, these mechanisms rely on PKA while the dependency later transitions onto CamKII (Luchkina et al., 2014). In line with this, iNs express higher levels of *Prkaa2* and *Prkca* (see Table 19). Albeit protein kinase A (*Prkaca, Prkacb, Prkacg, Prkar1a, Prkar1b, Prkar2a, Prkar2b*) was not found among the DEG, the protein kinase A subunit gamma 2 (*Prkag2*) was downregulated, similarly to *Gria4*. In general, several genes related to structural complexity were found to be downregulated, such as *Mef2c, Epha7, Rapgef4 (also known as Epac2), Ctnnb1, L1cam* (see Figure 5.40). In addition, the CaMKId transcript was found significantly downregulated (see Table 23). CaMKId has been shown to mediate transcription via the Ras/Erk signaling pathway in a Ca^{2+}-dependent way and strongly contributes to dendritic arborization, albeit mostly in a developmental context (Wayman et al., 2008).

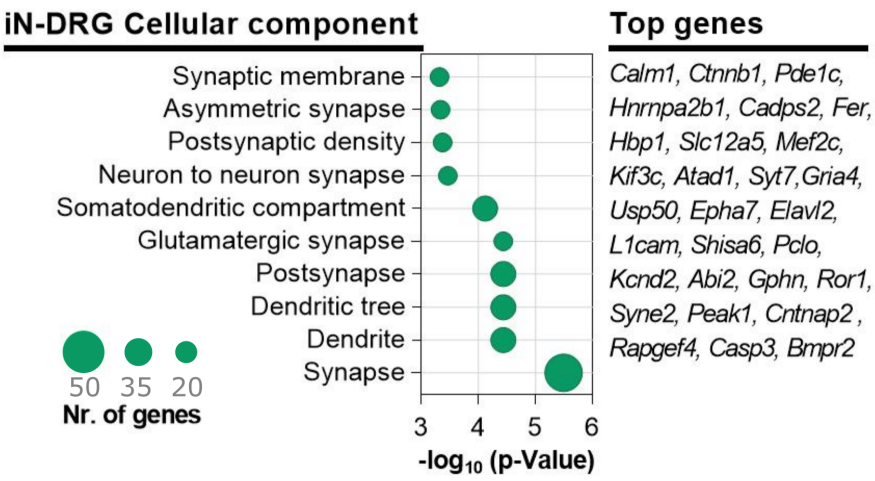

Figure 5.40: **GO term analysis of the iN-downregulated gene set.**
Go term analysis of iN-DRG set shows strong enrichment for cellular components such as 'post-/synapse', 'dendrite' or 'glutamatergic synapse'. Selected genes that were enriched in these pathways are highlighted on the right side.

Interestingly, when performing synapse-specific GO term analysis, genes significantly, and exclusively, enriched for structural components of the postsynapse (see Figure 5.41 *A*). Among the regulated genes in iNs, a small set of TFs could be identified. iNs display downregulation of 11 TFs *Fli1, St18, Kat7, Mef2c, Zfhx, Thrb, Ncor2, Purg, Prox1, Foxj3, Prdm8* and 8 cofactors (*Mapk14, Flna, Cdk8, Rps6ka3, Ddx17, Ccnh, Fer, Hnrnpa2b1*) (see Table 23), while upregulating only 6 TFs (*Zfp64, Pou2f2, Hivep3, Terf1, Atrx, Ash1l*) and 3 cofactors (*Pkn2, Tpr, Gps2*) in response to activity inhibition (see Table 22). Interestingly, only two TFs were commonly upregulated by iNs and eNs (*Zfhx2 and Thrb*). Moreover, iNs display upregulation of Ncor2 while eNs increase expression of Ncor1. Similarly, only two TFs were found to be commonly downregulated (*Pou2f2 and Hivep3*), while eNs downregulate *Hivep1* in addition. Interestingly, in the absence of activity, the transcriptional corepressors Ncor1/2 are known to suppress activity-dependent gene transcription via epigenetic silencing by recruiting histone deacetylases and have been shown to regulate gene expression in a developmental as well as homeostatic context (Iemolo et al., 2020). Among eN upregulated genes, the histone deacetylase Hdac8 could be detected, while iNs do not display regulation of such epigenetic modifiers. Ncor2, which is upregulated in iNs, was shown to be recruited by the TF Arnt2 in order to suppress activity-dependent gene transcription in silenced neurons (Sharma et al., 2019).

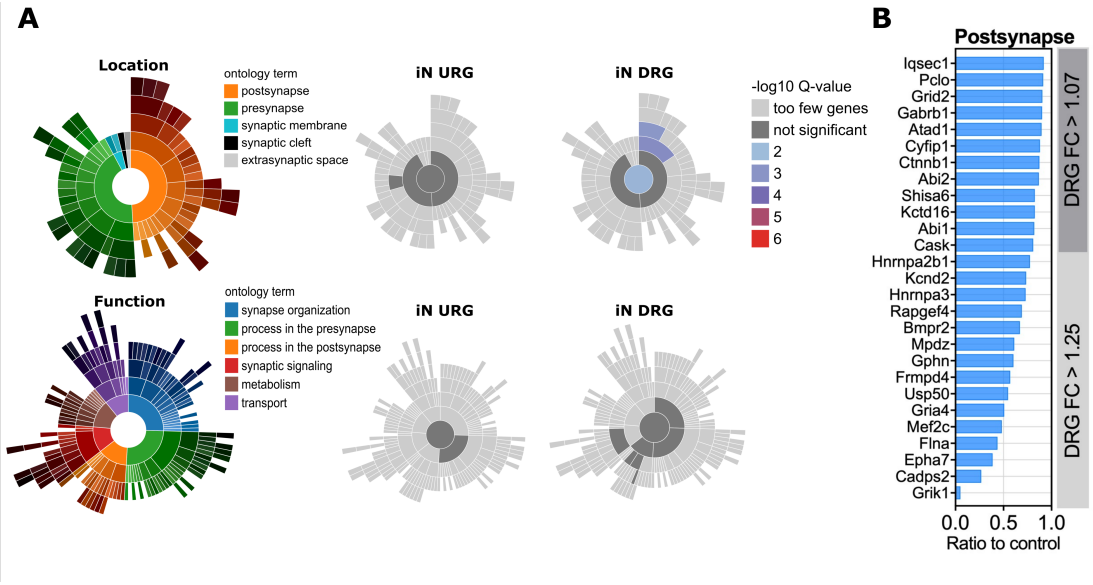

Figure 5.41: **Specific downregulation of postsynapse-related genes in inhibited iNs.** (**A**) Synapse-specific GO term analysis of iN up- and downregulated genes shows that iNs display downregulation of postsynapse-enriched genes. (**B**) Bar plot visualizing the fold changes of downregulated, postsynapse-enriched genes.

Due to the downregulation of multiple genes related to structural complexity, Sholl analysis was performed to characterize changes in the dendritic arbor morphology of iNs across conditions. In accordance with known functions of downregulated genes relating to morphological development, a reduced morphological complexity was observed in inhibited iNs compared to control iNs (see Figure 5.42). Moreover, a significant reduction in the number of primary branches was observed in inhibited iNs (see Figure 5.42). In summary, these data show that inhibition of activity leads to genome-wide gene regulation in iNs. Albeit the analysis revealed a limited number of regulated genes in iNs, the extent of regulation does resemble previous bulk sequencing studies (Schaukowitch et al., 2017). Surprisingly, induced transcriptional dynamics do not suggest a functional similarity with transcriptional dynamics observed in eNs as iNs do not display a strong transcriptional upregulation that would reflect homeostatic synaptic upscaling. Instead, iNs respond to activity inhibition by a remarkable downregulation of synapse-related genes, among which the critical AMPAR subunit GluA4 was detected. These data suggest that the cellular physiologies of iNs and eNs seem to be substantially different, which may reflect an acquisition of a distinct cellular phenotype or incomplete synaptic integration into the network of iNs.

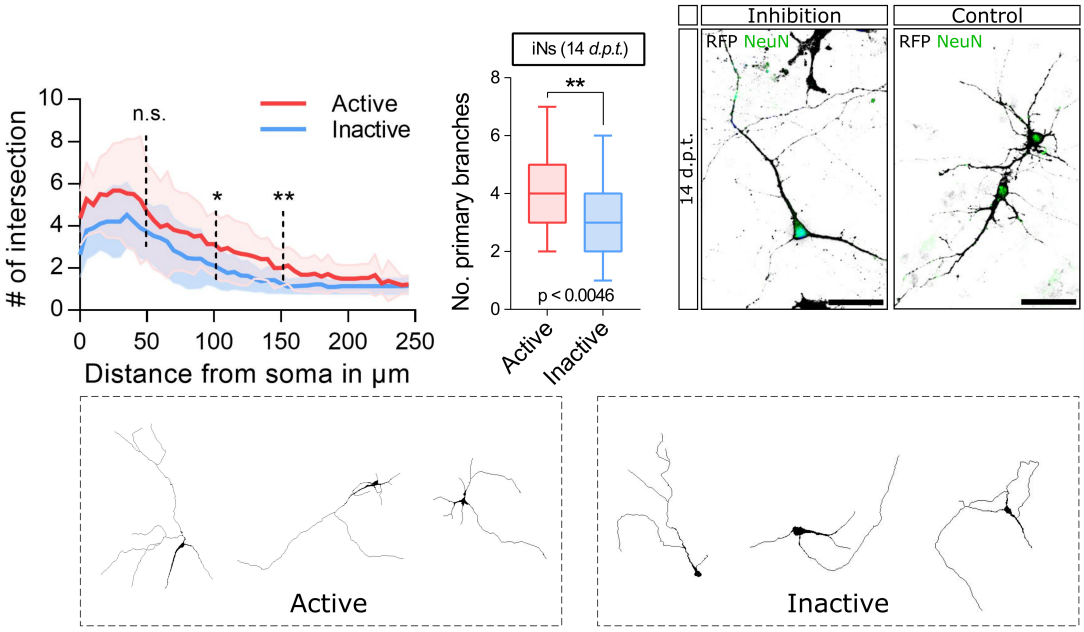

Figure 5.42: **Activity-dependent morphological changes in iNs.**
Activity was pharmacologically inhibited for 48 hours in cocultured neurons and morphological complexity was assessed in iNs using Sholl analysis. Additionally, the number of primary branches extending from the soma was manually counted. Immunocytochemical staining showing expression of NeuN and RFP in induced neurons. The color channel for the reporter was inverted in order to visualize detailed morphology. Representative images displaying morphological complexity in control and silenced condition (*bottom panel*). Scale bar, 40 µm.

5.4.4 *eN-upregulated genes in response to activity inhibition are highly expressed in iNs under basal condition*

Due to the minimal overlap of regulated genes between eNs and iNs, I reasoned that eN-URG may either not be expressed in iNs or that, due to extensive heterogeneity in neuronal types and maturation levels, single genes may display a higher variability in expression levels that would prevent the identification of clear shifts in gene expression across experimental conditions (active vs. inactive). Assessing expression dynamics of eN-regulated genes as whole sets of genes in iNs may therefore reveal a coherent shift in expression. In order to project the set of eN-URG and -DRG on iNs, a score was calculated by subtracting the average expression of a reference gene set from the average expression of the eN-URG and eN-DRG set, respectively by using ScanPy (see Table 15). The reference gene sets were randomly sampled from all genes expressed. The obtained signature scores were then visualized on the UMAP plot. The most striking observation to emerge from the data comparison was that eN-URG were found to be actually highly expressed by active iNs (see Figure 5.43 A *left*). Moreover, the expression levels of this gene set in iNs seem to be at least as high as those found in the inactive eN population.

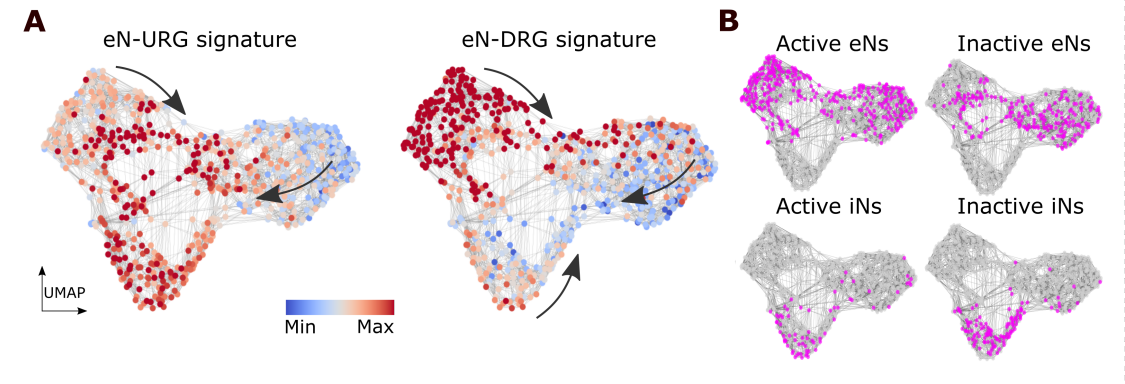

Figure 5.43: **Visualization of eN-regulated gene set signatures on UMAP plots.** (**A**) UMAP plots visualizing the eN-URG signature (*left*) and eN-DRG signature (*right*). (**B**) UMAP plots visualizing each of the four experimental groups.

Moreover, a seeming downregulation of eN-DRG could be appreciated based on mean expression values (see Figure 5.43 A *right*). In order to assess which genes of the eN-URG set were highly expressed in iNs, the list of eN-URG was compared to the list of regulated genes between active eNs and active iNs (see Figure 5.31 and Tables 18 and 19). This comparison identified a total of 192 genes that were significantly more highly expressed by active iNs compared to active eNs (see Figure 5.44 A). Intriguingly, iNs express this gene set at higher levels than expression levels detected in the inactive eNs (i.e. following upregulation) (see Figure 5.44 B). GO term analysis revealed that these genes significantly enrich for biological processes related to 'Neuron differentiation', 'cell projection organization', or 'positive regulation of transcription' (see Figure 5.44 C). In order to assess whether the high expression level of these genes reflects a more immature developmental stage of iNs as suggested by the observed functional enrichment categories, expression levels of genes were assessed in young (P8) and adult (P38) glutamatergic neurons derived from the S. Cheng et al., 2022 dataset. Interestingly, genes displayed a balanced distribution across developmental time points, with half of the genes being expressed at higher levels during early time points (41.3 %) and the other half expressed more highly during later time points (54.2 %) (see Figure 5.44 D), implying that high expression of this gene set is not necessarily reflecting the more immature phenotype of iNs compared to eNs.

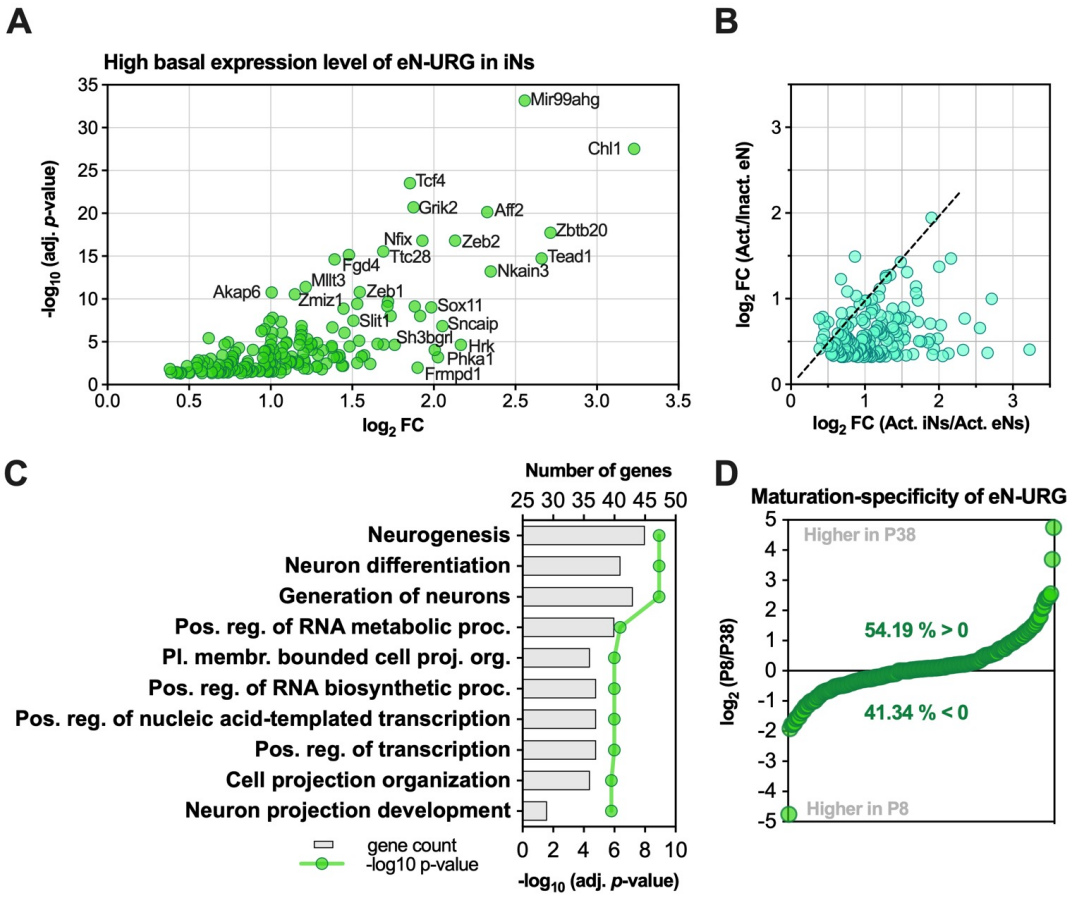

Figure 5.44: **eN-upregulated genes are highly expressed in iNs and are independent of distinct maturation stages.** (**A**) Visualization of eN-URG genes that were found to be highly expressed in active iNs (in comparison to active eNs). **(B)** Comparison between the $\log_2$ ratio of Active iNs/Active eNs expression values and $\log_2$ ratio of Active eNs/Inactive eNs. **(C)** GO term analysis of the eN-URG gene set that is highly expressed in active iNs. **(D)** Assessment of expression values of eN-URG set in postnatal (P8) and adult (P38) glutamatergic neurons taken from the S. Cheng et al., 2022 dataset available at www.singlecell.broadinstitute.org. Ratios were ordered according to size and visualize expression levels in both populations. Percentages given do not include the number of zeros, e.g. genes whose expression level did not differ between the distinct maturation stages assessed.

Next, I assessed whether the previously identified two iN populations, distinct in maturation stages, display distinct expression dynamics of the eN-URG set across the experimental conditions. Intriguingly, both iN populations, immature as well as mature ones, display a significantly higher expression level of the gene set compared to basally active eNs (Immature iNs: p-value = 0.0001, mature iNs: p-value $<$ 0.0001; see Figure 5.45 *left*). In contrast, the set of eN-DRG was found to be expressed at significantly lower levels by both iN populations (Immature iNs: p-value $<$ 0.0001, Mature iNs: p-value $<$ 0.0001; see Figure 5.45 *right*). Crucially, statistical analysis of expression levels between

the active and inactive iN populations revealed that mature iNs display a significant upregulation of the eN-URG set (p-value = 0.0128), despite expression of these genes at higher basal levels compared to eNs. Moreover, downregulation of the eN-DRG set was prominent as well (p-value = 0.0004). Immature iNs did not display any obvious upregulation (p-value = 0.8969) but significant downregulation (p-value = 0.0268).

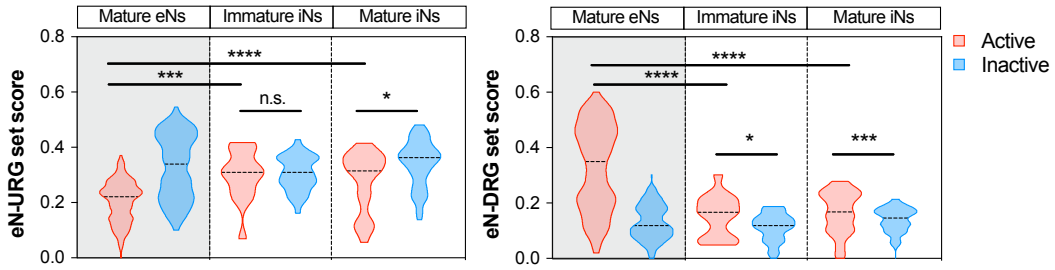

Figure 5.45: **Visualization of eN-regulated gene set signatures on UMAP plots.** (**A**) UMAP plots visualizing the eN-URG signature (*left*) and eN-DRG signature (*right*). (**B**) UMAP plots visualizing each of the four experimental groups.

Together, these analyses suggest that at least the more mature iN population displays signs of homeostatic synaptic upscaling hence reflecting functional integration into the network. The basally higher expression levels of genes that are identified as functionally relevant for synaptic plasticity processes most likely represent a relevant aspect of functional maturation in iNs which may correlate with the higher competing interest in synaptic integration.

5.5 ASSESSMENT OF SYNAPTIC INTEGRATION OF INS BY PHARMACOLOGICAL NETWORK ACTIVITY DISINHIBITION

The next experiment assessed whether activity-dependent gene regulation in iNs can be induced by acute network disinhibition. In order to test this, the next experiment focused on whether iNs display c-Fos upregulation in response to synaptic stimulation by modulating endogenous GABAergic signaling. Network activity was therefore disinhibited by exposing cultures to the $GABA_A$ receptor antagonist Bicuculline in order to increase excitatory firing. Alongside Bicuculline, cultures were treated with the K^+-channel inhibitor 4-Aminopyridine, which inhibits the repolarization phase and leads to an increased firing frequency. This protocol has been widely used to increase synaptic stimulation and activate synaptic NMDAR *in vitro* (Hoey et al., 2009; Hou et al., 2013; Karpova et al., 2013). Cocultures were treated for 15 min and activity was subsequently abolished using 1 µM TTX. Cells were then fixed after 1 and 3 hours and immunocytochemically labeled for c-Fos along and a neuronal marker. While the synaptic stimulation

paradigm strongly induced c-Fos upregulation in eNs after 1 hour (Control: 4.27 ± 0.14, 1 hour: 8.43 ± 0.19, $p < 0.0001$), c-Fos intensities remained unchanged 1 hour after treatment in iNs (Control 1.38 ± 0.07, 1 hour: 1.58 ± 0.11, see Figure 5.46). After 3 hours, c-Fos intensities in eNs drastically increase to an approximately 15-fold value (Control: 4.27 ± 0.14, 3 hours: 56.41 ± 0.96, $p < 0.0001$). These data suggest that Bicuculline/4-AP treatment leads to increased excitatory firing, resulting in strong c-Fos upregulation.

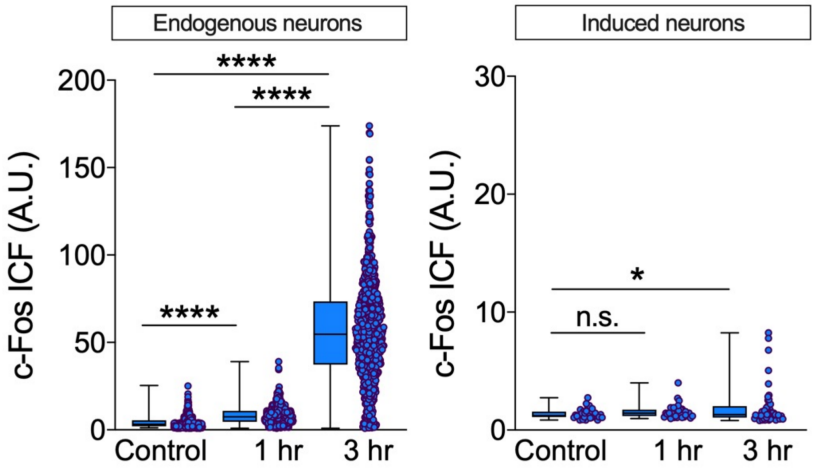

Figure 5.46: **Network activity disinhibition does not result in c-Fos upregulation in iNs.** Cocultured neurons were treated for 15 min with Bicuculline and 4-AP in order to disinhibit excitatory neurons and induce enhanced firing. Activity was ceased and the cultures were fixed 1 and 3 hours after treatment. c-Fos protein expression level was assessed via immunocytochemical stainings.

In comparison, iNs show no c-Fos upregulation 1 hour after treatment and only minimal upregulation following 3 hours (Control: 1.38 ± 0.07, 3 hours: 1.98 ± 0.25, $p < 0.0258$) These data suggest that iNs are not only poorly connected to GABAergic neurons (see Figure 5.47), but also do not receive (increased) synaptic input from excitatory neurons when these are disinhibited. In order to assess connectivity, the presence of GABAergic synapses onto cocultured neurons was first assessed by immunocytochemical staining via labeling of the presynaptic vesicular GABA transporter (vGAT) and the postsynaptic scaffold protein Gephyrin. The latter is a crucial component of functional GABAergic synapses and anchors glycine and $GABA_A$ receptors at their location in the membrane (Choii and Ko, 2015). In eNs, prominent expression of Gephyrin was observed which colocalized with vGAT expression, suggesting presence of functional GABAergic synapses onto eNs (see Figure 5.47). In comparison, iNs displayed only a few Gephyrin punctae around the soma and rarely along the dendrites. vGat punctae were more abundantly observed (see Figure 5.47).

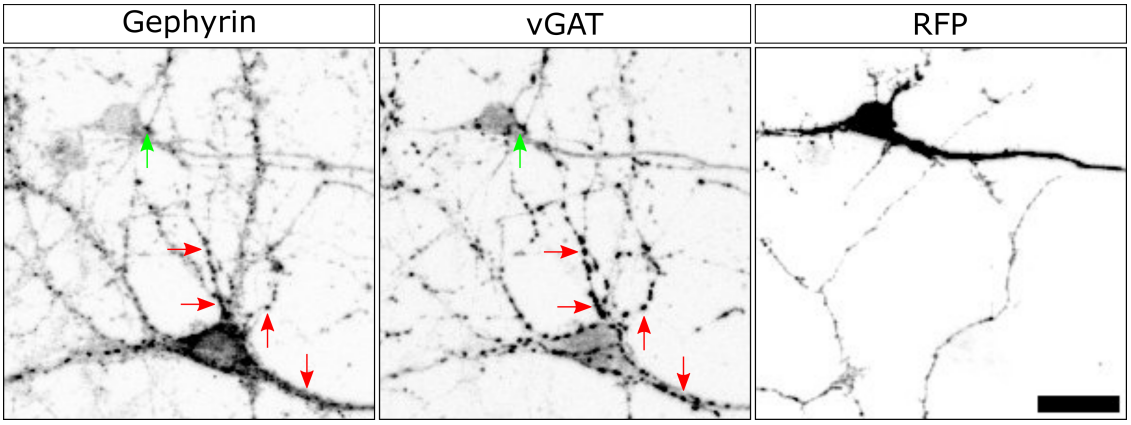

Figure 5.47: **Visualization of GABAergic synapses in coculture.**
Immunocytochemical staining visualizing GABAergic synapses in cocultured eNs and iNs. Dendrites and soma of eNs were decorated with presynaptic terminals containing vesicular GABA transporter (vGAT), which colocalized with the postsynaptic scaffold protein gephyrin. In comparison, iNs expressed less gephyrin and were decorated with fewer presynaptic terminals containing vGAT, out of which not all colocalize with gephyrin expression. Scale bar, 20 µm.

This allows the assumption that both neuronal populations receive presynaptic GABAergic contacts. However, compared to eNs, iNs display minimal expression of the postsynaptic element Gephyrin. This observation suggests an incomplete assembly of GABAergic synapses onto iNs and hence limited responsiveness to GABAergic signaling. The presence of glutamatergic synapses was then assessed immunocytochemically by assessing vGlut1 expression. Surprisingly, iNs were not appreciably decorated by vGlut1 punctae, unlike surrounding eNs (see Figure 5.48), despite the expression and activity-dependent regulation of multiple postsynaptic genes (see Figure 5.41). In sum, the data suggest that despite the ability of iNs to transcribe necessary postsynaptic-related genes, synaptic input from eNs may be very sparse. Indeed, the very limited response displayed by iNs to network disinhibition favors the former interpretation that synaptic integration seems limited.

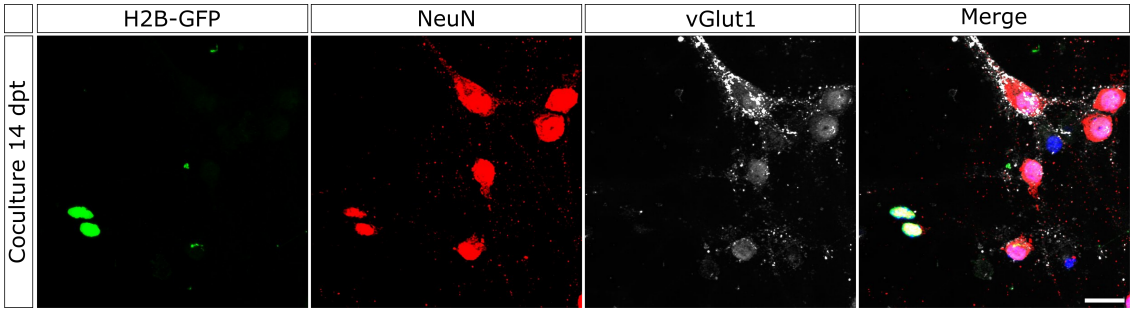

Figure 5.48: **Limited decoration of iNs with vGlut1 in coculture.**
Immunocytochemical staining of vGlut1 expression in endogenous and induced neurons cocultured for 14 *dpt*. Induced neurons express the reporter H2B-GFP. Scale bar, 20 µm.

6

DISCUSSION

Direct cellular reprogramming has expanded the potential for cell replacement therapeutic approaches following congenital or degenerative neuronal diseases as well as acute neuronal damage. The application, however, requires a comprehensive understanding of what iNs can and cannot functionally achieve once embedded within the adult, diseased brain. Despite comprehensive characterizations of glia-derived Neurog2-induced neurons regarding their basic neuronal functional features, little is known about the ability to respond to neuronal depolarization by inducing functionally relevant changes to their transcriptome. Neuronal plasticity is not only required for the restoration and maintenance of proper circuit functioning but is also a necessity for iNs to integrate into the pre-existing network. The work presented in this thesis focused on investigating whether iNs display the ability to implement meaningful transcriptional regulation in response to activity modulations. This was addressed first by performing an acute stimulation with subsequent assessment of the upregulation of IEGs. Next, chronic activity inhibition aimed to assess genome-wide transcriptional responses, reflecting homeostatic plasticity mechanisms as an indication of functional integration into the network. The mechanistic insights derived from this thesis improve our understanding of the molecular phenotype of iNs and eventually might be valuable in refining the iN differentiation process towards a functionally more mature and responsive phenotype.

6.1 INDUCED NEURONS DISPLAY ACTIVITY-DEPENDENT TRANSCRIPTIONAL RESPONSIVENESS TO FUNCTIONAL STIMULATION

Functional integration of iNs into an extant neuronal circuitry would support the regenerative potential of cellular reprogramming. Substantial evidence from previous reprogramming studies suggests the acquisition of neuron-specific morphology, functional features as well as protein expression (Heinrich et al., 2010; R. K. Tsunemoto et al., 2015). Crucially, iNs generate action potentials (Berninger et al., 2007) and display synaptic connections with surrounding neurons (Blum et al., 2011; Heinrich et al., 2010; Lentini et al., 2021; Tai et al., 2021). Yet, it remains unclear if and to which extent iNs possess the ability to meaningfully contribute to their surrounding network by coupling changes in activity to transcriptional regulation that ultimately leads to functional modification. Therefore, the first experiments addressed whether iNs display the ability to undergo activity-dependent gene transcription as a prerequisite for synaptic plasticity

mechanisms and whether such a form of neuronal activation would be detectable across the entire iN population. The readout chosen was IEG protein expression due to their rapid expression kinetics following transcriptional activation (Meenakshi et al., 2021) and the possibility of assessing single-cell expression levels via immunocytochemical stainings. For this, the activity of cocultured iNs and eNs was initially silenced overnight, neurons were then exposed to elevated KCl levels for 3 hours in order to induce robust membrane depolarization and to allow downstream gene expression changes to take place. The data presented shows that iNs can be 'activated' by stimulation protocols generally applied for testing the responsiveness of neurons (Bullitt, 1990) and do this as expected of maturing neurons in response to the applied external stimulation (e.g. upregulation of IEGs). Moreover, they display this ability when tested after a maturation period of 2 weeks *in vitro*. Two distinct and functionally relevant IEGs were selected as molecular markers in order to assess activity-induced transcriptional modulation, c-Fos as well as Arc. The IEG c-Fos is a TF that has been functionally extensively characterized and linked to processes underlying neuroplasticity (Abraham et al., 1991; Gandolfi et al., 2017; Guzowski et al., 2001; Minatohara et al., 2016). The observation that iNs display robust c-Fos upregulation in response to stimulation demonstrates that the molecular communication between synapse and nucleus is established and functional. Similarly, upon stimulation, iNs displayed upregulation of the effector protein Arc which, however, displayed restricted expression towards the soma, while eNs strongly displayed dendritic Arc expression (see Figure 5.15). Upon stimulation, rapid transcription of the IEG Arc is followed by trafficking towards dendrites with local translation at synapses, a process that is critical in synaptic plasticity and learning mechanisms (Ninomiya et al., 2016; Pastuzyn and Shepherd, 2017). The absence of Arc protein in iNs' dendrites therefore suggests either a transportation or local translation perturbation, e.g. Arc mRNA may either not be transported distally or translation may not be occurring despite mRNA presence in dendrites. Performing Single Molecule Fluorescence In Situ Hybridization (smFISH) would help address whether Arc mRNA localizes to dendrites. Interestingly, Arc protein translation has been described to also occur in the somatic cytoplasm following activity-dependent transcriptional activation, suggesting that translation of at least a small mRNA pool does not take place distally (Steward et al., 2015). Moreover, this finding implies that Arc mRNA may be mostly under active translational repression during distal transportation, with a small pool of mRNA molecules being not under this influence and that the ratio of locally versus distally translated mRNA may be different between iNs and eNs. The second scenario may be that Arc mRNA gets transported distally, but not locally translated. Local translation has been shown to be under the control of local synaptic signals (Schuman et al., 2006), hence distinct Arc protein localization may indirectly reflect the degree of synaptic integration of iNs. Interestingly, both c-Fos

and Arc were upregulated by a larger proportion of iNs and to higher expression levels compared to eNs. The fact that a higher percentage of iNs displays IEG upregulation than eNs may reflect distinct maturation stages: since neuronal circuits are established and shaped during early cortical development, it has been suggested that immature neurons are more responsive to activity modulations than more mature ones (X. Zhou et al., 2009). Different intensities of IEG expression may reflect distinct temporal dynamics of IEG regulation. IEG transcription occurs rapidly, reaches a maximum and declines within minutes to hours following stimulation (Tyssowski et al., 2018b). Different intensity levels between the majority of iNs and eNs may therefore suggest distinct temporal dynamics of IEG expression following stimulation: the maximum mRNA expression of the investigated rapid IEGs has been shown to be normally reached after 1 hour following stimulation (Tyssowski et al., 2018b) and protein expression usually peaks between 90 and 120 mins as detected by immunocytochemical staining (Meenakshi et al., 2021), depending on the activation of different signaling cascades (Tyssowski et al., 2018b). Distinct intensity levels may therefore suggest either the involvement of distinct signaling pathways in iNs and eNs or a common signaling pathway with distinct timing or magnitude. For further investigation, it would be suggested to assess distinct temporal dynamics by varying the stimulation duration, an experimental design that may suggest an involvement of distinct signaling cascades. Moreover, performing immunocytochemical stainings at distinct time points following stimulation would reveal the temporal dynamics at play. Additionally, with the currently available single-timepoint analysis, it is not possible to distinguish whether expression in a neuron is within the rising or falling phase of a binomial expression profile. The functional stimulation data were complemented with calcium imaging of cocultured neurons in order to indirectly reveal activity patterns of iNs and their relation to eNs' activity pattern. Albeit limited in scope, the calcium imaging experiments reveal that iNs display activity patterns that are in part synchronized with eN traces, but also show independent activity while eN traces are fully synchronized. Dissociated primary neuronal cultures have been extensively shown to display increasingly synchronized neuronal bursting activity over time which reflects ongoing network maturation (Cotterill et al., 2016; Kuijlaars et al., 2016). As such spontaneous neuronal activity constitutes an intrinsic neuronal property that regulates membrane receptor trafficking and, accordingly, efficacy of synaptic transmission these recordings suggest the presence of at least partial synaptic integration into the cortical network. Albeit suggestive, the available dataset would need to be expanded and analyzed in order to quantitatively assess synchronization between activity patterns observed in iNs and eNs. Moreover, calcium traces represent neuronal activity only indirectly. Hence, direct assessment of iN activity via electrophysiological recordings e.g. in response to stimulations, should be performed. Previous work could already

show that rat astroglia-derived Neurog2-induced neurons are able to form networks and display synchronous and rhythmic calcium traces upon bicuculline perfusion at later developmental stages, despite displaying minimal spontaneous calcium transients (Blum et al., 2011). Interestingly, in this work, iNs seemed to display overall more Ca $^{2+}$-transients than eNs. Previous studies could show that immature adult-born dentate granule cells were shown to display more Ca $^{2+}$-transients than mature ones, supporting the view of iNs and eNs being at distinct developmental stages (Danielson et al., 2016; Parylak et al., 2023). In sum, these data demonstrate that iNs robustly respond to membrane depolarization with the upregulation of prototypical activity-dependent gene products.

6.2 NEUROG2-INDUCED NEURONS DISPLAY SUBTYPE- AND MATURATION-SPECIFIC HETEROGENEOUS MOLECULAR SIGNATURES

Recent studies have begun to shed light on the remarkable diversity of neuronal subtypes in the mammalian brain that could only be appreciated by performing scRNA-seq profiling on samples comprising thousands of cells (Di Bella et al., 2021; Yao, Liu, et al., 2021). Intriguingly, while direct lineage reprogramming via single neurogenic TFs can achieve a broad diversity of neuronal types (Bocchi et al., 2022; Vignoles et al., 2019), it is not yet fully understood to which extent neuronal identity features (e.g. region-specific phenotypes, neurotransmitter identity, firing properties) can be recapitulated and how a desired neuronal phenotype can be obtained via ectopic expression of TFs (R. Tsunemoto et al., 2018). In fact, an increasing amount of studies have been suggesting that neurogenic TFs need to be accompanied by additional factors in order to specify defined neuronal subtypes (Bocchi et al., 2022; Luginbuhl et al., 2021; R. Tsunemoto et al., 2018; M. Zhou et al., 2021). Moreover, studies suggest that more precise cell fate engineering of distinct neuronal subtypes with desired functional output will advance disease modeling as well as therapeutic approaches for neurodegenerative diseases (Lentini et al., 2021; Lin et al., 2021b). In line with the existing literature, the data presented in this thesis show that astroglia-derived Neurog2-iNs acquire a highly diverse range of neuronal identities. Most surprisingly, the analysis identified two heterogeneous sets of glutamatergic and GABAergic neuronal subtypes within the iN population. Among glutamatergic Neurog2-iNs, a diverse range of cortical layer molecular identities could be identified, whereas a subset of iNs expressed inhibitory marker genes and were accordingly assigned GABAergic transcriptomic identities. These analyses were further supported by immunocytochemical stainings displaying subtype-specific marker expression in iNs (e.g. Satb2, Cux2, PV), albeit detected at low frequencies. These findings raise the question by which mechanisms ectopic expression of Neurog2 results in diverse reprogramming outcomes (Karow et al., 2018). During differentiation of nonoverlapping NPC popula-

tions, Neurog2 not only plays a fundamental role in the generation of multiple neuronal subtypes, e.g. glutamatergic, motor, dopaminergic as well as sensory neurons but also in inhibiting the generation of a GABAergic neuronal identity (Hulme et al., 2022). This is achieved by e.g. inhibiting Ascl1, a TF necessary for the generation of GABAergic neurons (Hulme et al., 2022). One possible explanation for the observed heterogeneity within the iN population, and specifically the observed segregation into excitatory as well as inhibitory neurons, could be biases in the reprogramming outcome due to distinct starting cell type identities and their unique repertoire of TFs, signaling molecules or cellular milieu (Rahmani et al., 2019). These factors modulate the reprogramming process, likely by affecting the ability of the reprogramming TFs to access and modulate their target genes, hence leading to diverse reprogramming outcomes. Such cell-type specific molecular properties will also likely interact with and modulate the impact of the activity of the gene products whose expression has been induced by TFs. Importantly, lineage relationships and the degree of similarity between a given starting cell type and the desired reprogramming product may influence the likelihood of a given reprogramming process taking place. In order to understand cell type composition within the glial cultures prior to iN characterization, I initially assessed the percentages of distinct glial types prior to retroviral targeting. Astroglia represent an attractive target cell type for direct reprogramming purposes into neuronal subtypes, especially in the *in vivo* context: they are derived from radial glia, e.g. the same glial population which gives rise to neuronal precursors during development (Malatesta et al., 2008). The close developmental relationship between astroglia and neurons therefore promises a higher success rate of lineage conversion towards neurons compared to other glial populations (Sareen and Svendsen, 2010). Moreover, different glial populations display region-specific molecular signatures (Tan et al., 2019). Intriguingly, astrocytes were shown to maintain their regional identity following astrocyte-to-neuron reprogramming, a feature that could be beneficial in obtaining region-specific neuronal subtypes (Bocchi et al., 2022; Herrero-Navarro et al., 2021). Finally, astroglial cells are abundantly present and display a high proliferative capacity following injury (Boghdadi et al., 2020). Neuroprotective as well as neurotoxic properties have been assigned to the expanding population (Karve et al., 2016). It may therefore be advantageous to convert neurotoxic astrocytes and reduce their detrimental effect, assuming their neurotoxic role does not ultimately lead to beneficial effects on neuronal network maintenance in the long term. In the utilized system, the big majority of cultured glia were found to be indeed GFAP-expressing astrocytes, however, several other glial populations (e.g. OPCs, microglia) could also be detected and transduced (see Figure 5.4). If no e.g. selective cell death or divergence onto a non-neuronal fate occurred within specific cell types following transduction, it is hence possible that these diverse cell types contributed to the generation of the iN pool and shaped the resulting extent of

distinct molecular identities. Importantly, in order to accurately determine the starting population, lineage tracing of the transduced population should be performed, which allows dissection of reprogramming and maturation efficiencies derived from distinct glial populations as well as identification of the resulting molecular identity. A previous study used NeuroD1, a TF associated with the differentiation of glutamatergic neurons, in order to aim for reprogramming astroglia into glutamatergic neurons. Intriguingly, astroglia as well NG2-glia were transduced and while astroglia exclusively adopted a glutamatergic neuronal fate, a major fraction of targeted NG2-glia could be converted into both, glutamatergic as well as GABAergic neurons (Guo et al., 2014). The study performed by Guo et al. therefore supports the findings of this part of the work and suggests another possible mechanistic interpretation of the data: the developmental origin of the starting cell dictates a persisting regional identity that, in turn, impacts the reprogramming outcome (Falk et al., 2021; Guo et al., 2014). As a pool of cortical NG2-glia originates from the ventral telencephalon and gives rise to oligodendroglia as well as astrocytes and has the potential to give rise to interneurons during development, the close lineage relationship to GABAergic neurons may be reflected in the reprogramming outcome (Dimou and Gallo, n.d.; Sánchez-González et al., 2020). Even though Neurog2 regulates glutamatergic neuron differentiation, additional factors may be necessary in order to shape the glutamatergic subtype phenotype which is not present in distinct glial cell types. Moreover, the genome accessibility may have been shaped by factors that have been present before and therefore restrict Neurog2 accessibility which in combination with present TFs results in an alternative fate, e.g. a GABAergic phenotype. For instance, interneuron-specific genes have been shown to exist in a more readily accessible state regarding their chromatin modifications in OPCs compared to astrocytes (Boshans et al., 2019). Another interesting perspective to consider involves Pax6, a TF expressed upstream of Neurog2, that has been shown to significantly contribute to neuronal subtype specification by restricting the competence of cortical progenitor cells of generating a broader range of neuronal types in response to various extracellular factors (Manuel et al., 2022). Intriguingly, when Pax6 was specifically deleted in the cortex, a small population of cortical progenitors were found to express Gsx2, Dlx and Gad genes and mapped onto GABAergic interneurons when the dataset was integrated with data from the embryonic ventral telencephalon (Manuel et al., 2022). Moreover, those cells also displayed altered expression of IEGs such as Jun or Fos (Manuel et al., 2022). Given these observations, it could be interesting to test the hypothesis of whether ectopic expression of Neurog2 in the absence of (preceded) Pax6 expression compared to expression of both factors may lead to distinct extents of observed subtype heterogeneity. Intriguingly, although several other systems have previously reported that bHLH TF expression alone specifies cellular identity, they have simultaneously highlighted that the addition of homeobox

TFs seems necessary in further specifying neuronal subtype identity, suggesting that the two processes of specification of cellular and subtype identity occur independently from each other (Fode et al., 1998; Hatakeyama et al., 2001). Moreover, studies have shown that neuronal neurotransmitter phenotype seems in fact a plastic neuronal feature that can be directly modified by distinct neuronal activity patterns, *in vitro* as well as *in vivo* (Bertels et al., 2022; Kirischuk et al., 2017; Spitzer, 2012), adding further complexity to the identification of neuronal subtype identity acquisition as neuronal identity continues to be connected to the expression of distinct neurotransmitters. Intriguingly, neuronal neurotransmitter respecification can occur as an activity-dependent process as part of a homeostatic mechanism in response to sustained network activity changes in order to conserve responsiveness (Spitzer, 2012). Taken together, these findings support the hypothesis that the lineage proximity as well as similarity of the starting as well as target cell types constitute potentially relevant aspects during lineage reprogramming processes. Interestingly, iNs display similarity towards a wide range of distinct cortical-layer specific identities, with the biggest proportion being upper-layer cortical neurons, suggesting that expression of Neurog2 may not be sufficient in specifying a defined molecular identity. On the other hand, and as suggested by others, external factors that affect neuronal maturation, such as e.g. specific guiding molecules, may be necessary for subtype specification (Klingler et al., 2021; X. Li et al., 2021; Telley et al., 2019). Interestingly, reprogramming iPSCs via Neurog2 towards a neuronal fate has similarly shown to lead to diverse neuronal subtypes (X. Li et al., 2021), while glial reprogramming in the cortex results in a deep-layer glutamatergic identity after only 10 d.p.t. (Gascón et al., 2016), which is in line with the function of Neurog2 during cortical development (S. Han et al., 2018; Schuurmans et al., 2004). Moreover, heterogeneous cortical layer-specific identities of iNs may reflect the influence of cortical domain- or layer-specific differences among the targeted astroglial populations, the most abundantly transduced cell type (Bayraktar et al., 2020; Herrero-Navarro et al., 2021; Mattugini et al., 2019). It is not fully understood if and to what extent biases exist in basal expression or genomic accessibility of neuronal subtype-specifying genes within the glia population and if such could play a role in biasing the reprogramming process. Moreover, Neurog2 is known to be involved in the induction of a broad range of neuronal types, but which additional factors contribute to the diversity is not fully understood (Falk et al., 2021). Nonetheless, the process of diversification seems recapitulated during astroglia-to-neuron reprogramming. With the use of scRNA-sequencing and a higher resolution in temporal sampling during the reprogramming process, molecular changes that occur during cell type conversion may be resolved and could reveal the underlying unfolding of transcriptional programs and whether these are mostly driven by the reprogramming TF or influenced by other factors. Of note, the analysis focused on the identification of cellular molecular identities (see

Figure 5.18), relied on reference datasets with a focused coverage of cortical neuronal types and the hippocampal formation, therefore, it can not be excluded that iNs may show a closer similarity to non-cortical neuronal types. For instance, Neurog2-mediated human iPSC-derived iNs have been shown to display a mixed signature of CNS as well as PNS neuronal types at 35 days of differentiation, which prevented the assignment of the iN clusters towards a more defined subtype identity (Lin et al., 2021b). However, the analysis performed here shows that iNs express clear cortical layer-specific neuronal gene signatures that are significantly distinct from one another. Despite the expression of several canonical layer-specific markers (e.g. *Satb2, Cux2, Ctip2, Foxp2*) at the transcript level, the corresponding gene products could rarely be detected at the protein level, suggesting an early phase of specification during which overall layer-specific transcriptional identity may be established prior to detectable levels of such known layer-specific marker proteins. Alternatively, these observations may also hint towards potentially abnormal neuronal RNA processing or translation, which may reflect incomplete glia-to-neuron fate conversion. Neuron-specific RNA-binding proteins (RBPs) have been shown to play a crucial role in the temporal regulation of subtype-specific TFs, such as regulation of Satb2 by the RBP Pumilio2, and contribute to the refinement of neuronal transcriptional programs (Harnett et al., 2022). As discussed earlier, the unexpected distribution of Arc expression upon iN stimulation may have been similarly a result of dysregulated translational processes and reinforces the possibility of misfunctioning translational or post-transcriptional control of gene expression in iNs. Interestingly, the iN population is composed of, at least, two main developmental stages despite being concomitantly transduced. Approximately half of the population displayed a transcriptional signature that resembled early cortical or hippocampal progenitors, while the remaining half displayed transcriptional signatures that most closely resembled well-differentiated excitatory cortical layer-specific neurons. This observation suggests the presence of distinct stages along one or possibly more differentiation trajectories. Intriguingly, the presence of iNs at distinct maturation stages, together with the observed diversity in neuronal subtypes, suggests that the direct environment may have different effects on distinct reprogramming trajectories with regard to the initial starting cell type heterogeneity and that the reprogramming trajectory may be guided by cell-autonomous as well as cell non-autonomous mechanisms. Although not applied within the scope of this thesis, tools designed to address this pattern, e.g. pseudotemporal trajectory inference, could be applied to datasets generated by sampling reprogramming at several time points and may reveal expression of distinct transcriptional programs throughout maturation that may ultimately guide progressive circuit integration. Taken together, the analysis performed in this thesis with the aim to define iN neuronal identities points to two distinct axes of diversity among the iN population: molecular subtype identities as well as develop-

mental stages. These observations suggest potential synergistic interactions between the employed TF and the intrinsic cellular context including its developmental stage and the origin of the starting cell population or the cellular environment. Importantly, such a highly heterogeneous iN population may result in the acquisition of heterogeneous functional qualities, which have to be taken into account during functional recovery strategies in a diseased environment.

6.3 TRANSCRIPTIONAL RESPONSE OF INDUCED NEURONS TO NETWORK ACTIVITY INHIBITION SUGGESTS LIMITED SYNAPTIC INTEGRATION INTO THE EXISTING CIRCUITRY

To explore transcriptional changes in the eN as well as iN populations following network activity modulation, single nucleus RNA sequencing (snRNA-Seq) was performed. As stated before, transcriptional profiling of neurons was also carried out with the aim of dissecting differences in neuronal identity and maturation stages between iNs and eNs. Moreover, transcript levels of neuron-defining features that dictate electrical excitability or synaptic connectivity were compared across the neuronal populations. To this end, DEG analysis was performed between both active (untreated) endogenous as well as induced neuronal populations in order to identify differential expression levels of functionally relevant genes of the synaptic machinery. It should be noted that synapse-associated mRNA are generally translated at the synapse, a cellular compartment that is lost during nuclear isolation, hence snRNA-seq data may not reliably capture the entire synaptic transcriptome (**Pekarek2022**). Yet, the transcriptome dataset contained hundreds of synapse-related genes in both neuronal populations at comparable expression levels. Foremost, the obtained DEG analysis results show that iNs transcribe genes necessary for the assembly of a postsynaptic compartment and, given adequate post-transcriptional processing, could therefore be structurally recognized by endogenous neurons as potential synaptic targets. Importantly, several synapse-associated genes whose expression levels are known to correlate with neuronal maturation were also differentially expressed between iNs and eNs (e.g. *CamK2a, PSD95, SNAP25*) (Tepe et al., 2018). Moreover, AMPAR subunits GluA1 and GluA2, which are known to mediate excitatory transmission as well as distinct forms of neuronal plasticity, were found to be similarly expressed between both neuronal populations (S. Cohen and Greenberg, 2008; Shimshek et al., 2017). However, the differential expression level of genes such as CamK2a or PSD95 suggests distinct functional maturation stages between iNs and eNs. Interestingly, Neurog2-mediated reprogramming of human PSCs into excitatory neurons has been shown to result in two functionally distinct populations that could be identified based on differential expression of CamK2a and display differential NMDAR-mediated synaptic transmission (Nehme et al., 2018). Of note, when screening for differential regulation of ion channels and receptors, the majority was transcribed at similar levels. Expression of the cation-chloride cotransporters (CCCs) was assessed as they are developmentally regulated and modulate GABAergic as well as glutamatergic signaling (Kaila et al., 2014). In particular, the CCCs NKCC1 (*Slc12a2*) and KCC2 (*Slc12a5*) were found to be expressed at similar levels between iNs and eNs, suggesting that iNs reached a developmental stage in which the flow of Cl- currents leads to a postsynaptic hyperpolarization, and thus to inhibition of synaptic transmission (Kaila et al., 2014). This plays a significant role

during proper neuronal signaling and establishment of connectivity (Kaila et al., 2014). In sum, the DGE analysis comparing untreated eNs and iNs reveals that iNs express most of pre- and postsynaptic-related genes similar to eNs and may therefore be well able to establish a functional pre- as well as postsynaptic compartment. Moreover, based on their transcriptional profile, iNs seem to be at a developmental stage in which they are equipped to be recognized as synaptic partners and, in turn, establish connections to neighboring mature neurons. Therefore, it was next assessed whether iNs display transcriptional signs of homeostatic synaptic plasticity when embedded into a cortical circuit and subjected to network silencing, a readout that would indicate established synaptic contacts with eNs and their functional integration. The data was obtained by performing DEG analysis between the active and inactive eN and iN populations, respectively. The analysis of genes showing differential expression between active and inactive (i.e. inhibited) eNs revealed a strong synaptic upscaling mechanism with hundreds of regulated genes that were previously shown to participate in HSP processes, and more specifically in synaptic upscaling (Dörrbaum et al., 2020; Schaukowitch et al., 2017). Conversely, iNs displayed significant modulation of only a small set of genes with smaller changes in expression levels. Of note, known functions of the regulated genes in iNs did not suggest a typical synaptic upscaling process taking place as assessed by individual inspection of gene function, GO term analysis or direct comparison to eN-regulated genes. Importantly, however, iNs do display activity-dependent gene regulation as they display transcriptional regulation of a neuronal functional gene set in response to activity inhibition. However, as pointed out, the transcriptional response is distinct from the one elicited in eNs, highlighting the importance of using bona fide transcription profiling for comparative analysis. There are several reasons why iNs may have been differentially impacted by network activity inhibition compared to eNs. First, differences in developmental stages have been shown to correlate with distinct synapse-related responses to activity deprivation (E. B. Han and Stevens, 2009). For instance, an *in vitro* study showed that while immature hippocampal neurons respond to 24 hours of activity inhibition by increasing the number of postsynaptic receptors, more mature neurons display instead an increase in synaptic vesicle number and hence an increased probability of neurotransmitter release (E. B. Han and Stevens, 2009). Interestingly, following 48 hours of activity inhibition, immature as well as mature hippocampal neurons respond with both pre- as well as postsynaptic mechanisms *in vitro* (E. B. Han and Stevens, 2009). A more recent study showed that activity inhibition in the visual cortex during the critical period (P24-P29) resulted in both excitatory synaptic upscaling as well as intrinsic homeostatic plasticity (i.e. membrane excitability), while in the adult cortex, neurons displayed excitatory synaptic upscaling, but no intrinsic homeostatic plasticity (Wen and Turrigiano, 2021). These studies show that the response to an identical stimulus is

significantly shaped by the neuronal maturation level. Moreover, maturing eNs seem to display already a functionally responsive phenotype early in their developmental trajectory while iNs at an equivalent time in culture seem to retain immature-like functional features. This may suggest either an impaired maturation process along a trajectory shared with eNs, or potentially an iN-specific maturation trajectory. In order to address differing maturation stages as potential drivers for distinct transcriptional responses, a comparative time-course analysis of age-matched eNs and iNs at distinct stages of differentiation/reprogramming could be performed. Moreover, eNs were already highly differentiated (e.g. expression of mature neuronal marker, synchronous activity pattern) by the time of coculturing with iNs, and underwent further maturation during the following two weeks. Additionally, intrinsic properties of eNs may likely be more advanced, as for instance detectable through their spontaneous activity. Their more refined synaptic connections may therefore be more receptive to network changes than newly forming connections established by iNs. Therefore, activity-dependent competitive processes during network wiring may disadvantage less mature iNs competing with eNs for synaptic input and result in iNs being not able to integrate and respond to synaptic activity modulations. Moreover, the dataset comprises a single time point along the iN maturation trajectory and can therefore not predict whether iNs may display HSP at later maturation stages. Although several attempts were made to prolong the culture duration and enable further iN maturation, it could not be maintained with a good iN viability beyond 2-3 weeks. Further experiments will be needed that investigate the inter- and intracellular mechanisms leading to iN death. Intriguingly, I have observed that the decline in iN numbers and viability is not as pronounced when cultured in monocultures, and could be kept beyond 2 weeks in culture, in line with what has been reported in previous studies (Heinrich et al., 2010). Previous studies provide evidence that with sufficient maturation time, iNs develop electrophysiological properties that are similar to those of eNs, however, the ability to undergo distinct synaptic plasticity mechanisms has yet to be examined. Interestingly, when dividing the iN population according to the two identified maturation stages and assessing their unique ability to display regulation of eN-regulated gene sets, mature iNs were found to regulate eN-URGs as well as eN-DRGs significantly stronger compared to immature iNs. Intriguingly, multiple studies suggest higher excitability and plasticity potential in immature neurons compared to mature neurons, raising the question of the relationship between electrophysiological properties and transcriptional responsiveness to activity modulations. Importantly, a recent study could show that, similarly to the observation made here, immature DGCs display less marked activity-induced transcriptional dynamics compared to more mature DGCs (Parylak et al., 2023). However, although this study points to reduced activity-dependent transcription in immature DGCs, the authors acknowledge multiple

other studies highlighting the observations of relevant functional contributions made by immature DGCs (Parylak et al., 2023). Interestingly, different forms of activity-dependent gene regulation have been not only reported in distinct developmental stages of cortical neurons but have also been suggested to occur in different layer-specific subtypes at a given developmental stage (Nehme et al., 2018; Nelson et al., 2022). Distinct neuronal layer-specific subtypes possess distinct connectivities, anatomical positions and functional properties including differences in their excitability and synaptic activity which are reflected in their distinct gene expression profiles (Nelson et al., 2022; Radnikow and Feldmeyer, 2018). Hence, it is possible that among the observed heterogeneity of distinct iN identities, differences in the inactivity-regulated gene set could be identified, but were masked by the pseudobulk DEG analysis. Another possible explanation for the diverging transcriptional responses to activity inhibition observed in iNs may be their lack of integration into the circuitry. Endogenous neuronal integration into pre-existing circuitry occurs in the adult brain in two regions, and, interestingly, in both regions, a major fraction of newborn neurons fail to survive and integrate (Tepe et al., 2018; Turnley et al., 2014). Intriguingly, the fate of newborn neurons has been shown to depend on the network activity level during synapse formation (Ge et al., 2008; Overman et al., 2012; Tepe et al., 2018; Turnley et al., 2014). For instance, modulation of activity in the olfactory bulb via odor discrimination learning has been shown to lead to increased survival of newborn neurons (Alonso et al., 2006; Turnley et al., 2014). In contrast, survival has been shown to be dependent on sensory experience during a critical period of integration (Turnley et al., 2014; Yamaguchi and Mori, 2005). Sensory deprivation does not only affect the survival of newborn neurons but also the density of their newly formed synapses (Kelsch et al., 2009). Therefore, it is possible that the network activity pattern influences the integration and survival of iNs and hence their capability to participate in homeostatic plasticity mechanisms. For instance, in synaptically-silenced neurons, the bHLH TF Arnt2 has been shown to mobilize the corepressor NCoR2 in order to suppress activity-dependent gene regulatory elements, ultimately leading to low basal expression levels of ARGs (Sharma et al., 2019). Similarly, when synaptic excitation is lacking, the histone deacetylase Hdac4, together with the TF Mef2, represses genes encoding for synapse-related proteins (Sando et al., 2012). Lack of synaptic input and calcium influx may be therefore leading to an adjusted gene regulatory network that does not allow short-term activity-dependent gene regulation. Long-term modulation of network activity may therefore allow integration of iNs into the network and could be experimentally induced pharmacologically or genetically. Similarly, modulation of intrinsic excitability of iNs may facilitate their integration, as it determines neuronal maturation and the development of synaptic connections to surrounding neurons (Sim et al., 2013). Of note, the hippocampus and the olfactory bulb are primed regions that allow the integration

of new, immature neurons, and hence may be more plastic than e.g. the cortex to begin with (Turnley et al., 2014). In line with this, dissociated rat hippocampal cultures were shown to continue generating newborn neurons, which synaptically integrated into the preexisting network *in vitro* (Cheyne et al., 2011). Intriguingly, recent studies have been focusing on assessing the integration of immature neurons of diverse origins into the cortex (Ballout et al., 2016; Espuny-Camacho et al., 2018; Falkner et al., 2016; Michelsen et al., 2015; Revah et al., 2022). Indeed, embryonic neurons transplanted into the visual cortex, a region that normally does not incorporate new neurons, mature into pyramidal neurons within several weeks and display not only highly accurate anatomical synaptic integration but also external stimulus-specific responses that are comparable to ones elicited by endogenous neurons (Espuny-Camacho et al., 2018; Falkner et al., 2016). Most intriguingly, the molecular functions driving these processes seem to be conserved across species, as human ESC-derived neurons have been shown to successfully integrate into the murine visual cortex as well (Espuny-Camacho et al., 2018). This highlights the potential of the cerebral cortex to allow new, immature neurons to synaptically integrate despite not being a neurogenic region. Importantly, recent studies are beginning to investigate if the integration of embryonic neurons can also occur in a diseased environment that is marked by reactive gliosis and inflammatory processes and have identified significant differences compared to a healthy environment (Grade et al., 2022). Therefore, the integration of iNs into a pre-existing network should be also assessed from this point of view. Moreover, there is reason to speculate whether distinct subtypes may display distinct abilities to integrate into a pre-existing network (Batista-Brito and Fishell, 2009). From a developmental perspective, inhibitory interneurons migrate into the cortex and integrate naturally into the maturing cortical network (Batista-Brito and Fishell, 2009). It may therefore be possible that due to distinct intrinsic properties, interneurons integrate more easily into pre-existing circuits. In fact, several studies could successfully show synaptic integration of glia-derived reprogrammed interneurons into pre-existing, injured circuits and the restoration of functional aspects (Gonzalez-Ramos et al., 2021; Lentini et al., 2021; Tai et al., 2021). In this regard, it would be interesting to dissect the elicited activity-dependent transcriptional dynamics based on neuronal subtype in order to assess whether induced GABAergic display stronger synapse-related regulation compared to the glutamatergic iN population. Most interestingly, although iNs undergo modulation of only a small percentage of the eN-activity regulated gene (ARG) set, they display under basal conditions already higher expression levels of eN-URGs compared to active eNs. Recent scRNAseq studies show that synapse-related genes are highly transcribed early during development in the mouse (Tepe et al., 2018) as well as the human cortex (Herring et al., 2022) prior to synaptic activity. High expression of these genes in iNs may therefore reflect their ongoing maturation process and would

suggest that integration may occur at later stages. On the other hand, this data may also suggest that iNs could basally already be in a state of deprived network activity input and possibly reflecting a lack of integration or in a hyperexcitable state due to high expression of synapse- and excitability-related genes. Interestingly, when synaptic integration of iNs was assessed by an acute pharmacological treatment known to induce burst firing with subsequent IEG detection, the data show that iNs are barely responsive compared to the observed strong IEG upregulation in eNs. Together with the absence of regulation of typical synaptic plasticity-associated genes following activity inhibition, this data suggests that iNs are not yet functionally integrated into the network, despite wide expression of synaptic machinery-related genes. In line with this, the maturation of iNs is likely constrained due to the lack of synaptic input by surrounding neurons. While the snRNA-seq data shows downregulation of postsynapse-related genes in iNs, the Sholl analysis displayed a reduced morphological complexity following 48 hours of activity inhibition. While it has yet to be assessed how eNs respond under these conditions to the applied activity modulation in terms of morphological reorganization, the observations suggest that iNs respond uniquely to activity inhibition. Both the downregulation of synapse-associated genes as well as the reduction in morphological complexity impact neuronal functionality and are observations that are distinct from the traditionally known synaptic scaling process occurring following prolonged activity deprivation. Future experiments assessing e.g. firing properties of iNs need to be performed in order to allow a better understanding of the functional significance of the processes taking place. Importantly, inadequate induction of HSP in electrically active iNs may either fail to induce compensation for changes in network activity levels or may potentially destabilize network activity itself, an aspect that should be monitored and assessed by e.g. electrophysiological recordings following activity modulations. In sum, iNs respond to activity inhibition with transcriptional regulation, however, their response suggests induction of a unique program that could reflect either their state, maturation stage or connectivity within the network. Functionally, the results discussed in this part demonstrate that the coupling between activity levels and transcriptional regulation differs between iNs and eNs. These differences suggest that the functional integration of iNs into a pre-existing network may be limited. However, it is possible that iNs possess the capacity to contribute to network dynamics by modifying the response of eNs by their activity patterns rather than undergoing dramatic transcriptional changes themselves, as proposed for immature adult-born dentate granule cells (Parylak et al., 2023). Needless to say, assessment of mRNA levels is insufficient for protein level prediction that allows a thorough understanding of physiological processes (Y. Liu et al., 2016). Transcriptomic profiling should ideally be complemented with functional analysis of iNs in order to comprehensively characterize biological phenotypes. Moreover, while

the reprogramming process ideally aims to fully recapitulate the desired cellular identity and its function, only partial accomplishment of the reprogramming outcome may still satisfy the functional requirements for cell replacement applications.

6.4 IDENTIFICATION OF AN EXTENSIVE TRANSCRIPTIONAL PROGRAM IN ENDOGENOUS NEURONS UNDERLYING SYNAPTIC SCALING

The main focus of the DEG analysis was to assess the genome-wide transcriptional response to network activity inhibition in iNs. The response elicited in co-existing eNs was used as a reference, but also provided new insights into the synaptic upscaling process. The analysis revealed that the synaptic transcriptome was extensively remodeled during homeostatic upscaling in eNs, with hundreds of genes being up- as well as downregulated following activity inhibition. Especially transcription of synaptic genes was affected by activity inhibition. Multiple regulated genes (e.g. *GluA1/2*, *Nrxn3*, *Syp*, *Synpo1*, *Syt1*, *Nos1*, *Camk2a*, *Plk2*, *Neto1*, *Ncam1* and more) could be detected that are already known to play a significant role during HSP (Desch et al., 2021; Dörrbaum et al., 2020; Schaukowitch et al., 2017). Moreover, eNs display regulation of the AMPAR subunit GluA2 (Gria2) in response to activity inhibition, indicative of modulation of mature synapses (X. Xu and Pozzo-Miller, 2017). As previous studies have described, homeostatic upscaling seems to be achieved by transcriptional up- as well as downregulation of synaptic genes (Schaukowitch et al., 2017), which was confirmed with this work. These genes are involved both at the pre- as well as postsynapse. For example, glutamate transporters at the presynapse have been shown to be upregulated following activity inhibition which likely contribute to a higher neurotransmitter quantal release (Schaukowitch et al., 2017). In line with this, this work shows a strong upregulation of the vGlut1 transporter (*Slc17a7*). Furthermore, apart from known activity-associated genes, this work reveals a significant set of neuronal development-associated genes (e.g. Zmiz1, Zeb2, Sema4f, Sez6, Nyap2) that are regulated in response to 48h of activity inhibition. Although the underlying genetic mechanisms responsible for synaptic architecture and remodeling are not yet fully understood, recent studies have begun to elucidate the role of developmental mechanisms on postnatal and adult synapse architecture. For instance, Pax6 has been shown to regulate the expression of multiple synaptic proteins during postnatal as well as adult cortical circuit formation (Tomas-Roca et al., 2022). Intriguingly, NeuroD2 was identified as a novel gene associated with homeostatic synaptic upscaling (see Figure 5.36). In eNs, NeuroD2 was strongly upregulated in response to activity inhibition and this finding was validated by RT-qPCR analysis (see Figure 5.36). While previous studies suggested that NeuroD2 is involved in synaptic maturation, the data presented in this study suggest an additional involvement in HSP in mature cortical neurons, although the precise mechanism remains to be further elucidated. Interestingly, while NeuroD2 is usually among the first TFs to be expressed in immature embryonic cortical neurons with expression maintained throughout life (Y. C. Chen et al., 2016), it could not be detected in iNs. Consistent with this observation is the high expression of reelin (*Reln*) in iNs, since NeuroD2 knockdown has been shown to result in a significant increase in

Reln expression (Guzelsoy et al., 2019). Interestingly, NeuroD2 is known to be activated by Ca^{2+} influx and therefore represents an interesting TF that seems to be involved in linking neuronal activity with gene transcription (Y. C. Chen et al., 2016; Ince-Dunn et al., 2006). NeuroD2-null mice display reduced excitatory synaptic currents mediated by AMPAR and NMDAR with disturbed synaptic transmission, underlining its significant role in synaptic maturation (Ince-Dunn et al., 2006). Studies have also pointed to its significant role in decreasing intrinsic neuronal excitability and hence promoting neuronal maturation and survival (Y. C. Chen et al., 2016). It may therefore be worth investigating the impact of concomitant overexpression of NeuroD2 along the reprogramming TF in order to boost synaptic maturation and long-term survival of iNs. Finally, it should be pointed out that by performing transcriptomic profiling following 48 hours of constant activity inhibition, there is e.g. a possibility that certain early activity-regulated target genes and TFs might remain unidentified due to decreasing expression levels from the onset of inhibition. Nonetheless, the analysis highlights multiple potential transcriptional regulators that could be manipulated in future experiments in order to e.g. promote functional maturation of iNs. Last but not least, this work highlights the regulation of multiple genes that are linked to several neurological disorders and hence emphasizes the functional relevance of the regulated gene sets. The observed association between activity inhibition-induced gene expression and risk genes of psychiatric disorders suggests an important role of the former for healthy cognitive functions. Taken together, these findings demonstrate that the pharmacological treatment induced transcriptional regulation of genes associated with homeostatic upscaling in eNs, with DEG being largely consistent with previous studies (Dörrbaum et al., 2020; Schaukowitch et al., 2017). Remarkably, this dataset provides an extensive list of DEGs, including TFs, on a single nucleus level, which have not yet been shown to be activity-modulated. Moreover, these results contribute to the further understanding of HSP mechanisms, as the identified set of regulated genes is broader than known from current literature and therefore suggests unknown or underappreciated mechanisms at play.

7

BIBLIOGRAPHY

Abbott, L. F., & Nelson, S. B. (2000). Synaptic plasticity: taming the beast. *Nature Neuroscience 2000 3:11*, *3*(11), 1178–1183. https://doi.org/10.1038/81453

Abe, K. (2008). Neural activity-dependent regulation of gene expression in developing and mature neurons. *Development, growth & differentiation*, *50*(4), 261–271. https://doi.org/10.1111/J.1440-169X.2008.00999.X

Abraham, W. C., Dragunow, M., & Tate, W. P. (1991). The role of immediate early genes in the stabilization of long-term potentiation. *Molecular Neurobiology*, *5*(2-4), 297–314. https://doi.org/10.1007/BF02935553

Ahlgren, H., Bas-Orth, C., Freitag, H. E., Hellwig, A., Ottersen, O. P., & Bading, H. (2014). The nuclear calcium signaling target, activating transcription factor 3 (ATF3), protects against dendrotoxicity and facilitates the recovery of synaptic transmission after an excitotoxic insult. *Journal of Biological Chemistry*, *289*(14), 9970–9982. https://doi.org/10.1074/JBC.M113.502914

Ahlmann-Eltze, C., & Huber, W. (2021). glmGamPoi: fitting Gamma-Poisson generalized linear models on single cell count data. *Bioinformatics*, *36*(24), 5701–5702. https://doi.org/10.1093/BIOINFORMATICS/BTAA1009

Aibar, S., González-Blas, C. B., Moerman, T., Huynh-Thu, V. A., Imrichova, H., Hulselmans, G., Rambow, F., Marine, J. C., Geurts, P., Aerts, J., Van Den Oord, J., Atak, Z. K., Wouters, J., & Aerts, S. (2017). SCENIC: single-cell regulatory network inference and clustering. *Nature Methods 2017 14:11*, *14*(11), 1083–1086. https://doi.org/10.1038/nmeth.4463

Alonso, M., Viollet, C., Gabellec, M. M., Meas-Yedid, V., Olivo-Marin, J. C., & Lledo, P. M. (2006). Olfactory Discrimination Learning Increases the Survival of Adult-Born Neurons in the Olfactory Bulb. *Journal of Neuroscience*, *26*(41), 10508–10513. https://doi.org/10.1523/JNEUROSCI.2633-06.2006

Amamoto, R., & Arlotta, P. (2014). Development-inspired reprogramming of the mammalian central nervous system. *Science (New York, N.Y.)*, *343*(6170). https://doi.org/10.1126/SCIENCE.1239882

Anderson, S., & Vanderhaeghen, P. (2014). Cortical neurogenesis from pluripotent stem cells: complexity emerging from simplicity. *Current opinion in neurobiology*, *27*, 151–157. https://doi.org/10.1016/J.CONB.2014.03.012

Anggono, V., Clem, R. L., & Huganir, R. L. (2011). PICK1 Loss of Function Occludes Homeostatic Synaptic Scaling. *The Journal of Neuroscience*, *31*(6), 2188. https://doi.org/10.1523/JNEUROSCI.5633-10.2011

Arendt, K. L., Sarti, F., & Chen, L. (2013). Chronic Inactivation of a Neural Circuit Enhances LTP by Inducing Silent Synapse Formation. *The Journal of Neuroscience*, *33*(5), 2087. https://doi.org/10.1523/JNEUROSCI.3880-12.2013

Arrázola, M. S., Varela-Nallar, L., Colombres, M., Toledo, E. M., Cruzat, F., Pavez, L., Assar, R., Aravena, A., González, M., Montecino, M., Maass, A., Martínez, S., & Inestrosa, N. C. (2009). Calcium/calmodulin-dependent protein kinase type IV is a target gene of the Wnt/β-catenin signaling pathway. *Journal of Cellular Physiology*, *221*(3), 658–667. https://doi.org/10.1002/JCP.21902

Aydin, B., Kakumanu, A., Rossillo, M., Moreno-Estellés, M., Garipler, G., Ringstad, N., Flames, N., Mahony, S., & Mazzoni, E. O. (2019). Proneural factors Ascl1 and Neurog2 contribute to neuronal subtype identities by establishing distinct chromatin landscapes. *Nature Neuroscience 2019 22:6*, *22*(6), 897–908. https://doi.org/10.1038/s41593-019-0399-y

Azevedo, F. A., Carvalho, L. R., Grinberg, L. T., Farfel, J. M., Ferretti, R. E., Leite, R. E., Filho, W. J., Lent, R., & Herculano-Houzel, S. (2009). Equal numbers of neuronal and nonneuronal cells make the human brain an isometrically scaled-up primate brain. *The Journal of comparative neurology*, *513*(5), 532–541. https://doi.org/10.1002/CNE.21974

Bading, H., Ginty, D. D., & Greenberg, M. E. (1993). Regulation of gene expression in hippocampal neurons by distinct calcium signaling pathways. *Science (New York, N.Y.)*, *260*(5105), 181–186. https://doi.org/10.1126/SCIENCE.8097060

Baker, N. E., & Brown, N. L. (2018). All in the family: proneural bHLH genes and neuronal diversity. *Development (Cambridge, England)*, *145*(9). https://doi.org/10.1242/DEV.159426

Bakken, T. E., Jorstad, N. L., Hu, Q., Lake, B. B., Tian, W., Kalmbach, B. E., Crow, M., Hodge, R. D., Krienen, F. M., Sorensen, S. A., Eggermont, J., Yao, Z., Aevermann, B. D., Aldridge, A. I., Bartlett, A., Bertagnolli, D., Casper, T., Castanon, R. G., Crichton, K., … Lein, E. S. (2021). Comparative cellular analysis of motor cortex in human, marmoset and mouse. *Nature*, *598*(7879), 111–119. https://doi.org/10.1038/S41586-021-03465-8

Ballout, N., Frappé, I., Péron, S., Jaber, M., Zibara, K., & Gaillard, A. (2016). Development and Maturation of Embryonic Cortical Neurons Grafted into the Damaged Adult Motor Cortex. *Frontiers in neural circuits*, *10*(AUG). https://doi.org/10.3389/FNCIR.2016.00055

Batista-Brito, R., & Fishell, G. (2009). Chapter 3 The Developmental Integration of Cortical Interneurons into a Functional Network. *Current Topics in Developmental Biology*, *87*(09), 81–118. https://doi.org/10.1016/S0070-2153(09)01203-4

Bats, C., Farrant, M., & Cull-Candy, S. G. (2013). A role of TARPs in the expression and plasticity of calcium-permeable AMPARs: Evidence from cerebellar neurons and glia. *Neuropharmacology*, *74*, 76. https://doi.org/10.1016/J.NEUROPHARM.2013.03.037

Bayer, K. U., Löhler, J., Schulman, H., & Harbers, K. (1999). Developmental expression of the CaM kinase II isoforms: Ubiquitous γ- and δ-CaM kinase II are the early isoforms and most abundant in the developing nervous system. *Molecular Brain Research*, *70*(1), 147–154. https://doi.org/10.1016/S0169-328X(99)00131-X

Bayraktar, O. A., Bartels, T., Holmqvist, S., Kleshchevnikov, V., Martirosyan, A., Polioudakis, D., Ben Haim, L., Young, A. M., Batiuk, M. Y., Prakash, K., Brown, A., Roberts, K., Paredes, M. F., Kawaguchi, R., Stockley, J. H., Sabeur, K., Chang, S. M., Huang, E., Hutchinson, P., … Rowitch, D. H. (2020). Astrocyte layers in the mammalian cerebral cortex revealed by a single-cell in situ transcriptomic map. *Nature Neuroscience 2020 23:4*, *23*(4), 500–509. https://doi.org/10.1038/s41593-020-0602-1

Béïque, J. C., Na, Y., Kuhl, D., Worley, P. F., & Huganir, R. L. (2011). Arc-dependent synapse-specific homeostatic plasticity. *Proceedings of the National Academy of Sciences of the United States of America*, *108*(2), 816–821. https://doi.org/10.1073/PNAS.1017914108

Ben-Arie, N., McCall, A. E., Berkman, S., Eichele, G., Bellen, H. J., & Zoghbi, H. Y. (1996). Evolutionary conservation of sequence and expression of the bHLH protein Atonal suggests a conserved role in neurogenesis. *Human molecular genetics*, *5*(9), 1207–1216. https://doi.org/10.1093/HMG/5.9.1207

Bender, K. J., Allen, C. B., Bender, V. A., & Feldman, D. E. (2006). Synaptic Basis for Whisker Deprivation-Induced Synaptic Depression in Rat Somatosensory Cortex. *Journal of Neuroscience*, *26*(16), 4155–4165. https://doi.org/10.1523/JNEUROSCI.0175-06.2006

Benito, E., & Barco, A. (2015). The Neuronal Activity-Driven Transcriptome. *Molecular Neurobiology*, *51*(3), 1071–1088. https://doi.org/10.1007/S12035-014-8772-Z/FIGURES/2

Bergsland, M., Werme, M., Malewicz, M., Perlmann, T., & Muhr, J. (2006). The establishment of neuronal properties is controlled by Sox4 and Sox11. *Genes & Development*, *20*(24), 3475. https://doi.org/10.1101/GAD.403406

Berninger, B., Costa, M. R., Koch, U., Schroeder, T., Sutor, B., Grothe, B., & Götz, M. (2007). Functional properties of neurons derived from in vitro reprogrammed postnatal

astroglia. *Journal of Neuroscience*, *27*(32), 8654–8664. https://doi.org/10.1523/JNEUROSCI.1615-07.2007

Bertels, H., Vicente-Ortiz, G., El Kanbi, K., & Takeoka, A. (2022). Neurotransmitter phenotype switching by spinal excitatory interneurons regulates locomotor recovery after spinal cord injury. *Nature Neuroscience 2022 25:5*, *25*(5), 617–629. https://doi.org/10.1038/s41593-022-01067-9

Bertrand, N., Castro, D. S., & Guillemot, F. (2002). Proneural genes and the specification of neural cell types. *Nature reviews. Neuroscience*, *3*(7), 517–530. https://doi.org/10.1038/NRN874

Bhaduri, A., Sandoval-Espinosa, C., Otero-Garcia, M., Oh, I., Yin, R., Eze, U. C., Nowakowski, T. J., & Kriegstein, A. R. (2021). An atlas of cortical arealization identifies dynamic molecular signatures. *Nature 2021 598:7879*, *598*(7879), 200–204. https://doi.org/10.1038/s41586-021-03910-8

Bird, A. (2002). DNA methylation patterns and epigenetic memory. *Genes & Development*, *16*(1), 6–21. https://doi.org/10.1101/GAD.947102

Bissen, D., Foss, F., & Acker-Palmer, A. (2019). AMPA receptors and their minions: auxiliary proteins in AMPA receptor trafficking. *Cellular and Molecular Life Sciences 2019 76:11*, *76*(11), 2133–2169. https://doi.org/10.1007/S00018-019-03068-7

Bito, H., Deisseroth, K., & Tsien, R. W. (1997). Ca2+-dependent regulation in neuronal gene expression. *Current opinion in neurobiology*, *7*(3), 419–429. https://doi.org/10.1016/S0959-4388(97)80072-4

Bliss, T. V., & Cooke, S. F. (2011). Long-term potentiation and long-term depression: a clinical perspective. *Clinics*, *66*(Suppl 1), 3. https://doi.org/10.1590/S1807-59322011001300002

Blum, R., Heinrich, C., Sánchez, R., Lepier, A., Gundelfinger, E. D., Berninger, B., & Götz, M. (2011). Neuronal network formation from reprogrammed early postnatal rat cortical glial cells. *Cerebral cortex (New York, N.Y. : 1991)*, *21*(2), 413–424. https://doi.org/10.1093/CERCOR/BHQ107

Bocchi, R., Masserdotti, G., & Götz, M. (2022). Direct neuronal reprogramming: Fast forward from new concepts toward therapeutic approaches. *Neuron*, *110*(3), 366–393. https://doi.org/10.1016/j.neuron.2021.11.023

Boghdadi, A. G., Teo, L., & Bourne, J. A. (2020). The Neuroprotective Role of Reactive Astrocytes after Central Nervous System Injury. *Journal of neurotrauma*, *37*(5), 681–691. https://doi.org/10.1089/NEU.2019.6938

Bonnefont, J., Tiberi, L., van den Ameele, J., Potier, D., Gaber, Z. B., Lin, X., Bilheu, A., Herpoel, A., Velez Bravo, F. D., Guillemot, F., Aerts, S., & Vanderhaeghen, P. (2019). Cortical Neurogenesis Requires Bcl6-Mediated Transcriptional Repression of Multiple Self-Renewal-Promoting Extrinsic Pathways. *Neuron*, *103*(6), 1096–

1108.e4. https://doi.org/10.1016/J.NEURON.2019.06.027/ATTACHMENT/8EFF5BA5-18D4-4A0B-80D5-441CAFB5BA3F/MMC6.XLSX

Bonnefont, J., & Vanderhaeghen, P. (2021). Neuronal fate acquisition and specification: time for a change. *Current opinion in neurobiology*, *66*, 195–204. https://doi.org/10.1016/J.CONB.2020.12.006

Boshans, L. L., Factor, D. C., Singh, V., Liu, J., Zhao, C., Mandoiu, I., Lu, Q. R., Casaccia, P., Tesar, P. J., & Nishiyama, A. (2019). The chromatin environment around interneuron genes in oligodendrocyte precursor cells and their potential for interneuron reprograming. *Frontiers in Neuroscience*, *13*(JUL), 829. https://doi.org/10.3389/FNINS.2019.00829/BIBTEX

Boulenouar, H., Benhatchi, H., Guermoudi, F., Oumiloud, A. H., & Rahoui, A. (2022). An actualized screening of schizophrenia-associated genes. *Egyptian Journal of Medical Human Genetics*, *23*(1), 1–12. https://doi.org/10.1186/S43042-022-00269-X/TABLES/2

Bragg-Gonzalo, L., De León Reyes, N. S., & Nieto, M. (2021). Genetic and activity dependent-mechanisms wiring the cortex: Two sides of the same coin. *Seminars in Cell & Developmental Biology*, *118*, 24–34. https://doi.org/10.1016/J.SEMCDB.2021.05.011

Brigidi, G. S., Hayes, M. G., Delos Santos, N. P., Hartzell, A. L., Texari, L., Lin, P. A., Bartlett, A., Ecker, J. R., Benner, C., Heinz, S., & Bloodgood, B. L. (2019). Genomic Decoding of Neuronal Depolarization by Stimulus-Specific NPAS4 Heterodimers. *Cell*, *179*(2), 373–391.e27. https://doi.org/10.1016/J.CELL.2019.09.004

Britanova, O., de Juan Romero, C., Cheung, A., Kwan, K. Y., Schwark, M., Gyorgy, A., Vogel, T., Akopov, S., Mitkovski, M., Agoston, D., Šestan, N., Molnár, Z., & Tarabykin, V. (2008). Satb2 Is a Postmitotic Determinant for Upper-Layer Neuron Specification in the Neocortex. *Neuron*, *57*(3), 378–392. https://doi.org/10.1016/J.NEURON.2007.12.028

Buchthal, B., Lau, D., Weiss, U., Weislogel, J. M., & Bading, H. (2012). Nuclear Calcium Signaling Controls Methyl-CpG-binding Protein 2 (MeCP2) Phosphorylation on Serine 421 following Synaptic Activity. *The Journal of Biological Chemistry*, *287*(37), 30967. https://doi.org/10.1074/JBC.M112.382507

Bullitt, E. (1990). Expression of c-fos-like protein as a marker for neuronal activity following noxious stimulation in the rat. *The Journal of comparative neurology*, *296*(4), 517–530. https://doi.org/10.1002/CNE.902960402

Canavero, S., & Cioni, B. (2011). Cerebral – Surface. *Essential Neuromodulation*, 17–46. https://doi.org/10.1016/B978-0-12-381409-8.00002-4

Cánovas, J., Berndt, F. A., Sepúlveda, H., Aguilar, R., Veloso, F. A., Montecino, M., Oliva, C., Maass, J. C., Sierralta, J., & Kukuljan, M. (2015). The Specification of Cortical

Subcerebral Projection Neurons Depends on the Direct Repression of TBR1 by CTIP1/BCL11a. *The Journal of Neuroscience*, *35*(19), 7552. https://doi.org/10.1523/JNEUROSCI.0169-15.2015

Cepko, C. L., Golden, J. A., Szele, F. G., & Lin, J. C. (1998). Lineage analysis in the vertebrate central nervous system. *Molecular and Cellular Approaches to Neural Development*. https://doi.org/10.1093/ACPROF:OSO/9780195111668.003.0011

Chahrour, M., Sung, Y. J., Shaw, C., Zhou, X., Wong, S. T., Qin, J., & Zoghbi, H. Y. (2008). MeCP2, a Key Contributor to Neurological Disease, Activates and Represses Transcription. *Science (New York, N.Y.)*, *320*(5880), 1224. https://doi.org/10.1126/SCIENCE.1153252

Chen, C., Lee, G. A., Pourmorady, A., Sock, E., & Donoghue, M. J. (2015). Orchestration of Neuronal Differentiation and Progenitor Pool Expansion in the Developing Cortex by SoxC Genes. *The Journal of Neuroscience*, *35*(29), 10629. https://doi.org/10.1523/JNEUROSCI.1663-15.2015

Chen, H., Huffman, J. E., Brody, J. A., Wang, C., Lee, S., Li, Z., Gogarten, S. M., Sofer, T., Bielak, L. F., Bis, J. C., Blangero, J., Bowler, R. P., Cade, B. E., Cho, M. H., Correa, A., Curran, J. E., de Vries, P. S., Glahn, D. C., Guo, X., … Lin, X. (2019). Efficient Variant Set Mixed Model Association Tests for Continuous and Binary Traits in Large-Scale Whole-Genome Sequencing Studies. *American journal of human genetics*, *104*(2), 260–274. https://doi.org/10.1016/j.ajhg.2018.12.012

Chen, J., Fuhler, N., Noguchi, K., & Dougherty, J. D. (2022). MYT1L is required for suppressing earlier neuronal development programs in the adult mouse brain. *bioRxiv*, 2022.10.17.512591. https://doi.org/10.1101/2022.10.17.512591

Chen, X., & Li, H. (2022). Neuronal reprogramming in treating spinal cord injury. *Neural Regeneration Research*, *17*(7), 1440. https://doi.org/10.4103/1673-5374.330590

Chen, Y., Wang, Y., Ertü Rk, A., Kallop, D., Jiang, Z., Weimer, R. M., Kaminker, J., & Sheng, M. (2014). Article Activity-Induced Nr4a1 Regulates Spine Density and Distribution Pattern of Excitatory Synapses in Pyramidal Neurons. *Neuron*, *83*, 431–443. https://doi.org/10.1016/j.neuron.2014.05.027

Chen, Y. C., Kuo, H. Y., Bornschein, U., Takahashi, H., Chen, S. Y., Lu, K. M., Yang, H. Y., Chen, G. M., Lin, J. R., Lee, Y. H., Chou, Y. C., Cheng, S. J., Chien, C. T., Enard, W., Hevers, W., Pääbo, S., Graybiel, A. M., & Liu, F. C. (2016). Foxp2 controls synaptic wiring of corticostriatal circuits and vocal communication by opposing Mef2c. *Nature Neuroscience 2016 19:11*, *19*(11), 1513–1522. https://doi.org/10.1038/nn.4380

Cheng, S., Butrus, S., Tan, L., Xu, R., Sagireddy, S., Trachtenberg, J. T., Shekhar, K., & Zipursky, S. L. (2022). Vision-dependent specification of cell types and function in

the developing cortex. *Cell*, *185*(2), 311–327.e24. https://doi.org/10.1016/J.CELL.2021.12.022

Cheng, X., Zhao, Y., Jiang, Q., Yang, J., Zhao, W., Taylor, I. A., Peng, Y. L., Wang, D., & Liu, J. (2019). Structural basis of dimerization and dual W-box DNA recognition by rice WRKY domain. *Nucleic Acids Research*, *47*(8), 4308–4318. https://doi.org/10.1093/nar/gkz113

Cheyne, J. E., Grant, L., Butler-Munro, C., Foote, J. W., Connor, B., & Montgomery, J. M. (2011). Synaptic integration of newly generated neurons in rat dissociated hippocampal cultures. *Molecular and cellular neurosciences*, *47*(3), 203–214. https://doi.org/10.1016/J.MCN.2011.04.006

Choii, G., & Ko, J. (2015). Gephyrin: a central GABAergic synapse organizer. *Experimental & Molecular Medicine 2015 47:4*, *47*(4), e158–e158. https://doi.org/10.1038/emm.2015.5

Chong, C. H., Li, Q., Mak, P. H. S., Ng, C. C. P., Leung, E. H. W., Tan, V. H., Chan, A. K. W., McAlonan, G., & Chan, S. Y. (2019). Lrrc7 mutant mice model developmental emotional dysregulation that can be alleviated by mGluR5 allosteric modulation. *Translational Psychiatry*, *9*(1). https://doi.org/10.1038/S41398-019-0580-9

Chouchane, M., Melo de Farias, A. R., Moura, D. M. d. S., Hilscher, M. M., Schroeder, T., Leão, R. N., & Costa, M. R. (2017). Lineage Reprogramming of Astroglial Cells from Different Origins into Distinct Neuronal Subtypes. *Stem cell reports*, *9*(1), 162–176. https://doi.org/10.1016/J.STEMCR.2017.05.009

Chung, S. W., Lewis, B. P., Rogasch, N. C., Saeki, T., Thomson, R. H., Hoy, K. E., Bailey, N. W., & Fitzgerald, P. B. (2017). Demonstration of short-term plasticity in the dorsolateral prefrontal cortex with theta burst stimulation: A TMS-EEG study. *Clinical neurophysiology : official journal of the International Federation of Clinical Neurophysiology*, *128*(7), 1117–1126. https://doi.org/10.1016/J.CLINPH.2017.04.005

Citri, A., & Malenka, R. C. (2007). Synaptic Plasticity: Multiple Forms, Functions, and Mechanisms. *Neuropsychopharmacology 2008 33:1*, *33*(1), 18–41. https://doi.org/10.1038/sj.npp.1301559

Clapham, D. E. (2007). Calcium Signaling. *Cell*, *131*(6), 1047–1058. https://doi.org/10.1016/j.cell.2007.11.028

Clark, E. A., Rutlin, M., Capano, L., Aviles, S., Saadon, J. R., Taneja, P., Zhang, Q., Bullis, J., Lauer, T., Myers, E., Schulmann, A., Forrest, D., & Nelson, S. B. (2020). Cortical RORβ is required for layer 4 transcriptional identity and barrel integrity. *eLife*, *9*, 1–45. https://doi.org/10.7554/ELIFE.52370

Clarke, Z. A., Andrews, T. S., Atif, J., Pouyabahar, D., Innes, B. T., MacParland, S. A., & Bader, G. D. (2021). Tutorial: guidelines for annotating single-cell transcriptomic

maps using automated and manual methods. *Nature Protocols 2021 16:6*, *16*(6), 2749–2764. https://doi.org/10.1038/s41596-021-00534-0

Cohen, S. M., Ma, H., Kuchibhotla, K. V., Watson, B. O., Buzsáki, G., Froemke, R. C., & Tsien, R. W. (2016). Excitation-Transcription Coupling in Parvalbumin-Positive Interneurons Employs a Novel CaM Kinase-Dependent Pathway Distinct from Excitatory Neurons. *Neuron*, *90*(2), 292–307. https://doi.org/10.1016/J.NEURON.2016.03.001

Cohen, S., & Greenberg, M. E. (2008). Communication between the synapse and the nucleus in neuronal development, plasticity, and disease. *Annual Review of Cell and Developmental Biology*, *24*, 183–209. https://doi.org/10.1146/annurev.cellbio.24.110707.175235

Colas, J. F., & Schoenwolf, G. C. (2001). Towards a cellular and molecular understanding of neurulation. *Developmental dynamics : an official publication of the American Association of Anatomists*, *221*(2), 117–145. https://doi.org/10.1002/DVDY.1144

Copp, A. J. (2005). Neurulation in the cranial region – normal and abnormal. *Journal of Anatomy*, *207*(5), 623. https://doi.org/10.1111/J.1469-7580.2005.00476.X

Cotterill, E., Charlesworth, P., Thomas, C. W., Paulsen, O., & Eglen, S. J. (2016). A comparison of computational methods for detecting bursts in neuronal spike trains and their application to human stem cell-derived neuronal networks. *Journal of neurophysiology*, *116*(2), 306–321. https://doi.org/10.1152/JN.00093.2016

Crux, S., Herms, J., & Dorostkar, M. M. (2018). Tcf4 regulates dendritic spine density and morphology in the adult brain. *PloS one*, *13*(6). https://doi.org/10.1371/JOURNAL.PONE.0199359

Cull-Candy, S., Kelly, L., & Farrant, M. (2006). Regulation of Ca2+-permeable AMPA receptors: synaptic plasticity and beyond. *Current opinion in neurobiology*, *16*(3), 288–297. https://doi.org/10.1016/J.CONB.2006.05.012

Danielson, N. B. B., Kaifosh, P., Zaremba, J. D. D., Lovett-Barron, M., Tsai, J., Denny, C. A. A., Balough, E. M. M., Goldberg, A. R. R., Drew, L. J. J., Hen, R., Losonczy, A., & Kheirbek, M. A. A. (2016). Distinct Contribution of Adult-Born Hippocampal Granule Cells to Context Encoding. *Neuron*, *90*(1), 101–112. https://doi.org/10.1016/j.neuron.2016.02.019

Davis, G. W. (2006). HOMEOSTATIC CONTROL OF NEURAL ACTIVITY: From Phenomenology to Molecular Design. *http://dx.doi.org/10.1146/annurev.neuro.28.061604.135751*, *29*, 307–323. https://doi.org/10.1146/ANNUREV.NEURO.28.061604.135751

Davis, M. W., & Jorgensen, E. M. (2022). ApE, A Plasmid Editor: A Freely Available DNA Manipulation and Visualization Program. *Frontiers in Bioinformatics*, *0*, 5. https://doi.org/10.3389/FBINF.2022.818619

Deeg, K. E., & Aizenman, C. D. (2011). Sensory modality–specific homeostatic plasticity in the developing optic tectum. *Nature Neuroscience 2011 14:5*, *14*(5), 548–550. https://doi.org/10.1038/nn.2772

Dehorter, N., Marichal, N., Marín, O., & Berninger, B. (2017). Tuning neural circuits by turning the interneuron knob. *Current opinion in neurobiology*, *42*, 144–151. https://doi.org/10.1016/J.CONB.2016.12.009

Dennis, D. J., Han, S., & Schuurmans, C. (2019). bHLH transcription factors in neural development, disease, and reprogramming. *Brain research*, *1705*, 48–65. https://doi.org/10.1016/J.BRAINRES.2018.03.013

Desai, A. R., & McConnell, S. K. (2000). Progressive restriction in fate potential by neural progenitors during cerebral cortical development. *Development (Cambridge, England)*, *127*(13), 2863–2872. https://doi.org/10.1242/DEV.127.13.2863

Desch, K., Langer, J. D., & Schuman, E. M. (2021). Dynamic bi-directional phosphorylation events associated with the reciprocal regulation of synapses during homeostatic up- and down-scaling. *Cell Reports*, *36*(8), 109583. https://doi.org/10.1016/J.CELREP.2021.109583

Di Bella, D. J., Habibi, E., Stickels, R. R., Scalia, G., Brown, J., Yadollahpour, P., Yang, S. M., Abbate, C., Biancalani, T., Macosko, E. Z., Chen, F., Regev, A., & Arlotta, P. (2021). Molecular logic of cellular diversification in the mouse cerebral cortex. *Nature 2021 595:7868*, *595*(7868), 554–559. https://doi.org/10.1038/s41586-021-03670-5

Dimou, L., & Gallo, V. (n.d.). NG2-glia and their functions in the central nervous system. https://doi.org/10.1002/glia.22859

Dörrbaum, A. R., Alvarez-Castelao, B., Nassim-Assir, B., Langer, J. D., & Schuman, E. M. (2020). Proteome dynamics during homeostatic scaling in cultured neurons. *eLife*, *9*. https://doi.org/10.7554/ELIFE.52939

Dudek, S. M., & Bear, M. F. (1992). Homosynaptic long-term depression in area CA1 of hippocampus and effects of N-methyl-D-aspartate receptor blockade. *Proceedings of the National Academy of Sciences of the United States of America*, *89*(10), 4363. https://doi.org/10.1073/PNAS.89.10.4363

Dynes, J. L., & Steward, O. (2007). Dynamics of bidirectional transport of Arc mRNA in neuronal dendrites. *The Journal of comparative neurology*, *500*(3), 433–447. https://doi.org/10.1002/CNE.21189

Ebert, D. H., & Greenberg, M. E. (2013). Activity-dependent neuronal signalling and autism spectrum disorder. *Nature*, *493*(7432), 327. https://doi.org/10.1038/NATURE11860

Eferl, R., & Wagner, E. F. (2003). AP-1: a double-edged sword in tumorigenesis. *Nature Reviews Cancer 2003 3:11*, *3*(11), 859–868. https://doi.org/10.1038/nrc1209

Elshazzly, M., Lopez, M. J., Reddy, V., & Caban, O. (2022). Embryology, Central Nervous System. *StatPearls*. https://www.ncbi.nlm.nih.gov/books/NBK526024/

Engert, F., & Bonhoeffer, T. (1999). Dendritic spine changes associated with hippocampal long-term synaptic plasticity. *Nature*, *399*(6731), 66–70. https://doi.org/10.1038/19978

Englund, C., Fink, A., Lau, C., Pham, D., Daza, R. A., Bulfone, A., Kowalczyk, T., & Hevner, R. F. (2005). Pax6, Tbr2, and Tbr1 are expressed sequentially by radial glia, intermediate progenitor cells, and postmitotic neurons in developing neocortex. *The Journal of neuroscience : the official journal of the Society for Neuroscience*, *25*(1), 247–251. https://doi.org/10.1523/JNEUROSCI.2899-04.2005

España, J., Valero, J., Miñano-Molina, A. J., Masgrau, R., Martín, E., Guardia-Laguarta, C., Lleó, A., Giménez-Llort, L., Rodríguez-Alvarez, J., & Saura, C. A. (2010). β-Amyloid Disrupts Activity-Dependent Gene Transcription Required for Memory through the CREB Coactivator CRTC1. *The Journal of Neuroscience*, *30*(28), 9402. https://doi.org/10.1523/JNEUROSCI.2154-10.2010

Espuny-Camacho, I., Michelsen, K. A., Linaro, D., Bilheu, A., Acosta-Verdugo, S., Herpoel, A., Giugliano, M., Gaillard, A., & Vanderhaeghen, P. (2018). Human Pluripotent Stem-Cell-Derived Cortical Neurons Integrate Functionally into the Lesioned Adult Murine Visual Cortex in an Area-Specific Way. *Cell reports*, *23*(9), 2732–2743. https://doi.org/10.1016/J.CELREP.2018.04.094

Falk, S., Han, D., & Karow, M. (2021). Cellular identity through the lens of direct lineage reprogramming. *Current Opinion in Genetics and Development*, *70*, 97–103. https://doi.org/10.1016/J.GDE.2021.06.015

Falkner, S., Grade, S., Dimou, L., Conzelmann, K. K., Bonhoeffer, T., Götz, M., & Hübener, M. (2016). Transplanted embryonic neurons integrate into adult neocortical circuits. *Nature*, *539*(7628), 248–253. https://doi.org/10.1038/NATURE20113

Fernandes, D., & Carvalho, A. L. (2016). Mechanisms of homeostatic plasticity in the excitatory synapse. *Journal of Neurochemistry*, *139*(6), 973–996. https://doi.org/10.1111/JNC.13687

Flavell, S. W., & Greenberg, M. E. (2008). Signaling mechanisms linking neuronal activity to gene expression and plasticity of the nervous system. *Annual review of neuroscience*, *31*, 563–590. https://doi.org/10.1146/ANNUREV.NEURO.31.060407.125631

Fode, C., Gradwohl, G., Morin, X., Dierich, A., LeMeur, M., Goridis, C., & Guillemot, F. (1998). The bHLH protein NEUROGENIN 2 is a determination factor for epibranchial placode-derived sensory neurons. *Neuron*, *20*(3), 483–494. https://doi.org/10.1016/S0896-6273(00)80989-7

Fox, K., & Stryker, M. (2017). Integrating Hebbian and homeostatic plasticity: introduction. *Philosophical Transactions of the Royal Society B: Biological Sciences*, *372*(1715). https://doi.org/10.1098/RSTB.2016.0413

Gachon, F., Fonjallaz, P., Damiola, F., Gos, P., Kodama, T., Zakany, J., Duboule, D., Petit, B., Tafti, M., & Schibler, U. (2004). The loss of circadian PAR bZip transcription factors results in epilepsy. *Genes & Development*, *18*(12), 1397. https://doi.org/10.1101/GAD.301404

Gaiano, N., Nye, J. S., & Fishell, G. (2000). Radial glial identity is promoted by Notch1 signaling in the murine forebrain. *Neuron*, *26*(2), 395–404. https://doi.org/10.1016/S0896-6273(00)81172-1

Galanis, C., & Vlachos, A. (2020). Hebbian and Homeostatic Synaptic Plasticity—Do Alterations of One Reflect Enhancement of the Other? *Frontiers in Cellular Neuroscience*, *14*, 50. https://doi.org/10.3389/FNCEL.2020.00050/BIBTEX

Gandolfi, D., Cerri, S., Mapelli, J., Polimeni, M., Tritto, S., Fuzzati-Armentero, M. T., Bigiani, A., Blandini, F., Mapelli, L., & D'Angelo, E. (2017). Activation of the CREB/c-Fos Pathway during Long-Term Synaptic Plasticity in the Cerebellum Granular Layer. *Frontiers in Cellular Neuroscience*, *11*. https://doi.org/10.3389/FNCEL.2017.00184

Gao, M., Sossa, K., Song, L., Errington, L., Cummings, L., Hwang, H., Kuhl, D., Worley, P., & Lee, H. K. (2010). A Specific Requirement of Arc/Arg3.1 for Visual Experience-Induced Homeostatic Synaptic Plasticity in Mouse Primary Visual Cortex. *The Journal of Neuroscience*, *30*(21), 7168–7178. https://doi.org/10.1523/JNEUROSCI.1067-10.2010

Gascón, S., Murenu, E., Masserdotti, G., Ortega, F., Russo, G. L., Petrik, D., Deshpande, A., Heinrich, C., Karow, M., Robertson, S. P., Schroeder, T., Beckers, J., Irmler, M., Berndt, C., Angeli, J. P., Conrad, M., Berninger, B., & Götz, M. (2016). Identification and Successful Negotiation of a Metabolic Checkpoint in Direct Neuronal Reprogramming. *Cell stem cell*, *18*(3), 396–409. https://doi.org/10.1016/J.STEM.2015.12.003

Gaspard, N., & Vanderhaeghen, P. (2011). Laminar fate specification in the cerebral cortex. *F1000 biology reports*, *3*(1). https://doi.org/10.3410/B3-6

Ge, S., Sailor, K. A., Ming, G. L., & Song, H. (2008). Synaptic integration and plasticity of new neurons in the adult hippocampus. *Journal of Physiology*, *586*(16), 3759–3765. https://doi.org/10.1113/JPHYSIOL.2008.155655

Georgias, C., Wasser, M., & Hinz, U. (1997). A basic-helix-loop-helix protein expressed in precursors of Drosophila longitudinal visceral muscles. *Mechanisms of Development*, *69*(1-2), 115–124. https://doi.org/10.1016/S0925-4773(97)00169-X

Gilbert., S. F. (2000). Developmental Biology - NCBI Bookshelf. Retrieved June 5, 2022, from https://www.ncbi.nlm.nih.gov/books/NBK9983/

Goel, A., Xu, L. W., Snyder, K. P., Song, L., Goenaga-Vazquez, Y., Megill, A., Takamiya, K., Huganir, R. L., & Lee, H. K. (2011). Phosphorylation of AMPA receptors is required for sensory deprivation-induced homeostatic synaptic plasticity. *PloS one*, *6*(3). https://doi.org/10.1371/JOURNAL.PONE.0018264

Gohlke, J. M., Armant, O., Parham, F. M., Smith, M. V., Zimmer, C., Castro, D. S., Nguyen, L., Parker, J. S., Gradwohl, G., Portier, C. J., & Guillemot, F. (2008). Characterization of the proneural gene regulatory network during mouse telencephalon development. *BMC Biology*, *6*(1), 1–18. https://doi.org/10.1186/1741-7007-6-15/FIGURES/5

Gonçalves, J. T., Schafer, S. T., & Gage, F. H. (2016). Adult Neurogenesis in the Hippocampus: From Stem Cells to Behavior. *Cell*, *167*(4), 897–914. https://doi.org/10.1016/J.CELL.2016.10.021

Gonzalez-Islas, C., Bülow, P., & Wenner, P. (2018). Regulation of synaptic scaling by action potential–independent miniature neurotransmission. *Journal of Neuroscience Research*, *96*(3), 348–353. https://doi.org/10.1002/jnr.24138

Gonzalez-Ramos, A., Waloschková, E., Mikroulis, A., Kokaia, Z., Bengzon, J., Ledri, M., Andersson, M., & Kokaia, M. (2021). Human stem cell-derived GABAergic neurons functionally integrate into human neuronal networks. *Scientific Reports 2021 11:1*, *11*(1), 1–16. https://doi.org/10.1038/s41598-021-01270-x

Götz, M., Nakafuku, M., & Petrik, D. (2016). Neurogenesis in the Developing and Adult Brain-Similarities and Key Differences. *Cold Spring Harbor perspectives in biology*, *8*(7). https://doi.org/10.1101/CSHPERSPECT.A018853

Götz, M., Stoykova, A., & Gruss, P. (1998). Pax6 controls radial glia differentiation in the cerebral cortex. *Neuron*, *21*(5), 1031–1044. https://doi.org/10.1016/S0896-6273(00)80621-2

Grade, S., Thomas, J., Zarb, Y., Thorwirth, M., Conzelmann, K. K., Hauck, S. M., & Götz, M. (2022). Brain injury environment critically influences the connectivity of transplanted neurons. *Science advances*, *8*(23). https://doi.org/10.1126/SCIADV.ABG9445

Grande, A., Sumiyoshi, K., López-Juárez, A., Howard, J., Sakthivel, B., Aronow, B., Campbell, K., & Nakafuku, M. (2013). Environmental impact on direct neuronal reprogramming in vivo in the adult brain. *Nature communications*, *4*. https://doi.org/10.1038/NCOMMS3373

Gray, J. M., & Spiegel, I. (2019). Cell-type-specific programs for activity-regulated gene expression. *Current Opinion in Neurobiology*, *56*, 33–39. https://doi.org/10.1016/j.conb.2018.11.001

Greenberg, M. E., & Ziff Edward B. (1984). Stimulation of 3T3 cells induces transcription of the c-fos proto-oncogene. *Nature 1984 311:5985*, *311*(5985), 433–438. https://doi.org/10.1038/311433a0

Guillemot, F., Lo, L. C., Johnson, J. E., Auerbach, A., Anderson, D. J., & Joyner, A. L. (1993). Mammalian achaete-scute homolog 1 is required for the early development of olfactory and autonomic neurons. *Cell*, *75*(3), 463–476. https://doi.org/10.1016/0092-8674(93)90381-Y

Guo, Z., Zhang, L., Wu, Z., Chen, Y., Wang, F., & Chen, G. (2014). In vivo direct reprogramming of reactive glial cells into functional neurons after brain injury and in an Alzheimer's disease model. *Cell stem cell*, *14*(2), 188–202. https://doi.org/10.1016/J.STEM.2013.12.001

Gurdon, J. B. (1962). The developmental capacity of nuclei taken from intestinal epithelium cells of feeding tadpoles - PubMed. Retrieved September 2, 2022, from https://pubmed.ncbi.nlm.nih.gov/13951335/

Guzelsoy, G., Akkaya, C., Atak, D., Dunn, C. D., Kabakcioglu, A., Ozlu, N., & Ince-Dunn, G. (2019). Terminal neuron localization to the upper cortical plate is controlled by the transcription factor NEUROD2. *Scientific Reports 2019 9:1*, *9*(1), 1–12. https://doi.org/10.1038/s41598-019-56171-x

Guzowski, J. F., Setlow, B., Wagner, E. K., & McGaugh, J. L. (2001). Experience-dependent gene expression in the rat hippocampus after spatial learning: a comparison of the immediate-early genes Arc, c-fos, and zif268. *The Journal of neuroscience : the official journal of the Society for Neuroscience*, *21*(14), 5089–5098. https://doi.org/10.1523/JNEUROSCI.21-14-05089.2001

Haines, D. E., & Mihailoff, G. A. (2018). The Telencephalon. *Fundamental Neuroscience for Basic and Clinical Applications: Fifth Edition*, 225–240.e1. https://doi.org/10.1016/B978-0-323-39632-5.00016-5

Han, E. B., & Stevens, C. F. (2009). Development regulates a switch between postand presynaptic strengthening in response to activity deprivation. *Proceedings of the National Academy of Sciences of the United States of America*, *106*(26), 10817–10822. https://doi.org/10.1073/pnas.0903603106

Han, S., Dennis, D. J., Balakrishnan, A., Dixit, R., Britz, O., Zinyk, D., Touahri, Y., Olender, T., Brand, M., Guillemot, F., Kurrasch, D., & Schuurmans, C. (2018). A non-canonical role for the proneural gene Neurog1 as a negative regulator of neocortical neurogenesis. *Development (Cambridge, England)*, *145*(19). https://doi.org/10.1242/DEV.157719

Hand, R., Bortone, D., Mattar, P., Nguyen, L., Heng, J. I. T., Guerrier, S., Boutt, E., Peters, E., Barnes, A. P., Parras, C., Schuurmans, C., Guillemot, F., & Polleux, F. (2005). Phosphorylation of Neurogenin2 specifies the migration properties and

the dendritic morphology of pyramidal neurons in the neocortex. *Neuron*, *48*(1), 45–62. https://doi.org/10.1016/J.NEURON.2005.08.032

Harnett, D., Ambrozkiewicz, M. C., Zinnall, U., Rusanova, A., Borisova, E., Drescher, A. N., Couce-Iglesias, M., Villamil, G., Dannenberg, R., Imami, K., Münster-Wandowski, A., Fauler, B., Mielke, T., Selbach, M., Landthaler, M., Spahn, C. M. T., Tarabykin, V., Ohler, U., & Kraushar, M. L. (2022). A critical period of translational control during brain development at codon resolution. *Nature Structural & Molecular Biology 2022 29:12*, *29*(12), 1277–1290. https://doi.org/10.1038/s41594-022-00882-9

Hatakeyama, J., Tomita, K., Inoue, T., & Kageyama, R. (2001). Roles of homeobox and bHLH genes in specification of a retinal cell type. *Development (Cambridge, England)*, *128*(8), 1313–1322. https://doi.org/10.1242/DEV.128.8.1313

Heavner, W. E., Lautz, J. D., Speed, H. E., Gniffke, E. P., Immendorf, K. B., Welsh, J. P., Baertsch, N. A., & Smith, S. E. (2021). Remodeling of the homer-shank interactome mediates homeostatic plasticity. *Science Signaling*, *14*(681), 7325. https://doi.org/10.1126/SCISIGNAL.ABD7325/SUPPL_FILE/ABD7325_SM.PDF activity-regulated postsynaptic protein interaction network (PIN) in mice. This PIN changed differentially to prolonged increases in activity compared to prolonged decreases and to the activity manipulations performed in culture compared to those performed in vivo. Some of the changes in this PIN did not occur in mice lacking either Homer1 or Shank3, scaffolding protein–encoding genes that are mutated in some patients with autism spectrum disorder. The findings begin to elucidate the complexity and context dependence of homeostatic synaptic plasticity

Heinrich, C., Bergami, M., Gascón, S., Lepier, A., Viganò, F., Dimou, L., Sutor, B., Berninger, B., & Götz, M. (2014). Sox2-mediated conversion of NG2 glia into induced neurons in the injured adult cerebral cortex. *Stem cell reports*, *3*(6), 1000–1014. https://doi.org/10.1016/J.STEMCR.2014.10.007

Heinrich, C., Blum, R., Gascón, S., Masserdotti, G., Tripathi, P., Sánchez, R., Tiedt, S., Schroeder, T., Götz, M., & Berninger, B. (2010). Directing astroglia from the cerebral cortex into subtype specific functional neurons. *PLoS biology*, *8*(5). https://doi.org/10.1371/JOURNAL.PBIO.1000373

Heinrich, C., Gascón, S., Masserdotti, G., Lepier, A., Sanchez, R., Simon-Ebert, T., Schroeder, T., Gøtz, M., & Berninger, B. (2011). Generation of subtype-specific neurons from postnatal astroglia of the mouse cerebral cortex. *Nature protocols*, *6*(2), 214–228. https://doi.org/10.1038/NPROT.2010.188

Heinrich, C., Götz, M., & Berninger, B. (2012). Reprogramming of postnatal astroglia of the mouse neocortex into functional, synapse-forming neurons. *Methods in molecular biology (Clifton, N.J.)*, *814*, 485–498. https://doi.org/10.1007/978-1-61779-452-0_32

Heins, N., Malatesta, P., Cecconi, F., Nakafuku, M., Tucker, K. L., Hack, M. A., Chapouton, P., Barde, Y. A., & Goötz, M. (2002). Glial cells generate neurons: the role of the transcription factor Pax6. *Nature neuroscience*, *5*(4), 308–315. https://doi.org/10.1038/NN828

Heir, R., & Stellwagen, D. (2020). TNF-Mediated Homeostatic Synaptic Plasticity: From in vitro to in vivo Models. *Frontiers in Cellular Neuroscience*, *14*, 297. https://doi.org/10.3389/FNCEL.2020.565841/BIBTEX

Henley, J. M., & Wilkinson, K. A. (2013). AMPA receptor trafficking and the mechanisms underlying synaptic plasticity and cognitive aging. *Dialogues in Clinical Neuroscience*, *15*(1), 11. https://doi.org/10.31887/DCNS.2013.15.1/JHENLEY

Herculano-Houzel, S., Mota, B., & Lent, R. (2006). Cellular scaling rules for rodent brains. *Proceedings of the National Academy of Sciences*, *103*(32), 12138–12143. https://doi.org/10.1073/pnas.0604911103

Herrero-Navarro, Á., Puche-Aroca, L., Moreno-Juan, V., Sempere-Ferràndez, A., Espinosa, A., Susín, R., Torres-Masjoan, L., Leyva-Díaz, E., Karow, M., Figueres-Oñate, M., López-Mascaraque, L., López-Atalaya, J. P., Berninger, B., & López-Bendito, G. (2021). Astrocytes and neurons share region-specific transcriptional signatures that confer regional identity to neuronal reprogramming. *Science advances*, *7*(15). https://doi.org/10.1126/SCIADV.ABE8978

Herring, C. A., Simmons, R. K., Freytag, S., Poppe, D., Moffet, J. J., Pflueger, J., Buckberry, S., Vargas-Landin, D. B., Clément, O., Echeverría, E. G., Sutton, G. J., Alvarez-Franco, A., Hou, R., Pflueger, C., McDonald, K., Polo, J. M., Forrest, A. R., Nowak, A. K., Voineagu, I., … Lister, R. (2022). Human prefrontal cortex gene regulatory dynamics from gestation to adulthood at single-cell resolution. *Cell*, *185*(23), 4428–4447.e28. https://doi.org/10.1016/J.CELL.2022.09.039/ATTACHMENT/553E2A11-824B-41B7-9A51-52D35A40D1A4/MMC6.XLSX

Higashimoto, T., Urbinati, F., Perumbeti, A., Jiang, G., Zarzuela, A., Chang, L. J., Kohn, D. B., & Malik, P. (2007). The woodchuck hepatitis virus post-transcriptional regulatory element reduces readthrough transcription from retroviral vectors. *Gene therapy*, *14*(17), 1298–1304. https://doi.org/10.1038/SJ.GT.3302979

Hippenmeyer, S. (2023). Principles of neural stem cell lineage progression: Insights from developing cerebral cortex. *Current opinion in neurobiology*, *79*. https://doi.org/10.1016/J.CONB.2023.102695

Hodge, R. D., Bakken, T. E., Miller, J. A., Smith, K. A., Barkan, E. R., Graybuck, L. T., Close, J. L., Long, B., Johansen, N., Penn, O., Yao, Z., Eggermont, J., Höllt, T., Levi, B. P., Shehata, S. I., Aevermann, B., Beller, A., Bertagnolli, D., Brouner, K., … Lein, E. S. (2019). Conserved cell types with divergent features in human versus mouse cortex. *Nature*, *573*(7772), 61–68. https://doi.org/10.1038/S41586-019-1506-7

Hoey, S. E., Williams, R. J., & Perkinton, M. S. (2009). Synaptic NMDA Receptor Activation Stimulates α-Secretase Amyloid Precursor Protein Processing and Inhibits Amyloid-β Production. *Journal of Neuroscience*, *29*(14), 4442–4460. https://doi.org/10.1523/JNEUROSCI.6017-08.2009

Hong, E. J., McCord, A. E., & Greenberg, M. E. (2008). A Biological Function for the Neuronal Activity-Dependent Component of Bdnf Transcription in the Development of Cortical Inhibition. *Neuron*, *60*(4), 610–624. https://doi.org/10.1016/j.neuron.2008.09.024

Hong, J. C. (2016). General Aspects of Plant Transcription Factor Families. *Plant Transcription Factors: Evolutionary, Structural and Functional Aspects*, 35–56. https://doi.org/10.1016/B978-0-12-800854-6.00003-8

Hou, H., Sun, L., Siddoway, B. A., Petralia, R. S., Yang, H., Gu, H., Nairn, A. C., & Xia, H. (2013). Synaptic NMDA receptor stimulation activates PP1 by inhibiting its phosphorylation by Cdk5. *Journal of Cell Biology*, *203*(3), 521–535. https://doi.org/10.1083/JCB.201303035

Hrvatin, S., Hochbaum, D. R., Nagy, M. A., Cicconet, M., Robertson, K., Cheadle, L., Zilionis, R., Ratner, A., Borges-Monroy, R., Klein, A. M., Sabatini, B. L., & Greenberg, M. E. (2018). Single-cell analysis of experience-dependent transcriptomic states in the mouse visual cortex. *Nature Neuroscience*, *21*(1), 120–129. https://doi.org/10.1038/s41593-017-0029-5

Huang, M., Pieraut, S., Cao, J., Polli, F. d. S., Roncace, V., Shen, G., & Maximov, A. (2022). Nr4a1 regulates inhibitory circuit structure and function in the mouse brain. *bioRxiv*, 2022.06.14.496205. https://doi.org/10.1101/2022.06.14.496205

Hulme, A. J., Maksour, S., St-Clair Glover, M., Miellet, S., & Dottori, M. (2022). Making neurons, made easy: The use of Neurogenin-2 in neuronal differentiation. *Stem cell reports*, *17*(1), 14–34. https://doi.org/10.1016/J.STEMCR.2021.11.015

Huupponen, J., Atanasova, T., Taira, T., & Lauri, S. E. (2016). GluA4 subunit of AMPA receptors mediates the early synaptic response to altered network activity in the developing hippocampus. *Journal of Neurophysiology*, *115*(6), 2989. https://doi.org/10.1152/JN.00435.2015

iN immature synapse, Gria4 GluA4

Ibata, K., Sun, Q., & Turrigiano, G. G. (2008). Rapid synaptic scaling induced by changes in postsynaptic firing. *Neuron*, *57*(6), 819–826. https://doi.org/10.1016/J.NEURON.2008.02.031

Ieda, M., Fu, J. D., Delgado-Olguin, P., Vedantham, V., Hayashi, Y., Bruneau, B. G., & Srivastava, D. (2010). Direct reprogramming of fibroblasts into functional cardiomyocytes by defined factors. *Cell*, *142*(3), 375–386. https://doi.org/10.1016/J.CELL.2010.07.002

Iemolo, A., Montilla-Perez, P., Lai, I. C., Meng, Y., Nolan, S., Wen, J., Rusu, I., Dulcis, D., & Telese, F. (2020). A cell type-specific expression map of NCoR1 and SMRT transcriptional co-repressors in the mouse brain. *The Journal of comparative neurology*, *528*(13), 2218. https://doi.org/10.1002/CNE.24886

Imayoshi, I., & Kageyama, R. (2014). bHLH factors in self-renewal, multipotency, and fate choice of neural progenitor cells. *Neuron*, *82*(1), 9–23. https://doi.org/10.1016/J.NEURON.2014.03.018

Ince-Dunn, G., Hall, B. J., Hu, S. C., Ripley, B., Huganir, R. L., Olson, J. M., Tapscott, S. J., & Ghosh, A. (2006). Regulation of Thalamocortical Patterning and Synaptic Maturation by NeuroD2. *Neuron*, *49*(5), 683–695. https://doi.org/10.1016/J.NEURON.2006.01.031

Inquimbert, P., Bartels, K., Babaniyi, O. B., Barrett, L. B., Tegeder, I., & Scholz, J. (2012). Peripheral nerve injury produces a sustained shift in the balance between glutamate release and uptake in the dorsal horn of the spinal cord. *Pain*, *153*(12), 2422. https://doi.org/10.1016/J.PAIN.2012.08.011

Isaac, J. T., Ashby, M., & McBain, C. J. (2007). The Role of the GluR2 Subunit in AMPA Receptor Function and Synaptic Plasticity. *Neuron*, *54*(6), 859–871. https://doi.org/10.1016/J.NEURON.2007.06.001

Jaafari, N., Henley, J. M., & Hanley, J. G. (2012). PICK1 Mediates Transient Synaptic Expression of GluA2-Lacking AMPA Receptors during Glycine-Induced AMPA Receptor Trafficking. *The Journal of Neuroscience*, *32*(34), 11618. https://doi.org/10.1523/JNEUROSCI.5068-11.2012

Jaeger, B. N., Linker, S. B., Parylak, S. L., Barron, J. J., Gallina, I. S., Saavedra, C. D., Fitzpatrick, C., Lim, C. K., Schafer, S. T., Lacar, B., Jessberger, S., & Gage, F. H. (2018). A novel environment-evoked transcriptional signature predicts reactivity in single dentate granule neurons. *Nature Communications 2018 9:1*, *9*(1), 1–15. https://doi.org/10.1038/s41467-018-05418-8

!! Cell-type specificity of activity levels and plasticity mechanisms suggests that later molecular processes may also differ across populations, including long-term changes underlying memory formation

Jang, S. S., & Chung, H. J. (2016). Emerging Link between Alzheimer's Disease and Homeostatic Synaptic Plasticity. *Neural plasticity*, *2016*. https://doi.org/10.1155/2016/7969272

Jeans, A. F., van Heusden, F. C., Al-Mubarak, B., Padamsey, Z., & Emptage, N. J. (2017). Homeostatic Presynaptic Plasticity Is Specifically Regulated by P/Q-type Ca2+ Channels at Mammalian Hippocampal Synapses. *Cell Reports*, *21*(2), 341. https://doi.org/10.1016/J.CELREP.2017.09.061

Kageyama, R., Ohtsuka, T., Shimojo, H., & Imayoshi, I. (2009). Dynamic regulation of Notch signaling in neural progenitor cells. *Current Opinion in Cell Biology*, *21*(6), 733–740. https://doi.org/10.1016/J.CEB.2009.08.009

Kaila, K., Price, T. J., Payne, J. A., Puskarjov, M., & Voipio, J. (2014). Cation-chloride cotransporters in neuronal development, plasticity and disease. *Nature Reviews Neuroscience 2014 15:10*, *15*(10), 637–654. https://doi.org/10.1038/nrn3819

Kandel, E. R. (2001). The molecular biology of memory storage: a dialogue between genes and synapses. *Science (New York, N.Y.)*, *294*(5544), 1030–1038. https://doi.org/10.1126/SCIENCE.1067020

Kanski, R., Van Strien, M. E., Van Tijn, P., & Hol, E. M. (2014). A star is born: new insights into the mechanism of astrogenesis. *Cellular and molecular life sciences : CMLS*, *71*(3), 433–447. https://doi.org/10.1007/S00018-013-1435-9

Karow, M., Gray Camp, J., Falk, S., Gerber, T., Pataskar, A., Gac-Santel, M., Kageyama, J., Brazovskaja, A., Garding, A., Fan, W., Riedemann, T., Casamassa, A., Smiyakin, A., Schichor, C., Götz, M., Tiwari, V. K., Treutlein, B., & Berninger, B. (2018). Direct pericyte-to-neuron reprogramming via unfolding of a neural stem cell-like program. *Nature Neuroscience 2018 21:7*, *21*(7), 932–940. https://doi.org/10.1038/s41593-018-0168-3

Karpova, A., Mikhaylova, M., Bera, S., Bär, J., Reddy, P. P., Behnisch, T., Rankovic, V., Spilker, C., Bethge, P., Sahin, J., Kaushik, R., Zuschratter, W., Kähne, T., Naumann, M., Gundelfinger, E. D., & Kreutz, M. R. (2013). Encoding and transducing the synaptic or extrasynaptic origin of NMDA receptor signals to the nucleus. *Cell*, *152*(5), 1119–1133. https://doi.org/10.1016/j.cell.2013.02.002

Karve, I. P., Taylor, J. M., & Crack, P. J. (2016). The contribution of astrocytes and microglia to traumatic brain injury. *British Journal of Pharmacology*, *173*(4), 692. https://doi.org/10.1111/BPH.13125

Keck, T., Keller, G. B., Jacobsen, R. I., Eysel, U. T., Bonhoeffer, T., & Hübener, M. (2013). Synaptic Scaling and Homeostatic Plasticity in the Mouse Visual Cortex In Vivo. *Neuron*, *80*(2), 327–334. https://doi.org/10.1016/J.NEURON.2013.08.018

Kelsch, W., Lin, C. W., Mosley, C. P., & Lois, C. (2009). A Critical Period for Activity-Dependent Synaptic Development during Olfactory Bulb Adult Neurogenesis. *The Journal of Neuroscience*, *29*(38), 11852. https://doi.org/10.1523/JNEUROSCI.2406-09.2009

Kempf, J., Knelles, K., Hersbach, B. A., Petrik, D., Riedemann, T., Bednarova, V., Janjic, A., Simon-Ebert, T., Enard, W., Smialowski, P., Götz, M., & Masserdotti, G. (2021). Heterogeneity of neurons reprogrammed from spinal cord astrocytes by the proneural factors Ascl1 and Neurogenin2. *Cell Reports*, *36*(3), 109409. https://doi.org/10.1016/J.CELREP.2021.109409

Kennedy, A. J., Rahn, E. J., Paulukaitis, B. S., Savell, K. E., Kordasiewicz, H. B., Wang, J., Lewis, J. W., Posey, J., Strange, S. K., Guzman-Karlsson, M. C., Phillips, S. E., Decker, K., Motley, S. T., Swayze, E. E., Ecker, D. J., Michael, T. P., Day, J. J., & Sweatt, J. D. (2016). Tcf4 Regulates Synaptic Plasticity, DNA Methylation, and Memory Function. *Cell Reports*, *16*(10), 2666–2685. https://doi.org/10.1016/J.CELREP.2016.08.004

Kharchenko, P. V., Silberstein, L., & Scadden, D. T. (2014). Bayesian approach to single-cell differential expression analysis. *Nature Methods 2014 11:7*, *11*(7), 740–742. https://doi.org/10.1038/nmeth.2967

Kilman, V., Van Rossum, M. C., & Turrigiano, G. G. (2002). Activity deprivation reduces miniature IPSC amplitude by decreasing the number of postsynaptic GABA(A) receptors clustered at neocortical synapses. *The Journal of neuroscience : the official journal of the Society for Neuroscience*, *22*(4), 1328–1337. https://doi.org/10.1523/JNEUROSCI.22-04-01328.2002

Kim, K. P., Choi, J., Yoon, J., Bruder, J. M., Shin, B., Kim, J., Arauzo-Bravo, M. J., Han, D., Wu, G., Han, D. W., Kim, J., Cramer, P., & Schöler, H. R. (2020). Permissive epigenomes endow reprogramming competence to transcriptional regulators. *Nature Chemical Biology 2020 17:1*, *17*(1), 47–56. https://doi.org/10.1038/s41589-020-0618-6

Kim, M. H., Radaelli, C., Thomsen, E. R., Monet, D., Chartrand, T., Jorstad, N. L., Mahoney, J. T., Taormina, M. J., Long, B., Baker, K., Bakken, T., Campagnola, L., Casper, T., Clark, M., Dee, N., D'orazi, F., Gamlin, C., Kalmbach, B., Kebede, S., … Lein, E. S. (2023). Target cell-specific synaptic dynamics of excitatory to inhibitory neuron connections in supragranular layers of human neocortex. *eLife*, *12*. https://doi.org/10.7554/ELIFE.81863

Kirischuk, S., Sinning, A., Blanquie, O., Yang, J. W., Luhmann, H. J., & Kilb, W. (2017). Modulation of Neocortical Development by Early Neuronal Activity: Physiology and Pathophysiology. *Frontiers in Cellular Neuroscience*, *11*. https://doi.org/10.3389/FNCEL.2017.00379

Kiselev, V. Y., Yiu, A., & Hemberg, M. (2018). scmap: projection of single-cell RNA-seq data across data sets. *Nature Methods 2018 15:5*, *15*(5), 359–362. https://doi.org/10.1038/nmeth.4644

Klingler, E., Francis, F., Jabaudon, D., & Cappello, S. (2021). Mapping the molecular and cellular complexity of cortical malformations. *Science*, *371*(6527). https://doi.org/10.1126/SCIENCE.ABA4517/ASSET/30CE620B-4299-4DF8-9AF3-C7A0EDEF631E/ASSETS/GRAPHIC/371_ABA4517_F5.JPEG

Kong, S. Y., Kim, W., Lee, H. R., & Kim, H. J. (2018). The histone demethylase KDM5A is required for the repression of astrocytogenesis and regulated by the translational

machinery in neural progenitor cells. *The FASEB Journal*, *32*(2), 1108. https://doi.org/10.1096/FJ.201700780R

Koo, B., Lee, K. H., li Ming, G., Yoon, K. J., & Song, H. (2023). Setting the clock of neural progenitor cells during mammalian corticogenesis. *Seminars in cell & developmental biology*, *142*. https://doi.org/10.1016/J.SEMCDB.2022.05.013

Koopmans, F., van Nierop, P., Andres-Alonso, M., Byrnes, A., Cijsouw, T., Coba, M. P., Cornelisse, L. N., Farrell, R. J., Goldschmidt, H. L., Howrigan, D. P., Hussain, N. K., Imig, C., de Jong, A. P., Jung, H., Kohansalnodehi, M., Kramarz, B., Lipstein, N., Lovering, R. C., MacGillavry, H., … Verhage, M. (2019). SynGO: An Evidence-Based, Expert-Curated Knowledge Base for the Synapse. *Neuron*, *103*(2), 217–234.e4. https://doi.org/10.1016/J.NEURON.2019.05.002

Kovach, C., Dixit, R., Li, S., Mattar, P., Wilkinson, G., Elsen, G. E., Kurrasch, D. M., Hevner, R. F., & Schuurmans, C. (2013). Neurog2 simultaneously activates and represses alternative gene expression programs in the developing neocortex. *Cerebral cortex (New York, N.Y. : 1991)*, *23*(8), 1884–1900. https://doi.org/10.1093/CERCOR/BHS176

Krukoff, T. L. (2003). c-fos Expression as a Marker of Functional Activity in the Brain: Immunohistochemistry. *Cell Neurobiology Techniques*, 213–230. https://doi.org/10.1385/0-89603-510-7:213

Kuijlaars, J., Oyelami, T., Diels, A., Rohrbacher, J., Versweyveld, S., Meneghello, G., Tuefferd, M., Verstraelen, P., Detrez, J. R., Verschuuren, M., De Vos, W. H., Meert, T., Peeters, P. J., Cik, M., Nuydens, R., Brône, B., & Verheyen, A. (2016). Sustained synchronized neuronal network activity in a human astrocyte co-culture system OPEN. *Nature Publishing Group*. https://doi.org/10.1038/srep36529

La Manno, G., Siletti, K., Furlan, A., Gyllborg, D., Vinsland, E., Mossi Albiach, A., Mattsson Langseth, C., Khven, I., Lederer, A. R., Dratva, L. M., Johnsson, A., Nilsson, M., Lönnerberg, P., & Linnarsson, S. (2021). Molecular architecture of the developing mouse brain. *Nature*, *596*(7870), 92–96. https://doi.org/10.1038/S41586-021-03775-X

Lacar, B., Linker, S. B., Jaeger, B. N., Krishnaswami, S., Barron, J., Kelder, M., Parylak, S., Paquola, A., Venepally, P., Novotny, M., O'Connor, C., Fitzpatrick, C., Erwin, J., Hsu, J. Y., Husband, D., McConnell, M. J., Lasken, R., & Gage, F. H. (2016). Nuclear RNA-seq of single neurons reveals molecular signatures of activation. *Nature Communications 2016 7:1*, *7*(1), 1–13. https://doi.org/10.1038/ncomms11022

Lacomme, M., Liaubet, L., Pituello, F., & Bel-Vialar, S. (2012). NEUROG2 Drives Cell Cycle Exit of Neuronal Precursors by Specifically Repressing a Subset of Cyclins Acting at the G1 and S Phases of the Cell Cycle. *Molecular and Cellular Biology*, *32*(13), 2596. https://doi.org/10.1128/MCB.06745-11

Lahne, M., Nagashima, M., Hyde, D. R., & Hitchcock, P. F. (2020). Reprogramming Müller Glia to Regenerate Retinal Neurons. *Annual review of vision science*, *6*, 171–193. https://doi.org/10.1146/ANNUREV-VISION-121219-081808

Langille, J. J., & Brown, R. E. (2018). The Synaptic Theory of Memory: A Historical Survey and Reconciliation of Recent Opposition. *Frontiers in Systems Neuroscience*, *12*, 52. https://doi.org/10.3389/FNSYS.2018.00052

Latchman, D. S. (1997). Transcription factors: An overview. *International Journal of Biochemistry and Cell Biology*, *29*(12), 1305–1312. https://doi.org/10.1016/S1357-2725(97)00085-X

Lee, A. G., Capanzana, R., Brockhurst, J., Cheng, M. Y., Buckmaster, C. L., Absher, D., Schatzberg, A. F., & Lyons, D. M. (2016). Learning to cope with stress modulates anterior cingulate cortex stargazin expression in monkeys and mice. *Neurobiology of learning and memory*, *131*, 95–100. https://doi.org/10.1016/J.NLM.2016.03.015

Lee, H. K., & Kirkwood, A. (2019). Mechanisms of Homeostatic Synaptic Plasticity in vivo. *Frontiers in Cellular Neuroscience*, *13*, 520. https://doi.org/10.3389/FNCEL.2019.00520/BIBTEX

Lee, K. Y., Royston, S. E., Vest, M. O., Ley, D. J., Lee, S., Bolton, E. C., & Chung, H. J. (2015). N-methyl-D-aspartate receptors mediate activity-dependent down-regulation of potassium channel genes during the expression of homeostatic intrinsic plasticity. *Molecular Brain*, *8*(1), 1–16. https://doi.org/10.1186/s13041-015-0094-1

LeMasson, G., Marder, E., & Abbott, L. F. (1993). Activity-dependent regulation of conductances in model neurons. *Science (New York, N.Y.)*, *259*(5103), 1915–1917. https://doi.org/10.1126/SCIENCE.8456317

Lentini, C., D'Orange, M., Marichal, N., Trottmann, M.-M., Vignoles, R., Foucault, L., Verrier, C., Massera, C., Raineteau, O., Conzelmann, K.-K., Rival-Gervier, S., Depaulis, A., Berninger, B., & Heinrich, C. (2021). Reprogramming reactive glia into interneurons reduces chronic seizure activity in a mouse model of mesial temporal lobe epilepsy. *Cell Stem Cell*. https://doi.org/10.1016/J.STEM.2021.09.002

Leslie, J. H., & Nedivi, E. (2011). Activity-regulated genes as mediators of neural circuit plasticity. *Progress in neurobiology*, *94*(3), 223–237. https://doi.org/10.1016/J.PNEUROBIO.2011.05.002

Leung, H.-W., Wei, G., Foo, Q., & Vandongen, A. M. J. (2019). Arc Regulates Transcription of Genes for Plasticity, Excitability and Alzheimer's Disease. *bioRxiv*, 833988. https://doi.org/10.1101/833988

Li, S., Mattar, P., Zinyk, D., Singh, K., Chaturvedi, C. P., Kovach, C., Dixit, R., Kurrasch, D. M., Ma, Y. C., Chan, J. A., Wallace, V., Dilworth, F. J., Brand, M., & Schuurmans, C. (2012). GSK3 Temporally Regulates Neurogenin 2 Proneural Activity in the

Neocortex. *Journal of Neuroscience*, *32*(23), 7791–7805. https://doi.org/10.1523/JNEUROSCI.1309-12.2012

Li, X., Liu, G., Yang, L., Li, Z., Zhang, Z., Xu, Z., Cai, Y., Du, H., Su, Z., Wang, Z., Duan, Y., Chen, H., Shang, Z., You, Y., Zhang, Q., He, M., Chen, B., & Yang, Z. (2021). Decoding Cortical Glial Cell Development. *Neuroscience Bulletin*, *37*(4), 440–460. https://doi.org/10.1007/S12264-021-00640-9/FIGURES/9

Li, Y., Fan, T., Li, X., Liu, L., Mao, F., Li, Y., Miao, Z., Zeng, C., Song, W., Pan, J., Zhou, S., Wang, H., Wang, Y., & Sun, Z. S. (2022). Npas3 deficiency impairs cortical astrogenesis and induces autistic-like behaviors. *Cell reports*, *40*(9). https://doi.org/10.1016/J.CELREP.2022.111289

Libé-Philippot, B., & Vanderhaeghen, P. (2021). Cellular and Molecular Mechanisms Linking Human Cortical Development and Evolution. *Annual Review of Genetics*, *55*, 555–581. https://doi.org/10.1146/annurev-genet-071719

Lin, H. C., He, Z., Ebert, S., Schörnig, M., Santel, M., Nikolova, M. T., Weigert, A., Hevers, W., Kasri, N. N., Taverna, E., Camp, J. G., & Treutlein, B. (2021a). NGN2 induces diverse neuron types from human pluripotency. *Stem Cell Reports*, *16*(9), 2118–2127. https://doi.org/10.1016/J.STEMCR.2021.07.006

Lin, H. C., He, Z., Ebert, S., Schörnig, M., Santel, M., Nikolova, M. T., Weigert, A., Hevers, W., Kasri, N. N., Taverna, E., Camp, J. G., & Treutlein, B. (2021b). NGN2 induces diverse neuron types from human pluripotency. *Stem Cell Reports*, *16*(9), 2118–2127. https://doi.org/10.1016/J.STEMCR.2021.07.006

Lisman, J., Yasuda, R., & Raghavachari, S. (2012). Mechanisms of CaMKII action in long-term potentiation. *Nature reviews. Neuroscience*, *13*(3), 169. https://doi.org/10.1038/NRN3192

Little, S. C., & Mullins, M. C. (2006). Extracellular modulation of BMP activity in patterning the dorsoventral axis. *Birth Defects Research Part C: Embryo Today: Reviews*, *78*(3), 224–242. https://doi.org/10.1002/BDRC.20079

Liu, J., Yang, M., Su, M., Liu, B., Zhou, K., Sun, C., Ba, R., Yu, B., Zhang, B., Zhang, Z., Fan, W., Wang, K., Zhong, M., Han, J., & Zhao, C. (2022). FOXG1 sequentially orchestrates subtype specification of postmitotic cortical projection neurons. *Science advances*, *8*(21). https://doi.org/10.1126/SCIADV.ABH3568

Liu, Y., Beyer, A., & Aebersold, R. (2016). On the Dependency of Cellular Protein Levels on mRNA Abundance. *Cell*, *165*(3), 535–550. https://doi.org/10.1016/J.CELL.2016.03.014

Llorca, A., & Deogracias, R. (2022). Origin, Development, and Synaptogenesis of Cortical Interneurons. *Frontiers in neuroscience*, *16*. https://doi.org/10.3389/FNINS.2022.929469

Lo, L., Dormand, E., Greenwood, A., & Anderson, D. J. (2002). Comparison of the generic neuronal differentiation and neuron subtype specification functions of mammalian achaete-scute and atonal homologs in cultured neural progenitor cells. *Development (Cambridge, England)*, *129*(7), 1553–1567. https://doi.org/10.1242/DEV.129.7.1553

Lohmann, C., & Kessels, H. W. (2014). The developmental stages of synaptic plasticity. *The Journal of physiology*, *592*(1), 13–31. https://doi.org/10.1113/JPHYSIOL.2012.235119

Louros, S. R., Hooks, B. M., Litvina, L., Carvalho, A. L., & Chen, C. (2014). A Role for Stargazin in Experience-Dependent Plasticity. *Cell reports*, *7*(5), 1614. https://doi.org/10.1016/J.CELREP.2014.04.054

Love, M. I., Huber, W., & Anders, S. (2014). Moderated estimation of fold change and dispersion for RNA-seq data with DESeq2. *Genome Biology*, *15*(12), 1–21. https://doi.org/10.1186/S13059-014-0550-8/FIGURES/9

Lubin, F. D., Roth, T. L., & Sweatt, J. D. (2008). Epigenetic regulation of BDNF gene transcription in the consolidation of fear memory. *The Journal of neuroscience : the official journal of the Society for Neuroscience*, *28*(42), 10576–10586. https://doi.org/10.1523/JNEUROSCI.1786-08.2008

Luchkina, N. V., Huupponen, J., Clarke, V. R., Coleman, S. K., Keinänen, K., Taira, T., & Lauri, S. E. (2014). Developmental switch in the kinase dependency of long-term potentiation depends on expression of GluA4 subunit-containing AMPA receptors. *Proceedings of the National Academy of Sciences of the United States of America*, *111*(11), 4321–4326. https://doi.org/10.1073/PNAS.1315769111/SUPPL_FILE/PNAS.201315769SI.PDF

Luecken, M. D., & Theis, F. J. (2019). Current best practices in single-cell RNA-seq analysis: a tutorial. *Molecular Systems Biology*, *15*(6). https://doi.org/10.15252/MSB.20188746

Luginbuhl, J., Kouno, T., Nakano, R., Chater, T. E., Sivaraman, D. M., Kishima, M., Roudnicky, F., Carninci, P., Plessy, C., & Shin, J. W. (2021). Decoding Neuronal Diversification by Multiplexed Single-cell RNA-Seq. *Stem cell reports*, *16*(4), 810–824. https://doi.org/10.1016/J.STEMCR.2021.02.006

Luo, C., Keown, C. L., Kurihara, L., Zhou, J., He, Y., Li, J., Castanon, R., Lucero, J., Nery, J. R., Sandoval, J. P., Bui, B., Sejnowski, T. J., Harkins, T. T., Mukamel, E. A., Behrens, M. M., & Ecker, J. R. (2017). Single-cell methylomes identify neuronal subtypes and regulatory elements in mammalian cortex. *Science (New York, N.Y.)*, *357*(6351), 600–604. https://doi.org/10.1126/SCIENCE.AAN3351

Lüscher, C., & Malenka, R. C. (2012). NMDA Receptor-Dependent Long-Term Potentiation and Long-Term Depression (LTP/LTD). *Cold Spring Harbor Perspectives in Biology*, *4*(6), 1–15. https://doi.org/10.1101/CSHPERSPECT.A005710

Lyford, G. L., Yamagata, K., Kaufmann, W. E., Barnes, C. A., Sanders, L. K., Copeland, N. G., Gilbert, D. J., Jenkins, N. A., Lanahan, A. A., & Worley, P. F. (1995). Arc, a growth factor and activity-regulated gene, encodes a novel cytoskeleton-associated protein that is enriched in neuronal dendrites. *Neuron*, *14*(2), 433–445. https://doi.org/10.1016/0896-6273(95)90299-6

Lyst, M. J., Ekiert, R., Ebert, D. H., Merusi, C., Nowak, J., Selfridge, J., Guy, J., Kastan, N. R., Robinson, N. D., De Lima Alves, F., Rappsilber, J., Greenberg, M. E., & Bird, A. (2013). Rett syndrome mutations abolish the interaction of MeCP2 with the NCoR/SMRT co-repressor. *Nature neuroscience*, *16*(7), 898–902. https://doi.org/10.1038/NN.3434

Ma, Y. C., Song, M. R., Park, J. P., Henry Ho, H. Y., Hu, L., Kurtev, M. V., Zieg, J., Ma, Q., Pfaff, S. L., & Greenberg, M. E. (2008). Regulation of Motor Neuron Specification by GSK3-Mediated Phosphorylation of Neurogenin 2. *Neuron*, *58*(1), 65. https://doi.org/10.1016/J.NEURON.2008.01.037

Madabhushi, R., & Kim, T.-K. (2018). Emerging themes in neuronal activity-dependent gene expression HHS Public Access. *Mol Cell Neurosci*, *87*, 27–34. https://doi.org/10.1016/j.mcn.2017.11.009

Maffei, A., & Turrigiano, G. G. (2008). Multiple Modes of Network Homeostasis in Visual Cortical Layer 2/3. *The Journal of Neuroscience*, *28*(17), 4377. https://doi.org/10.1523/JNEUROSCI.5298-07.2008

Malatesta, P., Hartfuss, E., & Götz, M. (2000). Isolation of radial glial cells by fluorescent-activated cell sorting reveals a neuronal lineage. *Development (Cambridge, England)*, *127*(24), 5253–5263. https://doi.org/10.1242/DEV.127.24.5253

Malatesta, P., Appolloni, I., & Calzolari, F. (2008). Radial glia and neural stem cells. *Cell and Tissue Research*, *331*(1), 165–178. https://doi.org/10.1007/S00441-007-0481-8/FIGURES/5

Malatesta, P., Hack, M. A., Hartfuss, E., Kettenmann, H., Klinkert, W., Kirchhoff, F., & Götz, M. (2003). Neuronal or glial progeny: regional differences in radial glia fate. *Neuron*, *37*(5), 751–764. https://doi.org/10.1016/S0896-6273(03)00116-8

Malik, A. N., Vierbuchen, T., Hemberg, M., Rubin, A. A., Ling, E., Couch, C. H., Stroud, H., Spiegel, I., Farh, K. K. H., Harmin, D. A., & Greenberg, M. E. (2014). Genome-wide identification and characterization of functional neuronal activity-dependent enhancers. *Nature Neuroscience*, *17*(10), 1330–1339. https://doi.org/10.1038/NN.3808

Mall, M., Kareta, M. S., Chanda, S., Ahlenius, H., Perotti, N., Zhou, B., Grieder, S. D., Ge, X., Drake, S., Euong Ang, C., Walker, B. M., Vierbuchen, T., Fuentes, D. R., Brennecke, P., Nitta, K. R., Jolma, A., Steinmetz, L. M., Taipale, J., Südhof, T. C., & Wernig, M. (2017). Myt1l safeguards neuronal identity by actively repressing many non-neuronal fates. *Nature 2016 544:7649*, *544*(7649), 245–249. https://doi.org/10.1038/nature21722

Mann, R., Mulligan, R. C., & Baltimore, D. (1983). Construction of a retrovirus packaging mutant and its use to produce helper-free defective retrovirus. *Cell*, *33*(1), 153–159. https://doi.org/10.1016/0092-8674(83)90344-6

Manuel, M., Tan, K. B., Kozic, Z., Molinek, M., Marcos, T. S., Razak, M. F. A., Dobolyi, D., Dobie, R., Henderson, B. E., Henderson, N. C., Chan, W. K., Daw, M. I., Mason, J. O., & Price, D. J. (2022). Pax6 limits the competence of developing cerebral cortical cells to respond to inductive intercellular signals. *PLOS Biology*, *20*(9), e3001563. https://doi.org/10.1371/JOURNAL.PBIO.3001563

Mao, W., Salzberg, A. C., Uchigashima, M., Hasegawa, Y., Hock, H., Watanabe, M., Akbarian, S., Kawasawa, Y. I., & Futai, K. (2018). Activity-Induced Regulation of Synaptic Strength through the Chromatin Reader L3mbtl1. *Cell reports*, *23*(11), 3209–3222. https://doi.org/10.1016/J.CELREP.2018.05.028

Mardinly, A. R., Spiegel, I., Patrizi, A., Centofante, E., Bazinet, J. E., Tzeng, C. P., Mandel-Brehm, C., Harmin, D. A., Adesnik, H., Fagiolini, M., & Greenberg, M. E. (2016). Sensory experience regulates cortical inhibition by inducing IGF-1 in VIP neurons. *Nature*, *531*(7594), 371. https://doi.org/10.1038/NATURE17187

Martynoga, B., Drechsel, D., & Guillemot, F. (2012). Molecular Control of Neurogenesis: A View from the Mammalian Cerebral Cortex. *Cold Spring Harbor Perspectives in Biology*, *4*(10). https://doi.org/10.1101/CSHPERSPECT.A008359

Masserdotti, G., Gillotin, S., Sutor, B., Drechsel, D., Irmler, M., Jørgensen, H. F., Sass, S., Theis, F. J., Beckers, J., Berninger, B., Guillemot, F., & Götz, M. (2015). Transcriptional Mechanisms of Proneural Factors and REST in Regulating Neuronal Reprogramming of Astrocytes. *Cell Stem Cell*, *17*(1), 74–88. https://doi.org/10.1016/j.stem.2015.05.014

Matsuzaki, M., Honkura, N., Ellis-Davies, G. C., & Kasai, H. (2004). Structural basis of long-term potentiation in single dendritic spines. *Nature 2004 429:6993*, *429*(6993), 761–766. https://doi.org/10.1038/nature02617

Mattugini, N., Bocchi, R., Scheuss, V., Russo, G. L., Torper, O., Lao, C. L., & Götz, M. (2019). Inducing Different Neuronal Subtypes from Astrocytes in the Injured Mouse Cerebral Cortex. *Neuron*, *103*(6), 1086–1095.e5. https://doi.org/10.1016/J.NEURON.2019.08.009

McInnes, L., Healy, J., & Melville, J. (2018). UMAP: Uniform Manifold Approximation and Projection for Dimension Reduction. https://doi.org/10.48550/arxiv.1802.03426

McKenna, W. L., Betancourt, J., Larkin, K. A., Abrams, B., Guo, C., Rubenstein, J. L., & Chen, B. (2011). Tbr1 and Fezf2 Regulate Alternate Corticofugal Neuronal Identities during Neocortical Development. *The Journal of Neuroscience*, *31*(2), 549. https://doi.org/10.1523/JNEUROSCI.4131-10.2011

McKenna, W. L., Ortiz-Londono, C. F., Mathew, T. K., Hoang, K., Katzman, S., & Chen, B. (2015). Mutual regulation between Satb2 and Fezf2 promotes subcerebral projection neuron identity in the developing cerebral cortex. *Proceedings of the National Academy of Sciences of the United States of America*, *112*(37), 11702–11707. https://doi.org/10.1073/PNAS.1504144112/-/DCSUPPLEMENTAL

McLaughlin, C. N., & Broihier, H. T. (2018). Keeping Neurons Young and Foxy: FoxOs Promote Neuronal Plasticity. *Trends in Genetics*, *34*(1), 65–78. https://doi.org/10.1016/j.tig.2017.10.002

McMahon, J. A., Takada, S., Zimmerman, L. B., Fan, C. M., Harland, R. M., & McMahon, A. P. (1998). Noggin-mediated antagonism of BMP signaling is required for growth and patterning of the neural tube and somite. *Genes & Development*, *12*(10), 1438. https://doi.org/10.1101/GAD.12.10.1438

Meenakshi, P., Kumar, S., & Balaji, J. (2021). In vivo imaging of immediate early gene expression dynamics segregates neuronal ensemble of memories of dual events. *Molecular brain*, *14*(1), 102. https://doi.org/10.1186/S13041-021-00798-3/FIGURES/6

Michelsen, K. A., Acosta-Verdugo, S., Benoit-Marand, M., Espuny-Camacho, I., Gaspard, N., Saha, B., Gaillard, A., & Vanderhaeghen, P. (2015). Area-specific reestablishment of damaged circuits in the adult cerebral cortex by cortical neurons derived from mouse embryonic stem cells. *Neuron*, *85*(5), 982–997. https://doi.org/10.1016/J.NEURON.2015.02.001

Minatohara, K., Akiyoshi, M., & Okuno, H. (2016). Role of immediate-early genes in synaptic plasticity and neuronal ensembles underlying the memory trace. *Frontiers in Molecular Neuroscience*, *8*(JAN2016), 1–11. https://doi.org/10.3389/fnmol.2015.00078

Mircea, M., & Semrau, S. (2021). How a cell decides its own fate: a single-cell view of molecular mechanisms and dynamics of cell-type specification. *Biochemical Society Transactions*, *49*(6), 2509. https://doi.org/10.1042/BST20210135

Mitsis, T., Efthimiadou, A., Bacopoulou, F., Vlachakis, D., Chrousos, G. P., & Eliopoulos, E. (2020). Transcription factors and evolution: An integral part of gene expression (Review). *World Academy of Sciences Journal*, *2*(1), 3–8. https://doi.org/10.3892/WASJ.2020.32/HTML

Molyneaux, B. J., Arlotta, P., Menezes, J. R., & Macklis, J. D. (2007). Neuronal subtype specification in the cerebral cortex. *Nature Reviews Neuroscience*, *8*(6), 427–437. https://doi.org/10.1038/nrn2151

Morrison, S. J. (2001). Neuronal differentiation: proneural genes inhibit gliogenesis. *Current biology : CB*, *11*(9). https://doi.org/10.1016/S0960-9822(01)00191-9

Mu, L., Berti, L., Masserdotti, G., Covic, M., Michaelidis, T. M., Doberauer, K., Merz, K., Rehfeld, F., Haslinger, A., Wegner, M., Sock, E., Lefebvre, V., Couillard-Despres, S., Aigner, L., Berninger, B., & Chichung Lie, D. (2012). SoxC transcription factors are required for neuronal differentiation in adult hippocampal neurogenesis. *The Journal of neuroscience : the official journal of the Society for Neuroscience*, *32*(9), 3067–3080. https://doi.org/10.1523/JNEUROSCI.4679-11.2012

Muhr, J., & Hagey, D. W. (2021). The cell cycle and differentiation as integrated processes: Cyclins and CDKs reciprocally regulate Sox and Notch to balance stem cell maintenance. *BioEssays*, *43*(7), 2000285. https://doi.org/10.1002/BIES.202000285

Murphy, T. H., Worley, P. F., & Baraban, J. M. (1991). L-type voltage-sensitive calcium channels mediate synaptic activation of immediate early genes. *Neuron*, *7*(4), 625–635. https://doi.org/10.1016/0896-6273(91)90375-A

Nägerl, U. V., Eberhorn, N., Cambridge, S. B., & Bonhoeffer, T. (2004). Bidirectional activity-dependent morphological plasticity in hippocampal neurons. *Neuron*, *44*(5), 759–767. https://doi.org/10.1016/j.neuron.2004.11.016

NARAHASHI, T., MOORE, J. W., & SCOTT, W. R. (1964). Tetrodotoxin Blockage of Sodium Conductance Increase in Lobster Giant Axons. *The Journal of General Physiology*, *47*(5), 965. https://doi.org/10.1085/JGP.47.5.965

Nehme, R., Zuccaro, E., Ghosh, S. D., Li, C., Sherwood, J. L., Pietilainen, O., Barrett, L. E., Limone, F., Worringer, K. A., Kommineni, S., Zang, Y., Cacchiarelli, D., Meissner, A., Adolfsson, R., Haggarty, S., Madison, J., Muller, M., Arlotta, P., Fu, Z., … Eggan, K. (2018). Combining NGN2 Programming with Developmental Patterning Generates Human Excitatory Neurons with NMDAR-Mediated Synaptic Transmission. *Cell Reports*, *23*(8), 2509–2523. https://doi.org/10.1016/J.CELREP.2018.04.066/ATTACHMENT/9A4B4328-D3F7-4A51-96A9-41EE59DBAE23/MMC2.XLSX

Nelson, E. D., Maynard, K. R., Nicholas, K. R., Tran, M. N., Divecha, H. R., Collado-Torres, L., Hicks, S. C., & Martinowich, K. (2022). Activity-regulated gene expression across cell types of the mouse hippocampus. *bioRxiv*, 2022.11.23.517593. https://doi.org/10.1101/2022.11.23.517593

Nieto, M., Monuki, E. S., Tang, H., Imitola, J., Haubst, N., Khoury, S. J., Cunningham, J., Gotz, M., & Walsh, C. A. (2004). Expression of Cux-1 and Cux-2 in the subventric-

ular zone and upper layers II-IV of the cerebral cortex. *The Journal of comparative neurology*, *479*(2), 168–180. https://doi.org/10.1002/CNE.20322

Nieto, M., Schuurmans, C., Britz, O., & Guillemot, F. (2001). Neural bHLH genes control the neuronal versus glial fate decision in cortical progenitors. *Neuron*, *29*(2), 401–413. https://doi.org/10.1016/S0896-6273(01)00214-8

Ninomiya, K., Ohno, M., & Kataoka, N. (2016). Dendritic transport element of human arc mRNA confers RNA degradation activity in a translation-dependent manner. *Genes to Cells*, *21*(11), 1263–1269. https://doi.org/10.1111/GTC.12439

Niu, W., Zang, T., Smith, D. K., Vue, T. Y., Zou, Y., Bachoo, R., Johnson, J. E., & Zhang, C. L. (2015). SOX2 reprograms resident astrocytes into neural progenitors in the adult brain. *Stem Cell Reports*, *4*(5), 780–794. https://doi.org/10.1016/j.stemcr.2015.03.006

Noack, F., Vangelisti, S., Raffl, G., Carido, M., Diwakar, J., Chong, F., & Bonev, B. (2022). Multimodal profiling of the transcriptional regulatory landscape of the developing mouse cortex identifies Neurog2 as a key epigenome remodeler. *Nature Neuroscience*, *25*(2), 154–167. https://doi.org/10.1038/s41593-021-01002-4

Oberst, P., Fièvre, S., Baumann, N., Concetti, C., Bartolini, G., & Jabaudon, D. (2019). Temporal plasticity of apical progenitors in the developing mouse neocortex. *Nature*. https://doi.org/10.1038/s41586-019-1515-6

O'Brien, R. J., Kamboj, S., Ehlers, M. D., Rosen, K. R., Fischbach, G. D., & Huganir, R. L. (1998). Activity-dependent modulation of synaptic AMPA receptor accumulation. *Neuron*, *21*(5), 1067–1078. https://doi.org/10.1016/S0896-6273(00)80624-8

Ory, D. S., Neugeborent, B. A., & Mulligantt, R. C. (1996). A stable human-derived packaging cell line for production of high titer retrovirus/vesicular stomatitis virus G pseudotypes. *Proceedings of the National Academy of Sciences*, *93*(21), 11400–11406. https://doi.org/10.1073/PNAS.93.21.11400

Overman, J. J., Clarkson, A. N., Wanner, I. B., Overman, W. T., Eckstein, I., Maguire, J. L., Dinov, I. D., Toga, A. W., & Carmichael, S. T. (2012). A role for ephrin-A5 in axonal sprouting, recovery, and activity-dependent plasticity after stroke. *Proceedings of the National Academy of Sciences of the United States of America*, *109*(33). https://doi.org/10.1073/PNAS.1204386109

Parylak, S. L., Qiu, F., Linker, S. B., Gallina, I. S., Lim, C. K., Preciado, D., McDonald, A. H., Zhou, X., & Gage, F. H. (2023). Neuronal activity-related transcription is blunted in immature compared to mature dentate granule cells. *Hippocampus*. https://doi.org/10.1002/HIPO.23515

Pastuzyn, E. D., & Shepherd, J. D. (2017). Activity-Dependent Arc Expression and Homeostatic Synaptic Plasticity Are Altered in Neurons from a Mouse Model of

Angelman Syndrome. *Frontiers in Molecular Neuroscience*, *10*. https://doi.org/10.3389/FNMOL.2017.00234

Payne, H. L. (2008). Molecular Membrane Biology The role of transmembrane AMPA receptor regulatory proteins (TARPs) in neurotransmission and receptor trafficking (Review) The role of transmembrane AMPA receptor regulatory proteins (TARPs) in neurotransmission and receptor tra. https://doi.org/10.1080/09687680801986480

Penrod, R. D., Kumar, J., Smith, L. N., McCalley, D., Nentwig, T. B., Hughes, B. W., Barry, G. M., Glover, K., Taniguchi, M., & Cowan, C. W. (2019). Activity-regulated cytoskeleton-associated protein (Arc/Arg3.1) regulates anxiety- and novelty-related behaviors. *Genes, brain, and behavior*, *18*(7). https://doi.org/10.1111/GBB.12561

Pozo, K., & Goda, Y. (2010). Unraveling mechanisms of homeostatic synaptic plasticity. *Neuron*, *66*(3), 337. https://doi.org/10.1016/J.NEURON.2010.04.028

Purves, D., Augustine, G., & Fitzpatrick, D. (2001). The Initial Formation of the Nervous System: Gastrulation and Neurulation - Neuroscience - NCBI Bookshelf. Retrieved June 4, 2022, from https://www.ncbi.nlm.nih.gov/books/NBK10993/

Radnikow, G., & Feldmeyer, D. (2018). Layer- and cell type-specific modulation of excitatory neuronal activity in the neocortex. *Frontiers in Neuroanatomy*, *12*, 1. https://doi.org/10.3389/FNANA.2018.00001/BIBTEX

Rahmani, E., Schweiger, R., Rhead, B., Criswell, L. A., Barcellos, L. F., Eskin, E., Rosset, S., Sankararaman, S., & Halperin, E. (2019). Cell-type-specific resolution epigenetics without the need for cell sorting or single-cell biology. *Nature Communications 2019 10:1*, *10*(1), 1–11. https://doi.org/10.1038/s41467-019-11052-9

Rakic, P. (2000). Radial Unit Hypothesis of Neocortical Expansion. *Novartis Foundation Symposium*, *228*, 30–45. https://doi.org/10.1002/0470846631.CH3

Rambousek, L., Gschwind, T., Lafourcade, C., Paterna, J. C., Dib, L., Fritschy, J. M., & Fontana, A. (2020). Aberrant expression of PAR bZIP transcription factors is associated with epileptogenesis, focus on hepatic leukemia factor. *Scientific Reports 2020 10:1*, *10*(1), 1–16. https://doi.org/10.1038/s41598-020-60638-7

Rannals, M. D., & Kapur, J. (2011). Homeostatic Strengthening of Inhibitory Synapses Is Mediated by the Accumulation of GABAA Receptors. *The Journal of Neuroscience*, *31*(48), 17701. https://doi.org/10.1523/JNEUROSCI.4476-11.2011

Ravanpay, A. C., Hansen, S. J., & Olson, J. M. (2010). Transcriptional inhibition of REST by NeuroD2 during neuronal differentiation. *Molecular and cellular neurosciences*, *44*(2), 178–189. https://doi.org/10.1016/J.MCN.2010.03.006

Revah, O., Gore, F., Kelley, K. W., Andersen, J., Sakai, N., Chen, X., Li, M. Y., Birey, F., Yang, X., Saw, N. L., Baker, S. W., Amin, N. D., Kulkarni, S., Mudipalli, R., Cui,

B., Nishino, S., Grant, G. A., Knowles, J. K., Shamloo, M., … Pașca, S. P. (2022). Maturation and circuit integration of transplanted human cortical organoids. *Nature 2022 610:7931*, *610*(7931), 319–326. https://doi.org/10.1038/s41586-022-05277-w

Risso, D., Perraudeau, F., Gribkova, S., Dudoit, S., & Vert, J. P. (2018). A general and flexible method for signal extraction from single-cell RNA-seq data. *Nature Communications 2018 9:1*, *9*(1), 1–17. https://doi.org/10.1038/s41467-017-02554-5

Robinson, M. D., McCarthy, D. J., & Smyth, G. K. (2010). edgeR: a Bioconductor package for differential expression analysis of digital gene expression data. *Bioinformatics*, *26*(1), 139–140. https://doi.org/10.1093/BIOINFORMATICS/BTP616

Rodriguez, G., Mesik, L., Gao, M., Parkins, S., Saha, R., & Lee, H. K. (2019). Disruption of NMDAR Function Prevents Normal Experience-Dependent Homeostatic Synaptic Plasticity in Mouse Primary Visual Cortex. *The Journal of neuroscience : the official journal of the Society for Neuroscience*, *39*(39), 7664–7673. https://doi.org/10.1523/JNEUROSCI.2117-18.2019

Roussos, P., Guennewig, B., Kaczorowski, D. C., Barry, G., & Brennand, K. J. (2016). Activity-Dependent Changes in Gene Expression in Schizophrenia Human-Induced Pluripotent Stem Cell Neurons. *JAMA psychiatry*, *73*(11), 1180–1188. https://doi.org/10.1001/JAMAPSYCHIATRY.2016.2575

Runge, K., Mathieu, R., Bugeon, S., Lafi, S., Beurrier, C., Sahu, S., Schaller, F., Loubat, A., Herault, L., Gaillard, S., Pallesi-Pocachard, E., Montheil, A., Bosio, A., Rosenfeld, J. A., Hudson, E., Lindstrom, K., Mercimek-Andrews, S., Jeffries, L., van Haeringen, A., … de Chevigny, A. (2021). Disruption of NEUROD2 causes a neurodevelopmental syndrome with autistic features via cell-autonomous defects in forebrain glutamatergic neurons. *Molecular Psychiatry 2021 26:11*, *26*(11), 6125–6148. https://doi.org/10.1038/s41380-021-01179-x

Sahara, S., Yanagawa, Y., O'Leary, D. D., & Stevens, C. F. (2012). The Fraction of Cortical GABAergic Neurons Is Constant from Near the Start of Cortical Neurogenesis to Adulthood. *The Journal of Neuroscience*, *32*(14), 4755. https://doi.org/10.1523/JNEUROSCI.6412-11.2012

Sainsbury, S., Bernecky, C., & Cramer, P. (2015). Structural basis of transcription initiation by RNA polymerase II. *Nature reviews. Molecular cell biology*, *16*(3), 129–143. https://doi.org/10.1038/NRM3952

Sánchez-González, R., Bribián, A., & López-Mascaraque, L. (2020). Cell Fate Potential of NG2 Progenitors. *Scientific Reports 2020 10:1*, *10*(1), 1–12. https://doi.org/10.1038/s41598-020-66753-9

Sanders, S. J., & Mason, C. E. (2016). The Newly Emerging View of the Genome. *Genomics, Circuits, and Pathways in Clinical Neuropsychiatry*, 3–26. https://doi.org/10.1016/B978-0-12-800105-9.00001-9

Sanderson, J. L., Scott, J. D., & Dell'Acqua, M. L. (2018). Control of Homeostatic Synaptic Plasticity by AKAP-Anchored Kinase and Phosphatase Regulation of Ca 2+-Permeable AMPA Receptors. *The Journal of neuroscience : the official journal of the Society for Neuroscience*, *38*(11), 2863–2876. https://doi.org/10.1523/JNEUROSCI.2362-17.2018

Sando, R., Gounko, N., Pieraut, S., Liao, L., Yates, J., & Maximov, A. (2012). HDAC4 governs a transcriptional program essential for synaptic plasticity and memory. *Cell*, *151*(4), 821–834. https://doi.org/10.1016/J.CELL.2012.09.037

Sardi, S. P., Murtie, J., Koirala, S., Patten, B. A., & Corfas, G. (2006). Presenilin-dependent ErbB4 nuclear signaling regulates the timing of astrogenesis in the developing brain. *Cell*, *127*(1), 185–197. https://doi.org/10.1016/J.CELL.2006.07.037

Sareen, D., & Svendsen, C. N. (2010). Stem cell biologists sure play a mean pinball. *Nature Biotechnology 2010 28:4*, *28*(4), 333–335. https://doi.org/10.1038/nbt0410-333

Scala, F., Kobak, D., Bernabucci, M., Bernaerts, Y., Cadwell, C. R., Castro, J. R., Hartmanis, L., Jiang, X., Laturnus, S., Miranda, E., Mulherkar, S., Tan, Z. H., Yao, Z., Zeng, H., Sandberg, R., Berens, P., & Tolias, A. S. (2021). Phenotypic variation of transcriptomic cell types in mouse motor cortex. *Nature*, *598*(7879), 144–150. https://doi.org/10.1038/S41586-020-2907-3

Scala, F., Kobak, D., Shan, S., Bernaerts, Y., Laturnus, S., Cadwell, C. R., Hartmanis, L., Froudarakis, E., Castro, J. R., Tan, Z. H., Papadopoulos, S., Patel, S. S., Sandberg, R., Berens, P., Jiang, X., & Tolias, A. S. (2019). Layer 4 of mouse neocortex differs in cell types and circuit organization between sensory areas. *Nature Communications 2019 10:1*, *10*(1), 1–12. https://doi.org/10.1038/s41467-019-12058-z

Scandaglia, M., Lopez-Atalaya, J. P., Medrano-Fernandez, A., Lopez-Cascales, M. T., del Blanco, B., Lipinski, M., Benito, E., Olivares, R., Iwase, S., Shi, Y., & Barco, A. (2017). Loss of Kdm5c Causes Spurious Transcription and Prevents the Fine-Tuning of Activity-Regulated Enhancers in Neurons. *Cell Reports*, *21*(1), 47–59. https://doi.org/10.1016/J.CELREP.2017.09.014

Schaukowitch, K., Reese, A. L., Kim, S. K., Kilaru, G., Joo, J. Y., Kavalali, E. T., & Kim, T. K. (2017). An Intrinsic Transcriptional Program Underlying Synaptic Scaling during Activity Suppression. *Cell reports*, *18*(6), 1512–1526. https://doi.org/10.1016/J.CELREP.2017.01.033

Schmid, R. S., McGrath, B., Berechid, B. E., Boyles, B., Marchionni, M., Šestan, N., & Anton, E. S. (2003). Neuregulin 1–erbB2 signaling is required for the establishment of radial glia and their transformation into astrocytes in cerebral cortex. *Proceedings*

of the National Academy of Sciences of the United States of America, *100*(7), 4251. https://doi.org/10.1073/PNAS.0630496100

Schuman, E. M., Dynes, J. L., & Steward, O. (2006). Synaptic Regulation of Translation of Dendritic mRNAs. *The Journal of Neuroscience*, *26*(27), 7143. https://doi.org/10.1523/JNEUROSCI.1796-06.2006

Schuurmans, C., Armant, O., Nieto, M., Stenman, J. M., Britz, O., Klenin, N., Brown, C., Langevin, L. M., Seibt, J., Tang, H., Cunningham, J. M., Dyck, R., Walsh, C., Campbell, K., Polleux, F., & Guillemot, F. (2004). Sequential phases of cortical specification involve Neurogenin-dependent and -independent pathways. *The EMBO Journal*, *23*(14), 2892–2902. https://doi.org/10.1038/SJ.EMBOJ.7600278

Seredenina, T., & Luthi-Carter, R. (2012). What have we learned from gene expression profiles in Huntington's disease? *Neurobiology of disease*, *45*(1), 83–98. https://doi.org/10.1016/J.NBD.2011.07.001

Sharif, N., Calzolari, F., & Berninger, B. (2021). Direct In Vitro Reprogramming of Astrocytes into Induced Neurons. *Methods in Molecular Biology*, *2352*, 13–29. https://doi.org/10.1007/978-1-0716-1601-7_2

Sharma, N., Pollina, E. A., Nagy, M. A., Yap, E. L., DiBiase, F. A., Hrvatin, S., Hu, L., Lin, C., & Greenberg, M. E. (2019). ARNT2 Tunes Activity-Dependent Gene Expression through NCoR2-Mediated Repression and NPAS4-Mediated Activation. *Neuron*, *102*(2), 390–406.e9. https://doi.org/10.1016/J.NEURON.2019.02.007

Shepherd, J. D., & Bear, M. F. (2011). New views of Arc, a master regulator of synaptic plasticity. *Nature neuroscience*, *14*(3), 279–284. https://doi.org/10.1038/NN.2708

Shimojo, H., Ohtsuka, T., & Kageyama, R. (2008). Oscillations in Notch Signaling Regulate Maintenance of Neural Progenitors. *Neuron*, *58*(1), 52–64. https://doi.org/10.1016/J.NEURON.2008.02.014

Shimshek, D. R., Bus, T., Schupp, B., Jensen, V., Marx, V., Layer, L. E., & Köhr, G. (2017). Different Forms of AMPA Receptor Mediated LTP and Their Correlation to the Spatial Working Memory Formation. *Frontiers in Molecular Neuroscience — www.frontiersin.org*, *1*, 214. https://doi.org/10.3389/fnmol.2017.00214

Sim, S., Antolin, S., Lin, C. W., Lin, Y. X., & Lois, C. (2013). Increased cell-intrinsic excitability induces synaptic changes in new neurons in the adult dentate gyrus that require Npas4. *The Journal of neuroscience : the official journal of the Society for Neuroscience*, *33*(18), 7928–7940. https://doi.org/10.1523/JNEUROSCI.1571-12.2013

Smith, D. K., Yang, J., Liu, M. L., & Zhang, C. L. (2016). Small Molecules Modulate Chromatin Accessibility to Promote NEUROG2-Mediated Fibroblast-to-Neuron Reprogramming. *Stem Cell Reports*, *7*(5), 955. https://doi.org/10.1016/J.STEMCR.2016.09.013

Soneson, C., & Robinson, M. D. (2018). Bias, robustness and scalability in single-cell differential expression analysis. *Nature methods*, *15*(4), 255–261. https://doi.org/10.1038/NMETH.4612

Spiegel, I., Mardinly, A. R., Gabel, H. W., Bazinet, J. E., Couch, C. H., Tzeng, C. P., Harmin, D. A., & Greenberg, M. E. (2014). Npas4 regulates excitatory-inhibitory balance within neural circuits through cell-type-specific gene programs. *Cell*, *157*(5), 1216–1229. https://doi.org/10.1016/j.cell.2014.03.058

Spitz, F., & Furlong, E. E. (2012). Transcription factors: from enhancer binding to developmental control. *Nature Reviews Genetics 2012 13:9*, *13*(9), 613–626. https://doi.org/10.1038/nrg3207

Spitzer, N. C. (2012). Activity-dependent neurotransmitter respecification. https://doi.org/10.1038/nrn3154

Steward, O., Farris, S., Pirbhoy, P. S., Darnell, J., & Van Driesche, S. J. (2015). Localization and local translation of Arc/Arg3.1 mRNA at synapses: Some observations and paradoxes. *Frontiers in Molecular Neuroscience*, *7*(JAN), 1–15. https://doi.org/10.3389/FNMOL.2014.00101/BIBTEX

Stuart, T., Butler, A., Hoffman, P., Hafemeister, C., Papalexi, E., Mauck, W. M., Hao, Y., Stoeckius, M., Smibert, P., & Satija, R. (2019). Comprehensive Integration of Single-Cell Data. *Cell*, *177*(7), 1888–1902.e21. https://doi.org/10.1016/J.CELL.2019.05.031/ATTACHMENT/2F8B9EBE-54E6-43EB-9EF2-949B6BDA8BA2/MMC3.PDF

Sun, A. X., Yuan, Q., Tan, S., Xiao, Y., Wang, D., Khoo, A. T. T., Sani, L., Tran, H. D., Kim, P., Chiew, Y. S., Lee, K. J., Yen, Y. C., Ng, H. H., Lim, B., & Je, H. S. (2016). Direct Induction and Functional Maturation of Forebrain GABAergic Neurons from Human Pluripotent Stem Cells. *Cell Reports*, *16*(7), 1942–1953. https://doi.org/10.1016/j.celrep.2016.07.035

Suter, D. M., Tirefort, D., Julien, S., & Krause, K.-H. (2009). A Sox1 to Pax6 switch drives neuroectoderm to radial glia progression during differentiation of mouse embryonic stem cells. *Stem cells (Dayton, Ohio)*, *27*(1), 49–58. https://doi.org/10.1634/STEMCELLS.2008-0319

Tai, W., Wu, W., Wang, L. L., Ni, H., Chen, C., Yang, J., Zang, T., Zou, Y., Xu, X. M., & Zhang, C. L. (2021). In vivo reprogramming of NG2 glia enables adult neurogenesis and functional recovery following spinal cord injury. *Cell Stem Cell*, *28*(5), 923–937.e4. https://doi.org/10.1016/J.STEM.2021.02.009

Takahashi, K., & Yamanaka, S. (2006). Induction of pluripotent stem cells from mouse embryonic and adult fibroblast cultures by defined factors. *Cell*, *126*(4), 663–676. https://doi.org/10.1016/J.CELL.2006.07.024

Takouda, J., Katada, S., & Nakashima, K. (2017). Emerging mechanisms underlying astrogenesis in the developing mammalian brain. *Proceedings of the Japan Academy.*

Series B, Physical and biological sciences, *93*(6), 386–398. https://doi.org/10.2183/PJAB.93.024

Tamura, M., Amano, T., & Shiroishi, T. (2014). The Hand2 Gene Dosage Effect in Developmental Defects and Human Congenital Disorders. *Current Topics in Developmental Biology*, *110*, 129–152. https://doi.org/10.1016/B978-0-12-405943-6.00003-8

Tan, Y. L., Yuan, Y., & Tian, L. (2019). Microglial regional heterogeneity and its role in the brain. *Molecular Psychiatry 2019 25:2*, *25*(2), 351–367. https://doi.org/10.1038/s41380-019-0609-8

Taverna, E., Götz, M., & Huttner, W. B. (2014). The Cell Biology of Neurogenesis: Toward an Understanding of the Development and Evolution of the Neocortex. *http://dx.doi.org/10.1146/annurev-cellbio-101011-155801*, *30*, 465–502. https://doi.org/10.1146/ANNUREV-CELLBIO-101011-155801

Telley, L., Agirman, G., Prados, J., Amberg, N., Fièvre, S., Oberst, P., Bartolini, G., Vitali, I., Cadilhac, C., Hippenmeyer, S., Nguyen, L., Dayer, A., & Jabaudon, D. (2019). Temporal patterning of apical progenitors and their daughter neurons in the developing neocortex. *Science*, *364*(6440). https://doi.org/10.1126/SCIENCE.AAV2522/SUPPL_FILE/AAV2522_TELLEY_SM.PDF

Tepe, B., Hill, M. C., Pekarek, B. T., Hunt, P. J., Martin, T. J., Martin, J. F., & Arenkiel, B. R. (2018). Single-Cell RNA-Seq of Mouse Olfactory Bulb Reveals Cellular Heterogeneity and Activity-Dependent Molecular Census of Adult-Born Neurons. *Cell reports*, *25*(10), 2689–2703.e3. https://doi.org/10.1016/J.CELREP.2018.11.034

Thalhammer, A., & Cingolani, L. A. (2014). Cell adhesion and homeostatic synaptic plasticity. *Neuropharmacology*, *78*(100), 23–30. https://doi.org/10.1016/J.NEUROPHARM.2013.03.015

Thanasios, A., & Apavassiliou, G. P. (1995). Transcription Factors. *Molecular Medicine*, *332*(1), 45–47. https://doi.org/10.1056/NEJM199501053320108

Thomas, J., Martinez-Reza, M. F., Thorwirth, M., Zarb, Y., Conzelmann, K. K., Hauck, S. M., Grade, S., & Götz, M. (2022). Excessive local host-graft connectivity in aging and amyloid-loaded brain. *Science advances*, *8*(23). https://doi.org/10.1126/SCIADV.ABG9287

Tien, N. W., & Kerschensteiner, D. (2018). Homeostatic plasticity in neural development. *Neural Development 2018 13:1*, *13*(1), 1–7. https://doi.org/10.1186/S13064-018-0105-X

Tomas-Roca, L., Qiu, Z., Fransén, E., Gokhale, R., Bulovaite, E., Price, D. J., Komiyama, N. H., & Grant, S. G. N. (2022). Developmental disruption and restoration of brain synaptome architecture in the murine Pax6 neurodevelopmental disease model. *Nature Communications 2022 13:1*, *13*(1), 1–13. https://doi.org/10.1038/s41467-022-34131-w

Tomita, K., Moriyoshi, K., Nakanishi, S., Guillemot, F., & Kageyama, R. (2000). Mammalian achaete–scute and atonal homologs regulate neuronal versus glial fate determination in the central nervous system. *The EMBO Journal*, *19*(20), 5460. https://doi.org/10.1093/EMBOJ/19.20.5460

Tong Ihn Lee, & Young, R. A. (2003). Transcription of eukaryotic protein-coding genes. *https://doi.org/10.1146/annurev.genet.34.1.77*, *34*, 77–137. https://doi.org/10.1146/ANNUREV.GENET.34.1.77

Tsunemoto, R., Lee, S., Szucs, A., Chubukov, P., Sokolova, I., Blanchard, J. W., Eade, K. T., Bruggemann, J., Wu, C., Torkamani, A., Sanna, P. P., & Baldwin, K. K. (2018). Diverse reprogramming codes for neuronal identity. *Nature*, *557*(7705), 375–380. https://doi.org/10.1038/s41586-018-0103-5

Tsunemoto, R. K., Eade, K. T., Blanchard, J. W., & Baldwin, K. K. (2015). Embj201591402. *34*(11), 1445–1455.

Turnley, A. M., Basrai, H. S., & Christie, K. J. (2014). Is integration and survival of newborn neurons the bottleneck for effective neural repair by endogenous neural precursor cells? *Frontiers in Neuroscience*, *8*(8 FEB). https://doi.org/10.3389/FNINS.2014.00029

Turrigiano, G. G., Leslie, K. R., Desai, N. S., Rutherford, L. C., & Nelson, S. B. (1998). Activity-dependent scaling of quantal amplitude in neocortical neurons. *Nature*, *391*(6670), 892–896. https://doi.org/10.1038/36103

Turrigiano, G. (2011). Too many cooks? Intrinsic and synaptic homeostatic mechanisms in cortical circuit refinement. *Annual review of neuroscience*, *34*, 89–103. https://doi.org/10.1146/ANNUREV-NEURO-060909-153238

Turrigiano, G. (2012). Homeostatic Synaptic Plasticity: Local and Global Mechanisms for Stabilizing Neuronal Function. *Cold Spring Harbor Perspectives in Biology*, *4*(1). https://doi.org/10.1101/CSHPERSPECT.A005736

Turrigiano, G., Abbott, L. F., & Marder, E. (1994). Activity-dependent changes in the intrinsic properties of cultured neurons. *Science (New York, N.Y.)*, *264*(5161), 974–977. https://doi.org/10.1126/SCIENCE.8178157

The homeostatic control of intrinsic excitability was brought to the forefront by experiments that followed the fate of a neuron that was removed from its circuit and placed in isolated cell cul- ture (Turrigiano et al., 1994). Over a period of days, the isolated neuron rebalanced ion channel surface expression and restored intrinsic firing properties that were characteristic of that cell in vivo. The effect was shown to be both activity and calcium dependent.

Turrigiano, G. G. (1999). Homeostatic plasticity in neuronal networks: the more things change, the more they stay the same. *Trends in Neurosciences*, *22*(5), 221–227. https://doi.org/10.1016/S0166-2236(98)01341-1

Turrigiano, G. G. (2008). The Self-Tuning Neuron: Synaptic Scaling of Excitatory Synapses. *Cell*, *135*(3), 422. https://doi.org/10.1016/J.CELL.2008.10.008

Turrigiano, G. G. (2017). The dialectic of Hebb and homeostasis. *Philosophical Transactions of the Royal Society B: Biological Sciences*, *372*(1715). https://doi.org/10.1098/RSTB.2016.0258

Turrigiano, G. G., & Nelson, S. B. (2004). Homeostatic plasticity in the developing nervous system. *Nature Reviews Neuroscience 2004 5:2*, *5*(2), 97–107. https://doi.org/10.1038/nrn1327

Tyssowski, K. M., DeStefino, N. R., Cho, J. H., Dunn, C. J., Poston, R. G., Carty, C. E., Jones, R. D., Chang, S. M., Romeo, P., Wurzelmann, M. K., Ward, J. M., Andermann, M. L., Saha, R. N., Dudek, S. M., & Gray, J. M. (2018a). Different Neuronal Activity Patterns Induce Different Gene Expression Programs. *Neuron*, *98*(3), 530–546.e11. https://doi.org/10.1016/j.neuron.2018.04.001

Tyssowski, K. M., DeStefino, N. R., Cho, J. H., Dunn, C. J., Poston, R. G., Carty, C. E., Jones, R. D., Chang, S. M., Romeo, P., Wurzelmann, M. K., Ward, J. M., Andermann, M. L., Saha, R. N., Dudek, S. M., & Gray, J. M. (2018b). Different Neuronal Activity Patterns Induce Different Gene Expression Programs. *Neuron*, *98*(3), 530–546.e11. https://doi.org/10.1016/j.neuron.2018.04.001

Valakh, V., Aelita Zhu, X., Wise, D., Van Hooser, S., Schectman, R., Kirk, R., & Nelson, S. B. (n.d.). A transcriptional constraint mechanism limits the homeostatic response to activity deprivation in mammalian neocortex. https://doi.org/10.1101/2021.10.20.465163

Valakh, V., Zhu, X. A., Wise, D., Hooser, S. V., Schectman, R., Cepeda, I., Kirk, R., O'Toole, S., & Nelson, S. B. (2021). A transcriptional constraint mechanism limits the homeostatic response to activity deprivation in mammalian neocortex. *bioRxiv*, 2021.10.20.465163. https://doi.org/10.1101/2021.10.20.465163

Van den Berge, K., Perraudeau, F., Soneson, C., Love, M. I., Risso, D., Vert, J. P., Robinson, M. D., Dudoit, S., & Clement, L. (2018). Observation weights unlock bulk RNA-seq tools for zero inflation and single-cell applications. *Genome Biology*, *19*(1), 1–17. https://doi.org/10.1186/S13059-018-1406-4/FIGURES/6

Vierbuchen, T., Ling, E., Cowley, C. J., Couch, C. H., Wang, X., Harmin, D. A., Roberts, C. W., & Greenberg, M. E. (2017). AP-1 Transcription Factors and the BAF Complex Mediate Signal-Dependent Enhancer Selection. *Molecular cell*, *68*(6), 1067–1082.e12. https://doi.org/10.1016/J.MOLCEL.2017.11.026

Vierbuchen, T., Ostermeier, A., Pang, Z. P., Kokubu, Y., Südhof, T. C., & Wernig, M. (2010). Direct conversion of fibroblasts to functional neurons by defined factors. *Nature*, *463*(7284), 1035–1041. https://doi.org/10.1038/NATURE08797

Vignoles, R., Lentini, C., D'Orange, M., & Heinrich, C. (2019). Direct Lineage Reprogramming for Brain Repair: Breakthroughs and Challenges. *Trends in Molecular Medicine*, *25*(10), 897–914. https://doi.org/10.1016/j.molmed.2019.06.006

Vihma, H., Luhakooder, M., Pruunsild, P., & Timmusk, T. (2016). Regulation of different human NFAT isoforms by neuronal activity. *Journal of neurochemistry*, *137*(3), 394–408. https://doi.org/10.1111/JNC.13568

Villalba, A., Götz, M., & Borrell, V. (2021). The regulation of cortical neurogenesis. *Current Topics in Developmental Biology*, *142*, 1–66. https://doi.org/10.1016/BS.CTDB.2020.10.003

Vitureira, N., & Goda, Y. (2013). The interplay between Hebbian and homeostatic synaptic plasticity. *Journal of Cell Biology*, *203*(2), 175–186. https://doi.org/10.1083/JCB.201306030

Wamsley, B., & Fishell, G. (2017). Genetic and activity-dependent mechanisms underlying interneuron diversity. *Nature Reviews Neuroscience 2017 18:5*, *18*(5), 299–309. https://doi.org/10.1038/nrn.2017.30

Wang, H. Y., Hsieh, P. F., Huang, D. F., Chin, P. S., Chou, C. H., Tung, C. C., Chen, S. Y., Lee, L. J., Gau, S. S. F., & Huang, H. S. (2015). RBFOX3/NeuN is Required for Hippocampal Circuit Balance and Function. *Scientific Reports 2015 5:1*, *5*(1), 1–16. https://doi.org/10.1038/srep17383

Wang, H. L., Zhang, Z., Hintze, M., & Chen, L. (2011). Decrease in Calcium Concentration Triggers Neuronal Retinoic Acid Synthesis during Homeostatic Synaptic Plasticity. *The Journal of Neuroscience*, *31*(49), 17764. https://doi.org/10.1523/JNEUROSCI.3964-11.2011

Wang, T., Li, B., Nelson, C. E., & Nabavi, S. (2019). Comparative analysis of differential gene expression analysis tools for single-cell RNA sequencing data. *BMC Bioinformatics*, *20*(1), 1–16. https://doi.org/10.1186/S12859-019-2599-6/TABLES/7

Wayman, G. A., Lee, Y. S., Tokumitsu, H., Silva, A., & Soderling, T. R. (2008). Calmodulin-kinases: modulators of neuronal development and plasticity. *Neuron*, *59*(6), 914–931. https://doi.org/10.1016/J.NEURON.2008.08.021

Wen, W., & Turrigiano, G. G. (2021). Developmental Regulation of Homeostatic Plasticity in Mouse Primary Visual Cortex. https://doi.org/10.1523/JNEUROSCI.1200-21.2021

West, A. E., Chen, W. G., Dalva, M. B., Dolmetsch, R. E., Kornhauser, J. M., Shaywitz, A. J., Takasu, M. A., Tao, X., & Greenberg, M. E. (2001). Calcium regulation of neuronal gene expression. *Proceedings of the National Academy of Sciences of the United States of America*, *98*(20), 11024–11031. https://doi.org/10.1073/PNAS.191352298/ASSET/EA6FED01-834A-47EA-95D6-F9AF4D2F3AD6/ASSETS/GRAPHIC/PQ1913522004.JPEG

West, A. E., & Greenberg, M. E. (2011). Neuronal activity-regulated gene transcription in synapse development and cognitive function. *Cold Spring Harbor Perspectives in Biology*, *3*(6), 1–21. https://doi.org/10.1101/cshperspect.a005744

Whitt, J. L., Petrus, E., & Lee, H. K. (2014). Experience-dependent homeostatic synaptic plasticity in neocortex. *Neuropharmacology*, *78*(100), 45–54. https://doi.org/10.1016/J.NEUROPHARM.2013.02.016

Wilkinson, G., Dennis, D., & Schuurmans, C. (2013). Proneural genes in neocortical development. *Neuroscience*, *253*, 256–273. https://doi.org/10.1016/j.neuroscience.2013.08.029

Winnubst, J., & Arber, S. (2021). A census of cell types in the brain's motor cortex. *Nature 2021 598:7879*, *598*(7879), 33–34. https://doi.org/10.1038/d41586-021-02493-8

Wisniewska, M. B. (2013). Physiological Role of β-Catenin/TCF Signaling in Neurons of the Adult Brain. *Neurochemical Research*, *38*(6), 1144. https://doi.org/10.1007/S11064-013-0980-9

Wittmann, M. T., & Häberle, B. M. (2018). Linking the Neuropsychiatric Disease Gene TCF4 to Neuronal Activity-Dependent Regulatory Networks. *The Journal of Neuroscience*, *38*(11), 2653. https://doi.org/10.1523/JNEUROSCI.3475-17.2018

Wolf, F. A., Angerer, P., & Theis, F. J. (2018). SCANPY: Large-scale single-cell gene expression data analysis. *Genome Biology*, *19*(1), 1–5. https://doi.org/10.1186/S13059-017-1382-0/FIGURES/1

Wu, G. Y., Deisseroth, K., & Tsien, R. W. (2001). Activity-dependent CREB phosphorylation: Convergence of a fast, sensitive calmodulin kinase pathway and a slow, less sensitive mitogen-activated protein kinase pathway. *Proceedings of the National Academy of Sciences of the United States of America*, *98*(5), 2808–2813. https://doi.org/10.1073/PNAS.051634198/ASSET/C0180C93-4322-4177-8F21-54519636BCA5/ASSETS/GRAPHIC/PQ0516341005.JPEG

Wu, X., Li, Y., Crise, B., & Burgess, S. M. (2003). Transcription start regions in the human genome are favored targets for MLV integration. *Science (New York, N.Y.)*, *300*(5626), 1749–1751. https://doi.org/10.1126/SCIENCE.1083413

Xu, J., Du, Y., & Deng, H. (2015). Direct Lineage Reprogramming: Strategies, Mechanisms, and Applications. *Cell Stem Cell*, *16*(2), 119–134. https://doi.org/10.1016/J.STEM.2015.01.013

Xu, X., & Pozzo-Miller, L. (2017). EEA1 restores homeostatic synaptic plasticity in hippocampal neurons from Rett syndrome mice. *The Journal of Physiology*, *595*(16), 5699–5712. https://doi.org/10.1113/JP274450
MECP2 !!!

Yamaguchi, M., & Mori, K. (2005). Critical period for sensory experience-dependent survival of newly generated granule cells in the adult mouse olfactory bulb.

Proceedings of the National Academy of Sciences of the United States of America, *102*(27), 9697–9702. https://doi.org/10.1073/PNAS.0406082102

Yang, N., Ng, Y. H., Pang, Z. P., Südhof, T. C., & Wernig, M. (2011). Induced Neuronal (iN) Cells: How to Make and Define a Neuron. *Cell stem cell*, *9*(6), 517. https://doi.org/10.1016/J.STEM.2011.11.015

Yang, Y., Yamada, T., Hill, K. K., Hemberg, M., Reddy, N. C., Cho, H. Y., Guthrie, A. N., Oldenborg, A., Heiney, S. A., Ohmae, S., Medina, J. F., Holy, T. E., & Bonni, A. (2016). Chromatin remodeling inactivates activity genes and regulates neural coding. *Science (New York, N.Y.)*, *353*(6296), 300–306. https://doi.org/10.1126/SCIENCE.AAD4225

Yao, Z., Liu, H., Xie, F., Fischer, S., Adkins, R. S., Aldridge, A. I., Ament, S. A., Bartlett, A., Behrens, M. M., Van den Berge, K., Bertagnolli, D., de Bézieux, H. R., Biancalani, T., Booeshaghi, A. S., Bravo, H. C., Casper, T., Colantuoni, C., Crabtree, J., Creasy, H., … Mukamel, E. A. (2021). A transcriptomic and epigenomic cell atlas of the mouse primary motor cortex. *Nature 2021 598:7879*, *598*(7879), 103–110. https://doi.org/10.1038/s41586-021-03500-8

Yao, Z., van Velthoven, C. T., Nguyen, T. N., Goldy, J., Sedeno-Cortes, A. E., Baftizadeh, F., Bertagnolli, D., Casper, T., Chiang, M., Crichton, K., Ding, S. L., Fong, O., Garren, E., Glandon, A., Gouwens, N. W., Gray, J., Graybuck, L. T., Hawrylycz, M. J., Hirschstein, D., … Zeng, H. (2021). A taxonomy of transcriptomic cell types across the isocortex and hippocampal formation. *Cell*, *184*(12), 3222–3241.e26. https://doi.org/10.1016/J.CELL.2021.04.021

Yap, E. L., & Greenberg, M. E. (2018). Activity-Regulated Transcription: Bridging the Gap between Neural Activity and Behavior. *Neuron*, *100*(2), 330–348. https://doi.org/10.1016/J.NEURON.2018.10.013

Yu, X., Chung, S., Chen, D. Y., Wang, S., Dodd, S. J., Walters, J. R., Isaac, J. T., & Koretsky, A. P. (2012). Thalamocortical Inputs Show Post-Critical-Period Plasticity. *Neuron*, *74*(4), 731–742. https://doi.org/10.1016/J.NEURON.2012.04.024

Zeisel, A., Hochgerner, H., Lönnerberg, P., Johnsson, A., Memic, F., van der Zwan, J., Häring, M., Braun, E., Borm, L. E., La Manno, G., Codeluppi, S., Furlan, A., Lee, K., Skene, N., Harris, K. D., Hjerling-Leffler, J., Arenas, E., Ernfors, P., Marklund, U., & Linnarsson, S. (2018). Molecular Architecture of the Mouse Nervous System. *Cell*, *174*(4), 999–1014.e22. https://doi.org/10.1016/J.CELL.2018.06.021

Zeng, H., & Sanes, J. R. (2017). Neuronal cell-type classification: challenges, opportunities and the path forward. *Nature reviews. Neuroscience*, *18*(9), 530–546. https://doi.org/10.1038/NRN.2017.85

Zhang, Y., Li, B., Cananzi, S., Han, C., Wang, L.-L., Zou, Y., Fu, Y.-X., Hon, G. C., & Zhang, C.-L. (2022). A single factor elicits multilineage reprogramming of astrocytes in

the adult mouse striatum. *Proceedings of the National Academy of Sciences*, *119*(11). https://doi.org/10.1073/PNAS.2107339119

Zhou, M., Tao, X., Sui, M., Cui, M., Liu, D., Wang, B., Wang, T., Zheng, Y., Luo, J., Mu, Y., Wan, F., Zhu, L. Q., & Zhang, B. (2021). Reprogramming astrocytes to motor neurons by activation of endogenous Ngn2 and Isl1. *Stem Cell Reports*, *16*(7), 1777–1791. https://doi.org/10.1016/j.stemcr.2021.05.020

Zhou, Q., Brown, J., Kanarek, A., Rajagopal, J., & Melton, D. A. (2008). In vivo reprogramming of adult pancreatic exocrine cells to beta-cells. *Nature*, *455*(7213), 627–632. https://doi.org/10.1038/NATURE07314

Zhou, X., Moon, C., Zheng, F., Luo, Y., Soellner, D., Nuñez, J. L., & Wang, H. (2009). NMDA-stimulated ERK1/2 Signaling and the Transcriptional Up-regulation of Plasticity-related Genes are Developmentally Regulated following in vitro Neuronal Maturation. *Journal of neuroscience research*, *87*(12), 2632. https://doi.org/10.1002/JNR.22103

Zhu, A., Ibrahim, J. G., & Love, M. I. (2019). Heavy-tailed prior distributions for sequence count data: removing the noise and preserving large differences. *Bioinformatics*, *35*(12), 2084–2092. https://doi.org/10.1093/BIOINFORMATICS/BTY895

BIBLIOGRAPHY

Abbott, L. F., & Nelson, S. B. (2000). Synaptic plasticity: taming the beast. *Nature Neuroscience 2000 3:11*, *3*(11), 1178–1183. https://doi.org/10.1038/81453

Abe, K. (2008). Neural activity-dependent regulation of gene expression in developing and mature neurons. *Development, growth & differentiation*, *50*(4), 261–271. https://doi.org/10.1111/J.1440-169X.2008.00999.X

Abraham, W. C., Dragunow, M., & Tate, W. P. (1991). The role of immediate early genes in the stabilization of long-term potentiation. *Molecular Neurobiology*, *5*(2-4), 297–314. https://doi.org/10.1007/BF02935553

Ahlgren, H., Bas-Orth, C., Freitag, H. E., Hellwig, A., Ottersen, O. P., & Bading, H. (2014). The nuclear calcium signaling target, activating transcription factor 3 (ATF3), protects against dendrotoxicity and facilitates the recovery of synaptic transmission after an excitotoxic insult. *Journal of Biological Chemistry*, *289*(14), 9970–9982. https://doi.org/10.1074/JBC.M113.502914

Ahlmann-Eltze, C., & Huber, W. (2021). glmGamPoi: fitting Gamma-Poisson generalized linear models on single cell count data. *Bioinformatics*, *36*(24), 5701–5702. https://doi.org/10.1093/BIOINFORMATICS/BTAA1009

Aibar, S., González-Blas, C. B., Moerman, T., Huynh-Thu, V. A., Imrichova, H., Hulselmans, G., Rambow, F., Marine, J. C., Geurts, P., Aerts, J., Van Den Oord, J., Atak, Z. K., Wouters, J., & Aerts, S. (2017). SCENIC: single-cell regulatory network inference and clustering. *Nature Methods 2017 14:11*, *14*(11), 1083–1086. https://doi.org/10.1038/nmeth.4463

Alonso, M., Viollet, C., Gabellec, M. M., Meas-Yedid, V., Olivo-Marin, J. C., & Lledo, P. M. (2006). Olfactory Discrimination Learning Increases the Survival of Adult-Born Neurons in the Olfactory Bulb. *Journal of Neuroscience*, *26*(41), 10508–10513. https://doi.org/10.1523/JNEUROSCI.2633-06.2006

Amamoto, R., & Arlotta, P. (2014). Development-inspired reprogramming of the mammalian central nervous system. *Science (New York, N.Y.)*, *343*(6170). https://doi.org/10.1126/SCIENCE.1239882

Anderson, S., & Vanderhaeghen, P. (2014). Cortical neurogenesis from pluripotent stem cells: complexity emerging from simplicity. *Current opinion in neurobiology*, *27*, 151–157. https://doi.org/10.1016/J.CONB.2014.03.012

Anggono, V., Clem, R. L., & Huganir, R. L. (2011). PICK1 Loss of Function Occludes Homeostatic Synaptic Scaling. *The Journal of Neuroscience*, *31*(6), 2188. https://doi.org/10.1523/JNEUROSCI.5633-10.2011

Arendt, K. L., Sarti, F., & Chen, L. (2013). Chronic Inactivation of a Neural Circuit Enhances LTP by Inducing Silent Synapse Formation. *The Journal of Neuroscience*, *33*(5), 2087. https://doi.org/10.1523/JNEUROSCI.3880-12.2013

Arrázola, M. S., Varela-Nallar, L., Colombres, M., Toledo, E. M., Cruzat, F., Pavez, L., Assar, R., Aravena, A., González, M., Montecino, M., Maass, A., Martínez, S., & Inestrosa, N. C. (2009). Calcium/calmodulin-dependent protein kinase type IV is a target gene of the Wnt/β-catenin signaling pathway. *Journal of Cellular Physiology*, *221*(3), 658–667. https://doi.org/10.1002/JCP.21902

Aydin, B., Kakumanu, A., Rossillo, M., Moreno-Estellés, M., Garipler, G., Ringstad, N., Flames, N., Mahony, S., & Mazzoni, E. O. (2019). Proneural factors Ascl1 and Neurog2 contribute to neuronal subtype identities by establishing distinct chromatin landscapes. *Nature Neuroscience 2019 22:6*, *22*(6), 897–908. https://doi.org/10.1038/s41593-019-0399-y

Azevedo, F. A., Carvalho, L. R., Grinberg, L. T., Farfel, J. M., Ferretti, R. E., Leite, R. E., Filho, W. J., Lent, R., & Herculano-Houzel, S. (2009). Equal numbers of neuronal and nonneuronal cells make the human brain an isometrically scaled-up primate brain. *The Journal of comparative neurology*, *513*(5), 532–541. https://doi.org/10.1002/CNE.21974

Bading, H., Ginty, D. D., & Greenberg, M. E. (1993). Regulation of gene expression in hippocampal neurons by distinct calcium signaling pathways. *Science (New York, N.Y.)*, *260*(5105), 181–186. https://doi.org/10.1126/SCIENCE.8097060

Baker, N. E., & Brown, N. L. (2018). All in the family: proneural bHLH genes and neuronal diversity. *Development (Cambridge, England)*, *145*(9). https://doi.org/10.1242/DEV.159426

Bakken, T. E., Jorstad, N. L., Hu, Q., Lake, B. B., Tian, W., Kalmbach, B. E., Crow, M., Hodge, R. D., Krienen, F. M., Sorensen, S. A., Eggermont, J., Yao, Z., Aevermann, B. D., Aldridge, A. I., Bartlett, A., Bertagnolli, D., Casper, T., Castanon, R. G., Crichton, K., … Lein, E. S. (2021). Comparative cellular analysis of motor cortex in human, marmoset and mouse. *Nature*, *598*(7879), 111–119. https://doi.org/10.1038/S41586-021-03465-8

Ballout, N., Frappé, I., Péron, S., Jaber, M., Zibara, K., & Gaillard, A. (2016). Development and Maturation of Embryonic Cortical Neurons Grafted into the Damaged Adult Motor Cortex. *Frontiers in neural circuits*, *10*(AUG). https://doi.org/10.3389/FNCIR.2016.00055

Batista-Brito, R., & Fishell, G. (2009). Chapter 3 The Developmental Integration of Cortical Interneurons into a Functional Network. *Current Topics in Developmental Biology*, *87*(09), 81–118. https://doi.org/10.1016/S0070-2153(09)01203-4

Bats, C., Farrant, M., & Cull-Candy, S. G. (2013). A role of TARPs in the expression and plasticity of calcium-permeable AMPARs: Evidence from cerebellar neurons and glia. *Neuropharmacology*, *74*, 76. https://doi.org/10.1016/J.NEUROPHARM.2013.03.037

Bayer, K. U., Löhler, J., Schulman, H., & Harbers, K. (1999). Developmental expression of the CaM kinase II isoforms: Ubiquitous γ- and δ-CaM kinase II are the early isoforms and most abundant in the developing nervous system. *Molecular Brain Research*, *70*(1), 147–154. https://doi.org/10.1016/S0169-328X(99)00131-X

Bayraktar, O. A., Bartels, T., Holmqvist, S., Kleshchevnikov, V., Martirosyan, A., Polioudakis, D., Ben Haim, L., Young, A. M., Batiuk, M. Y., Prakash, K., Brown, A., Roberts, K., Paredes, M. F., Kawaguchi, R., Stockley, J. H., Sabeur, K., Chang, S. M., Huang, E., Hutchinson, P., … Rowitch, D. H. (2020). Astrocyte layers in the mammalian cerebral cortex revealed by a single-cell in situ transcriptomic map. *Nature Neuroscience 2020 23:4*, *23*(4), 500–509. https://doi.org/10.1038/s41593-020-0602-1

Béïque, J. C., Na, Y., Kuhl, D., Worley, P. F., & Huganir, R. L. (2011). Arc-dependent synapse-specific homeostatic plasticity. *Proceedings of the National Academy of Sciences of the United States of America*, *108*(2), 816–821. https://doi.org/10.1073/PNAS.1017914108

Ben-Arie, N., McCall, A. E., Berkman, S., Eichele, G., Bellen, H. J., & Zoghbi, H. Y. (1996). Evolutionary conservation of sequence and expression of the bHLH protein Atonal suggests a conserved role in neurogenesis. *Human molecular genetics*, *5*(9), 1207–1216. https://doi.org/10.1093/HMG/5.9.1207

Bender, K. J., Allen, C. B., Bender, V. A., & Feldman, D. E. (2006). Synaptic Basis for Whisker Deprivation-Induced Synaptic Depression in Rat Somatosensory Cortex. *Journal of Neuroscience*, *26*(16), 4155–4165. https://doi.org/10.1523/JNEUROSCI.0175-06.2006

Benito, E., & Barco, A. (2015). The Neuronal Activity-Driven Transcriptome. *Molecular Neurobiology*, *51*(3), 1071–1088. https://doi.org/10.1007/S12035-014-8772-Z/FIGURES/2

Bergsland, M., Werme, M., Malewicz, M., Perlmann, T., & Muhr, J. (2006). The establishment of neuronal properties is controlled by Sox4 and Sox11. *Genes & Development*, *20*(24), 3475. https://doi.org/10.1101/GAD.403406

Berninger, B., Costa, M. R., Koch, U., Schroeder, T., Sutor, B., Grothe, B., & Götz, M. (2007). Functional properties of neurons derived from in vitro reprogrammed postnatal

astroglia. *Journal of Neuroscience*, *27*(32), 8654–8664. https://doi.org/10.1523/JNEUROSCI.1615-07.2007

Bertels, H., Vicente-Ortiz, G., El Kanbi, K., & Takeoka, A. (2022). Neurotransmitter phenotype switching by spinal excitatory interneurons regulates locomotor recovery after spinal cord injury. *Nature Neuroscience 2022 25:5*, *25*(5), 617–629. https://doi.org/10.1038/s41593-022-01067-9

Bertrand, N., Castro, D. S., & Guillemot, F. (2002). Proneural genes and the specification of neural cell types. *Nature reviews. Neuroscience*, *3*(7), 517–530. https://doi.org/10.1038/NRN874

Bhaduri, A., Sandoval-Espinosa, C., Otero-Garcia, M., Oh, I., Yin, R., Eze, U. C., Nowakowski, T. J., & Kriegstein, A. R. (2021). An atlas of cortical arealization identifies dynamic molecular signatures. *Nature 2021 598:7879*, *598*(7879), 200–204. https://doi.org/10.1038/s41586-021-03910-8

Bird, A. (2002). DNA methylation patterns and epigenetic memory. *Genes & Development*, *16*(1), 6–21. https://doi.org/10.1101/GAD.947102

Bissen, D., Foss, F., & Acker-Palmer, A. (2019). AMPA receptors and their minions: auxiliary proteins in AMPA receptor trafficking. *Cellular and Molecular Life Sciences 2019 76:11*, *76*(11), 2133–2169. https://doi.org/10.1007/S00018-019-03068-7

Bito, H., Deisseroth, K., & Tsien, R. W. (1997). Ca2+-dependent regulation in neuronal gene expression. *Current opinion in neurobiology*, *7*(3), 419–429. https://doi.org/10.1016/S0959-4388(97)80072-4

Bliss, T. V., & Cooke, S. F. (2011). Long-term potentiation and long-term depression: a clinical perspective. *Clinics*, *66*(Suppl 1), 3. https://doi.org/10.1590/S1807-59322011001300002

Blum, R., Heinrich, C., Sánchez, R., Lepier, A., Gundelfinger, E. D., Berninger, B., & Götz, M. (2011). Neuronal network formation from reprogrammed early postnatal rat cortical glial cells. *Cerebral cortex (New York, N.Y. : 1991)*, *21*(2), 413–424. https://doi.org/10.1093/CERCOR/BHQ107

Bocchi, R., Masserdotti, G., & Götz, M. (2022). Direct neuronal reprogramming: Fast forward from new concepts toward therapeutic approaches. *Neuron*, *110*(3), 366–393. https://doi.org/10.1016/j.neuron.2021.11.023

Boghdadi, A. G., Teo, L., & Bourne, J. A. (2020). The Neuroprotective Role of Reactive Astrocytes after Central Nervous System Injury. *Journal of neurotrauma*, *37*(5), 681–691. https://doi.org/10.1089/NEU.2019.6938

Bonnefont, J., Tiberi, L., van den Ameele, J., Potier, D., Gaber, Z. B., Lin, X., Bilheu, A., Herpoel, A., Velez Bravo, F. D., Guillemot, F., Aerts, S., & Vanderhaeghen, P. (2019). Cortical Neurogenesis Requires Bcl6-Mediated Transcriptional Repression of Multiple Self-Renewal-Promoting Extrinsic Pathways. *Neuron*, *103*(6), 1096–

1108.e4. https://doi.org/10.1016/J.NEURON.2019.06.027/ATTACHMENT/8EFF5BA5-18D4-4A0B-80D5-441CAFB5BA3F/MMC6.XLSX

Bonnefont, J., & Vanderhaeghen, P. (2021). Neuronal fate acquisition and specification: time for a change. *Current opinion in neurobiology*, *66*, 195–204. https://doi.org/10.1016/J.CONB.2020.12.006

Boshans, L. L., Factor, D. C., Singh, V., Liu, J., Zhao, C., Mandoiu, I., Lu, Q. R., Casaccia, P., Tesar, P. J., & Nishiyama, A. (2019). The chromatin environment around interneuron genes in oligodendrocyte precursor cells and their potential for interneuron reprograming. *Frontiers in Neuroscience*, *13*(JUL), 829. https://doi.org/10.3389/FNINS.2019.00829/BIBTEX

Boulenouar, H., Benhatchi, H., Guermoudi, F., Oumiloud, A. H., & Rahoui, A. (2022). An actualized screening of schizophrenia-associated genes. *Egyptian Journal of Medical Human Genetics*, *23*(1), 1–12. https://doi.org/10.1186/S43042-022-00269-X/TABLES/2

Bragg-Gonzalo, L., De León Reyes, N. S., & Nieto, M. (2021). Genetic and activity dependent-mechanisms wiring the cortex: Two sides of the same coin. *Seminars in Cell & Developmental Biology*, *118*, 24–34. https://doi.org/10.1016/J.SEMCDB.2021.05.011

Brigidi, G. S., Hayes, M. G., Delos Santos, N. P., Hartzell, A. L., Texari, L., Lin, P. A., Bartlett, A., Ecker, J. R., Benner, C., Heinz, S., & Bloodgood, B. L. (2019). Genomic Decoding of Neuronal Depolarization by Stimulus-Specific NPAS4 Heterodimers. *Cell*, *179*(2), 373–391.e27. https://doi.org/10.1016/J.CELL.2019.09.004

Britanova, O., de Juan Romero, C., Cheung, A., Kwan, K. Y., Schwark, M., Gyorgy, A., Vogel, T., Akopov, S., Mitkovski, M., Agoston, D., Šestan, N., Molnár, Z., & Tarabykin, V. (2008). Satb2 Is a Postmitotic Determinant for Upper-Layer Neuron Specification in the Neocortex. *Neuron*, *57*(3), 378–392. https://doi.org/10.1016/J.NEURON.2007.12.028

Buchthal, B., Lau, D., Weiss, U., Weislogel, J. M., & Bading, H. (2012). Nuclear Calcium Signaling Controls Methyl-CpG-binding Protein 2 (MeCP2) Phosphorylation on Serine 421 following Synaptic Activity. *The Journal of Biological Chemistry*, *287*(37), 30967. https://doi.org/10.1074/JBC.M112.382507

Bullitt, E. (1990). Expression of c-fos-like protein as a marker for neuronal activity following noxious stimulation in the rat. *The Journal of comparative neurology*, *296*(4), 517–530. https://doi.org/10.1002/CNE.902960402

Canavero, S., & Cioni, B. (2011). Cerebral – Surface. *Essential Neuromodulation*, 17–46. https://doi.org/10.1016/B978-0-12-381409-8.00002-4

Cánovas, J., Berndt, F. A., Sepúlveda, H., Aguilar, R., Veloso, F. A., Montecino, M., Oliva, C., Maass, J. C., Sierralta, J., & Kukuljan, M. (2015). The Specification of Cortical

Subcerebral Projection Neurons Depends on the Direct Repression of TBR1 by CTIP1/BCL11a. *The Journal of Neuroscience*, *35*(19), 7552. https://doi.org/10.1523/JNEUROSCI.0169-15.2015

Cepko, C. L., Golden, J. A., Szele, F. G., & Lin, J. C. (1998). Lineage analysis in the vertebrate central nervous system. *Molecular and Cellular Approaches to Neural Development*. https://doi.org/10.1093/ACPROF:OSO/9780195111668.003.0011

Chahrour, M., Sung, Y. J., Shaw, C., Zhou, X., Wong, S. T., Qin, J., & Zoghbi, H. Y. (2008). MeCP2, a Key Contributor to Neurological Disease, Activates and Represses Transcription. *Science (New York, N.Y.)*, *320*(5880), 1224. https://doi.org/10.1126/SCIENCE.1153252

Chen, C., Lee, G. A., Pourmorady, A., Sock, E., & Donoghue, M. J. (2015). Orchestration of Neuronal Differentiation and Progenitor Pool Expansion in the Developing Cortex by SoxC Genes. *The Journal of Neuroscience*, *35*(29), 10629. https://doi.org/10.1523/JNEUROSCI.1663-15.2015

Chen, H., Huffman, J. E., Brody, J. A., Wang, C., Lee, S., Li, Z., Gogarten, S. M., Sofer, T., Bielak, L. F., Bis, J. C., Blangero, J., Bowler, R. P., Cade, B. E., Cho, M. H., Correa, A., Curran, J. E., de Vries, P. S., Glahn, D. C., Guo, X., … Lin, X. (2019). Efficient Variant Set Mixed Model Association Tests for Continuous and Binary Traits in Large-Scale Whole-Genome Sequencing Studies. *American journal of human genetics*, *104*(2), 260–274. https://doi.org/10.1016/j.ajhg.2018.12.012

Chen, J., Fuhler, N., Noguchi, K., & Dougherty, J. D. (2022). MYT1L is required for suppressing earlier neuronal development programs in the adult mouse brain. *bioRxiv*, 2022.10.17.512591. https://doi.org/10.1101/2022.10.17.512591

Chen, X., & Li, H. (2022). Neuronal reprogramming in treating spinal cord injury. *Neural Regeneration Research*, *17*(7), 1440. https://doi.org/10.4103/1673-5374.330590

Chen, Y., Wang, Y., Ertü Rk, A., Kallop, D., Jiang, Z., Weimer, R. M., Kaminker, J., & Sheng, M. (2014). Article Activity-Induced Nr4a1 Regulates Spine Density and Distribution Pattern of Excitatory Synapses in Pyramidal Neurons. *Neuron*, *83*, 431–443. https://doi.org/10.1016/j.neuron.2014.05.027

Chen, Y. C., Kuo, H. Y., Bornschein, U., Takahashi, H., Chen, S. Y., Lu, K. M., Yang, H. Y., Chen, G. M., Lin, J. R., Lee, Y. H., Chou, Y. C., Cheng, S. J., Chien, C. T., Enard, W., Hevers, W., Pääbo, S., Graybiel, A. M., & Liu, F. C. (2016). Foxp2 controls synaptic wiring of corticostriatal circuits and vocal communication by opposing Mef2c. *Nature Neuroscience 2016 19:11*, *19*(11), 1513–1522. https://doi.org/10.1038/nn.4380

Cheng, S., Butrus, S., Tan, L., Xu, R., Sagireddy, S., Trachtenberg, J. T., Shekhar, K., & Zipursky, S. L. (2022). Vision-dependent specification of cell types and function in

the developing cortex. *Cell*, *185*(2), 311–327.e24. https://doi.org/10.1016/J.CELL.2021.12.022

Cheng, X., Zhao, Y., Jiang, Q., Yang, J., Zhao, W., Taylor, I. A., Peng, Y. L., Wang, D., & Liu, J. (2019). Structural basis of dimerization and dual W-box DNA recognition by rice WRKY domain. *Nucleic Acids Research*, *47*(8), 4308–4318. https://doi.org/10.1093/nar/gkz113

Cheyne, J. E., Grant, L., Butler-Munro, C., Foote, J. W., Connor, B., & Montgomery, J. M. (2011). Synaptic integration of newly generated neurons in rat dissociated hippocampal cultures. *Molecular and cellular neurosciences*, *47*(3), 203–214. https://doi.org/10.1016/J.MCN.2011.04.006

Choii, G., & Ko, J. (2015). Gephyrin: a central GABAergic synapse organizer. *Experimental & Molecular Medicine 2015 47:4*, *47*(4), e158–e158. https://doi.org/10.1038/emm.2015.5

Chong, C. H., Li, Q., Mak, P. H. S., Ng, C. C. P., Leung, E. H. W., Tan, V. H., Chan, A. K. W., McAlonan, G., & Chan, S. Y. (2019). Lrrc7 mutant mice model developmental emotional dysregulation that can be alleviated by mGluR5 allosteric modulation. *Translational Psychiatry*, *9*(1). https://doi.org/10.1038/S41398-019-0580-9

Chouchane, M., Melo de Farias, A. R., Moura, D. M. d. S., Hilscher, M. M., Schroeder, T., Leão, R. N., & Costa, M. R. (2017). Lineage Reprogramming of Astroglial Cells from Different Origins into Distinct Neuronal Subtypes. *Stem cell reports*, *9*(1), 162–176. https://doi.org/10.1016/J.STEMCR.2017.05.009

Chung, S. W., Lewis, B. P., Rogasch, N. C., Saeki, T., Thomson, R. H., Hoy, K. E., Bailey, N. W., & Fitzgerald, P. B. (2017). Demonstration of short-term plasticity in the dorsolateral prefrontal cortex with theta burst stimulation: A TMS-EEG study. *Clinical neurophysiology : official journal of the International Federation of Clinical Neurophysiology*, *128*(7), 1117–1126. https://doi.org/10.1016/J.CLINPH.2017.04.005

Citri, A., & Malenka, R. C. (2007). Synaptic Plasticity: Multiple Forms, Functions, and Mechanisms. *Neuropsychopharmacology 2008 33:1*, *33*(1), 18–41. https://doi.org/10.1038/sj.npp.1301559

Clapham, D. E. (2007). Calcium Signaling. *Cell*, *131*(6), 1047–1058. https://doi.org/10.1016/j.cell.2007.11.028

Clark, E. A., Rutlin, M., Capano, L., Aviles, S., Saadon, J. R., Taneja, P., Zhang, Q., Bullis, J., Lauer, T., Myers, E., Schulmann, A., Forrest, D., & Nelson, S. B. (2020). Cortical RORβ is required for layer 4 transcriptional identity and barrel integrity. *eLife*, *9*, 1–45. https://doi.org/10.7554/ELIFE.52370

Clarke, Z. A., Andrews, T. S., Atif, J., Pouyabahar, D., Innes, B. T., MacParland, S. A., & Bader, G. D. (2021). Tutorial: guidelines for annotating single-cell transcriptomic

maps using automated and manual methods. *Nature Protocols 2021 16:6*, *16*(6), 2749–2764. https://doi.org/10.1038/s41596-021-00534-0

Cohen, S. M., Ma, H., Kuchibhotla, K. V., Watson, B. O., Buzsáki, G., Froemke, R. C., & Tsien, R. W. (2016). Excitation-Transcription Coupling in Parvalbumin-Positive Interneurons Employs a Novel CaM Kinase-Dependent Pathway Distinct from Excitatory Neurons. *Neuron*, *90*(2), 292–307. https://doi.org/10.1016/J.NEURON.2016.03.001

Cohen, S., & Greenberg, M. E. (2008). Communication between the synapse and the nucleus in neuronal development, plasticity, and disease. *Annual Review of Cell and Developmental Biology*, *24*, 183–209. https://doi.org/10.1146/annurev.cellbio.24.110707.175235

Colas, J. F., & Schoenwolf, G. C. (2001). Towards a cellular and molecular understanding of neurulation. *Developmental dynamics : an official publication of the American Association of Anatomists*, *221*(2), 117–145. https://doi.org/10.1002/DVDY.1144

Copp, A. J. (2005). Neurulation in the cranial region – normal and abnormal. *Journal of Anatomy*, *207*(5), 623. https://doi.org/10.1111/J.1469-7580.2005.00476.X

Cotterill, E., Charlesworth, P., Thomas, C. W., Paulsen, O., & Eglen, S. J. (2016). A comparison of computational methods for detecting bursts in neuronal spike trains and their application to human stem cell-derived neuronal networks. *Journal of neurophysiology*, *116*(2), 306–321. https://doi.org/10.1152/JN.00093.2016

Crux, S., Herms, J., & Dorostkar, M. M. (2018). Tcf4 regulates dendritic spine density and morphology in the adult brain. *PloS one*, *13*(6). https://doi.org/10.1371/JOURNAL.PONE.0199359

Cull-Candy, S., Kelly, L., & Farrant, M. (2006). Regulation of Ca2+-permeable AMPA receptors: synaptic plasticity and beyond. *Current opinion in neurobiology*, *16*(3), 288–297. https://doi.org/10.1016/J.CONB.2006.05.012

Danielson, N. B. B., Kaifosh, P., Zaremba, J. D. D., Lovett-Barron, M., Tsai, J., Denny, C. A. A., Balough, E. M. M., Goldberg, A. R. R., Drew, L. J. J., Hen, R., Losonczy, A., & Kheirbek, M. A. A. (2016). Distinct Contribution of Adult-Born Hippocampal Granule Cells to Context Encoding. *Neuron*, *90*(1), 101–112. https://doi.org/10.1016/j.neuron.2016.02.019

Davis, G. W. (2006). HOMEOSTATIC CONTROL OF NEURAL ACTIVITY: From Phenomenology to Molecular Design. *http://dx.doi.org/10.1146/annurev.neuro.28.061604.135751*, *29*, 307–323. https://doi.org/10.1146/ANNUREV.NEURO.28.061604.135751

Davis, M. W., & Jorgensen, E. M. (2022). ApE, A Plasmid Editor: A Freely Available DNA Manipulation and Visualization Program. *Frontiers in Bioinformatics*, *0*, 5. https://doi.org/10.3389/FBINF.2022.818619

Deeg, K. E., & Aizenman, C. D. (2011). Sensory modality–specific homeostatic plasticity in the developing optic tectum. *Nature Neuroscience 2011 14:5*, *14*(5), 548–550. https://doi.org/10.1038/nn.2772

Dehorter, N., Marichal, N., Marín, O., & Berninger, B. (2017). Tuning neural circuits by turning the interneuron knob. *Current opinion in neurobiology*, *42*, 144–151. https://doi.org/10.1016/J.CONB.2016.12.009

Dennis, D. J., Han, S., & Schuurmans, C. (2019). bHLH transcription factors in neural development, disease, and reprogramming. *Brain research*, *1705*, 48–65. https://doi.org/10.1016/J.BRAINRES.2018.03.013

Desai, A. R., & McConnell, S. K. (2000). Progressive restriction in fate potential by neural progenitors during cerebral cortical development. *Development (Cambridge, England)*, *127*(13), 2863–2872. https://doi.org/10.1242/DEV.127.13.2863

Desch, K., Langer, J. D., & Schuman, E. M. (2021). Dynamic bi-directional phosphorylation events associated with the reciprocal regulation of synapses during homeostatic up- and down-scaling. *Cell Reports*, *36*(8), 109583. https://doi.org/10.1016/J.CELREP.2021.109583

Di Bella, D. J., Habibi, E., Stickels, R. R., Scalia, G., Brown, J., Yadollahpour, P., Yang, S. M., Abbate, C., Biancalani, T., Macosko, E. Z., Chen, F., Regev, A., & Arlotta, P. (2021). Molecular logic of cellular diversification in the mouse cerebral cortex. *Nature 2021 595:7868*, *595*(7868), 554–559. https://doi.org/10.1038/s41586-021-03670-5

Dimou, L., & Gallo, V. (n.d.). NG2-glia and their functions in the central nervous system. https://doi.org/10.1002/glia.22859

Dörrbaum, A. R., Alvarez-Castelao, B., Nassim-Assir, B., Langer, J. D., & Schuman, E. M. (2020). Proteome dynamics during homeostatic scaling in cultured neurons. *eLife*, *9*. https://doi.org/10.7554/ELIFE.52939

Dudek, S. M., & Bear, M. F. (1992). Homosynaptic long-term depression in area CA1 of hippocampus and effects of N-methyl-D-aspartate receptor blockade. *Proceedings of the National Academy of Sciences of the United States of America*, *89*(10), 4363. https://doi.org/10.1073/PNAS.89.10.4363

Dynes, J. L., & Steward, O. (2007). Dynamics of bidirectional transport of Arc mRNA in neuronal dendrites. *The Journal of comparative neurology*, *500*(3), 433–447. https://doi.org/10.1002/CNE.21189

Ebert, D. H., & Greenberg, M. E. (2013). Activity-dependent neuronal signalling and autism spectrum disorder. *Nature*, *493*(7432), 327. https://doi.org/10.1038/NATURE11860

Eferl, R., & Wagner, E. F. (2003). AP-1: a double-edged sword in tumorigenesis. *Nature Reviews Cancer 2003 3:11*, *3*(11), 859–868. https://doi.org/10.1038/nrc1209

Elshazzly, M., Lopez, M. J., Reddy, V., & Caban, O. (2022). Embryology, Central Nervous System. *StatPearls*. https://www.ncbi.nlm.nih.gov/books/NBK526024/

Engert, F., & Bonhoeffer, T. (1999). Dendritic spine changes associated with hippocampal long-term synaptic plasticity. *Nature*, *399*(6731), 66–70. https://doi.org/10.1038/19978

Englund, C., Fink, A., Lau, C., Pham, D., Daza, R. A., Bulfone, A., Kowalczyk, T., & Hevner, R. F. (2005). Pax6, Tbr2, and Tbr1 are expressed sequentially by radial glia, intermediate progenitor cells, and postmitotic neurons in developing neocortex. *The Journal of neuroscience : the official journal of the Society for Neuroscience*, *25*(1), 247–251. https://doi.org/10.1523/JNEUROSCI.2899-04.2005

España, J., Valero, J., Miñano-Molina, A. J., Masgrau, R., Martín, E., Guardia-Laguarta, C., Lleó, A., Giménez-Llort, L., Rodríguez-Alvarez, J., & Saura, C. A. (2010). β-Amyloid Disrupts Activity-Dependent Gene Transcription Required for Memory through the CREB Coactivator CRTC1. *The Journal of Neuroscience*, *30*(28), 9402. https://doi.org/10.1523/JNEUROSCI.2154-10.2010

Espuny-Camacho, I., Michelsen, K. A., Linaro, D., Bilheu, A., Acosta-Verdugo, S., Herpoel, A., Giugliano, M., Gaillard, A., & Vanderhaeghen, P. (2018). Human Pluripotent Stem-Cell-Derived Cortical Neurons Integrate Functionally into the Lesioned Adult Murine Visual Cortex in an Area-Specific Way. *Cell reports*, *23*(9), 2732–2743. https://doi.org/10.1016/J.CELREP.2018.04.094

Falk, S., Han, D., & Karow, M. (2021). Cellular identity through the lens of direct lineage reprogramming. *Current Opinion in Genetics and Development*, *70*, 97–103. https://doi.org/10.1016/J.GDE.2021.06.015

Falkner, S., Grade, S., Dimou, L., Conzelmann, K. K., Bonhoeffer, T., Götz, M., & Hübener, M. (2016). Transplanted embryonic neurons integrate into adult neocortical circuits. *Nature*, *539*(7628), 248–253. https://doi.org/10.1038/NATURE20113

Fernandes, D., & Carvalho, A. L. (2016). Mechanisms of homeostatic plasticity in the excitatory synapse. *Journal of Neurochemistry*, *139*(6), 973–996. https://doi.org/10.1111/JNC.13687

Flavell, S. W., & Greenberg, M. E. (2008). Signaling mechanisms linking neuronal activity to gene expression and plasticity of the nervous system. *Annual review of neuroscience*, *31*, 563–590. https://doi.org/10.1146/ANNUREV.NEURO.31.060407.125631

Fode, C., Gradwohl, G., Morin, X., Dierich, A., LeMeur, M., Goridis, C., & Guillemot, F. (1998). The bHLH protein NEUROGENIN 2 is a determination factor for epibranchial placode-derived sensory neurons. *Neuron*, *20*(3), 483–494. https://doi.org/10.1016/S0896-6273(00)80989-7

Fox, K., & Stryker, M. (2017). Integrating Hebbian and homeostatic plasticity: introduction. *Philosophical Transactions of the Royal Society B: Biological Sciences*, *372*(1715). https://doi.org/10.1098/RSTB.2016.0413

Gachon, F., Fonjallaz, P., Damiola, F., Gos, P., Kodama, T., Zakany, J., Duboule, D., Petit, B., Tafti, M., & Schibler, U. (2004). The loss of circadian PAR bZip transcription factors results in epilepsy. *Genes & Development*, *18*(12), 1397. https://doi.org/10.1101/GAD.301404

Gaiano, N., Nye, J. S., & Fishell, G. (2000). Radial glial identity is promoted by Notch1 signaling in the murine forebrain. *Neuron*, *26*(2), 395–404. https://doi.org/10.1016/S0896-6273(00)81172-1

Galanis, C., & Vlachos, A. (2020). Hebbian and Homeostatic Synaptic Plasticity—Do Alterations of One Reflect Enhancement of the Other? *Frontiers in Cellular Neuroscience*, *14*, 50. https://doi.org/10.3389/FNCEL.2020.00050/BIBTEX

Gandolfi, D., Cerri, S., Mapelli, J., Polimeni, M., Tritto, S., Fuzzati-Armentero, M. T., Bigiani, A., Blandini, F., Mapelli, L., & D'Angelo, E. (2017). Activation of the CREB/c-Fos Pathway during Long-Term Synaptic Plasticity in the Cerebellum Granular Layer. *Frontiers in Cellular Neuroscience*, *11*. https://doi.org/10.3389/FNCEL.2017.00184

Gao, M., Sossa, K., Song, L., Errington, L., Cummings, L., Hwang, H., Kuhl, D., Worley, P., & Lee, H. K. (2010). A Specific Requirement of Arc/Arg3.1 for Visual Experience-Induced Homeostatic Synaptic Plasticity in Mouse Primary Visual Cortex. *The Journal of Neuroscience*, *30*(21), 7168–7178. https://doi.org/10.1523/JNEUROSCI.1067-10.2010

Gascón, S., Murenu, E., Masserdotti, G., Ortega, F., Russo, G. L., Petrik, D., Deshpande, A., Heinrich, C., Karow, M., Robertson, S. P., Schroeder, T., Beckers, J., Irmler, M., Berndt, C., Angeli, J. P., Conrad, M., Berninger, B., & Götz, M. (2016). Identification and Successful Negotiation of a Metabolic Checkpoint in Direct Neuronal Reprogramming. *Cell stem cell*, *18*(3), 396–409. https://doi.org/10.1016/J.STEM.2015.12.003

Gaspard, N., & Vanderhaeghen, P. (2011). Laminar fate specification in the cerebral cortex. *F1000 biology reports*, *3*(1). https://doi.org/10.3410/B3-6

Ge, S., Sailor, K. A., Ming, G. L., & Song, H. (2008). Synaptic integration and plasticity of new neurons in the adult hippocampus. *Journal of Physiology*, *586*(16), 3759–3765. https://doi.org/10.1113/JPHYSIOL.2008.155655

Georgias, C., Wasser, M., & Hinz, U. (1997). A basic-helix-loop-helix protein expressed in precursors of Drosophila longitudinal visceral muscles. *Mechanisms of Development*, *69*(1-2), 115–124. https://doi.org/10.1016/S0925-4773(97)00169-X

Gilbert., S. F. (2000). Developmental Biology - NCBI Bookshelf. Retrieved June 5, 2022, from https://www.ncbi.nlm.nih.gov/books/NBK9983/

Goel, A., Xu, L. W., Snyder, K. P., Song, L., Goenaga-Vazquez, Y., Megill, A., Takamiya, K., Huganir, R. L., & Lee, H. K. (2011). Phosphorylation of AMPA receptors is required for sensory deprivation-induced homeostatic synaptic plasticity. *PloS one*, *6*(3). https://doi.org/10.1371/JOURNAL.PONE.0018264

Gohlke, J. M., Armant, O., Parham, F. M., Smith, M. V., Zimmer, C., Castro, D. S., Nguyen, L., Parker, J. S., Gradwohl, G., Portier, C. J., & Guillemot, F. (2008). Characterization of the proneural gene regulatory network during mouse telencephalon development. *BMC Biology*, *6*(1), 1–18. https://doi.org/10.1186/1741-7007-6-15/FIGURES/5

Gonçalves, J. T., Schafer, S. T., & Gage, F. H. (2016). Adult Neurogenesis in the Hippocampus: From Stem Cells to Behavior. *Cell*, *167*(4), 897–914. https://doi.org/10.1016/J.CELL.2016.10.021

Gonzalez-Islas, C., Bülow, P., & Wenner, P. (2018). Regulation of synaptic scaling by action potential–independent miniature neurotransmission. *Journal of Neuroscience Research*, *96*(3), 348–353. https://doi.org/10.1002/jnr.24138

Gonzalez-Ramos, A., Waloschková, E., Mikroulis, A., Kokaia, Z., Bengzon, J., Ledri, M., Andersson, M., & Kokaia, M. (2021). Human stem cell-derived GABAergic neurons functionally integrate into human neuronal networks. *Scientific Reports 2021 11:1*, *11*(1), 1–16. https://doi.org/10.1038/s41598-021-01270-x

Götz, M., Nakafuku, M., & Petrik, D. (2016). Neurogenesis in the Developing and Adult Brain-Similarities and Key Differences. *Cold Spring Harbor perspectives in biology*, *8*(7). https://doi.org/10.1101/CSHPERSPECT.A018853

Götz, M., Stoykova, A., & Gruss, P. (1998). Pax6 controls radial glia differentiation in the cerebral cortex. *Neuron*, *21*(5), 1031–1044. https://doi.org/10.1016/S0896-6273(00)80621-2

Grade, S., Thomas, J., Zarb, Y., Thorwirth, M., Conzelmann, K. K., Hauck, S. M., & Götz, M. (2022). Brain injury environment critically influences the connectivity of transplanted neurons. *Science advances*, *8*(23). https://doi.org/10.1126/SCIADV.ABG9445

Grande, A., Sumiyoshi, K., López-Juárez, A., Howard, J., Sakthivel, B., Aronow, B., Campbell, K., & Nakafuku, M. (2013). Environmental impact on direct neuronal reprogramming in vivo in the adult brain. *Nature communications*, *4*. https://doi.org/10.1038/NCOMMS3373

Gray, J. M., & Spiegel, I. (2019). Cell-type-specific programs for activity-regulated gene expression. *Current Opinion in Neurobiology*, *56*, 33–39. https://doi.org/10.1016/j.conb.2018.11.001

Greenberg, M. E., & Ziff Edward B. (1984). Stimulation of 3T3 cells induces transcription of the c-fos proto-oncogene. *Nature 1984 311:5985*, *311*(5985), 433–438. https://doi.org/10.1038/311433a0

Guillemot, F., Lo, L. C., Johnson, J. E., Auerbach, A., Anderson, D. J., & Joyner, A. L. (1993). Mammalian achaete-scute homolog 1 is required for the early development of olfactory and autonomic neurons. *Cell*, *75*(3), 463–476. https://doi.org/10.1016/0092-8674(93)90381-Y

Guo, Z., Zhang, L., Wu, Z., Chen, Y., Wang, F., & Chen, G. (2014). In vivo direct reprogramming of reactive glial cells into functional neurons after brain injury and in an Alzheimer's disease model. *Cell stem cell*, *14*(2), 188–202. https://doi.org/10.1016/J.STEM.2013.12.001

Gurdon, J. B. (1962). The developmental capacity of nuclei taken from intestinal epithelium cells of feeding tadpoles - PubMed. Retrieved September 2, 2022, from https://pubmed.ncbi.nlm.nih.gov/13951335/

Guzelsoy, G., Akkaya, C., Atak, D., Dunn, C. D., Kabakcioglu, A., Ozlu, N., & Ince-Dunn, G. (2019). Terminal neuron localization to the upper cortical plate is controlled by the transcription factor NEUROD2. *Scientific Reports 2019 9:1*, *9*(1), 1–12. https://doi.org/10.1038/s41598-019-56171-x

Guzowski, J. F., Setlow, B., Wagner, E. K., & McGaugh, J. L. (2001). Experience-dependent gene expression in the rat hippocampus after spatial learning: a comparison of the immediate-early genes Arc, c-fos, and zif268. *The Journal of neuroscience : the official journal of the Society for Neuroscience*, *21*(14), 5089–5098. https://doi.org/10.1523/JNEUROSCI.21-14-05089.2001

Haines, D. E., & Mihailoff, G. A. (2018). The Telencephalon. *Fundamental Neuroscience for Basic and Clinical Applications: Fifth Edition*, 225–240.e1. https://doi.org/10.1016/B978-0-323-39632-5.00016-5

Han, E. B., & Stevens, C. F. (2009). Development regulates a switch between postand presynaptic strengthening in response to activity deprivation. *Proceedings of the National Academy of Sciences of the United States of America*, *106*(26), 10817–10822. https://doi.org/10.1073/pnas.0903603106

Han, S., Dennis, D. J., Balakrishnan, A., Dixit, R., Britz, O., Zinyk, D., Touahri, Y., Olender, T., Brand, M., Guillemot, F., Kurrasch, D., & Schuurmans, C. (2018). A non-canonical role for the proneural gene Neurog1 as a negative regulator of neocortical neurogenesis. *Development (Cambridge, England)*, *145*(19). https://doi.org/10.1242/DEV.157719

Hand, R., Bortone, D., Mattar, P., Nguyen, L., Heng, J. I. T., Guerrier, S., Boutt, E., Peters, E., Barnes, A. P., Parras, C., Schuurmans, C., Guillemot, F., & Polleux, F. (2005). Phosphorylation of Neurogenin2 specifies the migration properties and

the dendritic morphology of pyramidal neurons in the neocortex. *Neuron*, *48*(1), 45–62. https://doi.org/10.1016/J.NEURON.2005.08.032

Harnett, D., Ambrozkiewicz, M. C., Zinnall, U., Rusanova, A., Borisova, E., Drescher, A. N., Couce-Iglesias, M., Villamil, G., Dannenberg, R., Imami, K., Münster-Wandowski, A., Fauler, B., Mielke, T., Selbach, M., Landthaler, M., Spahn, C. M. T., Tarabykin, V., Ohler, U., & Kraushar, M. L. (2022). A critical period of translational control during brain development at codon resolution. *Nature Structural & Molecular Biology 2022 29:12*, *29*(12), 1277–1290. https://doi.org/10.1038/s41594-022-00882-9

Hatakeyama, J., Tomita, K., Inoue, T., & Kageyama, R. (2001). Roles of homeobox and bHLH genes in specification of a retinal cell type. *Development (Cambridge, England)*, *128*(8), 1313–1322. https://doi.org/10.1242/DEV.128.8.1313

Heavner, W. E., Lautz, J. D., Speed, H. E., Gniffke, E. P., Immendorf, K. B., Welsh, J. P., Baertsch, N. A., & Smith, S. E. (2021). Remodeling of the homer-shank interactome mediates homeostatic plasticity. *Science Signaling*, *14*(681), 7325. https://doi.org/10.1126/SCISIGNAL.ABD7325/SUPPL_FILE/ABD7325_SM.PDF activity-regulated postsynaptic protein interaction network (PIN) in mice. This PIN changed differentially to prolonged increases in activity compared to prolonged decreases and to the activity manipulations performed in culture compared to those performed in vivo. Some of the changes in this PIN did not occur in mice lacking either Homer1 or Shank3, scaffolding protein–encoding genes that are mutated in some patients with autism spectrum disorder. The findings begin to elucidate the complexity and context dependence of homeostatic synaptic plasticity

Heinrich, C., Bergami, M., Gascón, S., Lepier, A., Viganò, F., Dimou, L., Sutor, B., Berninger, B., & Götz, M. (2014). Sox2-mediated conversion of NG2 glia into induced neurons in the injured adult cerebral cortex. *Stem cell reports*, *3*(6), 1000–1014. https://doi.org/10.1016/J.STEMCR.2014.10.007

Heinrich, C., Blum, R., Gascón, S., Masserdotti, G., Tripathi, P., Sánchez, R., Tiedt, S., Schroeder, T., Götz, M., & Berninger, B. (2010). Directing astroglia from the cerebral cortex into subtype specific functional neurons. *PLoS biology*, *8*(5). https://doi.org/10.1371/JOURNAL.PBIO.1000373

Heinrich, C., Gascón, S., Masserdotti, G., Lepier, A., Sanchez, R., Simon-Ebert, T., Schroeder, T., Gøtz, M., & Berninger, B. (2011). Generation of subtype-specific neurons from postnatal astroglia of the mouse cerebral cortex. *Nature protocols*, *6*(2), 214–228. https://doi.org/10.1038/NPROT.2010.188

Heinrich, C., Götz, M., & Berninger, B. (2012). Reprogramming of postnatal astroglia of the mouse neocortex into functional, synapse-forming neurons. *Methods in molecular biology (Clifton, N.J.)*, *814*, 485–498. https://doi.org/10.1007/978-1-61779-452-0_32

Heins, N., Malatesta, P., Cecconi, F., Nakafuku, M., Tucker, K. L., Hack, M. A., Chapouton, P., Barde, Y. A., & Goötz, M. (2002). Glial cells generate neurons: the role of the transcription factor Pax6. *Nature neuroscience*, *5*(4), 308–315. https://doi.org/10.1038/NN828

Heir, R., & Stellwagen, D. (2020). TNF-Mediated Homeostatic Synaptic Plasticity: From in vitro to in vivo Models. *Frontiers in Cellular Neuroscience*, *14*, 297. https://doi.org/10.3389/FNCEL.2020.565841/BIBTEX

Henley, J. M., & Wilkinson, K. A. (2013). AMPA receptor trafficking and the mechanisms underlying synaptic plasticity and cognitive aging. *Dialogues in Clinical Neuroscience*, *15*(1), 11. https://doi.org/10.31887/DCNS.2013.15.1/JHENLEY

Herculano-Houzel, S., Mota, B., & Lent, R. (2006). Cellular scaling rules for rodent brains. *Proceedings of the National Academy of Sciences*, *103*(32), 12138–12143. https://doi.org/10.1073/pnas.0604911103

Herrero-Navarro, Á., Puche-Aroca, L., Moreno-Juan, V., Sempere-Ferràndez, A., Espinosa, A., Susín, R., Torres-Masjoan, L., Leyva-Díaz, E., Karow, M., Figueres-Oñate, M., López-Mascaraque, L., López-Atalaya, J. P., Berninger, B., & López-Bendito, G. (2021). Astrocytes and neurons share region-specific transcriptional signatures that confer regional identity to neuronal reprogramming. *Science advances*, *7*(15). https://doi.org/10.1126/SCIADV.ABE8978

Herring, C. A., Simmons, R. K., Freytag, S., Poppe, D., Moffet, J. J., Pflueger, J., Buckberry, S., Vargas-Landin, D. B., Clément, O., Echeverría, E. G., Sutton, G. J., Alvarez-Franco, A., Hou, R., Pflueger, C., McDonald, K., Polo, J. M., Forrest, A. R., Nowak, A. K., Voineagu, I., … Lister, R. (2022). Human prefrontal cortex gene regulatory dynamics from gestation to adulthood at single-cell resolution. *Cell*, *185*(23), 4428–4447.e28. https://doi.org/10.1016/J.CELL.2022.09.039/ATTACHMENT/553E2A11-824B-41B7-9A51-52D35A40D1A4/MMC6.XLSX

Higashimoto, T., Urbinati, F., Perumbeti, A., Jiang, G., Zarzuela, A., Chang, L. J., Kohn, D. B., & Malik, P. (2007). The woodchuck hepatitis virus post-transcriptional regulatory element reduces readthrough transcription from retroviral vectors. *Gene therapy*, *14*(17), 1298–1304. https://doi.org/10.1038/SJ.GT.3302979

Hippenmeyer, S. (2023). Principles of neural stem cell lineage progression: Insights from developing cerebral cortex. *Current opinion in neurobiology*, *79*. https://doi.org/10.1016/J.CONB.2023.102695

Hodge, R. D., Bakken, T. E., Miller, J. A., Smith, K. A., Barkan, E. R., Graybuck, L. T., Close, J. L., Long, B., Johansen, N., Penn, O., Yao, Z., Eggermont, J., Höllt, T., Levi, B. P., Shehata, S. I., Aevermann, B., Beller, A., Bertagnolli, D., Brouner, K., … Lein, E. S. (2019). Conserved cell types with divergent features in human versus mouse cortex. *Nature*, *573*(7772), 61–68. https://doi.org/10.1038/S41586-019-1506-7

Hoey, S. E., Williams, R. J., & Perkinton, M. S. (2009). Synaptic NMDA Receptor Activation Stimulates α-Secretase Amyloid Precursor Protein Processing and Inhibits Amyloid-β Production. *Journal of Neuroscience*, *29*(14), 4442–4460. https://doi.org/10.1523/JNEUROSCI.6017-08.2009

Hong, E. J., McCord, A. E., & Greenberg, M. E. (2008). A Biological Function for the Neuronal Activity-Dependent Component of Bdnf Transcription in the Development of Cortical Inhibition. *Neuron*, *60*(4), 610–624. https://doi.org/10.1016/j.neuron.2008.09.024

Hong, J. C. (2016). General Aspects of Plant Transcription Factor Families. *Plant Transcription Factors: Evolutionary, Structural and Functional Aspects*, 35–56. https://doi.org/10.1016/B978-0-12-800854-6.00003-8

Hou, H., Sun, L., Siddoway, B. A., Petralia, R. S., Yang, H., Gu, H., Nairn, A. C., & Xia, H. (2013). Synaptic NMDA receptor stimulation activates PP1 by inhibiting its phosphorylation by Cdk5. *Journal of Cell Biology*, *203*(3), 521–535. https://doi.org/10.1083/JCB.201303035

Hrvatin, S., Hochbaum, D. R., Nagy, M. A., Cicconet, M., Robertson, K., Cheadle, L., Zilionis, R., Ratner, A., Borges-Monroy, R., Klein, A. M., Sabatini, B. L., & Greenberg, M. E. (2018). Single-cell analysis of experience-dependent transcriptomic states in the mouse visual cortex. *Nature Neuroscience*, *21*(1), 120–129. https://doi.org/10.1038/s41593-017-0029-5

Huang, M., Pieraut, S., Cao, J., Polli, F. d. S., Roncace, V., Shen, G., & Maximov, A. (2022). Nr4a1 regulates inhibitory circuit structure and function in the mouse brain. *bioRxiv*, 2022.06.14.496205. https://doi.org/10.1101/2022.06.14.496205

Hulme, A. J., Maksour, S., St-Clair Glover, M., Miellet, S., & Dottori, M. (2022). Making neurons, made easy: The use of Neurogenin-2 in neuronal differentiation. *Stem cell reports*, *17*(1), 14–34. https://doi.org/10.1016/J.STEMCR.2021.11.015

Huupponen, J., Atanasova, T., Taira, T., & Lauri, S. E. (2016). GluA4 subunit of AMPA receptors mediates the early synaptic response to altered network activity in the developing hippocampus. *Journal of Neurophysiology*, *115*(6), 2989. https://doi.org/10.1152/JN.00435.2015

iN immature synapse, Gria4 GluA4

Ibata, K., Sun, Q., & Turrigiano, G. G. (2008). Rapid synaptic scaling induced by changes in postsynaptic firing. *Neuron*, *57*(6), 819–826. https://doi.org/10.1016/J.NEURON.2008.02.031

Ieda, M., Fu, J. D., Delgado-Olguin, P., Vedantham, V., Hayashi, Y., Bruneau, B. G., & Srivastava, D. (2010). Direct reprogramming of fibroblasts into functional cardiomyocytes by defined factors. *Cell*, *142*(3), 375–386. https://doi.org/10.1016/J.CELL.2010.07.002

Iemolo, A., Montilla-Perez, P., Lai, I. C., Meng, Y., Nolan, S., Wen, J., Rusu, I., Dulcis, D., & Telese, F. (2020). A cell type-specific expression map of NCoR1 and SMRT transcriptional co-repressors in the mouse brain. *The Journal of comparative neurology*, *528*(13), 2218. https://doi.org/10.1002/CNE.24886

Imayoshi, I., & Kageyama, R. (2014). bHLH factors in self-renewal, multipotency, and fate choice of neural progenitor cells. *Neuron*, *82*(1), 9–23. https://doi.org/10.1016/J.NEURON.2014.03.018

Ince-Dunn, G., Hall, B. J., Hu, S. C., Ripley, B., Huganir, R. L., Olson, J. M., Tapscott, S. J., & Ghosh, A. (2006). Regulation of Thalamocortical Patterning and Synaptic Maturation by NeuroD2. *Neuron*, *49*(5), 683–695. https://doi.org/10.1016/J.NEURON.2006.01.031

Inquimbert, P., Bartels, K., Babaniyi, O. B., Barrett, L. B., Tegeder, I., & Scholz, J. (2012). Peripheral nerve injury produces a sustained shift in the balance between glutamate release and uptake in the dorsal horn of the spinal cord. *Pain*, *153*(12), 2422. https://doi.org/10.1016/J.PAIN.2012.08.011

Isaac, J. T., Ashby, M., & McBain, C. J. (2007). The Role of the GluR2 Subunit in AMPA Receptor Function and Synaptic Plasticity. *Neuron*, *54*(6), 859–871. https://doi.org/10.1016/J.NEURON.2007.06.001

Jaafari, N., Henley, J. M., & Hanley, J. G. (2012). PICK1 Mediates Transient Synaptic Expression of GluA2-Lacking AMPA Receptors during Glycine-Induced AMPA Receptor Trafficking. *The Journal of Neuroscience*, *32*(34), 11618. https://doi.org/10.1523/JNEUROSCI.5068-11.2012

Jaeger, B. N., Linker, S. B., Parylak, S. L., Barron, J. J., Gallina, I. S., Saavedra, C. D., Fitzpatrick, C., Lim, C. K., Schafer, S. T., Lacar, B., Jessberger, S., & Gage, F. H. (2018). A novel environment-evoked transcriptional signature predicts reactivity in single dentate granule neurons. *Nature Communications 2018 9:1*, *9*(1), 1–15. https://doi.org/10.1038/s41467-018-05418-8

!! Cell-type specificity of activity levels and plasticity mechanisms suggests that later molecular processes may also differ across populations, including long-term changes underlying memory formation

Jang, S. S., & Chung, H. J. (2016). Emerging Link between Alzheimer's Disease and Homeostatic Synaptic Plasticity. *Neural plasticity*, *2016*. https://doi.org/10.1155/2016/7969272

Jeans, A. F., van Heusden, F. C., Al-Mubarak, B., Padamsey, Z., & Emptage, N. J. (2017). Homeostatic Presynaptic Plasticity Is Specifically Regulated by P/Q-type Ca2+ Channels at Mammalian Hippocampal Synapses. *Cell Reports*, *21*(2), 341. https://doi.org/10.1016/J.CELREP.2017.09.061

Kageyama, R., Ohtsuka, T., Shimojo, H., & Imayoshi, I. (2009). Dynamic regulation of Notch signaling in neural progenitor cells. *Current Opinion in Cell Biology*, *21*(6), 733–740. https://doi.org/10.1016/J.CEB.2009.08.009

Kaila, K., Price, T. J., Payne, J. A., Puskarjov, M., & Voipio, J. (2014). Cation-chloride cotransporters in neuronal development, plasticity and disease. *Nature Reviews Neuroscience 2014 15:10*, *15*(10), 637–654. https://doi.org/10.1038/nrn3819

Kandel, E. R. (2001). The molecular biology of memory storage: a dialogue between genes and synapses. *Science (New York, N.Y.)*, *294*(5544), 1030–1038. https://doi.org/10.1126/SCIENCE.1067020

Kanski, R., Van Strien, M. E., Van Tijn, P., & Hol, E. M. (2014). A star is born: new insights into the mechanism of astrogenesis. *Cellular and molecular life sciences : CMLS*, *71*(3), 433–447. https://doi.org/10.1007/S00018-013-1435-9

Karow, M., Gray Camp, J., Falk, S., Gerber, T., Pataskar, A., Gac-Santel, M., Kageyama, J., Brazovskaja, A., Garding, A., Fan, W., Riedemann, T., Casamassa, A., Smiyakin, A., Schichor, C., Götz, M., Tiwari, V. K., Treutlein, B., & Berninger, B. (2018). Direct pericyte-to-neuron reprogramming via unfolding of a neural stem cell-like program. *Nature Neuroscience 2018 21:7*, *21*(7), 932–940. https://doi.org/10.1038/s41593-018-0168-3

Karpova, A., Mikhaylova, M., Bera, S., Bär, J., Reddy, P. P., Behnisch, T., Rankovic, V., Spilker, C., Bethge, P., Sahin, J., Kaushik, R., Zuschratter, W., Kähne, T., Naumann, M., Gundelfinger, E. D., & Kreutz, M. R. (2013). Encoding and transducing the synaptic or extrasynaptic origin of NMDA receptor signals to the nucleus. *Cell*, *152*(5), 1119–1133. https://doi.org/10.1016/j.cell.2013.02.002

Karve, I. P., Taylor, J. M., & Crack, P. J. (2016). The contribution of astrocytes and microglia to traumatic brain injury. *British Journal of Pharmacology*, *173*(4), 692. https://doi.org/10.1111/BPH.13125

Keck, T., Keller, G. B., Jacobsen, R. I., Eysel, U. T., Bonhoeffer, T., & Hübener, M. (2013). Synaptic Scaling and Homeostatic Plasticity in the Mouse Visual Cortex In Vivo. *Neuron*, *80*(2), 327–334. https://doi.org/10.1016/J.NEURON.2013.08.018

Kelsch, W., Lin, C. W., Mosley, C. P., & Lois, C. (2009). A Critical Period for Activity-Dependent Synaptic Development during Olfactory Bulb Adult Neurogenesis. *The Journal of Neuroscience*, *29*(38), 11852. https://doi.org/10.1523/JNEUROSCI.2406-09.2009

Kempf, J., Knelles, K., Hersbach, B. A., Petrik, D., Riedemann, T., Bednarova, V., Janjic, A., Simon-Ebert, T., Enard, W., Smialowski, P., Götz, M., & Masserdotti, G. (2021). Heterogeneity of neurons reprogrammed from spinal cord astrocytes by the proneural factors Ascl1 and Neurogenin2. *Cell Reports*, *36*(3), 109409. https://doi.org/10.1016/J.CELREP.2021.109409

Kennedy, A. J., Rahn, E. J., Paulukaitis, B. S., Savell, K. E., Kordasiewicz, H. B., Wang, J., Lewis, J. W., Posey, J., Strange, S. K., Guzman-Karlsson, M. C., Phillips, S. E., Decker, K., Motley, S. T., Swayze, E. E., Ecker, D. J., Michael, T. P., Day, J. J., & Sweatt, J. D. (2016). Tcf4 Regulates Synaptic Plasticity, DNA Methylation, and Memory Function. *Cell Reports*, *16*(10), 2666–2685. https://doi.org/10.1016/J.CELREP.2016.08.004

Kharchenko, P. V., Silberstein, L., & Scadden, D. T. (2014). Bayesian approach to single-cell differential expression analysis. *Nature Methods 2014 11:7*, *11*(7), 740–742. https://doi.org/10.1038/nmeth.2967

Kilman, V., Van Rossum, M. C., & Turrigiano, G. G. (2002). Activity deprivation reduces miniature IPSC amplitude by decreasing the number of postsynaptic GABA(A) receptors clustered at neocortical synapses. *The Journal of neuroscience : the official journal of the Society for Neuroscience*, *22*(4), 1328–1337. https://doi.org/10.1523/JNEUROSCI.22-04-01328.2002

Kim, K. P., Choi, J., Yoon, J., Bruder, J. M., Shin, B., Kim, J., Arauzo-Bravo, M. J., Han, D., Wu, G., Han, D. W., Kim, J., Cramer, P., & Schöler, H. R. (2020). Permissive epigenomes endow reprogramming competence to transcriptional regulators. *Nature Chemical Biology 2020 17:1*, *17*(1), 47–56. https://doi.org/10.1038/s41589-020-0618-6

Kim, M. H., Radaelli, C., Thomsen, E. R., Monet, D., Chartrand, T., Jorstad, N. L., Mahoney, J. T., Taormina, M. J., Long, B., Baker, K., Bakken, T., Campagnola, L., Casper, T., Clark, M., Dee, N., D'orazi, F., Gamlin, C., Kalmbach, B., Kebede, S., … Lein, E. S. (2023). Target cell-specific synaptic dynamics of excitatory to inhibitory neuron connections in supragranular layers of human neocortex. *eLife*, *12*. https://doi.org/10.7554/ELIFE.81863

Kirischuk, S., Sinning, A., Blanquie, O., Yang, J. W., Luhmann, H. J., & Kilb, W. (2017). Modulation of Neocortical Development by Early Neuronal Activity: Physiology and Pathophysiology. *Frontiers in Cellular Neuroscience*, *11*. https://doi.org/10.3389/FNCEL.2017.00379

Kiselev, V. Y., Yiu, A., & Hemberg, M. (2018). scmap: projection of single-cell RNA-seq data across data sets. *Nature Methods 2018 15:5*, *15*(5), 359–362. https://doi.org/10.1038/nmeth.4644

Klingler, E., Francis, F., Jabaudon, D., & Cappello, S. (2021). Mapping the molecular and cellular complexity of cortical malformations. *Science*, *371*(6527). https://doi.org/10.1126/SCIENCE.ABA4517/ASSET/30CE620B-4299-4DF8-9AF3-C7A0EDEF631E/ASSETS/GRAPHIC/371_ABA4517_F5.JPEG

Kong, S. Y., Kim, W., Lee, H. R., & Kim, H. J. (2018). The histone demethylase KDM5A is required for the repression of astrocytogenesis and regulated by the translational

machinery in neural progenitor cells. *The FASEB Journal*, *32*(2), 1108. https://doi.org/10.1096/FJ.201700780R

Koo, B., Lee, K. H., li Ming, G., Yoon, K. J., & Song, H. (2023). Setting the clock of neural progenitor cells during mammalian corticogenesis. *Seminars in cell & developmental biology*, *142*. https://doi.org/10.1016/J.SEMCDB.2022.05.013

Koopmans, F., van Nierop, P., Andres-Alonso, M., Byrnes, A., Cijsouw, T., Coba, M. P., Cornelisse, L. N., Farrell, R. J., Goldschmidt, H. L., Howrigan, D. P., Hussain, N. K., Imig, C., de Jong, A. P., Jung, H., Kohansalnodehi, M., Kramarz, B., Lipstein, N., Lovering, R. C., MacGillavry, H., ... Verhage, M. (2019). SynGO: An Evidence-Based, Expert-Curated Knowledge Base for the Synapse. *Neuron*, *103*(2), 217–234.e4. https://doi.org/10.1016/J.NEURON.2019.05.002

Kovach, C., Dixit, R., Li, S., Mattar, P., Wilkinson, G., Elsen, G. E., Kurrasch, D. M., Hevner, R. F., & Schuurmans, C. (2013). Neurog2 simultaneously activates and represses alternative gene expression programs in the developing neocortex. *Cerebral cortex (New York, N.Y. : 1991)*, *23*(8), 1884–1900. https://doi.org/10.1093/CERCOR/BHS176

Krukoff, T. L. (2003). c-fos Expression as a Marker of Functional Activity in the Brain: Immunohistochemistry. *Cell Neurobiology Techniques*, 213–230. https://doi.org/10.1385/0-89603-510-7:213

Kuijlaars, J., Oyelami, T., Diels, A., Rohrbacher, J., Versweyveld, S., Meneghello, G., Tuefferd, M., Verstraelen, P., Detrez, J. R., Verschuuren, M., De Vos, W. H., Meert, T., Peeters, P. J., Cik, M., Nuydens, R., Brône, B., & Verheyen, A. (2016). Sustained synchronized neuronal network activity in a human astrocyte co-culture system OPEN. *Nature Publishing Group*. https://doi.org/10.1038/srep36529

La Manno, G., Siletti, K., Furlan, A., Gyllborg, D., Vinsland, E., Mossi Albiach, A., Mattsson Langseth, C., Khven, I., Lederer, A. R., Dratva, L. M., Johnsson, A., Nilsson, M., Lönnerberg, P., & Linnarsson, S. (2021). Molecular architecture of the developing mouse brain. *Nature*, *596*(7870), 92–96. https://doi.org/10.1038/S41586-021-03775-X

Lacar, B., Linker, S. B., Jaeger, B. N., Krishnaswami, S., Barron, J., Kelder, M., Parylak, S., Paquola, A., Venepally, P., Novotny, M., O'Connor, C., Fitzpatrick, C., Erwin, J., Hsu, J. Y., Husband, D., McConnell, M. J., Lasken, R., & Gage, F. H. (2016). Nuclear RNA-seq of single neurons reveals molecular signatures of activation. *Nature Communications 2016 7:1*, *7*(1), 1–13. https://doi.org/10.1038/ncomms11022

Lacomme, M., Liaubet, L., Pituello, F., & Bel-Vialar, S. (2012). NEUROG2 Drives Cell Cycle Exit of Neuronal Precursors by Specifically Repressing a Subset of Cyclins Acting at the G1 and S Phases of the Cell Cycle. *Molecular and Cellular Biology*, *32*(13), 2596. https://doi.org/10.1128/MCB.06745-11

Lahne, M., Nagashima, M., Hyde, D. R., & Hitchcock, P. F. (2020). Reprogramming Müller Glia to Regenerate Retinal Neurons. *Annual review of vision science*, *6*, 171–193. https://doi.org/10.1146/ANNUREV-VISION-121219-081808

Langille, J. J., & Brown, R. E. (2018). The Synaptic Theory of Memory: A Historical Survey and Reconciliation of Recent Opposition. *Frontiers in Systems Neuroscience*, *12*, 52. https://doi.org/10.3389/FNSYS.2018.00052

Latchman, D. S. (1997). Transcription factors: An overview. *International Journal of Biochemistry and Cell Biology*, *29*(12), 1305–1312. https://doi.org/10.1016/S1357-2725(97)00085-X

Lee, A. G., Capanzana, R., Brockhurst, J., Cheng, M. Y., Buckmaster, C. L., Absher, D., Schatzberg, A. F., & Lyons, D. M. (2016). Learning to cope with stress modulates anterior cingulate cortex stargazin expression in monkeys and mice. *Neurobiology of learning and memory*, *131*, 95–100. https://doi.org/10.1016/J.NLM.2016.03.015

Lee, H. K., & Kirkwood, A. (2019). Mechanisms of Homeostatic Synaptic Plasticity in vivo. *Frontiers in Cellular Neuroscience*, *13*, 520. https://doi.org/10.3389/FNCEL.2019.00520/BIBTEX

Lee, K. Y., Royston, S. E., Vest, M. O., Ley, D. J., Lee, S., Bolton, E. C., & Chung, H. J. (2015). N-methyl-D-aspartate receptors mediate activity-dependent down-regulation of potassium channel genes during the expression of homeostatic intrinsic plasticity. *Molecular Brain*, *8*(1), 1–16. https://doi.org/10.1186/s13041-015-0094-1

LeMasson, G., Marder, E., & Abbott, L. F. (1993). Activity-dependent regulation of conductances in model neurons. *Science (New York, N.Y.)*, *259*(5103), 1915–1917. https://doi.org/10.1126/SCIENCE.8456317

Lentini, C., D'Orange, M., Marichal, N., Trottmann, M.-M., Vignoles, R., Foucault, L., Verrier, C., Massera, C., Raineteau, O., Conzelmann, K.-K., Rival-Gervier, S., Depaulis, A., Berninger, B., & Heinrich, C. (2021). Reprogramming reactive glia into interneurons reduces chronic seizure activity in a mouse model of mesial temporal lobe epilepsy. *Cell Stem Cell*. https://doi.org/10.1016/J.STEM.2021.09.002

Leslie, J. H., & Nedivi, E. (2011). Activity-regulated genes as mediators of neural circuit plasticity. *Progress in neurobiology*, *94*(3), 223–237. https://doi.org/10.1016/J.PNEUROBIO.2011.05.002

Leung, H.-W., Wei, G., Foo, Q., & Vandongen, A. M. J. (2019). Arc Regulates Transcription of Genes for Plasticity, Excitability and Alzheimer's Disease. *bioRxiv*, 833988. https://doi.org/10.1101/833988

Li, S., Mattar, P., Zinyk, D., Singh, K., Chaturvedi, C. P., Kovach, C., Dixit, R., Kurrasch, D. M., Ma, Y. C., Chan, J. A., Wallace, V., Dilworth, F. J., Brand, M., & Schuurmans, C. (2012). GSK3 Temporally Regulates Neurogenin 2 Proneural Activity in the

Neocortex. *Journal of Neuroscience*, *32*(23), 7791–7805. https://doi.org/10.1523/JNEUROSCI.1309-12.2012

Li, X., Liu, G., Yang, L., Li, Z., Zhang, Z., Xu, Z., Cai, Y., Du, H., Su, Z., Wang, Z., Duan, Y., Chen, H., Shang, Z., You, Y., Zhang, Q., He, M., Chen, B., & Yang, Z. (2021). Decoding Cortical Glial Cell Development. *Neuroscience Bulletin*, *37*(4), 440–460. https://doi.org/10.1007/S12264-021-00640-9/FIGURES/9

Li, Y., Fan, T., Li, X., Liu, L., Mao, F., Li, Y., Miao, Z., Zeng, C., Song, W., Pan, J., Zhou, S., Wang, H., Wang, Y., & Sun, Z. S. (2022). Npas3 deficiency impairs cortical astrogenesis and induces autistic-like behaviors. *Cell reports*, *40*(9). https://doi.org/10.1016/J.CELREP.2022.111289

Libé-Philippot, B., & Vanderhaeghen, P. (2021). Cellular and Molecular Mechanisms Linking Human Cortical Development and Evolution. *Annual Review of Genetics*, *55*, 555–581. https://doi.org/10.1146/annurev-genet-071719

Lin, H. C., He, Z., Ebert, S., Schörnig, M., Santel, M., Nikolova, M. T., Weigert, A., Hevers, W., Kasri, N. N., Taverna, E., Camp, J. G., & Treutlein, B. (2021a). NGN2 induces diverse neuron types from human pluripotency. *Stem Cell Reports*, *16*(9), 2118–2127. https://doi.org/10.1016/J.STEMCR.2021.07.006

Lin, H. C., He, Z., Ebert, S., Schörnig, M., Santel, M., Nikolova, M. T., Weigert, A., Hevers, W., Kasri, N. N., Taverna, E., Camp, J. G., & Treutlein, B. (2021b). NGN2 induces diverse neuron types from human pluripotency. *Stem Cell Reports*, *16*(9), 2118–2127. https://doi.org/10.1016/J.STEMCR.2021.07.006

Lisman, J., Yasuda, R., & Raghavachari, S. (2012). Mechanisms of CaMKII action in long-term potentiation. *Nature reviews. Neuroscience*, *13*(3), 169. https://doi.org/10.1038/NRN3192

Little, S. C., & Mullins, M. C. (2006). Extracellular modulation of BMP activity in patterning the dorsoventral axis. *Birth Defects Research Part C: Embryo Today: Reviews*, *78*(3), 224–242. https://doi.org/10.1002/BDRC.20079

Liu, J., Yang, M., Su, M., Liu, B., Zhou, K., Sun, C., Ba, R., Yu, B., Zhang, B., Zhang, Z., Fan, W., Wang, K., Zhong, M., Han, J., & Zhao, C. (2022). FOXG1 sequentially orchestrates subtype specification of postmitotic cortical projection neurons. *Science advances*, *8*(21). https://doi.org/10.1126/SCIADV.ABH3568

Liu, Y., Beyer, A., & Aebersold, R. (2016). On the Dependency of Cellular Protein Levels on mRNA Abundance. *Cell*, *165*(3), 535–550. https://doi.org/10.1016/J.CELL.2016.03.014

Llorca, A., & Deogracias, R. (2022). Origin, Development, and Synaptogenesis of Cortical Interneurons. *Frontiers in neuroscience*, *16*. https://doi.org/10.3389/FNINS.2022.929469

Lo, L., Dormand, E., Greenwood, A., & Anderson, D. J. (2002). Comparison of the generic neuronal differentiation and neuron subtype specification functions of mammalian achaete-scute and atonal homologs in cultured neural progenitor cells. *Development (Cambridge, England)*, *129*(7), 1553–1567. https://doi.org/10.1242/DEV.129.7.1553

Lohmann, C., & Kessels, H. W. (2014). The developmental stages of synaptic plasticity. *The Journal of physiology*, *592*(1), 13–31. https://doi.org/10.1113/JPHYSIOL.2012.235119

Louros, S. R., Hooks, B. M., Litvina, L., Carvalho, A. L., & Chen, C. (2014). A Role for Stargazin in Experience-Dependent Plasticity. *Cell reports*, *7*(5), 1614. https://doi.org/10.1016/J.CELREP.2014.04.054

Love, M. I., Huber, W., & Anders, S. (2014). Moderated estimation of fold change and dispersion for RNA-seq data with DESeq2. *Genome Biology*, *15*(12), 1–21. https://doi.org/10.1186/S13059-014-0550-8/FIGURES/9

Lubin, F. D., Roth, T. L., & Sweatt, J. D. (2008). Epigenetic regulation of BDNF gene transcription in the consolidation of fear memory. *The Journal of neuroscience : the official journal of the Society for Neuroscience*, *28*(42), 10576–10586. https://doi.org/10.1523/JNEUROSCI.1786-08.2008

Luchkina, N. V., Huupponen, J., Clarke, V. R., Coleman, S. K., Keinänen, K., Taira, T., & Lauri, S. E. (2014). Developmental switch in the kinase dependency of long-term potentiation depends on expression of GluA4 subunit-containing AMPA receptors. *Proceedings of the National Academy of Sciences of the United States of America*, *111*(11), 4321–4326. https://doi.org/10.1073/PNAS.1315769111/SUPPL_FILE/PNAS.201315769SI.PDF

Luecken, M. D., & Theis, F. J. (2019). Current best practices in single-cell RNA-seq analysis: a tutorial. *Molecular Systems Biology*, *15*(6). https://doi.org/10.15252/MSB.20188746

Luginbuhl, J., Kouno, T., Nakano, R., Chater, T. E., Sivaraman, D. M., Kishima, M., Roudnicky, F., Carninci, P., Plessy, C., & Shin, J. W. (2021). Decoding Neuronal Diversification by Multiplexed Single-cell RNA-Seq. *Stem cell reports*, *16*(4), 810–824. https://doi.org/10.1016/J.STEMCR.2021.02.006

Luo, C., Keown, C. L., Kurihara, L., Zhou, J., He, Y., Li, J., Castanon, R., Lucero, J., Nery, J. R., Sandoval, J. P., Bui, B., Sejnowski, T. J., Harkins, T. T., Mukamel, E. A., Behrens, M. M., & Ecker, J. R. (2017). Single-cell methylomes identify neuronal subtypes and regulatory elements in mammalian cortex. *Science (New York, N.Y.)*, *357*(6351), 600–604. https://doi.org/10.1126/SCIENCE.AAN3351

Lüscher, C., & Malenka, R. C. (2012). NMDA Receptor-Dependent Long-Term Potentiation and Long-Term Depression (LTP/LTD). *Cold Spring Harbor Perspectives in Biology*, *4*(6), 1–15. https://doi.org/10.1101/CSHPERSPECT.A005710

Lyford, G. L., Yamagata, K., Kaufmann, W. E., Barnes, C. A., Sanders, L. K., Copeland, N. G., Gilbert, D. J., Jenkins, N. A., Lanahan, A. A., & Worley, P. F. (1995). Arc, a growth factor and activity-regulated gene, encodes a novel cytoskeleton-associated protein that is enriched in neuronal dendrites. *Neuron*, *14*(2), 433–445. https://doi.org/10.1016/0896-6273(95)90299-6

Lyst, M. J., Ekiert, R., Ebert, D. H., Merusi, C., Nowak, J., Selfridge, J., Guy, J., Kastan, N. R., Robinson, N. D., De Lima Alves, F., Rappsilber, J., Greenberg, M. E., & Bird, A. (2013). Rett syndrome mutations abolish the interaction of MeCP2 with the NCoR/SMRT co-repressor. *Nature neuroscience*, *16*(7), 898–902. https://doi.org/10.1038/NN.3434

Ma, Y. C., Song, M. R., Park, J. P., Henry Ho, H. Y., Hu, L., Kurtev, M. V., Zieg, J., Ma, Q., Pfaff, S. L., & Greenberg, M. E. (2008). Regulation of Motor Neuron Specification by GSK3-Mediated Phosphorylation of Neurogenin 2. *Neuron*, *58*(1), 65. https://doi.org/10.1016/J.NEURON.2008.01.037

Madabhushi, R., & Kim, T.-K. (2018). Emerging themes in neuronal activity-dependent gene expression HHS Public Access. *Mol Cell Neurosci*, *87*, 27–34. https://doi.org/10.1016/j.mcn.2017.11.009

Maffei, A., & Turrigiano, G. G. (2008). Multiple Modes of Network Homeostasis in Visual Cortical Layer 2/3. *The Journal of Neuroscience*, *28*(17), 4377. https://doi.org/10.1523/JNEUROSCI.5298-07.2008

Malatesta, P., Hartfuss, E., & Götz, M. (2000). Isolation of radial glial cells by fluorescent-activated cell sorting reveals a neuronal lineage. *Development (Cambridge, England)*, *127*(24), 5253–5263. https://doi.org/10.1242/DEV.127.24.5253

Malatesta, P., Appolloni, I., & Calzolari, F. (2008). Radial glia and neural stem cells. *Cell and Tissue Research*, *331*(1), 165–178. https://doi.org/10.1007/S00441-007-0481-8/FIGURES/5

Malatesta, P., Hack, M. A., Hartfuss, E., Kettenmann, H., Klinkert, W., Kirchhoff, F., & Götz, M. (2003). Neuronal or glial progeny: regional differences in radial glia fate. *Neuron*, *37*(5), 751–764. https://doi.org/10.1016/S0896-6273(03)00116-8

Malik, A. N., Vierbuchen, T., Hemberg, M., Rubin, A. A., Ling, E., Couch, C. H., Stroud, H., Spiegel, I., Farh, K. K. H., Harmin, D. A., & Greenberg, M. E. (2014). Genome-wide identification and characterization of functional neuronal activity-dependent enhancers. *Nature Neuroscience*, *17*(10), 1330–1339. https://doi.org/10.1038/NN.3808

Mall, M., Kareta, M. S., Chanda, S., Ahlenius, H., Perotti, N., Zhou, B., Grieder, S. D., Ge, X., Drake, S., Euong Ang, C., Walker, B. M., Vierbuchen, T., Fuentes, D. R., Brennecke, P., Nitta, K. R., Jolma, A., Steinmetz, L. M., Taipale, J., Südhof, T. C., & Wernig, M. (2017). Myt1l safeguards neuronal identity by actively repressing many non-neuronal fates. *Nature 2016 544:7649*, *544*(7649), 245–249. https://doi.org/10.1038/nature21722

Mann, R., Mulligan, R. C., & Baltimore, D. (1983). Construction of a retrovirus packaging mutant and its use to produce helper-free defective retrovirus. *Cell*, *33*(1), 153–159. https://doi.org/10.1016/0092-8674(83)90344-6

Manuel, M., Tan, K. B., Kozic, Z., Molinek, M., Marcos, T. S., Razak, M. F. A., Dobolyi, D., Dobie, R., Henderson, B. E., Henderson, N. C., Chan, W. K., Daw, M. I., Mason, J. O., & Price, D. J. (2022). Pax6 limits the competence of developing cerebral cortical cells to respond to inductive intercellular signals. *PLOS Biology*, *20*(9), e3001563. https://doi.org/10.1371/JOURNAL.PBIO.3001563

Mao, W., Salzberg, A. C., Uchigashima, M., Hasegawa, Y., Hock, H., Watanabe, M., Akbarian, S., Kawasawa, Y. I., & Futai, K. (2018). Activity-Induced Regulation of Synaptic Strength through the Chromatin Reader L3mbtl1. *Cell reports*, *23*(11), 3209–3222. https://doi.org/10.1016/J.CELREP.2018.05.028

Mardinly, A. R., Spiegel, I., Patrizi, A., Centofante, E., Bazinet, J. E., Tzeng, C. P., Mandel-Brehm, C., Harmin, D. A., Adesnik, H., Fagiolini, M., & Greenberg, M. E. (2016). Sensory experience regulates cortical inhibition by inducing IGF-1 in VIP neurons. *Nature*, *531*(7594), 371. https://doi.org/10.1038/NATURE17187

Martynoga, B., Drechsel, D., & Guillemot, F. (2012). Molecular Control of Neurogenesis: A View from the Mammalian Cerebral Cortex. *Cold Spring Harbor Perspectives in Biology*, *4*(10). https://doi.org/10.1101/CSHPERSPECT.A008359

Masserdotti, G., Gillotin, S., Sutor, B., Drechsel, D., Irmler, M., Jørgensen, H. F., Sass, S., Theis, F. J., Beckers, J., Berninger, B., Guillemot, F., & Götz, M. (2015). Transcriptional Mechanisms of Proneural Factors and REST in Regulating Neuronal Reprogramming of Astrocytes. *Cell Stem Cell*, *17*(1), 74–88. https://doi.org/10.1016/j.stem.2015.05.014

Matsuzaki, M., Honkura, N., Ellis-Davies, G. C., & Kasai, H. (2004). Structural basis of long-term potentiation in single dendritic spines. *Nature 2004 429:6993*, *429*(6993), 761–766. https://doi.org/10.1038/nature02617

Mattugini, N., Bocchi, R., Scheuss, V., Russo, G. L., Torper, O., Lao, C. L., & Götz, M. (2019). Inducing Different Neuronal Subtypes from Astrocytes in the Injured Mouse Cerebral Cortex. *Neuron*, *103*(6), 1086–1095.e5. https://doi.org/10.1016/J.NEURON.2019.08.009

McInnes, L., Healy, J., & Melville, J. (2018). UMAP: Uniform Manifold Approximation and Projection for Dimension Reduction. https://doi.org/10.48550/arxiv.1802.03426

McKenna, W. L., Betancourt, J., Larkin, K. A., Abrams, B., Guo, C., Rubenstein, J. L., & Chen, B. (2011). Tbr1 and Fezf2 Regulate Alternate Corticofugal Neuronal Identities during Neocortical Development. *The Journal of Neuroscience*, *31*(2), 549. https://doi.org/10.1523/JNEUROSCI.4131-10.2011

McKenna, W. L., Ortiz-Londono, C. F., Mathew, T. K., Hoang, K., Katzman, S., & Chen, B. (2015). Mutual regulation between Satb2 and Fezf2 promotes subcerebral projection neuron identity in the developing cerebral cortex. *Proceedings of the National Academy of Sciences of the United States of America*, *112*(37), 11702–11707. https://doi.org/10.1073/PNAS.1504144112/-/DCSUPPLEMENTAL

McLaughlin, C. N., & Broihier, H. T. (2018). Keeping Neurons Young and Foxy: FoxOs Promote Neuronal Plasticity. *Trends in Genetics*, *34*(1), 65–78. https://doi.org/10.1016/j.tig.2017.10.002

McMahon, J. A., Takada, S., Zimmerman, L. B., Fan, C. M., Harland, R. M., & McMahon, A. P. (1998). Noggin-mediated antagonism of BMP signaling is required for growth and patterning of the neural tube and somite. *Genes & Development*, *12*(10), 1438. https://doi.org/10.1101/GAD.12.10.1438

Meenakshi, P., Kumar, S., & Balaji, J. (2021). In vivo imaging of immediate early gene expression dynamics segregates neuronal ensemble of memories of dual events. *Molecular brain*, *14*(1), 102. https://doi.org/10.1186/S13041-021-00798-3/FIGURES/6

Michelsen, K. A., Acosta-Verdugo, S., Benoit-Marand, M., Espuny-Camacho, I., Gaspard, N., Saha, B., Gaillard, A., & Vanderhaeghen, P. (2015). Area-specific reestablishment of damaged circuits in the adult cerebral cortex by cortical neurons derived from mouse embryonic stem cells. *Neuron*, *85*(5), 982–997. https://doi.org/10.1016/J.NEURON.2015.02.001

Minatohara, K., Akiyoshi, M., & Okuno, H. (2016). Role of immediate-early genes in synaptic plasticity and neuronal ensembles underlying the memory trace. *Frontiers in Molecular Neuroscience*, *8*(JAN2016), 1–11. https://doi.org/10.3389/fnmol.2015.00078

Mircea, M., & Semrau, S. (2021). How a cell decides its own fate: a single-cell view of molecular mechanisms and dynamics of cell-type specification. *Biochemical Society Transactions*, *49*(6), 2509. https://doi.org/10.1042/BST20210135

Mitsis, T., Efthimiadou, A., Bacopoulou, F., Vlachakis, D., Chrousos, G. P., & Eliopoulos, E. (2020). Transcription factors and evolution: An integral part of gene expression (Review). *World Academy of Sciences Journal*, *2*(1), 3–8. https://doi.org/10.3892/WASJ.2020.32/HTML

Molyneaux, B. J., Arlotta, P., Menezes, J. R., & Macklis, J. D. (2007). Neuronal subtype specification in the cerebral cortex. *Nature Reviews Neuroscience*, *8*(6), 427–437. https://doi.org/10.1038/nrn2151

Morrison, S. J. (2001). Neuronal differentiation: proneural genes inhibit gliogenesis. *Current biology : CB*, *11*(9). https://doi.org/10.1016/S0960-9822(01)00191-9

Mu, L., Berti, L., Masserdotti, G., Covic, M., Michaelidis, T. M., Doberauer, K., Merz, K., Rehfeld, F., Haslinger, A., Wegner, M., Sock, E., Lefebvre, V., Couillard-Despres, S., Aigner, L., Berninger, B., & Chichung Lie, D. (2012). SoxC transcription factors are required for neuronal differentiation in adult hippocampal neurogenesis. *The Journal of neuroscience : the official journal of the Society for Neuroscience*, *32*(9), 3067–3080. https://doi.org/10.1523/JNEUROSCI.4679-11.2012

Muhr, J., & Hagey, D. W. (2021). The cell cycle and differentiation as integrated processes: Cyclins and CDKs reciprocally regulate Sox and Notch to balance stem cell maintenance. *BioEssays*, *43*(7), 2000285. https://doi.org/10.1002/BIES.202000285

Murphy, T. H., Worley, P. F., & Baraban, J. M. (1991). L-type voltage-sensitive calcium channels mediate synaptic activation of immediate early genes. *Neuron*, *7*(4), 625–635. https://doi.org/10.1016/0896-6273(91)90375-A

Nägerl, U. V., Eberhorn, N., Cambridge, S. B., & Bonhoeffer, T. (2004). Bidirectional activity-dependent morphological plasticity in hippocampal neurons. *Neuron*, *44*(5), 759–767. https://doi.org/10.1016/j.neuron.2004.11.016

NARAHASHI, T., MOORE, J. W., & SCOTT, W. R. (1964). Tetrodotoxin Blockage of Sodium Conductance Increase in Lobster Giant Axons. *The Journal of General Physiology*, *47*(5), 965. https://doi.org/10.1085/JGP.47.5.965

Nehme, R., Zuccaro, E., Ghosh, S. D., Li, C., Sherwood, J. L., Pietilainen, O., Barrett, L. E., Limone, F., Worringer, K. A., Kommineni, S., Zang, Y., Cacchiarelli, D., Meissner, A., Adolfsson, R., Haggarty, S., Madison, J., Muller, M., Arlotta, P., Fu, Z., … Eggan, K. (2018). Combining NGN2 Programming with Developmental Patterning Generates Human Excitatory Neurons with NMDAR-Mediated Synaptic Transmission. *Cell Reports*, *23*(8), 2509–2523. https://doi.org/10.1016/J.CELREP.2018.04.066/ATTACHMENT/9A4B4328-D3F7-4A51-96A9-41EE59DBAE23/MMC2.XLSX

Nelson, E. D., Maynard, K. R., Nicholas, K. R., Tran, M. N., Divecha, H. R., Collado-Torres, L., Hicks, S. C., & Martinowich, K. (2022). Activity-regulated gene expression across cell types of the mouse hippocampus. *bioRxiv*, 2022.11.23.517593. https://doi.org/10.1101/2022.11.23.517593

Nieto, M., Monuki, E. S., Tang, H., Imitola, J., Haubst, N., Khoury, S. J., Cunningham, J., Gotz, M., & Walsh, C. A. (2004). Expression of Cux-1 and Cux-2 in the subventric-

ular zone and upper layers II-IV of the cerebral cortex. *The Journal of comparative neurology*, *479*(2), 168–180. https://doi.org/10.1002/CNE.20322

Nieto, M., Schuurmans, C., Britz, O., & Guillemot, F. (2001). Neural bHLH genes control the neuronal versus glial fate decision in cortical progenitors. *Neuron*, *29*(2), 401–413. https://doi.org/10.1016/S0896-6273(01)00214-8

Ninomiya, K., Ohno, M., & Kataoka, N. (2016). Dendritic transport element of human arc mRNA confers RNA degradation activity in a translation-dependent manner. *Genes to Cells*, *21*(11), 1263–1269. https://doi.org/10.1111/GTC.12439

Niu, W., Zang, T., Smith, D. K., Vue, T. Y., Zou, Y., Bachoo, R., Johnson, J. E., & Zhang, C. L. (2015). SOX2 reprograms resident astrocytes into neural progenitors in the adult brain. *Stem Cell Reports*, *4*(5), 780–794. https://doi.org/10.1016/j.stemcr.2015.03.006

Noack, F., Vangelisti, S., Raffl, G., Carido, M., Diwakar, J., Chong, F., & Bonev, B. (2022). Multimodal profiling of the transcriptional regulatory landscape of the developing mouse cortex identifies Neurog2 as a key epigenome remodeler. *Nature Neuroscience*, *25*(2), 154–167. https://doi.org/10.1038/s41593-021-01002-4

Oberst, P., Fièvre, S., Baumann, N., Concetti, C., Bartolini, G., & Jabaudon, D. (2019). Temporal plasticity of apical progenitors in the developing mouse neocortex. *Nature*. https://doi.org/10.1038/s41586-019-1515-6

O'Brien, R. J., Kamboj, S., Ehlers, M. D., Rosen, K. R., Fischbach, G. D., & Huganir, R. L. (1998). Activity-dependent modulation of synaptic AMPA receptor accumulation. *Neuron*, *21*(5), 1067–1078. https://doi.org/10.1016/S0896-6273(00)80624-8

Ory, D. S., Neugeborent, B. A., & Mulligantt, R. C. (1996). A stable human-derived packaging cell line for production of high titer retrovirus/vesicular stomatitis virus G pseudotypes. *Proceedings of the National Academy of Sciences*, *93*(21), 11400–11406. https://doi.org/10.1073/PNAS.93.21.11400

Overman, J. J., Clarkson, A. N., Wanner, I. B., Overman, W. T., Eckstein, I., Maguire, J. L., Dinov, I. D., Toga, A. W., & Carmichael, S. T. (2012). A role for ephrin-A5 in axonal sprouting, recovery, and activity-dependent plasticity after stroke. *Proceedings of the National Academy of Sciences of the United States of America*, *109*(33). https://doi.org/10.1073/PNAS.1204386109

Parylak, S. L., Qiu, F., Linker, S. B., Gallina, I. S., Lim, C. K., Preciado, D., McDonald, A. H., Zhou, X., & Gage, F. H. (2023). Neuronal activity-related transcription is blunted in immature compared to mature dentate granule cells. *Hippocampus*. https://doi.org/10.1002/HIPO.23515

Pastuzyn, E. D., & Shepherd, J. D. (2017). Activity-Dependent Arc Expression and Homeostatic Synaptic Plasticity Are Altered in Neurons from a Mouse Model of

Angelman Syndrome. *Frontiers in Molecular Neuroscience*, *10*. https://doi.org/10.3389/FNMOL.2017.00234

Payne, H. L. (2008). Molecular Membrane Biology The role of transmembrane AMPA receptor regulatory proteins (TARPs) in neurotransmission and receptor trafficking (Review) The role of transmembrane AMPA receptor regulatory proteins (TARPs) in neurotransmission and receptor tra. https://doi.org/10.1080/09687680801986480

Penrod, R. D., Kumar, J., Smith, L. N., McCalley, D., Nentwig, T. B., Hughes, B. W., Barry, G. M., Glover, K., Taniguchi, M., & Cowan, C. W. (2019). Activity-regulated cytoskeleton-associated protein (Arc/Arg3.1) regulates anxiety- and novelty-related behaviors. *Genes, brain, and behavior*, *18*(7). https://doi.org/10.1111/GBB.12561

Pozo, K., & Goda, Y. (2010). Unraveling mechanisms of homeostatic synaptic plasticity. *Neuron*, *66*(3), 337. https://doi.org/10.1016/J.NEURON.2010.04.028

Purves, D., Augustine, G., & Fitzpatrick, D. (2001). The Initial Formation of the Nervous System: Gastrulation and Neurulation - Neuroscience - NCBI Bookshelf. Retrieved June 4, 2022, from https://www.ncbi.nlm.nih.gov/books/NBK10993/

Radnikow, G., & Feldmeyer, D. (2018). Layer- and cell type-specific modulation of excitatory neuronal activity in the neocortex. *Frontiers in Neuroanatomy*, *12*, 1. https://doi.org/10.3389/FNANA.2018.00001/BIBTEX

Rahmani, E., Schweiger, R., Rhead, B., Criswell, L. A., Barcellos, L. F., Eskin, E., Rosset, S., Sankararaman, S., & Halperin, E. (2019). Cell-type-specific resolution epigenetics without the need for cell sorting or single-cell biology. *Nature Communications 2019 10:1*, *10*(1), 1–11. https://doi.org/10.1038/s41467-019-11052-9

Rakic, P. (2000). Radial Unit Hypothesis of Neocortical Expansion. *Novartis Foundation Symposium*, *228*, 30–45. https://doi.org/10.1002/0470846631.CH3

Rambousek, L., Gschwind, T., Lafourcade, C., Paterna, J. C., Dib, L., Fritschy, J. M., & Fontana, A. (2020). Aberrant expression of PAR bZIP transcription factors is associated with epileptogenesis, focus on hepatic leukemia factor. *Scientific Reports 2020 10:1*, *10*(1), 1–16. https://doi.org/10.1038/s41598-020-60638-7

Rannals, M. D., & Kapur, J. (2011). Homeostatic Strengthening of Inhibitory Synapses Is Mediated by the Accumulation of GABAA Receptors. *The Journal of Neuroscience*, *31*(48), 17701. https://doi.org/10.1523/JNEUROSCI.4476-11.2011

Ravanpay, A. C., Hansen, S. J., & Olson, J. M. (2010). Transcriptional inhibition of REST by NeuroD2 during neuronal differentiation. *Molecular and cellular neurosciences*, *44*(2), 178–189. https://doi.org/10.1016/J.MCN.2010.03.006

Revah, O., Gore, F., Kelley, K. W., Andersen, J., Sakai, N., Chen, X., Li, M. Y., Birey, F., Yang, X., Saw, N. L., Baker, S. W., Amin, N. D., Kulkarni, S., Mudipalli, R., Cui,

B., Nishino, S., Grant, G. A., Knowles, J. K., Shamloo, M., … Pașca, S. P. (2022). Maturation and circuit integration of transplanted human cortical organoids. *Nature 2022 610:7931*, *610*(7931), 319–326. https://doi.org/10.1038/s41586-022-05277-w

Risso, D., Perraudeau, F., Gribkova, S., Dudoit, S., & Vert, J. P. (2018). A general and flexible method for signal extraction from single-cell RNA-seq data. *Nature Communications 2018 9:1*, *9*(1), 1–17. https://doi.org/10.1038/s41467-017-02554-5

Robinson, M. D., McCarthy, D. J., & Smyth, G. K. (2010). edgeR: a Bioconductor package for differential expression analysis of digital gene expression data. *Bioinformatics*, *26*(1), 139–140. https://doi.org/10.1093/BIOINFORMATICS/BTP616

Rodriguez, G., Mesik, L., Gao, M., Parkins, S., Saha, R., & Lee, H. K. (2019). Disruption of NMDAR Function Prevents Normal Experience-Dependent Homeostatic Synaptic Plasticity in Mouse Primary Visual Cortex. *The Journal of neuroscience : the official journal of the Society for Neuroscience*, *39*(39), 7664–7673. https://doi.org/10.1523/JNEUROSCI.2117-18.2019

Roussos, P., Guennewig, B., Kaczorowski, D. C., Barry, G., & Brennand, K. J. (2016). Activity-Dependent Changes in Gene Expression in Schizophrenia Human-Induced Pluripotent Stem Cell Neurons. *JAMA psychiatry*, *73*(11), 1180–1188. https://doi.org/10.1001/JAMAPSYCHIATRY.2016.2575

Runge, K., Mathieu, R., Bugeon, S., Lafi, S., Beurrier, C., Sahu, S., Schaller, F., Loubat, A., Herault, L., Gaillard, S., Pallesi-Pocachard, E., Montheil, A., Bosio, A., Rosenfeld, J. A., Hudson, E., Lindstrom, K., Mercimek-Andrews, S., Jeffries, L., van Haeringen, A., … de Chevigny, A. (2021). Disruption of NEUROD2 causes a neurodevelopmental syndrome with autistic features via cell-autonomous defects in forebrain glutamatergic neurons. *Molecular Psychiatry 2021 26:11*, *26*(11), 6125–6148. https://doi.org/10.1038/s41380-021-01179-x

Sahara, S., Yanagawa, Y., O'Leary, D. D., & Stevens, C. F. (2012). The Fraction of Cortical GABAergic Neurons Is Constant from Near the Start of Cortical Neurogenesis to Adulthood. *The Journal of Neuroscience*, *32*(14), 4755. https://doi.org/10.1523/JNEUROSCI.6412-11.2012

Sainsbury, S., Bernecky, C., & Cramer, P. (2015). Structural basis of transcription initiation by RNA polymerase II. *Nature reviews. Molecular cell biology*, *16*(3), 129–143. https://doi.org/10.1038/NRM3952

Sánchez-González, R., Bribián, A., & López-Mascaraque, L. (2020). Cell Fate Potential of NG2 Progenitors. *Scientific Reports 2020 10:1*, *10*(1), 1–12. https://doi.org/10.1038/s41598-020-66753-9

Sanders, S. J., & Mason, C. E. (2016). The Newly Emerging View of the Genome. *Genomics, Circuits, and Pathways in Clinical Neuropsychiatry*, 3–26. https://doi.org/10.1016/B978-0-12-800105-9.00001-9

Sanderson, J. L., Scott, J. D., & Dell'Acqua, M. L. (2018). Control of Homeostatic Synaptic Plasticity by AKAP-Anchored Kinase and Phosphatase Regulation of Ca 2+-Permeable AMPA Receptors. *The Journal of neuroscience : the official journal of the Society for Neuroscience*, *38*(11), 2863–2876. https://doi.org/10.1523/JNEUROSCI.2362-17.2018

Sando, R., Gounko, N., Pieraut, S., Liao, L., Yates, J., & Maximov, A. (2012). HDAC4 governs a transcriptional program essential for synaptic plasticity and memory. *Cell*, *151*(4), 821–834. https://doi.org/10.1016/J.CELL.2012.09.037

Sardi, S. P., Murtie, J., Koirala, S., Patten, B. A., & Corfas, G. (2006). Presenilin-dependent ErbB4 nuclear signaling regulates the timing of astrogenesis in the developing brain. *Cell*, *127*(1), 185–197. https://doi.org/10.1016/J.CELL.2006.07.037

Sareen, D., & Svendsen, C. N. (2010). Stem cell biologists sure play a mean pinball. *Nature Biotechnology 2010 28:4*, *28*(4), 333–335. https://doi.org/10.1038/nbt0410-333

Scala, F., Kobak, D., Bernabucci, M., Bernaerts, Y., Cadwell, C. R., Castro, J. R., Hartmanis, L., Jiang, X., Laturnus, S., Miranda, E., Mulherkar, S., Tan, Z. H., Yao, Z., Zeng, H., Sandberg, R., Berens, P., & Tolias, A. S. (2021). Phenotypic variation of transcriptomic cell types in mouse motor cortex. *Nature*, *598*(7879), 144–150. https://doi.org/10.1038/S41586-020-2907-3

Scala, F., Kobak, D., Shan, S., Bernaerts, Y., Laturnus, S., Cadwell, C. R., Hartmanis, L., Froudarakis, E., Castro, J. R., Tan, Z. H., Papadopoulos, S., Patel, S. S., Sandberg, R., Berens, P., Jiang, X., & Tolias, A. S. (2019). Layer 4 of mouse neocortex differs in cell types and circuit organization between sensory areas. *Nature Communications 2019 10:1*, *10*(1), 1–12. https://doi.org/10.1038/s41467-019-12058-z

Scandaglia, M., Lopez-Atalaya, J. P., Medrano-Fernandez, A., Lopez-Cascales, M. T., del Blanco, B., Lipinski, M., Benito, E., Olivares, R., Iwase, S., Shi, Y., & Barco, A. (2017). Loss of Kdm5c Causes Spurious Transcription and Prevents the Fine-Tuning of Activity-Regulated Enhancers in Neurons. *Cell Reports*, *21*(1), 47–59. https://doi.org/10.1016/J.CELREP.2017.09.014

Schaukowitch, K., Reese, A. L., Kim, S. K., Kilaru, G., Joo, J. Y., Kavalali, E. T., & Kim, T. K. (2017). An Intrinsic Transcriptional Program Underlying Synaptic Scaling during Activity Suppression. *Cell reports*, *18*(6), 1512–1526. https://doi.org/10.1016/J.CELREP.2017.01.033

Schmid, R. S., McGrath, B., Berechid, B. E., Boyles, B., Marchionni, M., Šestan, N., & Anton, E. S. (2003). Neuregulin 1–erbB2 signaling is required for the establishment of radial glia and their transformation into astrocytes in cerebral cortex. *Proceedings*

of the National Academy of Sciences of the United States of America, *100*(7), 4251. https://doi.org/10.1073/PNAS.0630496100

Schuman, E. M., Dynes, J. L., & Steward, O. (2006). Synaptic Regulation of Translation of Dendritic mRNAs. *The Journal of Neuroscience*, *26*(27), 7143. https://doi.org/10.1523/JNEUROSCI.1796-06.2006

Schuurmans, C., Armant, O., Nieto, M., Stenman, J. M., Britz, O., Klenin, N., Brown, C., Langevin, L. M., Seibt, J., Tang, H., Cunningham, J. M., Dyck, R., Walsh, C., Campbell, K., Polleux, F., & Guillemot, F. (2004). Sequential phases of cortical specification involve Neurogenin-dependent and -independent pathways. *The EMBO Journal*, *23*(14), 2892–2902. https://doi.org/10.1038/SJ.EMBOJ.7600278

Seredenina, T., & Luthi-Carter, R. (2012). What have we learned from gene expression profiles in Huntington's disease? *Neurobiology of disease*, *45*(1), 83–98. https://doi.org/10.1016/J.NBD.2011.07.001

Sharif, N., Calzolari, F., & Berninger, B. (2021). Direct In Vitro Reprogramming of Astrocytes into Induced Neurons. *Methods in Molecular Biology*, *2352*, 13–29. https://doi.org/10.1007/978-1-0716-1601-7_2

Sharma, N., Pollina, E. A., Nagy, M. A., Yap, E. L., DiBiase, F. A., Hrvatin, S., Hu, L., Lin, C., & Greenberg, M. E. (2019). ARNT2 Tunes Activity-Dependent Gene Expression through NCoR2-Mediated Repression and NPAS4-Mediated Activation. *Neuron*, *102*(2), 390–406.e9. https://doi.org/10.1016/J.NEURON.2019.02.007

Shepherd, J. D., & Bear, M. F. (2011). New views of Arc, a master regulator of synaptic plasticity. *Nature neuroscience*, *14*(3), 279–284. https://doi.org/10.1038/NN.2708

Shimojo, H., Ohtsuka, T., & Kageyama, R. (2008). Oscillations in Notch Signaling Regulate Maintenance of Neural Progenitors. *Neuron*, *58*(1), 52–64. https://doi.org/10.1016/J.NEURON.2008.02.014

Shimshek, D. R., Bus, T., Schupp, B., Jensen, V., Marx, V., Layer, L. E., & Köhr, G. (2017). Different Forms of AMPA Receptor Mediated LTP and Their Correlation to the Spatial Working Memory Formation. *Frontiers in Molecular Neuroscience — www.frontiersin.org*, *1*, 214. https://doi.org/10.3389/fnmol.2017.00214

Sim, S., Antolin, S., Lin, C. W., Lin, Y. X., & Lois, C. (2013). Increased cell-intrinsic excitability induces synaptic changes in new neurons in the adult dentate gyrus that require Npas4. *The Journal of neuroscience : the official journal of the Society for Neuroscience*, *33*(18), 7928–7940. https://doi.org/10.1523/JNEUROSCI.1571-12.2013

Smith, D. K., Yang, J., Liu, M. L., & Zhang, C. L. (2016). Small Molecules Modulate Chromatin Accessibility to Promote NEUROG2-Mediated Fibroblast-to-Neuron Reprogramming. *Stem Cell Reports*, *7*(5), 955. https://doi.org/10.1016/J.STEMCR.2016.09.013

Soneson, C., & Robinson, M. D. (2018). Bias, robustness and scalability in single-cell differential expression analysis. *Nature methods*, *15*(4), 255–261. https://doi.org/10.1038/NMETH.4612

Spiegel, I., Mardinly, A. R., Gabel, H. W., Bazinet, J. E., Couch, C. H., Tzeng, C. P., Harmin, D. A., & Greenberg, M. E. (2014). Npas4 regulates excitatory-inhibitory balance within neural circuits through cell-type-specific gene programs. *Cell*, *157*(5), 1216–1229. https://doi.org/10.1016/j.cell.2014.03.058

Spitz, F., & Furlong, E. E. (2012). Transcription factors: from enhancer binding to developmental control. *Nature Reviews Genetics 2012 13:9*, *13*(9), 613–626. https://doi.org/10.1038/nrg3207

Spitzer, N. C. (2012). Activity-dependent neurotransmitter respecification. https://doi.org/10.1038/nrn3154

Steward, O., Farris, S., Pirbhoy, P. S., Darnell, J., & Van Driesche, S. J. (2015). Localization and local translation of Arc/Arg3.1 mRNA at synapses: Some observations and paradoxes. *Frontiers in Molecular Neuroscience*, *7*(JAN), 1–15. https://doi.org/10.3389/FNMOL.2014.00101/BIBTEX

Stuart, T., Butler, A., Hoffman, P., Hafemeister, C., Papalexi, E., Mauck, W. M., Hao, Y., Stoeckius, M., Smibert, P., & Satija, R. (2019). Comprehensive Integration of Single-Cell Data. *Cell*, *177*(7), 1888–1902.e21. https://doi.org/10.1016/J.CELL.2019.05.031/ATTACHMENT/2F8B9EBE-54E6-43EB-9EF2-949B6BDA8BA2/MMC3.PDF

Sun, A. X., Yuan, Q., Tan, S., Xiao, Y., Wang, D., Khoo, A. T. T., Sani, L., Tran, H. D., Kim, P., Chiew, Y. S., Lee, K. J., Yen, Y. C., Ng, H. H., Lim, B., & Je, H. S. (2016). Direct Induction and Functional Maturation of Forebrain GABAergic Neurons from Human Pluripotent Stem Cells. *Cell Reports*, *16*(7), 1942–1953. https://doi.org/10.1016/j.celrep.2016.07.035

Suter, D. M., Tirefort, D., Julien, S., & Krause, K.-H. (2009). A Sox1 to Pax6 switch drives neuroectoderm to radial glia progression during differentiation of mouse embryonic stem cells. *Stem cells (Dayton, Ohio)*, *27*(1), 49–58. https://doi.org/10.1634/STEMCELLS.2008-0319

Tai, W., Wu, W., Wang, L. L., Ni, H., Chen, C., Yang, J., Zang, T., Zou, Y., Xu, X. M., & Zhang, C. L. (2021). In vivo reprogramming of NG2 glia enables adult neurogenesis and functional recovery following spinal cord injury. *Cell Stem Cell*, *28*(5), 923–937.e4. https://doi.org/10.1016/J.STEM.2021.02.009

Takahashi, K., & Yamanaka, S. (2006). Induction of pluripotent stem cells from mouse embryonic and adult fibroblast cultures by defined factors. *Cell*, *126*(4), 663–676. https://doi.org/10.1016/J.CELL.2006.07.024

Takouda, J., Katada, S., & Nakashima, K. (2017). Emerging mechanisms underlying astrogenesis in the developing mammalian brain. *Proceedings of the Japan Academy.*

Series B, Physical and biological sciences, *93*(6), 386–398. https://doi.org/10.2183/PJAB.93.024

Tamura, M., Amano, T., & Shiroishi, T. (2014). The Hand2 Gene Dosage Effect in Developmental Defects and Human Congenital Disorders. *Current Topics in Developmental Biology*, *110*, 129–152. https://doi.org/10.1016/B978-0-12-405943-6.00003-8

Tan, Y. L., Yuan, Y., & Tian, L. (2019). Microglial regional heterogeneity and its role in the brain. *Molecular Psychiatry 2019 25:2*, *25*(2), 351–367. https://doi.org/10.1038/s41380-019-0609-8

Taverna, E., Götz, M., & Huttner, W. B. (2014). The Cell Biology of Neurogenesis: Toward an Understanding of the Development and Evolution of the Neocortex. *http://dx.doi.org/10.1146/annurev-cellbio-101011-155801*, *30*, 465–502. https://doi.org/10.1146/ANNUREV-CELLBIO-101011-155801

Telley, L., Agirman, G., Prados, J., Amberg, N., Fièvre, S., Oberst, P., Bartolini, G., Vitali, I., Cadilhac, C., Hippenmeyer, S., Nguyen, L., Dayer, A., & Jabaudon, D. (2019). Temporal patterning of apical progenitors and their daughter neurons in the developing neocortex. *Science*, *364*(6440). https://doi.org/10.1126/SCIENCE.AAV2522/SUPPL_FILE/AAV2522_TELLEY_SM.PDF

Tepe, B., Hill, M. C., Pekarek, B. T., Hunt, P. J., Martin, T. J., Martin, J. F., & Arenkiel, B. R. (2018). Single-Cell RNA-Seq of Mouse Olfactory Bulb Reveals Cellular Heterogeneity and Activity-Dependent Molecular Census of Adult-Born Neurons. *Cell reports*, *25*(10), 2689–2703.e3. https://doi.org/10.1016/J.CELREP.2018.11.034

Thalhammer, A., & Cingolani, L. A. (2014). Cell adhesion and homeostatic synaptic plasticity. *Neuropharmacology*, *78*(100), 23–30. https://doi.org/10.1016/J.NEUROPHARM.2013.03.015

Thanasios, A., & Apavassiliou, G. P. (1995). Transcription Factors. *Molecular Medicine*, *332*(1), 45–47. https://doi.org/10.1056/NEJM199501053320108

Thomas, J., Martinez-Reza, M. F., Thorwirth, M., Zarb, Y., Conzelmann, K. K., Hauck, S. M., Grade, S., & Götz, M. (2022). Excessive local host-graft connectivity in aging and amyloid-loaded brain. *Science advances*, *8*(23). https://doi.org/10.1126/SCIADV.ABG9287

Tien, N. W., & Kerschensteiner, D. (2018). Homeostatic plasticity in neural development. *Neural Development 2018 13:1*, *13*(1), 1–7. https://doi.org/10.1186/S13064-018-0105-X

Tomas-Roca, L., Qiu, Z., Fransén, E., Gokhale, R., Bulovaite, E., Price, D. J., Komiyama, N. H., & Grant, S. G. N. (2022). Developmental disruption and restoration of brain synaptome architecture in the murine Pax6 neurodevelopmental disease model. *Nature Communications 2022 13:1*, *13*(1), 1–13. https://doi.org/10.1038/s41467-022-34131-w

Tomita, K., Moriyoshi, K., Nakanishi, S., Guillemot, F., & Kageyama, R. (2000). Mammalian achaete–scute and atonal homologs regulate neuronal versus glial fate determination in the central nervous system. *The EMBO Journal*, *19*(20), 5460. https://doi.org/10.1093/EMBOJ/19.20.5460

Tong Ihn Lee, & Young, R. A. (2003). Transcription of eukaryotic protein-coding genes. *https://doi.org/10.1146/annurev.genet.34.1.77*, *34*, 77–137. https://doi.org/10.1146/ANNUREV.GENET.34.1.77

Tsunemoto, R., Lee, S., Szucs, A., Chubukov, P., Sokolova, I., Blanchard, J. W., Eade, K. T., Bruggemann, J., Wu, C., Torkamani, A., Sanna, P. P., & Baldwin, K. K. (2018). Diverse reprogramming codes for neuronal identity. *Nature*, *557*(7705), 375–380. https://doi.org/10.1038/s41586-018-0103-5

Tsunemoto, R. K., Eade, K. T., Blanchard, J. W., & Baldwin, K. K. (2015). Embj201591402. *34*(11), 1445–1455.

Turnley, A. M., Basrai, H. S., & Christie, K. J. (2014). Is integration and survival of newborn neurons the bottleneck for effective neural repair by endogenous neural precursor cells? *Frontiers in Neuroscience*, *8*(8 FEB). https://doi.org/10.3389/FNINS.2014.00029

Turrigiano, G. G., Leslie, K. R., Desai, N. S., Rutherford, L. C., & Nelson, S. B. (1998). Activity-dependent scaling of quantal amplitude in neocortical neurons. *Nature*, *391*(6670), 892–896. https://doi.org/10.1038/36103

Turrigiano, G. (2011). Too many cooks? Intrinsic and synaptic homeostatic mechanisms in cortical circuit refinement. *Annual review of neuroscience*, *34*, 89–103. https://doi.org/10.1146/ANNUREV-NEURO-060909-153238

Turrigiano, G. (2012). Homeostatic Synaptic Plasticity: Local and Global Mechanisms for Stabilizing Neuronal Function. *Cold Spring Harbor Perspectives in Biology*, *4*(1). https://doi.org/10.1101/CSHPERSPECT.A005736

Turrigiano, G., Abbott, L. F., & Marder, E. (1994). Activity-dependent changes in the intrinsic properties of cultured neurons. *Science (New York, N.Y.)*, *264*(5161), 974–977. https://doi.org/10.1126/SCIENCE.8178157

The homeostatic control of intrinsic excitability was brought to the forefront by experiments that followed the fate of a neuron that was removed from its circuit and placed in isolated cell cul- ture (Turrigiano et al., 1994). Over a period of days, the isolated neuron rebalanced ion channel surface expression and restored intrinsic firing properties that were characteristic of that cell in vivo. The effect was shown to be both activity and calcium dependent.

Turrigiano, G. G. (1999). Homeostatic plasticity in neuronal networks: the more things change, the more they stay the same. *Trends in Neurosciences*, *22*(5), 221–227. https://doi.org/10.1016/S0166-2236(98)01341-1

Turrigiano, G. G. (2008). The Self-Tuning Neuron: Synaptic Scaling of Excitatory Synapses. *Cell*, *135*(3), 422. https://doi.org/10.1016/J.CELL.2008.10.008

Turrigiano, G. G. (2017). The dialectic of Hebb and homeostasis. *Philosophical Transactions of the Royal Society B: Biological Sciences*, *372*(1715). https://doi.org/10.1098/RSTB.2016.0258

Turrigiano, G. G., & Nelson, S. B. (2004). Homeostatic plasticity in the developing nervous system. *Nature Reviews Neuroscience 2004 5:2*, *5*(2), 97–107. https://doi.org/10.1038/nrn1327

Tyssowski, K. M., DeStefino, N. R., Cho, J. H., Dunn, C. J., Poston, R. G., Carty, C. E., Jones, R. D., Chang, S. M., Romeo, P., Wurzelmann, M. K., Ward, J. M., Andermann, M. L., Saha, R. N., Dudek, S. M., & Gray, J. M. (2018a). Different Neuronal Activity Patterns Induce Different Gene Expression Programs. *Neuron*, *98*(3), 530–546.e11. https://doi.org/10.1016/j.neuron.2018.04.001

Tyssowski, K. M., DeStefino, N. R., Cho, J. H., Dunn, C. J., Poston, R. G., Carty, C. E., Jones, R. D., Chang, S. M., Romeo, P., Wurzelmann, M. K., Ward, J. M., Andermann, M. L., Saha, R. N., Dudek, S. M., & Gray, J. M. (2018b). Different Neuronal Activity Patterns Induce Different Gene Expression Programs. *Neuron*, *98*(3), 530–546.e11. https://doi.org/10.1016/j.neuron.2018.04.001

Valakh, V., Aelita Zhu, X., Wise, D., Van Hooser, S., Schectman, R., Kirk, R., & Nelson, S. B. (n.d.). A transcriptional constraint mechanism limits the homeostatic response to activity deprivation in mammalian neocortex. https://doi.org/10.1101/2021.10.20.465163

Valakh, V., Zhu, X. A., Wise, D., Hooser, S. V., Schectman, R., Cepeda, I., Kirk, R., O'Toole, S., & Nelson, S. B. (2021). A transcriptional constraint mechanism limits the homeostatic response to activity deprivation in mammalian neocortex. *bioRxiv*, 2021.10.20.465163. https://doi.org/10.1101/2021.10.20.465163

Van den Berge, K., Perraudeau, F., Soneson, C., Love, M. I., Risso, D., Vert, J. P., Robinson, M. D., Dudoit, S., & Clement, L. (2018). Observation weights unlock bulk RNA-seq tools for zero inflation and single-cell applications. *Genome Biology*, *19*(1), 1–17. https://doi.org/10.1186/S13059-018-1406-4/FIGURES/6

Vierbuchen, T., Ling, E., Cowley, C. J., Couch, C. H., Wang, X., Harmin, D. A., Roberts, C. W., & Greenberg, M. E. (2017). AP-1 Transcription Factors and the BAF Complex Mediate Signal-Dependent Enhancer Selection. *Molecular cell*, *68*(6), 1067–1082.e12. https://doi.org/10.1016/J.MOLCEL.2017.11.026

Vierbuchen, T., Ostermeier, A., Pang, Z. P., Kokubu, Y., Südhof, T. C., & Wernig, M. (2010). Direct conversion of fibroblasts to functional neurons by defined factors. *Nature*, *463*(7284), 1035–1041. https://doi.org/10.1038/NATURE08797

Vignoles, R., Lentini, C., D'Orange, M., & Heinrich, C. (2019). Direct Lineage Reprogramming for Brain Repair: Breakthroughs and Challenges. *Trends in Molecular Medicine*, *25*(10), 897–914. https://doi.org/10.1016/j.molmed.2019.06.006

Vihma, H., Luhakooder, M., Pruunsild, P., & Timmusk, T. (2016). Regulation of different human NFAT isoforms by neuronal activity. *Journal of neurochemistry*, *137*(3), 394–408. https://doi.org/10.1111/JNC.13568

Villalba, A., Götz, M., & Borrell, V. (2021). The regulation of cortical neurogenesis. *Current Topics in Developmental Biology*, *142*, 1–66. https://doi.org/10.1016/BS.CTDB.2020.10.003

Vitureira, N., & Goda, Y. (2013). The interplay between Hebbian and homeostatic synaptic plasticity. *Journal of Cell Biology*, *203*(2), 175–186. https://doi.org/10.1083/JCB.201306030

Wamsley, B., & Fishell, G. (2017). Genetic and activity-dependent mechanisms underlying interneuron diversity. *Nature Reviews Neuroscience 2017 18:5*, *18*(5), 299–309. https://doi.org/10.1038/nrn.2017.30

Wang, H. Y., Hsieh, P. F., Huang, D. F., Chin, P. S., Chou, C. H., Tung, C. C., Chen, S. Y., Lee, L. J., Gau, S. S. F., & Huang, H. S. (2015). RBFOX3/NeuN is Required for Hippocampal Circuit Balance and Function. *Scientific Reports 2015 5:1*, *5*(1), 1–16. https://doi.org/10.1038/srep17383

Wang, H. L., Zhang, Z., Hintze, M., & Chen, L. (2011). Decrease in Calcium Concentration Triggers Neuronal Retinoic Acid Synthesis during Homeostatic Synaptic Plasticity. *The Journal of Neuroscience*, *31*(49), 17764. https://doi.org/10.1523/JNEUROSCI.3964-11.2011

Wang, T., Li, B., Nelson, C. E., & Nabavi, S. (2019). Comparative analysis of differential gene expression analysis tools for single-cell RNA sequencing data. *BMC Bioinformatics*, *20*(1), 1–16. https://doi.org/10.1186/S12859-019-2599-6/TABLES/7

Wayman, G. A., Lee, Y. S., Tokumitsu, H., Silva, A., & Soderling, T. R. (2008). Calmodulin-kinases: modulators of neuronal development and plasticity. *Neuron*, *59*(6), 914–931. https://doi.org/10.1016/J.NEURON.2008.08.021

Wen, W., & Turrigiano, G. G. (2021). Developmental Regulation of Homeostatic Plasticity in Mouse Primary Visual Cortex. https://doi.org/10.1523/JNEUROSCI.1200-21.2021

West, A. E., Chen, W. G., Dalva, M. B., Dolmetsch, R. E., Kornhauser, J. M., Shaywitz, A. J., Takasu, M. A., Tao, X., & Greenberg, M. E. (2001). Calcium regulation of neuronal gene expression. *Proceedings of the National Academy of Sciences of the United States of America*, *98*(20), 11024–11031. https://doi.org/10.1073/PNAS.191352298/ASSET/EA6FED01-834A-47EA-95D6-F9AF4D2F3AD6/ASSETS/GRAPHIC/PQ1913522004.JPEG

West, A. E., & Greenberg, M. E. (2011). Neuronal activity-regulated gene transcription in synapse development and cognitive function. *Cold Spring Harbor Perspectives in Biology*, *3*(6), 1–21. https://doi.org/10.1101/cshperspect.a005744

Whitt, J. L., Petrus, E., & Lee, H. K. (2014). Experience-dependent homeostatic synaptic plasticity in neocortex. *Neuropharmacology*, *78*(100), 45–54. https://doi.org/10.1016/J.NEUROPHARM.2013.02.016

Wilkinson, G., Dennis, D., & Schuurmans, C. (2013). Proneural genes in neocortical development. *Neuroscience*, *253*, 256–273. https://doi.org/10.1016/j.neuroscience.2013.08.029

Winnubst, J., & Arber, S. (2021). A census of cell types in the brain's motor cortex. *Nature 2021 598:7879*, *598*(7879), 33–34. https://doi.org/10.1038/d41586-021-02493-8

Wisniewska, M. B. (2013). Physiological Role of β-Catenin/TCF Signaling in Neurons of the Adult Brain. *Neurochemical Research*, *38*(6), 1144. https://doi.org/10.1007/S11064-013-0980-9

Wittmann, M. T., & Häberle, B. M. (2018). Linking the Neuropsychiatric Disease Gene TCF4 to Neuronal Activity-Dependent Regulatory Networks. *The Journal of Neuroscience*, *38*(11), 2653. https://doi.org/10.1523/JNEUROSCI.3475-17.2018

Wolf, F. A., Angerer, P., & Theis, F. J. (2018). SCANPY: Large-scale single-cell gene expression data analysis. *Genome Biology*, *19*(1), 1–5. https://doi.org/10.1186/S13059-017-1382-0/FIGURES/1

Wu, G. Y., Deisseroth, K., & Tsien, R. W. (2001). Activity-dependent CREB phosphorylation: Convergence of a fast, sensitive calmodulin kinase pathway and a slow, less sensitive mitogen-activated protein kinase pathway. *Proceedings of the National Academy of Sciences of the United States of America*, *98*(5), 2808–2813. https://doi.org/10.1073/PNAS.051634198/ASSET/C0180C93-4322-4177-8F21-54519636BCA5/ASSETS/GRAPHIC/PQ0516341005.JPEG

Wu, X., Li, Y., Crise, B., & Burgess, S. M. (2003). Transcription start regions in the human genome are favored targets for MLV integration. *Science (New York, N.Y.)*, *300*(5626), 1749–1751. https://doi.org/10.1126/SCIENCE.1083413

Xu, J., Du, Y., & Deng, H. (2015). Direct Lineage Reprogramming: Strategies, Mechanisms, and Applications. *Cell Stem Cell*, *16*(2), 119–134. https://doi.org/10.1016/J.STEM.2015.01.013

Xu, X., & Pozzo-Miller, L. (2017). EEA1 restores homeostatic synaptic plasticity in hippocampal neurons from Rett syndrome mice. *The Journal of Physiology*, *595*(16), 5699–5712. https://doi.org/10.1113/JP274450
MECP2 !!!

Yamaguchi, M., & Mori, K. (2005). Critical period for sensory experience-dependent survival of newly generated granule cells in the adult mouse olfactory bulb.

Proceedings of the National Academy of Sciences of the United States of America, *102*(27), 9697–9702. https://doi.org/10.1073/PNAS.0406082102

Yang, N., Ng, Y. H., Pang, Z. P., Südhof, T. C., & Wernig, M. (2011). Induced Neuronal (iN) Cells: How to Make and Define a Neuron. *Cell stem cell*, *9*(6), 517. https://doi.org/10.1016/J.STEM.2011.11.015

Yang, Y., Yamada, T., Hill, K. K., Hemberg, M., Reddy, N. C., Cho, H. Y., Guthrie, A. N., Oldenborg, A., Heiney, S. A., Ohmae, S., Medina, J. F., Holy, T. E., & Bonni, A. (2016). Chromatin remodeling inactivates activity genes and regulates neural coding. *Science (New York, N.Y.)*, *353*(6296), 300–306. https://doi.org/10.1126/SCIENCE.AAD4225

Yao, Z., Liu, H., Xie, F., Fischer, S., Adkins, R. S., Aldridge, A. I., Ament, S. A., Bartlett, A., Behrens, M. M., Van den Berge, K., Bertagnolli, D., de Bézieux, H. R., Biancalani, T., Booeshaghi, A. S., Bravo, H. C., Casper, T., Colantuoni, C., Crabtree, J., Creasy, H., … Mukamel, E. A. (2021). A transcriptomic and epigenomic cell atlas of the mouse primary motor cortex. *Nature 2021 598:7879*, *598*(7879), 103–110. https://doi.org/10.1038/s41586-021-03500-8

Yao, Z., van Velthoven, C. T., Nguyen, T. N., Goldy, J., Sedeno-Cortes, A. E., Baftizadeh, F., Bertagnolli, D., Casper, T., Chiang, M., Crichton, K., Ding, S. L., Fong, O., Garren, E., Glandon, A., Gouwens, N. W., Gray, J., Graybuck, L. T., Hawrylycz, M. J., Hirschstein, D., … Zeng, H. (2021). A taxonomy of transcriptomic cell types across the isocortex and hippocampal formation. *Cell*, *184*(12), 3222–3241.e26. https://doi.org/10.1016/J.CELL.2021.04.021

Yap, E. L., & Greenberg, M. E. (2018). Activity-Regulated Transcription: Bridging the Gap between Neural Activity and Behavior. *Neuron*, *100*(2), 330–348. https://doi.org/10.1016/J.NEURON.2018.10.013

Yu, X., Chung, S., Chen, D. Y., Wang, S., Dodd, S. J., Walters, J. R., Isaac, J. T., & Koretsky, A. P. (2012). Thalamocortical Inputs Show Post-Critical-Period Plasticity. *Neuron*, *74*(4), 731–742. https://doi.org/10.1016/J.NEURON.2012.04.024

Zeisel, A., Hochgerner, H., Lönnerberg, P., Johnsson, A., Memic, F., van der Zwan, J., Häring, M., Braun, E., Borm, L. E., La Manno, G., Codeluppi, S., Furlan, A., Lee, K., Skene, N., Harris, K. D., Hjerling-Leffler, J., Arenas, E., Ernfors, P., Marklund, U., & Linnarsson, S. (2018). Molecular Architecture of the Mouse Nervous System. *Cell*, *174*(4), 999–1014.e22. https://doi.org/10.1016/J.CELL.2018.06.021

Zeng, H., & Sanes, J. R. (2017). Neuronal cell-type classification: challenges, opportunities and the path forward. *Nature reviews. Neuroscience*, *18*(9), 530–546. https://doi.org/10.1038/NRN.2017.85

Zhang, Y., Li, B., Cananzi, S., Han, C., Wang, L.-L., Zou, Y., Fu, Y.-X., Hon, G. C., & Zhang, C.-L. (2022). A single factor elicits multilineage reprogramming of astrocytes in

the adult mouse striatum. *Proceedings of the National Academy of Sciences*, *119*(11). https://doi.org/10.1073/PNAS.2107339119

Zhou, M., Tao, X., Sui, M., Cui, M., Liu, D., Wang, B., Wang, T., Zheng, Y., Luo, J., Mu, Y., Wan, F., Zhu, L. Q., & Zhang, B. (2021). Reprogramming astrocytes to motor neurons by activation of endogenous Ngn2 and Isl1. *Stem Cell Reports*, *16*(7), 1777–1791. https://doi.org/10.1016/j.stemcr.2021.05.020

Zhou, Q., Brown, J., Kanarek, A., Rajagopal, J., & Melton, D. A. (2008). In vivo reprogramming of adult pancreatic exocrine cells to beta-cells. *Nature*, *455*(7213), 627–632. https://doi.org/10.1038/NATURE07314

Zhou, X., Moon, C., Zheng, F., Luo, Y., Soellner, D., Nuñez, J. L., & Wang, H. (2009). NMDA-stimulated ERK1/2 Signaling and the Transcriptional Up-regulation of Plasticity-related Genes are Developmentally Regulated following in vitro Neuronal Maturation. *Journal of neuroscience research*, *87*(12), 2632. https://doi.org/10.1002/JNR.22103

Zhu, A., Ibrahim, J. G., & Love, M. I. (2019). Heavy-tailed prior distributions for sequence count data: removing the noise and preserving large differences. *Bioinformatics*, *35*(12), 2084–2092. https://doi.org/10.1093/BIOINFORMATICS/BTY895

8

APPENDIX

Table 16: Feature selection within reference datasets

Reference datasets	Top 100 variable genes
La Manno et al., 2021	Xist, Vim, Uchl1, Ube2c, U2af1, Tubb3, Tubb2b, Tubb2a, Tpi1, Tenm2, Tbcb, Tagln3, Stmn4, Stmn3, Stmn2, Sox11, Sf3b2, Set, Serpinh1, Scg5, Rtn4, Rtn1, Rpl30, Robo1, Rbfox2, Rbfox1, Ptprd, Ptn, Psmc4, Polr2m, Pfn2, Pcsk1n, Pclaf, Pcdh9, Pbx1, Nsg1, Nrxn3, Nrxn1, Nfib, Nedd4, Ndn, Ncam1, Nap1l1, Mllt11, Meis2, Mdk, Map2, Map1b, Magi2, Ly6h, Lsamp, Ldha, Kif5c, Kalrn, Ina, Igfbpl1, Igfbp2, Id3, Hspe1, Hspd1, Hsp90b1, Hnrnph3, Hist3h2ba, H2afy2, H2afy, Gpm6b, Glrx3, Gap43, G3bp1, Fxyd6, Fscn1, Fez1, Fabp7, Elavl4, Elavl3, Ebf1, Dpysl3, Ddah2, Dcc, Dbn1, Dbi, Ctnna2, Cpe, Cnn3, Celf4, Celf2, Cdkn1c, Cdk4, Cd81, Ccnd2, Cbx1, Capzb, Cadm1, Bzw2, Bex2, Auts2, Ank3, Adgrl3, Adgrb3, 6330403K07Rik
Yao, Liu, et al., 2021	Unc5d, Tmsb10, Tenm2, Syt1, Syp, Synpr, Sv2b, Snhg11, Sncb, Snap25, Slc24a2, Slc1a2, Slc17a7, Sgcz, Rtn1, Robo1, Rims1, Rbfox1, Rasgrp1, Ralyl, Ptprt, Ptprd, Phactr1, Pde1a, Pcsk2, Pcp4, Pcdh9, Pcdh15, Opcml, Nxph1, Ntm, Nrxn3, Nrxn1, Nrgn, Nrg3, Npas3, Nlgn1, Ndrg4, Nav3, Mgat4c, Meg3, Mef2c, Map1b, Luzp2, Lsamp, Lrrtm4, Lrfn5, Lingo2, Kctd16, Kcnq5, Kcnip4, Kcnh7, Kcnd2, Kcnc2, Hs6st3, Grm7, Grm5, Grip1, Grin2b, Grin2a, Gm28928, Glp2r, Galntl6, Gad2, Gad1, Gabrg3, Frmpd4, Fgf14, Fam155a, Etl4, Erbb4, Egfem1, Dpp10, Dlgap2, Dlg2, Csmd1, Cntnap5a, Cntnap2, Cntn5, Cntn4, Chrm3, Celf4, Celf2, Cck, Car10, Camk2n1, Calm2, Cadps, Cadm2, Cacna2d3, Basp1, Atp1b1, Asic2, Arpp21, Anks1b, Ank3, Adgrb3, Adarb2, 3110035E14Rik, 2900097C17Rik
Zeisel et al., 2018	Zcchc18, Ywhah, Ywhag, Xist, Vsnl1, Ugt8a, Uchl1, Tubb2a, Tuba4a, Ttc3, Tspan2, Tspan13, Trf, Thy1, Tagln3, Syt1, Syn2, Stmn3, Stmn2, Sparcl1, Snurf, Snhg11, Snca, Snap25, Slc8a1, Scn2a1, Scg5, Rtn1, Rgs4, Rasgrp1, Ptgds, Prkcb, Prkar1b, Ppp3r1, Ppp3cb, Ppp3ca, Plp1, Pja2, Pde1a, Pcsk2, Olfm1, Ntm, Nsg2, Nsf, Nrgn, Neurod6, Ndrg4, Ncdn, Napb, Mog, Mobp, Mllt11, Meg3, Mdh1, Mbp, Map1b Mal, Mag, Hpca, Gsn, Grm5, Grin2b, Gria2, Gria1, Gpm6a, Gda, Gap43, Gabra1, Ermn, Epha4, Enpp2, Eno2, Dnm1, Dlgap1, D3Bwg0562e, Cyfip2, Crym, Cryab, Cpe, Cnp, Cldn11, Chn1, Celf4, Celf2, Cd9, Cck, Car2, Camk2b, Camk2a, Basp1, Atp2b1, Atp1b1, Atp1a3, Atp1a2, Arpp21, Arf3, Apoe, Apod, 3110035E14Rik, 2900097C17Rik

8.1 CELL IDENTITY ASSIGNMENTS BASED ON SIMILARITY WITH REFERENCE CELLS

Table 17: Single cell projection onto 3 reference datasets

Reference dataset	Cluster annotation (Cell type)	Nr cells projected
Zeisel et al., 2018	CA1PyrInt	43
	Mgl1 (Immune system-related cell type)	11
	Astro2 (Astrocyte)	7
	Choroid	3
	Pvm2 (Perivascular macrophage)	2
	Astro1 (Astrocyte)	1
	Int1 (Interneuron subtype)	1
	Int10 (Interneuron subtype)	1
	Int13 (Interneuron subtype)	1
	Int4 (Interneuron subtype)	1
	Int7 (Interneuron subtype)	1
	S1PyrL4	1
La Manno et al., 2021	Cortical or hippocampal glutamatergic neuron	60
	Oligodendrocyte precursor cell	40
	Arachnoid barrier cells	6
	Pituitary neuroendocrine	6
	PreOPC	5
	Forebrain GABAergic	5
	Midbrain GABAergic	4
	Cerebellum GABAergic	4
	Committed oligodendrocyte precursor	3
	Erythrocyte	1
	Oligodendrocyte	1
	Perivascular fibroblast-like cells	1
	Platelet	1
Yao, Liu, et al., 2021	L2/3 IT CTX-1 (Intratelencephalic project. neuron)	177
	Astro (Astrocyte)	137
	L2 IT RHP (Intratelencephalic retrohippocampal)	137
	L2/3 IT PPP	81
	Vip (GABAergic neuron from CGE)	75
	Pvalb (GABAergic neuron from MGE)	34
	L4/5 IT CTX (Intratelencephalic project. neuron)	24
	L5 NP CTX (Near-projecting)	19
	L6b CTX	19
	L5 IT TPE-ENT (Intratelencephalic)	14
	L2/3 IT CTX-2	11
	Lamp5 (GABAergic neuron from CGE)	10
	CR (Cajal-Retzius, glutamatergic, layer 1)	6
	L6 CT CTX (Corticothalamic neuron)	6
	L6 IT CTX (Intratelencephalic projection neuron)	6
	Oligo (Oligodendrocyte)	6
	Sst (GABAergic neuron from MGE)	6

Continued on next page

Table 17 – continued from previous page

Reference dataset	Cluster annotation (Cell type)	Nr cells projected
	Car3 (IT project. neurons)	3
	L3 RSP-ACA (Retrosplenial, anterior cingulate cortex),	3
	L5 PT CTX (Pyramidal tract)	3
	Micro-PVM (Perivascular macrophage)	3
	SMC-Peri (Smooth muscle cell)	3
	Sncg (GABAergic neuron from CGE)	1
	Sst Chodl (Interneuron subtype)	1

8.2 SIGNIFICANTLY UPREGULATED GENES IN ACTIVE ENDOGENOUS NEURONS COMPARED TO ACTIVE INDUCED NEURONS

Table 18: Significantly upregulated genes in active endogenous neurons compared to active induced neurons ordered by descending $\log_2$ FC

Gene	$\log_2$ FC	p-value	Gene	$\log_2$ FC	p-value
Gda	3.78	0.0217	Gm17167	1.05	0.0140
A230006K03Rik	3.58	0.0270	Gm1992	1.05	0.0076
2010300C02Rik	3.55	0.0267	Raph1	1.04	0.0105
Dpp10	3.40	0.0000	Cacna1e	1.04	0.0000
Lmo7	3.30	0.0305	Sorcs2	1.04	0.0088
Cpne7	3.27	0.0438	Strbp	1.03	0.0000
Etl4	3.23	0.0000	Cit	1.01	0.0126
Lingo2	3.23	0.0000	Kcnma1	1.01	0.0000
Wdr17	3.20	0.0000	Frmd4a	1.01	0.0000
Cntn5	3.17	0.0000	Arhgap44	1.00	0.0019
Dlg2	3.08	0.0000	Ext1	1.00	0.0002
Ildr2	3.04	0.0445	Gm26871	1.00	0.0001
Cobl	2.96	0.0127	4930578G10Rik	0.99	0.0128
Ptprd	2.96	0.0000	Arpp21	0.99	0.0000
9530059O14Rik	2.86	0.0001	Actr3b	0.99	0.0273
Grm8	2.73	0.0001	Gm44151	0.99	0.0206
Ralyl	2.62	0.0000	Sv2b	0.98	0.0148
Fam81a	2.61	0.0213	Ndrg4	0.98	0.0222
Nkain2	2.41	0.0000	Dlgap3	0.98	0.0334
Phf24	2.41	0.0002	Tafa1	0.97	0.0250
Camk2a	2.40	0.0002	Cdkl2	0.97	0.0346
Frmpd4	2.33	0.0001	Slc25a3	0.96	0.0282
Lrfn5	2.32	0.0002	Gm36975	0.96	0.0048

Continued on next page

Table 18 – continued from previous page

Gene	log_2 FC	p-value	Gene	log_2 FC	p-value
Lgi1	2.32	0.0134	Ncam2	0.96	0.0281
St6gal2	2.29	0.0413	Il1rapl1	0.96	0.0002
Myrip	2.25	0.0056	Robo1	0.95	0.0034
Cfap69	2.24	0.0154	Mrtfb	0.95	0.0042
Dlgap2	2.20	0.0000	Sphkap	0.95	0.0183
Cnksr2	2.20	0.0000	Fstl4	0.95	0.0356
Nrg3os	2.19	0.0001	Fut9	0.94	0.0061
B230209E15Rik	2.18	0.0035	Numb	0.94	0.0057
Xylt1	2.17	0.0000	Ryr2	0.94	0.0084
Gm15738	2.16	0.0004	Mpc1	0.93	0.0367
Csmd1	2.15	0.0000	Grin2b	0.93	0.0000
Ncald	2.15	0.0000	Tiam1	0.93	0.0094
Gm15155	2.14	0.0116	Arl15	0.93	0.0006
Gabra1	2.13	0.0248	Ppp2r2c	0.93	0.0109
Atp2b4	2.11	0.0034	Pde4b	0.93	0.0030
Nwd2	2.11	0.0001	Lrrtm4	0.92	0.0022
Prickle2	2.07	0.0000	Mgat4c	0.92	0.0413
Agfg2	2.07	0.0222	Mapre3	0.92	0.0312
Slc20a1	2.04	0.0259	Gfod1	0.92	0.0445
Agbl4	2.03	0.0000	Lncpint	0.92	0.0006
Exoc6	2.02	0.0107	Atp2b1	0.92	0.0002
Syt1	1.99	0.0000	Atp2b2	0.92	0.0003
Snhg11	1.98	0.0000	Lingo1	0.91	0.0097
Nrg3	1.98	0.0000	Ttyh1	0.91	0.0343
Phactr1	1.97	0.0000	Ptprr	0.91	0.0286
Pde8b	1.97	0.0040	Prkaa2	0.90	0.0481
Gm37459	1.97	0.0256	Tusc3	0.90	0.0193
Adgrb3	1.95	0.0000	Klhl2	0.90	0.0222
Pde1a	1.95	0.0000	Ank	0.89	0.0116
Gabrb1	1.94	0.0000	Khdrbs2	0.89	0.0127
Ntng1	1.94	0.0260	Unc80	0.89	0.0008
Atp1a1	1.93	0.0095	Celf2	0.88	0.0000
Prickle1	1.90	0.0007	Tmem132b	0.88	0.0269
Pex5l	1.84	0.0000	Amph	0.87	0.0085
Kcnq5	1.82	0.0000	Camk2d	0.86	0.0258
Abca2	1.79	0.0236	Stxbp5l	0.86	0.0029
Hs3st4	1.76	0.0142	Chka	0.85	0.0081
Rasgef1a	1.75	0.0051	Lekr1	0.85	0.0428
Glp2r	1.74	0.0149	Mapk10	0.85	0.0003
Eno2	1.73	0.0189	Kcnj3	0.84	0.0086

Continued on next page

Table 18 – continued from previous page

Gene	$\log_2$ FC	p-value	Gene	$\log_2$ FC	p-value
Gabrg3	1.70	0.0030	Kcnab1	0.84	0.0305
Osbpl10	1.69	0.0082	Khdrbs3	0.83	0.0196
Pcdh9	1.68	0.0000	Ndrg3	0.83	0.0207
Vsnl1	1.68	0.0076	Rap1gap2	0.82	0.0259
Ndst3	1.65	0.0139	Slc8a1	0.82	0.0006
Epb41l4b	1.63	0.0042	Cacna2d1	0.82	0.0011
Sorbs2os	1.62	0.0000	Cacna1a	0.81	0.0000
Mtus2	1.62	0.0020	Chchd6	0.81	0.0267
Kcnip4	1.61	0.0000	Nlk	0.81	0.0071
Gm20642	1.58	0.0010	Nbea	0.81	0.0000
Rph3a	1.58	0.0399	Epha6	0.81	0.0360
Brinp2	1.58	0.0016	Dock3	0.81	0.0001
Rbfox1	1.58	0.0000	Acap2	0.81	0.0114
Cntn4	1.58	0.0037	Hivep2	0.80	0.0001
Asic2	1.56	0.0006	Armc9	0.80	0.0182
D130043K22Rik	1.55	0.0309	Smap1	0.79	0.0340
Dmtn	1.55	0.0184	Leng9	0.79	0.0486
R3hdm1	1.55	0.0000	Lysmd4	0.79	0.0445
Kctd16	1.54	0.0042	Csmd2	0.78	0.0035
Caln1	1.53	0.0001	Kcnt2	0.78	0.0172
Cdh18	1.52	0.0090	Clstn1	0.78	0.0288
Gm12394	1.52	0.0006	Map1b	0.78	0.0005
Kcnt1	1.50	0.0124	Cntn1	0.78	0.0012
Myo1d	1.49	0.0297	A330023F24Rik	0.77	0.0175
Hdac9	1.49	0.0000	Macrod2	0.77	0.0002
Vps13a	1.48	0.0002	Samd12	0.77	0.0029
Adcy8	1.46	0.0325	Grid1	0.77	0.0014
Rgs7	1.46	0.0000	Gpr158	0.76	0.0113
Pcsk2	1.46	0.0136	Zfp804b	0.76	0.0486
Mdga2	1.46	0.0000	Efr3a	0.76	0.0466
Snap25	1.45	0.0000	Epha5	0.76	0.0057
Brinp1	1.44	0.0041	Eif4g3	0.76	0.0002
Pcnx2	1.43	0.0194	Celf3	0.75	0.0445
Stx1a	1.42	0.0148	Rims1	0.75	0.0004
Oxr1	1.42	0.0000	Sybu	0.74	0.0059
Ntrk2	1.42	0.0000	Epb41l3	0.74	0.0275
Susd4	1.41	0.0046	Cdh13	0.74	0.0167
Car10	1.41	0.0135	Ctnnd2	0.73	0.0004
Grin2a	1.40	0.0000	Nlgn1	0.73	0.0004
Sorbs2	1.40	0.0000	Atrnl1	0.73	0.0040

Continued on next page

Table 18 – continued from previous page

Gene	log_2 FC	p-value	Gene	log_2 FC	p-value
Snph	1.40	0.0286	Hook1	0.73	0.0313
Ldb2	1.39	0.0225	Adam23	0.73	0.0348
Inpp4b	1.38	0.0022	Ahi1	0.72	0.0000
Mpped1	1.38	0.0129	Pakap	0.72	0.0307
Cacnb4	1.35	0.0000	Ncoa7	0.71	0.0139
Gucy1b1	1.34	0.0486	Gabbr2	0.71	0.0055
Nav3	1.31	0.0000	Dpp6	0.71	0.0042
Fam135b	1.31	0.0000	Ube3a	0.70	0.0013
Sipa1l1	1.31	0.0000	Tenm1	0.70	0.0273
Meg3	1.30	0.0000	Rimbp2	0.70	0.0283
Sgk3	1.30	0.0445	Malat1	0.69	0.0000
Zranb2	1.30	0.0000	Aak1	0.69	0.0008
Serpini1	1.29	0.0183	Arglu1	0.69	0.0071
Actn1	1.29	0.0067	Atp6v0a1	0.68	0.0097
Negr1	1.29	0.0000	Ank2	0.68	0.0000
Syt7	1.27	0.0008	Nrcam	0.67	0.0009
Arhgap26	1.26	0.0000	Fam189a1	0.67	0.0382
Fbxw7	1.26	0.0035	Gls	0.67	0.0024
Nos1ap	1.26	0.0013	Hdac4	0.66	0.0360
Pgbd5	1.26	0.0060	Dennd4a	0.66	0.0273
Mical2	1.25	0.0002	Tanc2	0.66	0.0003
Fgf12	1.24	0.0000	Lrfn2	0.65	0.0449
Dock9	1.24	0.0004	Syt16	0.65	0.0268
Sorl1	1.24	0.0154	Lrrc7	0.65	0.0002
Tox	1.23	0.0474	Pnn	0.65	0.0204
Kalrn	1.23	0.0000	Sh3rf3	0.64	0.0386
Grm3	1.23	0.0360	Rabgap1l	0.64	0.0108
Gm37240	1.22	0.0004	Large1	0.64	0.0042
Clstn3	1.22	0.0338	Rian	0.63	0.0002
Gm43376	1.22	0.0165	Hivep3	0.63	0.0073
Nrxn3	1.21	0.0000	Atp8a2	0.62	0.0235
Pclo	1.21	0.0000	Dlg1	0.62	0.0120
Cdr1os	1.21	0.0009	Scn2a	0.62	0.0117
Mef2c	1.21	0.0051	Arhgap32	0.62	0.0306
Lrrc4c	1.20	0.0000	Ablim1	0.62	0.0170
Mmp16	1.20	0.0002	Jakmip2	0.61	0.0171
Hecw2	1.19	0.0000	Rasal2	0.61	0.0297
Dalrd3	1.19	0.0081	Sntg1	0.61	0.0433
Ppfibp1	1.18	0.0214	Dmd	0.60	0.0160
Nebl	1.18	0.0066	Ube2b	0.60	0.0280

Continued on next page

Table 18 – continued from previous page

Gene	log_2 FC	p-value	Gene	log_2 FC	p-value
Nrg1	1.18	0.0003	Nrxn1	0.59	0.0003
Gabrb3	1.18	0.0000	Fry	0.59	0.0079
4430402I18Rik	1.18	0.0481	Tenm2	0.58	0.0429
Hcn1	1.17	0.0040	Dclk1	0.58	0.0039
Rnf112	1.17	0.0309	Tjp1	0.58	0.0143
Ldlrad4	1.17	0.0013	Pde4dip	0.57	0.0321
Csgalnact1	1.15	0.0321	Upp2	0.57	0.0362
Otud7a	1.14	0.0000	Spock1	0.57	0.0461
Dnm1	1.14	0.0048	Fgf14	0.57	0.0018
Grm5	1.14	0.0000	Mical3	0.56	0.0318
Ctnna3	1.13	0.0009	Dscam	0.55	0.0236
Gabrg2	1.13	0.0374	Snrnp70	0.55	0.0010
Shank2	1.13	0.0008	Ptprn	0.55	0.0450
Prkcg	1.13	0.0106	Dync1i1	0.55	0.0433
Cacna2d3	1.12	0.0125	Nell2	0.54	0.0359
Mctp1	1.12	0.0004	Dab1	0.54	0.0216
Robo2	1.11	0.0114	Celf4	0.53	0.0071
Nptn	1.10	0.0000	Gm20275	0.53	0.0429
Sv2a	1.09	0.0441	Ttc14	0.53	0.0215
Map7	1.09	0.0090	Prkn	0.52	0.0155
Gria3	1.09	0.0006	Fam155a	0.50	0.0253
Nup93	1.08	0.0254	Trank1	0.49	0.0313
Pdzd2	1.08	0.0352	Plekha5	0.47	0.0397
A830018L16Rik	1.07	0.0025	Pabpn1	0.47	0.0487
Ablim2	1.07	0.0389	Dync1i2	0.44	0.0273
Fmn1	1.06	0.0380	Cacna1d	0.40	0.0382
Atp1b1	1.06	0.0246	Ppp3ca	0.37	0.0426
Kcnj6	1.05	0.0294			

8.3 SIGNIFICANTLY UPREGULATED GENES IN ACTIVE INDUCED NEURONS COMPARED TO ACTIVE ENDOGENOUS NEURONS

Table 19: Significantly upregulated genes in active induced neurons compared to active endogenous neurons ordered by descending $\log_2$ FC

Gene	$\log_2$ FC	p-value	Gene	$\log_2$ FC	p-value
Cdh23	4.3889	9.6E-05	Smarcc1	1.0134	6.9E-05
Adgrg6	4.2810	1.3E-05	Map4k4	1.0123	1.5E-08
St18	4.0851	2.4E-16	Lrmda	1.0117	5.5E-05
Ccdc7b	3.8350	8.7E-07	Fam204a	1.0117	2.3E-02
Cd180	3.7210	3.0E-23	Coro1c	1.0099	1.9E-03
Sema3c	3.7057	1.3E-16	Dscaml1	1.0097	8.5E-07
Gm31706	3.5793	1.4E-11	Hnrnph1	1.0093	1.5E-04
Pde1c	3.4161	2.4E-14	Wdr76	1.0090	4.5E-02
Lama2	3.2391	6.0E-11	Ppip5k2	1.0087	1.3E-03
Chl1	3.2287	3.0E-28	Cenpv	1.0080	3.6E-03
Lyn	3.0199	2.5E-09	Elmo1	1.0078	4.9E-04
Lgmn	2.9777	1.5E-08	Khdrbs1	1.0077	6.4E-05
Zbtb20	2.7154	1.8E-18	Akap6	1.0075	1.7E-11
Tead1	2.6608	1.8E-15	Zfhx2os	1.0062	2.6E-03
Samsn1	2.6524	1.8E-03	Tcerg1	1.0044	5.1E-06
Ccbe1	2.6408	9.5E-12	Hpf1	1.0035	2.7E-02
Fbxl7	2.6355	2.2E-21	Sparcl1	1.0030	2.4E-02
Msrb3	2.6123	1.2E-03	Agbl1	1.0029	4.8E-02
Mir99ahg	2.5572	7.0E-34	Sugct	1.0028	3.6E-02
2610307P16Rik	2.5056	6.2E-09	C530008M17Rik	1.0022	5.8E-07
Fli1	2.4899	4.6E-02	Stox2	1.0015	2.3E-05
Ptpn14	2.4639	5.5E-04	2210408F21Rik	1.0008	4.8E-03
Alk	2.4496	6.5E-09	Fbxo10	0.9974	2.2E-03
Ankrd44	2.4413	3.4E-15	Arhgap12	0.9961	6.4E-04
Aoah	2.3947	4.4E-08	Vps36	0.9946	2.4E-02
Nkain3	2.3491	5.8E-14	Slc38a2	0.9945	3.1E-03
Aff2	2.3272	7.1E-21	Rfx7	0.9937	1.4E-07
Hexb	2.3177	3.7E-11	Sh3d19	0.9935	3.8E-03
Asxl3	2.3166	6.1E-10	Tut4	0.9935	3.9E-08
Gm11146	2.2988	4.9E-07	Samd4	0.9934	3.6E-03
Tspan18	2.2712	3.2E-04	Fgf13	0.9930	1.5E-02
Afap1	2.2662	3.7E-11	Clvs1	0.9914	8.5E-05
Chd7	2.2382	1.0E-10	Abcg1	0.9902	1.1E-02

Continued on next page

Table 19 – continued from previous page

Gene	$\log_2$ FC	p-value	Gene	$\log_2$ FC	p-value
Col18a1	2.2238	1.1E-03	Pip4k2a	0.9889	6.1E-03
Gm29260	2.2222	1.5E-03	Gramd1b	0.9875	5.5E-06
Cecr2	2.2108	1.4E-03	Map3k1	0.9874	3.1E-02
Igdcc4	2.1970	3.1E-12	Rnf182	0.9873	3.2E-02
Daam2	2.1941	7.8E-03	Wasf2	0.9867	2.6E-02
Gm11266	2.1927	2.6E-06	Dzip1	0.9857	5.8E-04
Sec61a1	2.1764	8.5E-06	Prim2	0.9853	2.8E-02
Hrk	2.1654	2.2E-05	Tox3	0.9819	1.4E-02
Zeb2	2.1307	1.5E-17	Acly	0.9799	7.5E-03
Marcks	2.1257	1.1E-04	Ikzf2	0.9797	2.7E-02
St8sia2	2.1244	1.8E-04	Tbc1d1	0.9775	2.7E-02
Pard3	2.1128	1.5E-17	Parp8	0.9757	6.1E-05
Cxxc5	2.0817	2.2E-04	Ece2	0.9728	2.3E-02
Ust	2.0810	3.1E-13	Mvb12b	0.9725	2.4E-04
Tns1	2.0723	1.4E-03	Cerk	0.9716	2.0E-02
Tmcc3	2.0676	6.1E-04	Zfp740	0.9706	3.6E-02
Heg1	2.0618	1.4E-05	Pola1	0.9692	1.0E-02
Sncaip	2.0539	1.4E-07	Runx1t1	0.9681	1.1E-04
Phka1	2.0259	6.4E-04	Unc13c	0.9666	4.1E-02
Wipf1	2.0162	1.5E-03	Ano3	0.9656	5.7E-03
Sh3bgrl	2.0061	8.6E-05	Tcf12	0.9654	1.2E-05
Deptor	2.0049	5.3E-04	Stard7	0.9638	8.0E-03
Spata13	1.9949	3.3E-06	E330009J07Rik	0.9632	1.8E-02
Smoc1	1.9879	5.7E-05	Trim2	0.9630	3.4E-07
Sox11	1.9857	9.1E-10	Ctnnb1	0.9616	5.6E-03
Zfp423	1.9833	1.2E-12	Hdac8	0.9609	1.4E-04
Pappa	1.9831	2.9E-02	Ssb	0.9604	4.0E-03
Zbtb9	1.9765	1.4E-04	Apaf1	0.9589	6.3E-03
Bicc1	1.9665	6.6E-04	Zup1	0.9587	3.4E-03
Shb	1.9515	9.9E-06	Tet1	0.9576	8.0E-03
Mtss1	1.9421	2.0E-20	Srsf3	0.9543	5.2E-03
Zfp385b	1.9416	5.5E-14	Nova2	0.9542	7.5E-04
Nfix	1.9310	1.5E-17	Syt9	0.9511	1.2E-02
Airn	1.9291	9.5E-09	Foxn3	0.9509	3.0E-06
Tmem65	1.9231	1.2E-06	Ppm1h	0.9476	6.4E-04
Rbms1	1.9209	1.7E-10	Sfpq	0.9445	5.6E-07
Chchd4	1.9187	1.2E-02	Gpsm1	0.9438	2.4E-02
Dennd2a	1.9173	9.6E-09	Mtr	0.9420	2.9E-02
Aida	1.9103	1.8E-04	Cbx3	0.9410	2.7E-02

Continued on next page

Table 19 – continued from previous page

Gene	log_2 FC	p-value	Gene	log_2 FC	p-value
Frmpd1	1.9018	1.0E-02	9130015G15Rik	0.9408	2.6E-02
Mdga1	1.8841	7.4E-10	Stau1	0.9377	1.3E-02
Pvt1	1.8777	2.3E-15	Morf4l1	0.9375	4.9E-03
Grik2	1.8749	2.0E-21	Zhx2	0.9374	3.1E-02
Tgfbr1	1.8677	3.9E-05	Gm20754	0.9351	2.6E-02
Tcf4	1.8543	3.0E-24	Arhgef4	0.9348	2.5E-02
Prox1	1.8508	1.1E-02	Tshz1	0.9346	4.7E-02
Tbc1d4	1.8457	1.1E-05	Rbmx	0.9335	5.5E-03
Angpt1	1.8350	1.3E-05	Ccdc171	0.9300	2.5E-02
Antxr2	1.8295	1.8E-02	Srbd1	0.9276	6.0E-03
Syne2	1.8294	3.3E-05	Col4a2	0.9265	4.8E-03
Map3k14	1.8063	1.5E-03	Rccd1	0.9263	2.9E-02
Bach2	1.8062	3.8E-18	Rsrc1	0.9256	1.8E-04
Cdyl	1.8011	1.0E-06	Rbfox3	0.9248	8.9E-09
Meis2	1.7964	1.9E-12	Tmem201	0.9243	2.3E-02
Soga1	1.7943	2.0E-09	Wbp1l	0.9215	8.5E-03
Mapk14	1.7919	3.9E-07	Lrp8os2	0.9189	3.9E-02
Igf2r	1.7916	7.3E-07	Rgs12	0.9132	4.0E-02
Ccnjl	1.7723	1.4E-02	Slc38a1	0.9113	3.7E-03
Cemip2	1.7719	1.6E-07	Ctnna1	0.9112	2.2E-02
Prdm8	1.7620	7.5E-04	Mcmbp	0.9097	2.0E-02
St5	1.7607	2.3E-05	Amy1	0.9091	1.4E-03
Ptbp3	1.7554	7.9E-06	Zfand6	0.9085	1.2E-02
Ghr	1.7544	6.1E-08	Vps37b	0.9071	1.3E-02
Erbin	1.7512	1.7E-10	5430405H02Rik	0.9064	4.5E-02
Fem1b	1.7479	2.4E-04	Rttn	0.9038	3.6E-02
Taco1	1.7403	3.6E-12	Kmt5b	0.9035	5.5E-03
Pag1	1.7348	9.5E-09	Nol4	0.9021	7.3E-05
Ankrd6	1.7258	4.3E-08	Atf7	0.8997	7.7E-04
Coro2b	1.7196	2.0E-10	Zfyve26	0.8995	3.7E-02
Nrp2	1.7179	6.6E-10	Trak1	0.8995	1.1E-04
Sdk1	1.7166	6.7E-10	Jpt1	0.8994	2.0E-02
Rin2	1.7131	1.0E-02	Kcmf1	0.8989	1.1E-02
Grik4	1.7069	1.3E-10	Abcd3	0.8978	4.3E-02
Elf2	1.7064	6.8E-05	Xist	0.8972	5.7E-05
Tgfb2	1.6954	1.8E-02	Pou2f1	0.8970	1.7E-04
Vav3	1.6932	2.1E-05	Dpysl5	0.8966	5.8E-04
Ttc28	1.6911	2.8E-16	Zfhx4	0.8963	2.8E-02
Col4a6	1.6909	1.2E-03	Tspan9	0.8962	4.3E-03

Continued on next page

Table 19 – continued from previous page

Gene	$\log_2$ FC	p-value	Gene	$\log_2$ FC	p-value
Clmp	1.6855	1.4E-06	Frmd5	0.8923	8.9E-05
Ephb1	1.6834	2.5E-07	Zfp57	0.8922	2.8E-02
Zc3h12c	1.6818	2.3E-05	Dpy19l4	0.8917	1.5E-02
Zfp9	1.6587	3.8E-03	Jak2	0.8902	1.4E-02
Qser1	1.6554	1.7E-05	Nav1	0.8900	2.5E-07
Lncppara	1.6530	8.4E-12	Lrp12	0.8897	4.3E-02
Parva	1.6515	7.4E-03	Pcnx3	0.8893	4.4E-02
Mxi1	1.6509	1.1E-03	Xpa	0.8870	1.7E-02
Lurap1l	1.6497	3.3E-03	Rbbp4	0.8865	2.0E-02
Fam107b	1.6488	7.1E-03	Tgfbr3	0.8836	3.1E-02
Dixdc1	1.6429	1.9E-09	Cand1	0.8822	4.0E-02
4930444A19Rik	1.6418	3.7E-04	Bcl7a	0.8820	3.4E-02
Ezh2	1.6206	7.8E-06	Flna	0.8777	3.6E-03
Paip1	1.6107	4.5E-05	Sacs	0.8747	4.6E-03
Disp3	1.6099	3.7E-03	Eda	0.8718	1.8E-02
Pcdh19	1.6050	6.4E-04	D130040H23Rik	0.8692	5.3E-03
Slc16a10	1.6006	4.3E-03	Rps6ka5	0.8683	1.3E-02
Frmd4b	1.5996	2.0E-07	Pak2	0.8679	1.3E-02
Cald1	1.5945	1.9E-06	Glt8d1	0.8660	3.1E-02
Cpq	1.5938	2.0E-03	Ptpn12	0.8645	4.0E-04
Nova1	1.5924	9.6E-05	Gm47283	0.8644	1.1E-04
Kat2b	1.5920	1.5E-05	Nudt3	0.8641	3.0E-03
9230114K14Rik	1.5885	2.3E-02	Smc3	0.8606	1.9E-03
Tmem196	1.5879	9.0E-03	Ythdc1	0.8579	1.2E-03
Fgfr1	1.5858	7.5E-07	Cers4	0.8577	3.4E-03
Ebf4	1.5852	4.7E-05	Smc6	0.8573	1.4E-02
Itpkb	1.5800	1.8E-02	Tsc22d2	0.8568	2.2E-02
Aim2	1.5780	3.5E-04	Txlna	0.8544	4.3E-02
Golim4	1.5759	1.0E-03	Adgrl2	0.8537	1.2E-02
Rreb1	1.5749	5.7E-03	Nhsl1	0.8528	3.4E-02
Sox4	1.5736	3.8E-04	Anp32a	0.8514	8.9E-03
Zmat4	1.5727	2.3E-05	Cpsf6	0.8508	2.9E-04
Ctc1	1.5655	2.9E-03	Thsd7a	0.8500	2.8E-02
Lhpp	1.5615	2.0E-03	Alms1	0.8484	2.0E-02
Ablim3	1.5571	5.3E-04	Zfyve16	0.8477	1.8E-02
Msi1	1.5550	4.2E-03	Kiz	0.8453	3.8E-02
Onecut2	1.5548	2.0E-04	Ube3b	0.8451	4.9E-02
Rai2	1.5521	6.5E-04	Cdon	0.8440	2.1E-02
Zeb1	1.5462	1.5E-11	Afg3l1	0.8439	2.6E-02

Continued on next page

Table 19 – continued from previous page

Gene	log_2 FC	p-value	Gene	log_2 FC	p-value
Mmd2	1.5425	7.4E-06	Lamc1	0.8430	1.6E-02
Phldb2	1.5326	2.1E-02	Nup210	0.8428	2.6E-02
Zmiz1	1.5310	3.6E-10	Ldb1	0.8427	4.6E-02
Rgma	1.5299	3.0E-03	Plppr3	0.8397	7.9E-03
Nek6	1.5270	1.3E-02	Hdac1	0.8397	2.8E-02
Zfp61	1.5270	1.0E-02	Akap13	0.8391	1.6E-02
Cpne3	1.5264	2.2E-03	Dop1b	0.8387	4.5E-04
Frem1	1.5230	2.2E-02	Exoc4	0.8383	7.1E-07
Sp3	1.5224	2.0E-04	Nedd4	0.8376	1.7E-06
Rerg	1.5144	2.9E-02	2610316D01Rik	0.8357	3.0E-02
2210414B05Rik	1.5119	1.9E-02	March7	0.8349	4.2E-03
Susd6	1.5082	3.3E-08	Rimklb	0.8349	2.1E-02
Scarb2	1.5029	1.9E-05	Evi5l	0.8288	9.3E-03
Gas2	1.4999	1.1E-03	Agps	0.8285	1.4E-02
Shf	1.4953	4.2E-03	Pcm1	0.8272	4.9E-06
Sp4	1.4898	1.9E-03	Tmlhe	0.8248	3.6E-02
Slc39a14	1.4844	7.2E-04	Luzp2	0.8209	2.9E-02
Synpr	1.4838	3.3E-05	Nhs	0.8199	2.5E-02
Fgd4	1.4798	7.1E-16	Cog4	0.8192	1.3E-02
Elf1	1.4798	1.3E-02	Tuba1a	0.8192	4.6E-02
Plpp4	1.4748	1.0E-02	Arhgef1	0.8144	3.2E-02
Ppp2r2d	1.4744	8.9E-05	Dstn	0.8126	4.7E-02
Rdx	1.4691	1.6E-06	Cbx1	0.8114	3.1E-02
Gdpd5	1.4664	4.6E-07	Gdap1	0.8105	2.2E-02
Slc4a7	1.4540	4.6E-06	Eif3a	0.8066	3.5E-02
Amotl1	1.4536	4.5E-03	Cask	0.8060	3.4E-05
Slit1	1.4527	8.7E-07	Mir100hg	0.8056	5.4E-05
Tmem131l	1.4472	1.3E-09	Nfxl1	0.8044	3.8E-02
Gm16337	1.4461	2.4E-03	Kmt2c	0.8033	1.3E-04
St6gal1	1.4457	7.4E-05	Cbfa2t2	0.8031	4.3E-03
Grik1	1.4444	6.4E-03	Dpp8	0.8027	5.9E-03
Adam12	1.4421	3.6E-05	Fam133b	0.8007	6.3E-03
Sh3yl1	1.4401	2.5E-02	Pde3b	0.7991	2.4E-02
Slc10a7	1.4392	8.9E-05	Stk3	0.7981	1.0E-03
Dnah17	1.4378	2.1E-03	Pgap1	0.7980	9.0E-03
Tmtc3	1.4371	6.0E-03	Prpf39	0.7973	2.0E-04
Ap1s2	1.4354	1.4E-02	Pmpca	0.7958	4.7E-02
Bbx	1.4311	2.7E-05	Acadsb	0.7957	1.3E-02
Dock11	1.4307	3.1E-04	Cwf19l2	0.7955	4.1E-03

Continued on next page

Table 19 – continued from previous page

Gene	$\log_2$ FC	p-value	Gene	$\log_2$ FC	p-value
Nedd4l	1.4243	1.6E-17	Glcci1	0.7898	3.9E-02
Glce	1.4239	6.8E-04	Plcb1	0.7893	6.0E-05
Nxn	1.4207	3.7E-04	Fam172a	0.7867	5.2E-04
Adamts6	1.4181	8.0E-03	Cadm3	0.7844	1.2E-02
Enox2	1.4080	6.2E-04	Chd4	0.7838	4.3E-04
Pltp	1.4027	4.1E-02	Ehmt1	0.7826	1.7E-04
Clcn5	1.3991	8.5E-04	Xrcc5	0.7823	3.2E-02
Igf2bp2	1.3963	6.6E-04	Pacs2	0.7794	4.4E-02
Irak1	1.3945	3.2E-03	Tbl1x	0.7780	1.3E-03
Ralgapa2	1.3917	2.3E-15	Ints8	0.7780	1.9E-02
Kif3c	1.3874	2.7E-05	Hnrnpa2b1	0.7772	1.5E-05
Btbd3	1.3863	6.4E-04	Ppp1r9a	0.7770	3.5E-04
Abcb1b	1.3843	2.3E-02	Kdm5a	0.7769	2.4E-03
Cd200	1.3821	1.1E-03	Vav2	0.7732	2.9E-02
Igsf3	1.3812	1.3E-04	Top2b	0.7722	8.8E-04
40057	1.3803	4.4E-03	Ube2e3	0.7717	4.8E-02
Ophn1	1.3787	2.0E-07	Ptpn4	0.7712	6.8E-04
Itga4	1.3784	2.9E-03	Tbc1d12	0.7703	1.9E-02
Ythdf2	1.3775	6.3E-03	Cnot1	0.7700	2.1E-04
Lrp8	1.3750	2.3E-07	Zfp280d	0.7675	1.9E-03
Nuak1	1.3749	5.0E-05	Nfatc3	0.7666	3.8E-02
Cblb	1.3742	3.1E-05	Ptprk	0.7664	1.3E-03
Znrf2	1.3741	1.5E-04	Arhgap20	0.7656	8.0E-04
Pkia	1.3726	4.7E-07	Zfp536	0.7654	3.0E-02
Sufu	1.3654	7.6E-03	Ccdc93	0.7644	3.0E-02
Tnfrsf21	1.3607	3.3E-03	Ube2h	0.7634	4.6E-04
Rsl1d1	1.3580	2.5E-03	Cnot6l	0.7628	2.8E-02
Git2	1.3568	1.3E-05	5031425E22Rik	0.7626	8.9E-03
Adcyap1r1	1.3502	3.6E-04	Evl	0.7609	4.2E-03
Sh3kbp1	1.3481	4.1E-09	Xpo7	0.7591	2.6E-03
Gmip	1.3471	7.7E-03	Dnajc24	0.7574	4.9E-02
Chn2	1.3469	3.0E-04	Igf1r	0.7571	2.1E-03
Ap3b1	1.3445	2.3E-09	U2af1	0.7555	4.6E-02
Atp7a	1.3421	6.9E-03	Hdac2	0.7525	3.9E-02
Kdm6b	1.3417	3.3E-03	Exoc2	0.7518	1.2E-02
Nfib	1.3417	1.9E-11	Zdhhc17	0.7511	6.9E-03
Zdhhc6	1.3356	9.0E-03	Fer	0.7510	4.1E-03
Idh2	1.3343	1.1E-02	Htt	0.7506	1.5E-03
Cfdp1	1.3334	3.7E-07	Gm26672	0.7505	5.9E-03

Continued on next page

Table 19 – continued from previous page

Gene	log_2 FC	p-value	Gene	log_2 FC	p-value
Sema5a	1.3321	5.0E-03	Atp11c	0.7489	4.8E-02
Hunk	1.3306	2.6E-04	Taok3	0.7479	2.6E-02
Sgce	1.3267	1.4E-04	Gpr137c	0.7467	2.3E-02
Prrt1	1.3257	2.8E-03	Rnft2	0.7461	4.6E-02
Ntng2	1.3211	9.8E-05	Asah1	0.7457	2.5E-02
Eif4e3	1.3198	2.0E-04	Gng2	0.7410	3.6E-03
Zfp605	1.3194	2.6E-02	Myef2	0.7403	6.0E-04
Maml3	1.3162	8.5E-06	Mbnl1	0.7395	4.1E-02
Cntn2	1.3153	1.6E-02	Eml6	0.7393	1.1E-05
Pot1b	1.3082	4.7E-03	4632427E13Rik	0.7383	3.7E-02
Ankrd24	1.3008	5.3E-04	Ssbp3	0.7367	4.0E-03
Mid1	1.3006	4.2E-04	Lamp2	0.7362	2.6E-02
Gm42047	1.2998	1.7E-02	Hnrnpd	0.7354	1.9E-02
Itpr1	1.2980	2.8E-08	Arid2	0.7337	1.8E-02
Cyfip1	1.2959	2.4E-06	Snx24	0.7313	4.9E-02
Unk	1.2956	5.3E-03	Syn3	0.7313	4.5E-03
B3galnt1	1.2954	2.9E-02	Pias1	0.7305	1.1E-02
Tnrc18	1.2936	9.1E-10	Ilf3	0.7291	1.9E-02
Ndufab1	1.2929	1.7E-02	Kif5c	0.7282	2.3E-05
Ubash3b	1.2904	3.6E-04	Zfp292	0.7272	3.6E-03
3110039M20Rik	1.2851	1.3E-05	Fcho2	0.7265	3.7E-03
Adamts18	1.2834	7.3E-03	Sae1	0.7263	4.1E-02
Cbfa2t3	1.2830	8.3E-03	Hnrnpr	0.7243	2.5E-03
Patz1	1.2803	2.4E-03	Lims1	0.7241	6.2E-03
Vash1	1.2748	4.1E-03	Pam	0.7230	4.5E-03
Cpne2	1.2635	2.4E-02	Nsmaf	0.7221	1.7E-02
Nop58	1.2597	5.3E-04	Srcap	0.7219	2.3E-02
Tsg101	1.2569	5.2E-03	Thoc2	0.7218	4.8E-04
Atat1	1.2559	5.1E-03	Cep95	0.7200	3.4E-02
Thap4	1.2545	2.5E-02	Ncam1	0.7184	2.1E-05
Caprin2	1.2532	2.4E-02	Mapre2	0.7175	6.0E-03
Plcb4	1.2522	8.7E-05	Ncl	0.7175	3.9E-02
Rbms3	1.2511	2.0E-05	Pbrm1	0.7173	3.2E-03
Gm50368	1.2504	4.6E-04	Lrrn2	0.7168	1.5E-02
Lpp	1.2498	1.6E-05	Klf7	0.7164	1.5E-03
Zfp704	1.2449	8.4E-09	Cttnbp2	0.7157	4.3E-05
Ddx3x	1.2447	5.3E-03	Bclaf1	0.7149	1.0E-03
Rab8b	1.2421	2.1E-03	Jak1	0.7130	2.7E-02
Ccser1	1.2413	4.7E-13	Jph1	0.7128	2.6E-02

Continued on next page

Table 19 – continued from previous page

Gene	log_2 FC	p-value	Gene	log_2 FC	p-value
Elavl2	1.2407	1.5E-05	Ncor2	0.7121	6.5E-03
Svil	1.2399	3.4E-02	Upf3b	0.7116	2.9E-02
Pik3c2b	1.2352	4.1E-03	Cyth3	0.7096	2.8E-02
Nasp	1.2351	1.2E-03	Foxo3	0.7096	3.7E-02
Cuedc1	1.2317	3.4E-05	Macrod1	0.7083	3.1E-03
Prag1	1.2267	1.3E-02	Nrp1	0.7074	3.0E-02
Stxbp6	1.2264	6.2E-03	Fyn	0.7059	1.6E-04
Slc35f3	1.2262	3.9E-05	Dennd5a	0.7056	1.5E-02
Ahdc1	1.2247	4.6E-06	Megf11	0.7046	4.7E-02
Paqr8	1.2240	4.0E-03	Ccdc88a	0.7045	3.7E-04
Arhgef10l	1.2239	5.2E-05	Ccz1	0.7045	3.0E-02
Pxylp1	1.2217	3.9E-02	Fus	0.7012	5.8E-04
Rarb	1.2209	2.5E-02	Dcx	0.7007	2.2E-02
Tmem267	1.2191	1.6E-02	Plxna2	0.7003	3.0E-04
Spats2l	1.2184	5.3E-03	Gse1	0.6977	1.4E-03
Dek	1.2168	1.2E-02	Tab2	0.6939	2.7E-02
Mdc1	1.2145	3.8E-02	Rsrc2	0.6937	1.2E-02
Mllt3	1.2144	4.0E-12	Kat6b	0.6937	2.4E-03
Ptma	1.2092	2.3E-03	Xrn2	0.6921	2.4E-03
Foxg1	1.2078	2.1E-03	Osbpl9	0.6919	5.0E-03
Appl2	1.2066	3.0E-03	Sema4d	0.6907	1.3E-02
Lhfpl2	1.2064	1.3E-02	Iars	0.6884	2.7E-02
Cnr1	1.2056	1.2E-03	Pitpnc1	0.6873	3.6E-02
Grin3a	1.2045	1.2E-02	Epha3	0.6873	4.4E-02
Stat3	1.2018	2.1E-04	Uck2	0.6856	2.9E-02
Numa1	1.1964	4.7E-05	Thra	0.6854	4.7E-03
Sh3pxd2b	1.1949	4.2E-03	Foxj3	0.6842	3.1E-02
Nkain1	1.1910	4.9E-03	Ptprs	0.6833	1.1E-05
Zfhx2	1.1906	4.7E-07	Phf14	0.6815	4.4E-04
Neo1	1.1897	1.5E-07	Phip	0.6807	5.5E-04
Cachd1	1.1885	1.3E-03	Tbc1d23	0.6797	2.6E-02
Phf20	1.1873	1.7E-06	Nfkb1	0.6787	3.0E-02
Ppp2r3c	1.1865	1.3E-02	Srek1	0.6769	2.4E-03
Daam1	1.1859	9.9E-09	Smarca2	0.6768	1.9E-02
Psen1	1.1842	1.7E-03	Kdm5b	0.6763	1.9E-03
Fam129b	1.1835	3.9E-02	Dennd4c	0.6763	4.0E-02
Zhx3	1.1816	5.1E-06	Wsb1	0.6755	2.3E-02
Chst11	1.1783	6.8E-05	Lrch3	0.6741	8.1E-03
Nfia	1.1766	2.3E-05	Senp7	0.6737	3.0E-03

Continued on next page

Table 19 – continued from previous page

Gene	log_2 FC	p-value	Gene	log_2 FC	p-value
Arhgap31	1.1760	2.6E-02	Supt20	0.6734	1.5E-02
Snx1	1.1746	1.0E-03	Klf12	0.6713	8.8E-03
Myt1	1.1733	2.2E-03	Abca5	0.6706	4.0E-02
Cnn3	1.1705	4.3E-02	Flnb	0.6601	9.0E-03
9130019P16Rik	1.1699	3.1E-02	Nxpe4	0.6583	3.3E-02
Pdlim5	1.1682	4.3E-03	Washc4	0.6570	2.5E-02
Pxdn	1.1678	1.8E-03	Setx	0.6563	1.8E-02
Extl3	1.1643	1.2E-03	Zcchc8	0.6510	4.5E-02
Kcnip1	1.1637	2.6E-03	Bicra	0.6502	3.9E-02
Slc38a10	1.1619	1.9E-02	Ccnd2	0.6461	2.7E-02
Dpf3	1.1611	1.7E-02	Sec63	0.6448	2.2E-02
Rad21	1.1603	4.3E-02	Bmpr2	0.6423	2.5E-02
E430024I08Rik	1.1572	3.7E-03	Ric1	0.6415	2.9E-02
Map3k20	1.1568	1.4E-02	Focad	0.6413	2.8E-03
Cemip	1.1494	6.7E-03	Tacc2	0.6399	4.5E-02
Kmt2e	1.1490	2.9E-11	Insr	0.6391	3.1E-02
Kcnk2	1.1485	5.6E-04	Cdk13	0.6348	1.3E-02
Kcnk10	1.1453	8.3E-06	Syncrip	0.6344	4.7E-02
Arid1b	1.1450	1.4E-08	Tial1	0.6344	1.5E-02
Qsox1	1.1440	1.8E-02	AW554918	0.6340	1.2E-02
B4galt1	1.1430	3.6E-02	Setbp1	0.6327	9.7E-04
Plcg1	1.1401	6.9E-05	Brd8	0.6321	4.2E-02
Cep830s	1.1357	4.5E-02	Ascc3	0.6315	2.0E-03
Vps37d	1.1348	2.5E-02	Apc	0.6289	6.5E-05
Slc41a2	1.1348	4.4E-04	Shoc2	0.6275	4.8E-02
St3gal4	1.1343	1.4E-02	Araf	0.6231	4.9E-02
Psd3	1.1341	1.8E-09	Arhgef2	0.6215	3.7E-02
Ddb1	1.1340	1.1E-02	Rere	0.6213	3.7E-06
Gm16279	1.1319	2.9E-02	Dock7	0.6155	3.3E-03
Srsf1	1.1316	4.2E-04	Eif4g1	0.6098	2.1E-02
Gdpd1	1.1304	7.3E-04	1500004A13Rik	0.6079	1.8E-02
Pabpc1	1.1294	5.2E-04	Tmeff1	0.6054	4.9E-02
Psd2	1.1287	5.1E-03	Gm3764	0.6043	1.9E-02
Zfp608	1.1284	3.5E-05	Maco1	0.6038	1.9E-02
Dcc	1.1278	3.4E-06	Glg1	0.6019	2.1E-02
Metap1d	1.1256	1.9E-03	Spag9	0.6008	1.4E-03
Dock1	1.1245	2.5E-03	Ep400	0.5999	9.9E-03
Hnrnpa1	1.1242	5.5E-05	Smg1	0.5996	7.5E-04
Igsf21	1.1226	5.5E-06	Mtdh	0.5993	3.6E-02

Continued on next page

Table 19 – continued from previous page

Gene	log_2 FC	p-value	Gene	log_2 FC	p-value
Stxbp4	1.1223	1.6E-03	Luc7l3	0.5959	1.4E-04
Kdm2b	1.1198	3.3E-04	Tiam2	0.5944	4.7E-02
Bmpr1a	1.1189	2.2E-03	Fubp1	0.5915	1.6E-03
Nup153	1.1184	3.1E-03	Akap9	0.5908	4.4E-03
Ptk7	1.1181	9.8E-03	Nsmce2	0.5907	2.0E-02
Utrn	1.1175	5.8E-04	Hipk2	0.5894	3.0E-02
Celsr3	1.1131	5.6E-03	Pdss2	0.5888	2.2E-02
Wnk1	1.1096	9.5E-07	Sltm	0.5845	3.1E-03
Zfp811	1.1088	3.1E-02	Kcnb2	0.5845	5.5E-03
Zfhx3	1.1070	1.1E-02	Atl1	0.5823	4.9E-02
Dleu2	1.1067	3.0E-06	Zfp148	0.5794	6.2E-03
Camk1d	1.1063	4.6E-10	Bcl9	0.5792	4.3E-02
Ccdc112	1.1047	1.3E-03	Usp47	0.5783	3.3E-02
Ss18	1.1025	3.9E-02	Zfp973	0.5777	1.7E-02
4930488L21Rik	1.1016	1.6E-02	Nln	0.5772	4.6E-02
Gm38102	1.1001	5.6E-03	Dnajc1	0.5755	2.6E-02
Fbxl4	1.0986	2.1E-02	Rnpc3	0.5754	1.2E-02
Msi2	1.0980	1.1E-05	Usp9x	0.5749	1.9E-02
Arid1a	1.0963	1.5E-05	Hook3	0.5746	1.7E-02
Reln	1.0958	3.1E-02	Atad2b	0.5741	2.6E-02
Pard3b	1.0939	3.6E-03	Clasp2	0.5729	7.8E-04
Cep120	1.0932	3.2E-04	Kcnn2	0.5709	2.7E-02
Cdk6	1.0921	3.2E-02	Mon2	0.5696	4.1E-02
Rhobtb3	1.0912	2.0E-03	Cnot4	0.5657	1.4E-02
Arf4	1.0902	1.6E-02	Ptprj	0.5643	3.1E-02
Slc44a5	1.0869	6.2E-04	Dhx9	0.5591	4.8E-02
Ccdc50	1.0865	1.2E-05	Paxbp1	0.5585	6.0E-03
Lipe	1.0859	1.4E-02	Xkr6	0.5583	2.1E-02
Aldh1l2	1.0799	4.5E-02	Auts2	0.5582	1.5E-03
E130308A19Rik	1.0785	1.1E-02	Ptpra	0.5524	3.3E-02
Mest	1.0763	1.8E-02	Atrx	0.5492	2.9E-03
Matr3	1.0734	1.9E-02	Tsc22d1	0.5465	2.2E-02
Gm16036	1.0728	4.9E-02	Rb1	0.5463	3.9E-02
Prkca	1.0722	4.5E-05	Tia1	0.5461	1.1E-02
Lmnb1	1.0719	2.3E-02	D430041D05Rik	0.5414	2.1E-02
Lpin1	1.0709	5.3E-03	Snx29	0.5396	4.4E-02
Sh3gl3	1.0690	2.3E-04	Hnrnpm	0.5396	3.2E-02
Pknox1	1.0689	3.7E-02	Naa15	0.5359	4.9E-02
Baz2b	1.0685	8.9E-07	Pde4d	0.5357	1.6E-02

Continued on next page

Table 19 – continued from previous page

Gene	log_2 FC	p-value	Gene	log_2 FC	p-value
Tmem44	1.0679	1.2E-02	Golga4	0.5325	4.5E-02
Fmnl2	1.0648	4.5E-08	Itch	0.5291	4.9E-02
Cd2ap	1.0620	2.3E-04	Clasp1	0.5264	7.2E-03
Ctps2	1.0620	1.1E-03	Kdm4c	0.5233	2.3E-02
BC065397	1.0614	3.8E-02	Eps15l1	0.5209	4.3E-02
Trim24	1.0606	2.2E-04	Ntrk3	0.5196	1.5E-02
Arl5a	1.0604	1.6E-02	4930402H24Rik	0.5186	2.2E-03
Gpr19	1.0602	3.6E-02	Crebbp	0.5156	2.5E-02
Prdm10	1.0555	6.6E-04	Srgap2	0.5127	1.2E-02
Dhtkd1	1.0550	2.9E-02	Aff4	0.5101	2.7E-02
Eml5	1.0548	3.7E-08	Zfp638	0.5073	1.2E-02
Crebrf	1.0526	1.4E-03	Dapk1	0.5047	3.9E-02
Col4a1	1.0517	8.0E-04	Zzef1	0.5043	3.6E-02
Dclk2	1.0510	3.2E-05	Csnk1g1	0.4969	3.8E-02
Ankmy2	1.0503	9.8E-03	Arhgap21	0.4896	1.3E-02
Pde9a	1.0489	3.3E-03	Kif21a	0.4890	6.7E-03
Ccdc82	1.0478	1.7E-02	Sf3b1	0.4860	1.7E-02
Cep170	1.0470	2.7E-06	Setd5	0.4825	2.8E-02
Sdc2	1.0446	4.4E-03	Rbm5	0.4766	1.7E-02
Fxyd6	1.0427	3.1E-02	Ctif	0.4741	4.6E-02
Ephb2	1.0396	1.4E-04	Senp6	0.4664	4.5E-02
Ppm1d	1.0374	2.4E-02	Dnm1l	0.4646	4.0E-02
Pik3c3	1.0344	2.6E-02	Scaper	0.4571	4.5E-02
Tdrd3	1.0336	1.4E-02	Mapt	0.4533	7.0E-03
Dpysl3	1.0305	1.1E-04	Tulp4	0.4532	4.0E-02
Rgs9	1.0302	3.2E-02	Ntm	0.4528	4.1E-02
Kif26b	1.0288	7.2E-04	Gnaq	0.4496	2.4E-02
Pik3r1	1.0281	3.5E-04	Ccar1	0.4473	4.8E-02
Rad18	1.0276	2.7E-02	Rbm26	0.4387	2.9E-02
Mbtps2	1.0273	7.0E-03	C130071C03Rik	0.4361	4.5E-02
Fam102b	1.0262	3.5E-02	Syn2	0.4321	4.5E-02
Nck2	1.0254	1.6E-04	Rbm39	0.4253	1.3E-02
Rad51b	1.0246	1.3E-02	Enox1	0.4239	2.9E-02
Mmp24	1.0243	9.7E-03	Sorbs1	0.4235	3.5E-02
4933406I18Rik	1.0243	6.2E-03	Ubr5	0.4228	2.5E-02
Podxl2	1.0221	9.7E-03	Kif1b	0.4098	9.8E-03
Tbc1d8	1.0200	3.2E-03	Exoc6b	0.4059	3.6E-02
Pik3ip1	1.0190	3.1E-02	Ctnna2	0.3974	2.3E-02
Slc39a11	1.0159	2.6E-03	Ank3	0.3956	1.2E-02

Continued on next page

Table 19 – continued from previous page

Gene	log_2 FC	p-value	Gene	log_2 FC	p-value
Adk	1.0155	8.0E-03	Ncor1	0.3904	3.9E-02
CAAA01118383.1	1.0153	1.1E-02	Ttc3	0.3828	1.5E-02
Actb	1.0151	2.8E-02	Rbm25	0.3674	4.2E-02

8.4 SIGNIFICANTLY UPREGULATED GENES IN INACTIVE ENDOGENOUS NEURONS

Table 20: Significantly upregulated genes in inactive endogenous neurons compared to active endogenous neurons ordered by descending log_2 FC

Gene	log_2 FC	p-value	Gene	log_2 FC	p-value
B930036N10Rik	2.3094	6.87E-04	2610008E11Rik	0.499	1.10E-02
Jun	2.2684	2.71E-04	Samd14	0.4981	5.69E-03
Tmsb4x	2.2023	1.81E-07	Socs2	0.4977	1.41E-02
Tmsb10	2.2019	2.93E-05	Cul4a	0.4976	7.24E-03
Nap1l5	2.1524	4.10E-06	Rragd	0.4974	7.58E-04
Prdx1	2.0641	1.41E-05	Atf2	0.4968	7.84E-08
Frmpd1	1.9464	3.32E-05	Sf3b2	0.4968	5.54E-03
Sv2c	1.931	5.53E-04	Med13l	0.4952	6.94E-08
Nos1	1.8941	3.81E-07	Hsp90ab1	0.4934	2.15E-08
Cdh19	1.864	5.95E-05	Pus10	0.4926	6.64E-04
Csdc2	1.6741	1.09E-05	Grb10	0.4915	1.28E-04
Btg2	1.6712	5.06E-03	Tcf4	0.491	4.44E-07
Ap2s1	1.6569	1.86E-07	Cpd	0.4905	1.65E-05
Atp5mpl	1.6299	9.14E-04	Gins2	0.4894	3.61E-02
Smoc2	1.5744	2.43E-04	Slc25a23	0.4892	4.34E-03
Cp	1.5708	3.11E-05	Csnk1g1	0.4887	3.18E-10
Sash1	1.5376	3.22E-05	Fnip1	0.4877	1.54E-10
Atp5md	1.5215	4.13E-06	Zfp157	0.4876	1.92E-03
Ndufa4	1.4954	1.48E-04	Trp53inp1	0.4852	7.46E-08
Rps6ka5	1.4922	4.85E-13	Zmiz1os1	0.4852	7.90E-03
Hrk	1.4691	7.46E-08	Zbtb44	0.4844	1.28E-02
Dynll1	1.4578	2.52E-06	Rpl6	0.4839	1.05E-06
4930578M01Rik	1.4431	3.40E-05	Fubp1	0.4839	2.02E-08
Synpr	1.4294	1.54E-06	Csnk1a1	0.4834	4.88E-08
Polr2a	1.4258	3.33E-07	Fbxo25	0.4829	3.08E-04
Cotl1	1.4175	7.70E-05	Dcaf7	0.4823	7.72E-04
Nnat	1.4131	1.80E-11	Ptk2	0.4818	1.46E-06

Continued on next page

Table 20 – continued from previous page

Gene	log_2 FC	p-value	Gene	log_2 FC	p-value
Asrgl1	1.4065	5.13E-05	Optn	0.4817	4.70E-03
Lrig1	1.3819	3.09E-05	Cpa6	0.4814	6.08E-03
Sh3bgrl	1.3722	3.28E-09	Rgs17	0.4805	2.77E-03
Btg1	1.3691	1.33E-03	Sod2	0.4801	5.08E-04
Gm1604a	1.3615	1.24E-13	Slc18b1	0.4793	6.46E-05
Cpne6	1.3486	3.77E-06	Astn2	0.4789	2.75E-07
Pnmal2	1.3317	5.80E-04	Sez6l2	0.4788	2.04E-04
B3glct	1.3295	4.70E-04	Ror1	0.4783	1.94E-02
Sox4	1.3089	3.64E-05	Prpsap2	0.4781	1.35E-02
Rdm1	1.2897	3.45E-03	Pdzrn4	0.4777	1.47E-03
Tceal9	1.2865	3.97E-03	Lrfn2	0.4769	8.53E-06
Atp6voc	1.2822	8.00E-07	Plppr3	0.4755	9.19E-03
Kdm6b	1.2775	3.22E-07	Shisa4	0.4746	5.19E-04
Cacnb2	1.2757	1.93E-18	Shkbp1	0.4744	3.06E-02
Adamts18	1.2648	3.06E-05	Cdk17	0.4731	7.56E-06
Gm973	1.2631	3.35E-04	Dock7	0.4728	4.16E-09
Scrt1	1.2626	4.71E-06	Calm2	0.4724	7.45E-06
Sub1	1.2484	2.27E-05	Gm35256	0.468	1.97E-07
Cbfa2t3	1.2425	6.53E-05	Trim17	0.4672	1.89E-03
9530026P05Rik	1.2422	1.41E-04	Chga	0.4666	9.09E-03
Rapgef3	1.2351	9.76E-04	Syt14	0.4662	3.03E-04
Itga8	1.2299	3.32E-10	Zfx	0.4653	4.04E-03
Smarca2	1.228	2.88E-13	Arl5a	0.4651	3.22E-02
Tubb3	1.2268	3.87E-09	Trip4	0.4647	3.60E-05
Sntb2	1.2268	9.20E-10	Yes1	0.4645	2.67E-06
Rps24	1.2265	1.09E-09	Chpt1	0.4645	2.27E-05
Glis3	1.2074	1.72E-06	Alms1	0.4628	4.27E-03
Atpif1	1.2063	2.37E-09	Bace1	0.4621	1.14E-02
Arrdc3	1.2057	9.14E-08	Cacng4	0.4618	7.01E-06
Fndc1	1.2051	3.08E-07	Map2k2	0.4608	7.26E-04
Synpo2	1.1873	4.17E-03	Dpp6	0.46	3.90E-07
Gpam	1.1779	1.21E-07	Micos10	0.4592	1.70E-03
Ptms	1.1751	1.27E-06	Snca	0.4587	7.52E-06
Neurod2	1.1742	1.17E-04	Snph	0.4587	3.33E-03
Egfr	1.151	1.13E-03	Phkb	0.4581	1.13E-06
Pik3r3	1.1504	1.35E-10	Bcr	0.4574	2.43E-04
Qk	1.1493	5.57E-08	Hecw1	0.4568	8.48E-06
Cops9	1.1476	8.97E-04	Gprasp1	0.4566	1.53E-06
Wipf2	1.1431	1.98E-06	Urgcp	0.4563	1.70E-04
Vav3	1.1426	1.13E-06	Pgr	0.4562	3.07E-02

Continued on next page

Table 20 – continued from previous page

Gene	log_2 FC	p-value	Gene	log_2 FC	p-value
Gm30382	1.1333	2.13E-04	Celf4	0.4555	3.48E-07
Enc1	1.124	4.43E-05	Spop	0.4554	9.80E-04
Stat3	1.1145	4.67E-11	Zdhhc20	0.4541	2.54E-03
Tmtc4	1.1134	3.32E-07	Inpp4b	0.4539	6.21E-04
Pgrmc1	1.1115	1.86E-07	Osbp2	0.4539	6.99E-03
Vat1l	1.0973	1.48E-07	Tmem131l	0.453	8.96E-06
Ano4	1.091	1.19E-09	Kif21a	0.4523	1.08E-05
Ube2h	1.0841	4.54E-16	Ccdc92	0.4522	4.36E-02
Cntnap4	1.0792	3.52E-06	Lrrc8d	0.4517	1.15E-06
Ptprz1	1.0747	4.93E-07	Ankrd12	0.4508	4.88E-05
Ttc28	1.0658	2.05E-10	Map2k6	0.4505	2.22E-04
Lrrc57	1.0559	8.75E-03	Ryr2	0.4502	4.44E-04
Paip2	1.0513	1.40E-14	Tpst1	0.4493	6.89E-04
Slc16a1	1.0441	1.07E-04	Pelp1	0.4474	1.44E-02
Col4a5	1.0432	9.77E-04	Tia1	0.4471	1.54E-10
Hist1h2be	1.032	2.52E-04	Nim1k	0.447	1.74E-03
Tgfbr3	1.0316	1.19E-05	Tle5	0.4469	1.08E-03
Zfhx2	1.0234	4.88E-08	Sbf2	0.4464	5.44E-08
Tef	1.0178	1.57E-09	Grm5	0.4459	8.17E-07
Gm13483	1.0121	5.17E-08	Rnf182	0.4456	2.71E-04
Atxn7l3b	1.0114	5.60E-04	Cblb	0.4453	1.67E-02
A230057D06Rik	1.0034	6.00E-19	Tmx4	0.4446	5.67E-06
Zbtb20	1.0009	2.53E-06	Snx12	0.4437	1.58E-09
Rbx1	0.9987	2.62E-03	Rsf1	0.4435	3.42E-04
Pard3b	0.9909	6.92E-06	Galnt13	0.4405	2.91E-04
Ppp1cb	0.9886	1.43E-13	Pcdh9	0.4402	2.96E-04
Sdk1	0.9798	3.51E-07	Sh3gl3	0.4392	2.60E-03
Zfhx2os	0.9762	2.42E-06	Tango2	0.4385	1.59E-04
Dynlrb1	0.9758	2.73E-03	Acbd6	0.436	2.41E-07
Sparcl1	0.9752	1.26E-06	Tcaf1	0.4359	1.17E-06
Jph4	0.9697	5.71E-13	Lrriq1	0.4339	5.90E-05
Matn2	0.9632	9.21E-04	Upf2	0.4331	1.11E-03
Abca8a	0.9625	9.17E-03	Tbc1d31	0.4316	3.60E-05
Stmn1	0.9622	1.22E-07	Sppl2a	0.4308	8.69E-03
Cox6b1	0.9563	3.08E-08	Kat6a	0.4307	1.46E-06
Prkag2	0.9558	3.75E-10	Rere	0.4303	2.39E-12
N4bp2	0.9553	1.55E-04	Fam126b	0.4293	1.12E-07
Gm5087	0.9533	1.71E-03	Gabrb2	0.4288	1.10E-04
Dhx40	0.9414	9.05E-06	Kansl3	0.4287	2.24E-02
Ccdc171	0.9348	2.76E-08	Cacng2	0.4282	1.91E-04

Continued on next page

Table 20 – continued from previous page

Gene	log_2 FC	p-value	Gene	log_2 FC	p-value
Rps8	0.9343	8.52E-08	Slc44a1	0.4277	1.27E-04
Sipa1l3	0.9282	4.74E-08	Kansl1	0.4273	1.14E-09
Ntsr1	0.9231	2.64E-04	Smg6	0.4265	1.73E-06
Nyap2	0.9192	1.52E-14	Baz2b	0.4261	1.06E-08
Gab1	0.9173	1.42E-07	Trerf1	0.426	8.29E-07
E430024P14Rik	0.9124	2.55E-03	Rnf165	0.4257	8.42E-04
Nek7	0.9073	5.48E-05	Camk2a	0.4242	3.36E-04
Pou2f2	0.8995	6.54E-06	Arid4b	0.4237	9.86E-06
Specc1	0.8995	8.55E-08	Esrrg	0.4237	1.03E-03
Rgma	0.8985	1.03E-06	Chst1	0.4221	4.04E-02
Sncb	0.8974	6.70E-05	Ndufb1-ps	0.4212	2.53E-05
Peli2	0.8924	2.08E-08	Mpp6	0.4211	9.37E-03
Cox7b	0.8897	4.37E-07	Pias1	0.4209	3.64E-03
Pabpc1	0.8858	1.54E-07	Rbbp6	0.4204	3.29E-05
Nuak1	0.8848	4.61E-11	Nsd1	0.4203	5.48E-09
Msi2	0.8751	1.92E-11	Zfp148	0.4199	2.96E-09
Dnajb4	0.8605	3.39E-06	4921511C10Rik	0.4195	2.01E-04
Ctsl	0.8585	1.14E-03	Gm9801	0.4192	3.38E-04
Srgap3	0.8511	5.53E-16	Ncor1	0.4188	1.55E-05
Lrrc4b	0.8455	6.62E-06	Rb1cc1	0.4184	1.94E-05
Stard13	0.8454	1.05E-03	Nfix	0.4182	4.67E-11
Hibadh	0.8445	1.85E-06	Nono	0.4168	3.38E-02
Tuba1a	0.8445	2.14E-09	Cdk19	0.4168	9.99E-09
Tmem117	0.8427	1.13E-07	Rassf8	0.4159	2.26E-02
Ncoa1	0.8374	6.00E-19	Fbxo10	0.4158	2.28E-04
Sema4f	0.8354	9.61E-03	Gm20754	0.4155	1.20E-02
Atp1a3	0.8338	2.96E-08	Rabl6	0.4151	1.06E-02
Trp53bp2	0.8338	3.86E-03	Sqstm1	0.414	5.53E-04
Plce1	0.8334	2.43E-04	B3galnt2	0.4139	8.12E-03
Slc44a5	0.8325	2.95E-06	Eml1	0.4138	1.07E-06
Thra	0.8308	5.71E-13	Nova2	0.4136	9.20E-04
Rbms2	0.8289	1.47E-05	Ywhaq	0.412	2.12E-05
Pcp4	0.8231	1.46E-06	Caprin1	0.4118	1.17E-05
Galnt16	0.8222	1.41E-04	Arpc1a	0.4118	1.82E-06
Grm1	0.8221	2.15E-07	Zfp948	0.4112	1.16E-07
Mbd5	0.8213	1.32E-12	Nfat5	0.4109	6.58E-08
Jund	0.8167	2.04E-03	Hlcs	0.4099	9.29E-05
Siah1a	0.8106	4.49E-05	Asxl1	0.4096	5.09E-06
Xiap	0.8062	2.22E-07	Rab40c	0.4077	6.32E-03
Ptma	0.806	4.57E-07	Gm10848	0.4074	2.13E-02

Continued on next page

Table 20 – continued from previous page

Gene	$\log_2$ FC	p-value	Gene	$\log_2$ FC	p-value
Nufip2	0.8037	1.17E-10	4921534H16Rik	0.4065	4.59E-02
Crtac1	0.8019	6.11E-08	Ypel3	0.4055	2.75E-03
Vcp	0.801	2.15E-07	Acadsb	0.4053	3.67E-08
Gabra2	0.7973	6.55E-08	Ypel4	0.4052	1.73E-02
Stim2	0.7935	1.83E-04	Chl1	0.4049	2.08E-08
Pten	0.7917	5.71E-13	Ddx6	0.4049	1.85E-03
Selenow	0.7893	1.36E-10	Myo6	0.4046	3.01E-06
Gm16083	0.7893	7.90E-09	Sfpq	0.4045	3.32E-10
Cntn2	0.7888	1.45E-06	Rtn3	0.4038	2.24E-09
Syn2	0.7887	8.54E-13	Aff2	0.4037	5.34E-06
Stox2	0.7878	4.28E-10	Arf3	0.4037	4.82E-04
Gm46102	0.7873	3.15E-03	Phc3	0.4023	3.85E-04
Disp3	0.7871	9.93E-04	Vps13a	0.4016	6.01E-06
Cntnap2	0.7827	3.79E-08	Prr12	0.4012	2.86E-02
Pnrc1	0.7782	8.58E-05	Gm14326	0.4011	3.67E-04
Lhfpl3	0.7773	4.10E-05	Pak7	0.4008	3.64E-05
Fgd4	0.7753	2.05E-10	Fam120b	0.4007	5.63E-04
Fam120c	0.7744	3.87E-09	Insr	0.3996	1.58E-08
Nxn	0.773	4.81E-05	Dner	0.3993	7.34E-04
Sem1	0.7714	2.37E-04	Slc24a2	0.399	1.66E-04
Sec24d	0.771	2.35E-04	Akap6	0.3984	2.91E-09
Nkain3	0.771	2.62E-05	Mbtd1	0.3969	8.26E-06
Gm32250	0.7696	1.47E-03	Rabep1	0.3968	4.69E-05
Slit1	0.7687	2.83E-06	Stmn2	0.3968	7.41E-09
Irs2	0.7668	6.07E-06	Riok1	0.3966	8.75E-03
Ttc3	0.7667	2.36E-21	Tnrc6c	0.3966	1.22E-05
Rgl1	0.7636	1.45E-09	Gm31356	0.3964	5.78E-03
Zfp462	0.7635	2.27E-09	Prag1	0.3958	9.86E-03
Gnb1l	0.7622	5.46E-03	Commd1	0.3953	5.43E-04
Pak3	0.7595	8.66E-10	Hook2	0.3952	1.45E-05
Trim2	0.7534	7.63E-16	Tmem130	0.395	1.26E-04
Cpe	0.7517	2.87E-10	4933406I18Rik	0.3948	3.65E-07
Fam214a	0.7501	2.27E-06	Mfsd13a	0.3945	2.94E-02
Zeb1	0.748	1.43E-10	Slc7a6os	0.393	1.04E-02
Ppia	0.7463	1.36E-10	Zfp280d	0.3927	1.37E-03
Disp2	0.7445	1.43E-04	Slc17a7	0.3924	2.19E-02
Kif1bp	0.7437	1.58E-06	Cables1	0.3921	1.25E-07
Tpd52l1	0.7436	8.46E-05	Ly6h	0.3915	4.70E-03
Bmerb1	0.7433	5.71E-13	Sesn3	0.3901	3.15E-05
Snrpg	0.7415	1.62E-06	Cfap54	0.3887	1.61E-04

Continued on next page

Table 20 – continued from previous page

Gene	log_2 FC	p-value	Gene	log_2 FC	p-value
Rapgef2	0.7397	9.37E-12	Dars2	0.3874	4.24E-02
Astn1	0.7384	7.91E-11	Kcnip1	0.3873	1.35E-02
Top1	0.7384	1.16E-07	Trim37	0.3869	1.59E-02
Ftx	0.7333	2.89E-08	Cdk12	0.3865	5.36E-04
Ptch1	0.7313	1.60E-04	Arhgap39	0.3856	6.68E-05
Nhs	0.7297	2.03E-06	Gm44151	0.3851	1.03E-02
Dapk1	0.7296	2.12E-07	Me1	0.3848	7.99E-03
Coro2b	0.728	2.77E-04	Slc38a2	0.3845	3.88E-04
Zmym4	0.725	1.62E-09	Itsn2	0.3839	4.60E-06
Arhgap12	0.721	6.35E-13	AU040320	0.3838	6.49E-03
Slc35f3	0.7207	4.41E-05	Pafah1b1	0.3833	4.83E-08
Zfp963	0.7162	8.51E-04	Wdr60	0.383	1.48E-02
Cdh9	0.7156	5.98E-04	Ddhd1	0.3825	5.24E-06
Rab30	0.7147	2.90E-09	Aak1	0.3823	4.22E-07
Ogfod1	0.7111	4.88E-04	Frmd5	0.3823	1.77E-05
Wnt5b	0.7103	1.74E-04	Smarcc1	0.3816	1.19E-05
Mdga1	0.7096	1.29E-05	Unc45a	0.3815	1.61E-03
Tab2	0.7066	1.71E-08	Senp1	0.3814	3.10E-03
Erbb4	0.706	5.95E-03	Ppp1r14c	0.3806	9.23E-05
Soat1	0.7048	3.48E-05	Flnb	0.3805	5.41E-03
Dync2h1	0.7035	1.54E-07	Tet3	0.3805	5.95E-06
Pigu	0.7023	2.63E-05	Dym	0.3802	6.98E-09
Mgat5b	0.7022	4.60E-05	Txnrd1	0.3798	2.53E-04
Tex15	0.7005	7.05E-05	Crtc3	0.3798	5.07E-03
Chgb	0.7005	2.99E-03	Dock4	0.3797	4.25E-05
Slc4a4	0.6987	1.21E-07	Retreg3	0.3789	2.61E-02
Eml6	0.6971	6.07E-11	Ndufv3	0.3785	3.15E-05
Syn1	0.6936	6.78E-09	Usp35	0.3784	4.51E-02
Phka1	0.6923	4.16E-07	Baz1b	0.378	2.69E-04
Mettl7a1	0.6908	5.07E-03	Srrm3	0.3779	1.31E-03
Slc24a4	0.6892	1.99E-03	Ints8	0.3779	4.44E-04
Kri1	0.6876	5.76E-03	Armh3	0.377	7.03E-05
Trpm3	0.6867	1.08E-04	Pnkp	0.3767	2.92E-02
Unc5c	0.6862	1.16E-05	Adgrl3	0.3764	1.85E-06
Mef2d	0.6857	5.01E-06	Stim1	0.376	9.62E-06
Ntm	0.6836	1.60E-08	Slc7a14	0.3752	9.61E-03
Ranbp9	0.6835	3.42E-07	Rnf180	0.3747	1.73E-05
Cadm1	0.6814	2.89E-09	Gnas	0.3739	2.30E-06
Itm2b	0.6812	1.78E-04	Enox2	0.3738	1.11E-03
Cntnap5a	0.6811	1.44E-03	Kif13b	0.3736	1.07E-02

Continued on next page

Table 20 – continued from previous page

Gene	log_2 FC	p-value	Gene	log_2 FC	p-value
Pxdn	0.6808	1.00E-06	Cux2	0.3734	1.46E-04
Dok6	0.6792	8.41E-08	Tacc2	0.3724	2.65E-02
Ahcyl2	0.6782	3.85E-07	Depdc5	0.372	8.68E-10
Ophn1	0.6729	1.89E-09	Hacd3	0.3717	3.01E-03
Ptpn4	0.6727	1.50E-12	Syt17	0.3715	1.10E-03
Dock10	0.6699	5.02E-05	Dcun1d3	0.3708	1.18E-03
Oaz2	0.669	8.99E-04	Pik3r1	0.3703	2.69E-04
Trafd1	0.6667	2.66E-03	Abcf1	0.3699	1.19E-02
Grin3a	0.6663	1.12E-03	Skp1a	0.3698	4.73E-05
Purb	0.6659	9.66E-07	Man1c1	0.3698	2.10E-03
Pakap.1	0.6646	2.99E-05	Tead1	0.3698	3.86E-03
Ibtk	0.6594	9.14E-06	Minpp1	0.3694	1.43E-04
Hivep3	0.6571	4.02E-09	Nfia	0.3688	4.48E-04
Mir99ahg	0.6571	5.76E-11	Tjp1	0.3683	8.12E-07
Gm20616	0.6546	1.98E-02	Camk2n1	0.3681	2.52E-06
Timp2	0.6541	6.84E-05	Mcts1	0.3676	3.39E-05
A330076H08Rik	0.6526	4.67E-11	Lrp6	0.3674	6.89E-04
Spata6	0.6524	1.48E-06	Tra2a	0.3672	6.33E-05
Elavl3	0.6515	2.84E-11	Spon1	0.3672	7.18E-05
Btbd3	0.6445	2.52E-04	Amer2	0.3667	4.00E-02
Susd6	0.6433	1.24E-07	Zfp57	0.3664	1.56E-02
Lman2l	0.6417	8.74E-07	Prkg1	0.3662	5.67E-04
Slc1a3	0.6408	2.20E-03	Ano3	0.3662	4.03E-05
Phf20	0.6402	3.16E-10	F13a1	0.3659	1.61E-02
Kctd4	0.6382	1.13E-02	Auts2	0.3653	3.40E-04
Basp1	0.6371	5.92E-08	Ankfy1	0.3641	1.05E-02
Nedd8	0.6359	2.02E-04	Slc16a2	0.3637	1.39E-02
H3f3b	0.6346	1.75E-04	Psmb7	0.3628	1.50E-02
Olfm2	0.6321	2.16E-05	Tubb4a	0.3627	2.29E-04
Pdlim5	0.6303	6.70E-08	Dtnb	0.3615	2.71E-07
Clcn3	0.6287	1.15E-06	Gm46218	0.3607	9.30E-04
Kmt2e	0.6279	8.11E-15	Zeb2	0.3606	2.86E-04
Rp9	0.6265	1.94E-04	Sox5	0.3601	3.22E-03
Esrra	0.6237	4.54E-05	Gtf2ird1	0.36	2.63E-03
Gfod2	0.6217	3.99E-04	Rbms3	0.36	2.27E-05
Epha5	0.6192	8.15E-08	Ralgapa2	0.3594	1.30E-08
Ccdc88a	0.619	5.95E-09	Nhsl1	0.3594	4.21E-05
5730522E02Rik	0.6188	2.96E-07	Bod1l	0.3593	7.08E-06
Ahdc1	0.6185	1.72E-04	Phc2	0.3592	1.27E-03
Fam13a	0.6148	1.75E-04	Peak1	0.359	5.25E-07

Continued on next page

Table 20 – continued from previous page

Gene	log_2 FC	p-value	Gene	log_2 FC	p-value
Maml2	0.614	2.32E-03	Gpr19	0.3588	9.09E-03
Prxl2c	0.6135	5.95E-03	Coq3	0.3582	7.24E-04
Glce	0.6134	6.53E-10	Zfr	0.3582	1.91E-05
Tmem59	0.6131	2.45E-05	A730081D07Rik	0.3579	1.28E-03
Xpr1	0.611	2.06E-08	Gm32618	0.3578	1.69E-02
Plcb4	0.6107	2.91E-08	Zhx3	0.3575	2.15E-03
Neto2	0.6097	1.29E-05	Wwc2	0.3573	9.01E-06
Nsg2	0.6074	6.31E-07	Sh3gl1	0.3567	1.25E-03
Dock1	0.6052	2.40E-06	Ino80dos	0.3556	2.48E-04
Calm1	0.6033	2.88E-13	Copa	0.3549	1.15E-04
Grin1	0.6026	8.50E-06	Med26	0.3545	1.34E-04
Map7	0.6013	1.71E-08	Tmem260	0.3535	5.35E-06
Nr3c2	0.5997	5.40E-04	Gm16105	0.3534	4.01E-02
Hdgfl3	0.5966	6.55E-08	Caln1	0.3531	4.26E-03
Upp2	0.5963	7.46E-09	H13	0.3529	9.50E-03
Setbp1	0.5934	3.65E-08	Qser1	0.3526	2.75E-03
Kcnq1ot1	0.5931	2.06E-08	Itm2c	0.3523	4.17E-04
Mllt3	0.5917	2.99E-09	Clstn2	0.3522	9.90E-03
Rufy1	0.585	5.63E-04	Pgap2	0.3518	5.29E-04
A330023F24Rik	0.5848	8.87E-07	Smyd3	0.3517	2.89E-04
Ik	0.5847	1.54E-02	Tspyl4	0.3517	6.06E-05
Ccar1	0.5832	6.04E-06	Tcerg1	0.3516	3.82E-03
Npas3	0.5817	1.74E-03	Atrx	0.3512	2.61E-05
Rbfox1	0.5812	1.37E-06	C2cd3	0.3501	3.84E-05
Synj2bp	0.5811	5.32E-04	Tmod2	0.35	2.27E-04
Vwa5b2	0.5805	1.66E-02	Cers4	0.3497	1.68E-07
Lpp	0.5789	3.22E-07	Fam118b	0.3494	1.42E-03
Sgms1	0.5783	1.89E-09	Larp4	0.349	4.56E-03
Actb	0.5771	3.32E-10	Ptpn13	0.3489	1.20E-04
Kctd1	0.5769	6.54E-07	Ifnar2	0.3487	4.14E-04
Gm42722	0.5751	7.95E-03	Ston2	0.3485	1.75E-03
Abcc4	0.5745	1.85E-05	Ikzf2	0.3484	3.82E-04
Grik1	0.5742	2.64E-03	Dennd2a	0.3483	1.86E-04
Lsamp	0.5738	3.59E-05	Dstyk	0.348	1.48E-03
Ranbp17	0.5715	1.38E-06	Gm6145	0.3478	7.26E-06
Dennd4c	0.5711	8.67E-07	Zmat1	0.3475	2.90E-05
Runx1t1	0.5658	1.78E-04	Chd8	0.347	7.91E-11
Safb	0.5655	1.92E-04	Cntrl	0.3467	5.16E-03
Zfyve9	0.5645	2.27E-05	Dnajb6	0.3457	5.83E-04
Naaladl2	0.5636	1.45E-09	Lsm7	0.3453	2.75E-02

Continued on next page

Table 20 – continued from previous page

Gene	log_2 FC	p-value	Gene	log_2 FC	p-value
Mmd2	0.5635	3.63E-06	Rnf185	0.3436	3.98E-04
Syn3	0.5625	6.11E-09	Plxna4	0.3434	4.67E-03
Khdrbs2	0.5616	5.48E-05	Rybp	0.3428	4.35E-04
Zfp282	0.5577	1.49E-02	Hps5	0.3422	1.73E-03
Taok3	0.5576	4.33E-05	Acbd5	0.3418	4.95E-02
Cdh13	0.557	9.20E-05	4632427E13Rik	0.3418	1.74E-04
Psd	0.5567	4.82E-04	Neto1	0.3415	2.84E-04
Ro60	0.5567	3.12E-04	Ube2r2	0.3415	1.76E-11
Iqcb1	0.5554	4.13E-06	Ablim3	0.3411	3.21E-02
Dgkg	0.5552	1.74E-04	Bcl9	0.341	1.78E-02
Atp5j	0.553	1.66E-06	Adgra1	0.3404	1.03E-03
Epc1	0.5524	2.34E-06	Nabp1	0.3401	3.71E-03
Snap47	0.5521	4.56E-04	Grk4	0.34	2.32E-02
Ankrd13c	0.5519	7.18E-05	B830012L14Rik	0.3397	1.94E-04
Nckap5	0.5484	2.40E-07	Mar 08	0.3396	7.99E-03
Dcaf6	0.5478	1.46E-07	Rab43	0.3395	2.32E-03
Tmcc1	0.5477	9.66E-13	Bmpr1a	0.3392	2.30E-05
Kazn	0.5474	3.80E-06	Anp32a	0.3386	3.84E-02
Spock2	0.5467	4.57E-07	Clvs1	0.3383	5.22E-09
Ywhaz	0.5466	1.86E-08	Kdm6a	0.338	1.92E-05
Fam168a	0.5464	1.07E-11	Gmeb1	0.3375	1.48E-02
Tmem38a	0.5463	6.97E-03	Zfp652	0.3367	1.47E-04
Ptprk	0.5459	9.23E-05	Prkca	0.3364	2.65E-04
Rab5b	0.5449	1.16E-03	Tmtc3	0.3362	5.57E-03
Dzip1	0.543	1.41E-06	Senp5	0.336	9.79E-03
Cep95	0.5428	2.28E-04	Smc3	0.3356	6.66E-04
Stx6	0.5423	2.11E-04	Dnajc1	0.3355	5.16E-04
Plppr2	0.5416	9.30E-04	Trim46	0.3348	7.39E-04
Gm14329	0.5395	2.73E-02	Dop1a	0.3341	5.95E-03
Dscaml1	0.5385	1.60E-06	Naxd	0.334	4.24E-02
Ak5	0.538	7.03E-05	Mtor	0.3339	1.61E-02
Etv6	0.5373	1.46E-06	Neo1	0.3334	4.54E-08
Sox11	0.5365	2.40E-06	Kdelr1	0.3332	1.78E-02
Ncam1	0.5353	6.08E-07	Cacna1e	0.3332	1.60E-04
Ntng2	0.535	1.29E-02	Gria1	0.3332	1.87E-03
Bex2	0.5349	3.88E-08	Dlg3	0.3331	2.68E-03
Cox7a2	0.5347	3.32E-05	Pbx1	0.3331	9.84E-04
Ubxn4	0.5331	1.32E-04	Ankrd11	0.3321	4.65E-05
Klhl24	0.5328	1.08E-02	Arid1a	0.3311	1.76E-05
Cdr1os	0.53	7.48E-09	Sncaip	0.3309	8.20E-04

Continued on next page

Table 20 – continued from previous page

Gene	log_2 FC	p-value	Gene	log_2 FC	p-value
Taok1	0.5293	4.40E-07	Ddx19b	0.3308	2.42E-02
Grik2	0.5269	3.08E-06	Porcn	0.3305	4.97E-02
Gabbr1	0.5268	1.61E-03	Usp33	0.3304	1.45E-02
Map4k4	0.5268	5.19E-09	Tsc22d2	0.3301	8.71E-04
9930021J03Rik	0.5266	1.58E-05	Tcf20	0.3301	7.33E-05
Ehmt1	0.5263	1.02E-06	3110039M20Rik	0.3293	1.03E-05
Zmiz1	0.5255	4.24E-05	Plk2	0.3293	2.43E-02
Ice2	0.5245	1.23E-02	5031425E22Rik	0.3292	1.15E-06
Arl15	0.5236	5.46E-05	Tbc1d23	0.3288	4.48E-02
Galnt14	0.5223	1.45E-03	Kif26b	0.3286	2.68E-02
Sorbs1	0.5209	4.51E-09	Snx4	0.3285	6.05E-03
Hdac8	0.5203	1.71E-08	Actl6b	0.3279	2.31E-02
Ssbp3	0.5198	2.96E-09	Syt1	0.3276	1.03E-03
Tsc22d4	0.5193	7.18E-04	Btbd7	0.3271	1.67E-07
Tmem164	0.5192	6.29E-04	Hexdc	0.3269	3.63E-03
Ssb	0.5191	1.22E-05	Ldlrad4	0.3266	5.55E-03
Tmem29	0.5189	9.58E-05	Ndufc2	0.3265	2.20E-04
Tut4	0.5181	3.42E-09	Adnp	0.3263	2.36E-06
Npepps	0.5176	1.05E-07	Tubb2a	0.3262	1.53E-07
Fmnl2	0.516	2.36E-10	Kdm5c	0.3261	2.68E-02
Carmil1	0.5147	5.32E-07	Gm6566	0.3261	8.45E-03
Apc2	0.5144	8.62E-03	Spint2	0.3259	1.85E-02
Sez6	0.5125	4.86E-04	Slc25a12	0.3255	7.12E-04
Cbx5	0.5116	6.35E-04	Cnr1	0.3255	8.26E-06
Ammecr1	0.5113	1.14E-02	Atp6voe	0.3254	2.73E-03
Mar 03	0.5106	3.71E-04	Pura	0.325	8.57E-04
Etfa	0.5105	1.83E-02	Frg1	0.3246	4.01E-02
Ppp1r13b	0.5104	7.07E-04	Cacng8	0.3245	5.41E-04
Zcchc18	0.5103	4.93E-04	Gm37679	0.3244	2.62E-02
Ubash3b	0.508	7.08E-06	Sema4d	0.3243	1.65E-02
Hnrnph3	0.508	5.41E-03	Zc3h13	0.3226	4.51E-03
Igf1r	0.5072	1.12E-09	Siah3	0.3225	1.58E-02
Eny2	0.507	2.14E-04	Phf21a	0.3223	6.08E-04
Mir100hg	0.5067	2.66E-07	Mbd2	0.3223	3.02E-04
Celf6	0.5066	2.75E-04	Arf4	0.3221	4.42E-05
Pag1	0.5065	4.49E-05	Ppp3ca	0.3221	2.26E-06
Smad3	0.5056	1.42E-02	Prrc2c	0.322	6.62E-06
Metap1d	0.5054	2.06E-03	Osbpl6	0.322	6.77E-04
Phlpp1	0.5029	2.39E-08	Ints6	0.3219	4.18E-08
Rap2a	0.5022	1.89E-03	Vps37b	0.3213	2.94E-02

Continued on next page

Table 20 – continued from previous page

Gene	log_2 FC	p-value	Gene	log_2 FC	p-value
Rspo2	0.5017	3.28E-03	Pitpnc1	0.3212	1.93E-05
St5	0.5014	3.35E-03	Usp29	0.3208	1.02E-06
Gpc5	0.5003	6.53E-03	Smurf2	0.3201	1.34E-04
Adcy9	0.5001	4.32E-07	Wasf2	0.3201	1.95E-03
Thada	0.5	6.96E-04	Foxo3	0.3201	8.11E-03
Sphkap	0.4992	2.05E-04			

8.5 SIGNIFICANT DOWNREGULATED GENES IN INACTIVE ENDOGENOUS NEURONS

Table 21: Significantly downregulated genes in inactive endogenous neurons compared to active endogenous neurons ordered by descending log_2 FC

Gene	log_2 FC	p-value	Gene	log_2 FC	p-value
Nr4a1	-2.5602	5.47E-05	Atad3a	-0.5255	2.76E-02
Gm5820	-2.4692	1.19E-05	P4ha1	-0.5227	4.24E-03
A830036E02Rik	-2.1229	4.15E-05	Hnrnpa3	-0.5221	9.42E-03
Vgf	-2.0741	4.05E-04	Crebzf	-0.5205	2.30E-02
Abca7	-1.8557	1.42E-05	Palmd	-0.5197	1.81E-02
Rad51ap2	-1.8151	1.59E-04	Gm28379	-0.519	2.49E-03
P4ha2	-1.8057	2.03E-03	Mttp	-0.5179	1.98E-02
Fras1	-1.7901	7.41E-08	Las1l	-0.5178	1.01E-02
Ptprr	-1.7251	9.03E-11	Gm16599	-0.5172	2.60E-03
Neurl1b	-1.7163	1.32E-04	Vgll4	-0.5149	7.29E-04
Gm36251	-1.6974	2.14E-05	Adgrb1	-0.5131	2.50E-03
Shc3	-1.6903	1.13E-07	Rnft1	-0.511	2.62E-02
Gng4	-1.6449	1.38E-03	Cdk5	-0.511	1.76E-02
Gm15563	-1.6198	1.10E-06	Snap25	-0.5096	2.55E-08
9630014M24Rik	-1.5866	6.43E-06	Rasal2	-0.5092	4.14E-04
Spred3	-1.5731	1.35E-04	Raph1	-0.5077	7.19E-05
Sqle	-1.535	6.98E-04	Cd163l1	-0.5075	3.12E-03
Jcad	-1.5118	1.29E-04	Agfg1	-0.5069	1.16E-03
Gm15243	-1.4518	2.13E-04	Prkci	-0.5045	8.08E-03
Hecw2	-1.4308	4.02E-20	Traf3ip1	-0.5038	6.73E-04
Pcsk1	-1.4299	3.68E-04	Gm50232	-0.5033	7.34E-04
Gm12027	-1.4217	4.43E-04	Nap1l1	-0.501	3.03E-03
Gm48677	-1.4181	2.48E-04	Pcyt2	-0.4991	1.40E-02

Continued on next page

Table 21 – continued from previous page

Gene	log_2 FC	p-value	Gene	log_2 FC	p-value
4933439C10Rik	-1.4116	2.39E-04	Entr1	-0.4987	2.06E-03
Dhcr24	-1.3963	1.15E-03	Ext1	-0.4987	5.04E-04
Myo16	-1.3963	1.24E-13	Ndrg4	-0.4972	2.32E-03
Gm15337	-1.3944	5.27E-04	Fam189a1	-0.4968	1.81E-03
Gm26953	-1.3537	1.56E-06	Agrn	-0.4964	4.89E-03
Gm34544	-1.3149	4.66E-03	Odc1	-0.4924	1.51E-02
Cmss1	-1.3139	9.60E-09	Ktn1	-0.4908	1.33E-05
Krt12	-1.295	1.03E-03	Sf1	-0.4906	8.92E-03
Msmo1	-1.2846	6.22E-04	Robo1	-0.4906	1.15E-03
Lss	-1.2691	5.32E-04	Arhgap26	-0.4898	4.93E-05
Hmgcr	-1.2648	5.48E-06	Gm32509	-0.4896	1.27E-02
Gm42609	-1.2541	1.66E-06	Rwdd1	-0.4886	7.34E-03
Rsrp1	-1.2441	2.36E-21	Rtbdn	-0.4885	1.66E-02
Strip1	-1.2415	9.49E-04	Rrp1	-0.4884	1.29E-02
Kcnn2	-1.2377	1.09E-10	Timm44	-0.4879	1.77E-03
Oca2	-1.2295	7.48E-04	Mgst3	-0.4862	3.12E-02
4933407I08Rik	-1.2233	3.32E-03	Ctnna3	-0.4834	1.76E-03
Gnptg	-1.2114	2.71E-07	Rb1	-0.4826	4.34E-03
Leng9	-1.2035	1.40E-08	Cnst	-0.4817	2.06E-02
Ncald	-1.1979	1.37E-10	Cdkl5	-0.4814	1.14E-03
Bcar3	-1.1749	7.67E-04	Gm46124	-0.4807	2.68E-02
Hectd2os	-1.1732	1.55E-03	Pigk	-0.4797	2.74E-03
A330093E20Rik	-1.1672	2.08E-07	Usp31	-0.4789	4.59E-05
Miat	-1.1627	8.79E-10	Gba2	-0.4782	1.31E-02
Fgf1	-1.155	8.56E-04	Zdhhc8	-0.4761	2.94E-02
Gm15594	-1.1545	4.95E-06	Iqgap1	-0.4741	5.69E-03
Gm21798	-1.1534	9.97E-05	Kcnq5	-0.4736	1.85E-03
Hsd17b12	-1.1455	6.36E-04	St6gal2	-0.472	2.85E-03
Adcy8	-1.1364	6.74E-06	Gm10308	-0.4709	2.52E-02
Camk4	-1.1357	4.33E-07	Cpne7	-0.4705	1.94E-02
Wdr17	-1.1276	1.29E-10	Tmem178	-0.4679	1.42E-05
2010300C02Rik	-1.1203	2.53E-07	Ddx1	-0.467	5.78E-03
Gm26873	-1.1189	4.32E-03	Arhgap32	-0.4653	2.82E-04
Loxl2	-1.0952	3.23E-04	Ppp1r7	-0.463	3.10E-02
Rtl1	-1.0915	1.27E-04	Uckl1os	-0.4629	1.62E-02
R3hdm1	-1.0909	1.00E-15	Gabra5	-0.4628	2.37E-03
Arglu1	-1.084	1.30E-11	Cnksr2	-0.4589	7.96E-04
Arpc5	-1.0821	2.51E-03	Foxk2	-0.4586	1.10E-02
Rph3a	-1.0783	2.88E-05	Gm15489	-0.458	1.58E-02

Continued on next page

Table 21 – continued from previous page

Gene	log_2 FC	p-value	Gene	log_2 FC	p-value
Hmgcs1	-1.0599	1.44E-04	Nfatc2	-0.4579	3.17E-02
B3gat1	-1.0469	1.46E-06	Setd4	-0.4556	7.39E-03
Etl4	-1.0461	1.91E-05	Ccnc	-0.4541	7.38E-03
Apbb1	-1.0457	1.16E-03	Stx2	-0.454	1.15E-03
Grm3	-1.0451	3.05E-07	Rps6ka3	-0.4535	2.65E-08
Ring1	-1.0429	1.36E-04	AU023762	-0.4535	1.55E-02
Atp11b	-1.039	1.09E-11	Krba1	-0.4528	2.76E-02
Dalrd3	-1.0277	1.26E-05	Cit	-0.4519	3.74E-05
Dnah7c	-1.0165	1.12E-02	Gpr158	-0.4515	2.23E-04
L3mbtl4	-1.0056	1.21E-02	Wdr43	-0.4507	9.17E-03
Homer2	-1.004	4.65E-04	Usp4	-0.4507	5.60E-03
Rapgef5	-0.9996	2.93E-08	Hs6st3	-0.4505	4.39E-03
Slc11a2	-0.9945	7.87E-04	Mlip	-0.4464	1.78E-02
Pex5l	-0.9924	1.58E-06	Gm20275	-0.4463	3.08E-05
Cap2	-0.9899	1.91E-04	Parp8	-0.446	1.80E-03
Gm20642	-0.9893	2.52E-09	Capza2	-0.4454	7.26E-03
Adam23	-0.9818	1.13E-07	Rasa1	-0.4454	1.12E-05
Ptpn5	-0.9803	6.41E-05	Rad9b	-0.445	1.12E-02
Actr3b	-0.9784	6.06E-09	Ubqln4	-0.445	2.90E-03
Sh3glb2	-0.9756	7.62E-04	Pcsk2	-0.4448	7.90E-03
Sorbs2os	-0.9707	1.67E-06	Gm11437	-0.4442	4.23E-02
Kcnt2	-0.9695	2.52E-08	Ipo5	-0.4437	7.50E-03
Chst8	-0.9677	4.48E-03	Ptprn	-0.442	1.22E-03
Cdh10	-0.9636	1.79E-06	Lars	-0.4399	3.60E-04
Dgkz	-0.9614	5.32E-06	Garem1	-0.4391	1.58E-02
Gm15810	-0.9584	1.30E-05	Asap2	-0.4387	2.35E-03
Gm46367	-0.9578	1.29E-03	Ddx39b	-0.4387	2.98E-03
Dlk2	-0.955	1.99E-03	Sptb	-0.4387	2.61E-02
Ngef	-0.9536	1.51E-03	4930532I03Rik	-0.4386	8.54E-04
Slc24a5	-0.9493	1.60E-05	Gga1	-0.4383	8.32E-04
Nars	-0.9487	1.33E-05	Pmpca	-0.438	2.24E-02
Hcn3	-0.9395	3.45E-03	Efna5	-0.4368	7.24E-03
Gm48321	-0.9381	1.85E-04	Syt7	-0.4368	8.81E-04
Gpatch2l	-0.9263	5.80E-03	Grm8	-0.4366	2.55E-03
Ppfibp1	-0.9201	2.67E-05	Arfgef2	-0.4365	5.39E-03
Nox1	-0.9138	9.08E-04	Nbea	-0.4365	4.53E-06
4930419G24Rik	-0.9066	5.00E-04	Malat1	-0.4355	2.75E-05
Cyp51	-0.9018	2.06E-03	Zfp827	-0.4354	6.28E-04
Unc13a	-0.9016	7.11E-08	Zfpm2	-0.4354	2.18E-02

Continued on next page

Table 21 – continued from previous page

Gene	log_2 FC	p-value	Gene	log_2 FC	p-value
A330015K06Rik	-0.8938	8.54E-04	Dlc1	-0.4339	9.86E-03
Gm11867	-0.89	2.81E-06	Dab2ip	-0.4326	1.06E-02
Brd9	-0.8892	1.03E-05	Dusp11	-0.4321	6.71E-07
Zbbx	-0.8844	2.87E-04	Synpo	-0.4316	3.40E-02
Tnpo2	-0.8838	1.61E-04	Efnb2	-0.4309	1.89E-02
Gm37459	-0.8831	1.48E-03	Rasgef1c	-0.4309	3.94E-02
Dnah5	-0.8827	5.85E-03	Htr1f	-0.4302	6.68E-03
Erich3	-0.8777	5.31E-03	Hps4	-0.4301	2.73E-02
Adam11	-0.8741	4.79E-03	Fam135a	-0.4296	8.53E-03
Srebf2	-0.8654	1.08E-04	Npy1r	-0.4287	1.38E-02
Fam81a	-0.8643	3.96E-04	Catspere2	-0.4284	9.97E-03
Rgs11	-0.8616	7.44E-04	Ddx47	-0.4274	4.40E-02
Gpi1	-0.8558	3.69E-05	C030047K22Rik	-0.4257	6.32E-03
Cacna1a	-0.8524	2.88E-13	Smarcd1	-0.4256	4.37E-02
Nrbp2	-0.8495	2.11E-05	Acsl6	-0.424	1.10E-03
Slc25a3	-0.8494	2.50E-04	Cnnm2	-0.4239	9.82E-03
Mir124a-1hg	-0.8411	2.30E-05	E130006D01Rik	-0.4228	4.10E-02
Hdac9	-0.8365	2.44E-06	Ica1	-0.4226	4.26E-03
Hivep1	-0.8254	1.91E-06	Cntln	-0.4218	1.10E-05
Cds1	-0.8246	2.60E-03	Elmo1	-0.42	1.28E-03
Gm49226	-0.8238	1.41E-02	Prmt8	-0.4199	1.95E-02
Adcy1	-0.8233	7.59E-06	Gm33228	-0.4188	1.47E-05
Srsf5	-0.8227	3.78E-07	Strbp	-0.4178	1.96E-06
Wls	-0.8225	9.41E-03	Aars	-0.4176	3.65E-02
Phactr1	-0.8215	4.03E-08	Begain	-0.4171	4.62E-02
Aimp1	-0.821	2.32E-03	4930430F08Rik	-0.4159	3.84E-02
Cacnb4	-0.8182	1.75E-07	Rnmt	-0.4158	3.16E-03
Golga7b	-0.8175	1.67E-02	Kalrn	-0.4156	9.43E-05
P2ry12	-0.8168	2.84E-03	Nav3	-0.4149	1.72E-04
Parp2	-0.8142	7.98E-03	9130024F11Rik	-0.4123	4.71E-02
Gm43376	-0.808	9.49E-05	Cpsf4l	-0.4116	2.56E-02
Son	-0.8046	1.37E-10	Ifrd1	-0.4109	5.70E-04
Gm15738	-0.8028	1.58E-07	Ankrd16	-0.4108	3.97E-02
Gm32926	-0.8028	1.66E-02	Slc1a1	-0.4097	1.99E-02
Gm37240	-0.7965	1.90E-07	Gm16867	-0.4082	3.12E-02
Gm32743	-0.7965	1.18E-02	Gm20721	-0.4079	4.24E-03
Hars2	-0.7956	1.17E-02	Tgfbrap1	-0.4069	2.86E-03
Pknox2	-0.7949	6.67E-06	Pde10a	-0.4064	3.65E-04
Osbpl8	-0.791	8.53E-07	Elmo2	-0.4064	1.50E-02

Continued on next page

Table 21 – continued from previous page

Gene	log_2 FC	p-value	Gene	log_2 FC	p-value
Slc7a1	-0.786	1.69E-05	Abcc5	-0.4055	1.42E-03
Mical2	-0.7785	7.08E-06	39692	-0.4044	1.71E-03
Pdzd2	-0.7709	1.03E-04	Phf24	-0.4039	2.44E-03
Stt3b	-0.7698	1.35E-06	Ano10	-0.4039	9.52E-03
Lin7a	-0.7697	1.46E-04	Dclk1	-0.4026	8.92E-06
Snrnp70	-0.7694	1.32E-12	Macrod1	-0.401	2.15E-03
Asb5	-0.7683	1.69E-02	Actr1b	-0.4004	2.22E-02
Prelid3a	-0.7637	2.06E-03	Ralgapa1	-0.3999	6.11E-04
Gm38134	-0.7581	3.65E-03	Galnt2	-0.3998	1.77E-05
Csnk2a2	-0.7564	4.89E-05	Glrx2	-0.399	2.49E-02
Plppr4	-0.7562	9.31E-06	4930517O19Rik	-0.3974	2.99E-02
Nab1	-0.7554	8.46E-03	Sipa1l1	-0.3969	1.36E-03
Brsk2	-0.7547	1.08E-04	Plpbp	-0.3966	3.87E-02
Dnajc13	-0.7547	6.98E-06	Ggact	-0.3962	4.09E-02
Gm12064	-0.7504	7.98E-03	Elavl2	-0.3957	1.51E-05
Gm10800	-0.7493	3.74E-03	Atg2b	-0.3954	4.82E-02
39326	-0.7484	6.57E-06	Inpp5a	-0.395	1.98E-03
Gm48239	-0.7457	5.94E-03	Sirpa	-0.3946	1.18E-02
Hip1r	-0.7438	8.75E-03	Arid5b	-0.3937	2.45E-03
Gpr26	-0.7412	2.88E-04	Dennd6b	-0.393	4.56E-02
Snx7	-0.7391	3.90E-03	Spg7	-0.3928	3.87E-02
Ccdc186	-0.7373	2.54E-03	Nmt2	-0.3917	7.36E-04
Efcab6	-0.7326	3.62E-03	Ptprg	-0.3915	4.44E-04
Npdc1	-0.729	5.16E-03	Vegfa	-0.39	4.34E-02
Ppp1r12c	-0.7289	3.30E-03	Fbxl16	-0.3898	3.08E-02
Tsix	-0.7284	7.69E-05	Dvl1	-0.3898	3.09E-02
Atp1a1	-0.7268	8.54E-04	Ube2ql1	-0.3882	7.85E-03
Mfn1	-0.7267	2.27E-06	Tmem108	-0.3873	7.83E-04
Leng8	-0.7253	1.79E-04	Magi1	-0.3865	5.53E-04
Slit3	-0.7242	3.15E-05	Mta1	-0.3852	3.81E-02
Nphp4	-0.723	1.32E-03	Myrip	-0.3851	2.11E-02
C2cd2	-0.7217	4.32E-03	Gm13963	-0.385	4.68E-03
Asph	-0.719	1.25E-04	Myh10	-0.3845	1.94E-03
Nsmaf	-0.7188	1.73E-03	Ndufaf7	-0.3843	3.98E-02
Arhgap10	-0.7169	8.28E-04	Dsel	-0.3831	2.40E-02
Hectd2	-0.7115	4.96E-06	Ttc39b	-0.3829	2.98E-02
Pfkp	-0.7076	2.35E-09	Srrm1	-0.3815	3.96E-04
Nrg3os	-0.7075	1.45E-05	Trank1	-0.3811	5.82E-04
Gm49678	-0.706	8.71E-05	Ndfip2	-0.3809	1.97E-07

Continued on next page

Table 21 – continued from previous page

Gene	log_2 FC	p-value	Gene	log_2 FC	p-value
Gm50368	-0.7038	1.70E-02	Hs6st2	-0.3785	5.56E-04
Thrb	-0.6936	2.28E-04	4930586N03Rik	-0.3782	5.23E-03
Slc16a4	-0.6925	1.05E-02	Ppm1l	-0.3772	7.61E-04
Ntng1	-0.6922	5.77E-03	Sars	-0.377	2.03E-03
4933413L06Rik	-0.6908	2.11E-03	Pnn	-0.3765	6.45E-03
Nln	-0.6895	1.17E-03	Setd3	-0.3763	1.10E-03
Srrm2	-0.689	1.89E-09	Lysmd4	-0.3752	2.66E-02
Gm16226	-0.6885	2.70E-03	Mrps27	-0.375	2.25E-02
Sh3rf3	-0.6875	9.17E-11	Cdk8	-0.3744	7.07E-17
2900026A02Rik	-0.6873	2.79E-03	Pam	-0.3732	5.29E-03
Tspan17	-0.6857	1.69E-02	Stx7	-0.3728	3.54E-04
Sgtb	-0.6831	6.34E-03	Ablim2	-0.3725	2.52E-02
R3hdm2	-0.678	4.87E-06	Gm15283	-0.3721	2.56E-02
Ddx17	-0.6774	1.45E-09	Flrt2	-0.3713	7.29E-04
Pgap1	-0.6768	8.15E-08	Gda	-0.3712	1.23E-02
Ift43	-0.6755	1.19E-03	Satb2	-0.371	3.89E-02
Camkv	-0.6739	4.24E-04	Tiam1	-0.371	1.54E-05
Lrrfip2	-0.6725	1.69E-03	Zfp445	-0.3709	5.26E-03
Usp3	-0.6716	1.08E-05	Akap7	-0.3701	2.03E-03
Kif21b	-0.6657	1.34E-03	Zfp945	-0.3674	1.19E-02
Zranb2	-0.6651	1.37E-10	Ppid	-0.3672	1.88E-02
Rab3c	-0.6633	5.44E-05	Psmd7	-0.3669	2.76E-06
Kcnh7	-0.6601	6.96E-06	Kcnip4	-0.3664	1.10E-02
4930480K15Rik	-0.6594	3.05E-03	Homer1	-0.3656	9.37E-07
Gm20752	-0.6593	8.09E-03	Eri2	-0.3653	4.47E-02
Arap2	-0.6576	6.45E-05	Aagab	-0.365	2.24E-02
Kcnk10	-0.6568	1.97E-07	Spred1	-0.3649	1.05E-03
Gm26854	-0.6565	4.97E-03	Wdr45b	-0.3649	4.08E-02
Celf3	-0.6555	2.64E-04	Ttll4	-0.3647	2.83E-02
Armh4	-0.6489	4.63E-03	Gm47071	-0.3642	2.54E-02
Cdk5rap3	-0.6478	1.64E-03	Dscam	-0.3629	7.65E-05
Gm16183	-0.6466	1.80E-03	Degs2	-0.3603	1.01E-02
4930483P17Rik	-0.6447	4.97E-03	Pgs1	-0.36	7.73E-03
Spred2	-0.6444	2.15E-05	Tet2	-0.3592	3.04E-05
Nedd4l	-0.6438	1.45E-09	Snapc1	-0.3592	1.82E-02
Rps6kb2	-0.6432	1.68E-03	Celf2	-0.3591	7.21E-04
Slc6a17	-0.6414	2.11E-05	Ube3a	-0.359	4.64E-03
Stx1a	-0.6397	2.44E-03	Vps13d	-0.3588	6.48E-03
Zranb3	-0.6396	6.52E-04	Dpy19l3	-0.3584	1.79E-04

Continued on next page

Table 21 – continued from previous page

Gene	log_2 FC	p-value	Gene	log_2 FC	p-value
Plppr5	-0.6385	1.23E-04	Ubp1	-0.3582	2.75E-02
Cx3cr1	-0.6355	1.43E-02	Mfsd6	-0.3578	1.61E-04
Rhobtb1	-0.6326	2.32E-02	4430402I18Rik	-0.357	4.01E-02
Gm42303	-0.6326	6.38E-04	Hmgn3	-0.357	1.40E-03
Lmbrd1	-0.6299	3.99E-06	Mroh1	-0.3567	2.68E-02
Rbpj	-0.6276	5.02E-03	Lrp8os2	-0.3567	3.26E-02
Fggy	-0.627	8.17E-07	Unc80	-0.3545	1.04E-05
D930016D06Rik	-0.6246	2.09E-03	5530401A14Rik	-0.354	9.29E-03
Galnt1	-0.6227	1.33E-03	Bcl11a	-0.3517	1.02E-02
Mctp1	-0.622	3.64E-05	Npr3	-0.3517	4.96E-02
Ankrd13d	-0.6181	2.64E-03	Kcnh1	-0.3516	7.51E-03
Kcnab1	-0.6155	8.79E-04	Slc22a17	-0.3516	6.99E-03
Map3k5	-0.6149	5.94E-03	Zdhhc2	-0.3514	2.79E-04
Gm26749	-0.6142	7.15E-04	Phka2	-0.3512	4.93E-02
Far10s	-0.6138	3.05E-03	D5Ertd615e	-0.3509	3.39E-02
Gm16054	-0.6111	1.18E-02	Rims1	-0.3506	5.37E-04
Hdac4	-0.6077	2.91E-05	40787	-0.3502	1.89E-05
Mrps5	-0.6074	5.20E-04	Chtop	-0.3499	7.01E-05
A630089N07Rik	-0.6051	7.29E-04	Ap2b1	-0.3497	3.37E-05
Ptprj	-0.6039	1.65E-06	Frmd3	-0.3496	1.67E-04
Xrcc6	-0.6037	1.43E-04	Rhobtb2	-0.3494	9.78E-03
Lyrm9	-0.6036	3.78E-03	Phactr3	-0.3492	1.34E-02
Shfl	-0.6036	1.21E-02	Gria2	-0.349	1.24E-04
Babam2	-0.6032	9.22E-06	Taf15	-0.3487	1.34E-02
Mrs2	-0.603	1.29E-02	Tshz3	-0.3487	4.69E-02
Gphn	-0.602	2.09E-09	Dgkd	-0.3472	3.87E-03
Rab3gap2	-0.5935	6.01E-04	Scd2	-0.3468	4.44E-04
Pcnp	-0.5919	9.50E-03	Herc2	-0.3467	1.59E-04
Pclo	-0.5917	1.00E-06	Ttll7	-0.3467	1.73E-02
Numb	-0.5916	2.28E-04	Mpped1	-0.3461	2.86E-02
Hps3	-0.591	8.16E-03	Ulk4	-0.3457	8.93E-04
Anapc5	-0.5903	3.17E-04	Dld	-0.3449	4.98E-02
Ndrg3	-0.5899	1.27E-04	Exoc6	-0.344	2.88E-02
Gm26917	-0.5887	1.02E-04	Drg1	-0.343	7.03E-03
Zfp385b	-0.5881	1.29E-05	Neurl1a	-0.3417	4.76E-03
Ildr2	-0.5873	5.04E-04	Ptpre	-0.3411	3.60E-05
Cttnbp2	-0.5872	9.57E-08	Nrxn3	-0.3398	8.36E-03
Tfrc	-0.5869	4.95E-03	Tbc1d9	-0.3395	1.20E-02
Oxr1	-0.5825	6.00E-05	Arpp21	-0.339	7.02E-04

Continued on next page

Table 21 – continued from previous page

Gene	log_2 FC	p-value	Gene	log_2 FC	p-value
Mbd6	-0.5794	1.63E-02	Atg9a	-0.3384	4.26E-02
Nlk	-0.5779	2.72E-06	Prkcb	-0.3378	1.79E-04
Atp8b2	-0.5767	1.06E-03	Rad51b	-0.3375	2.52E-02
Nwd2	-0.576	2.18E-03	Gm17106	-0.3371	3.04E-02
Osbpl1a	-0.5755	2.63E-03	Ptn	-0.3355	3.45E-03
Cog5	-0.5729	6.16E-06	Zfp131	-0.3353	9.86E-03
Mpped2	-0.5727	2.95E-03	Trp53bp1	-0.3353	2.26E-02
Tardbp	-0.5717	3.35E-03	Dctn2	-0.3351	4.78E-02
Dok5	-0.5712	9.57E-03	Gm15700	-0.335	5.08E-03
Pdzrn3	-0.5711	2.86E-03	Nol4	-0.3343	5.21E-06
Fbxw7	-0.5702	1.46E-09	Lrp3	-0.3331	4.98E-02
Cttn	-0.5662	2.12E-03	Patj	-0.3331	3.11E-03
Gm21954	-0.5658	2.54E-03	Prickle1	-0.3327	2.88E-03
Enah	-0.5656	5.16E-04	Grip1os2	-0.3326	4.28E-03
Bbs4	-0.5641	4.56E-03	Fbxo34	-0.3323	2.28E-02
Dip2b	-0.5631	7.89E-05	Spock1	-0.3322	1.43E-02
Mthfd1l	-0.563	1.75E-02	Tes	-0.3321	3.14E-02
Usp28	-0.5622	4.48E-03	Zmym1	-0.3314	1.48E-02
Plcl1	-0.558	7.25E-04	6530409C15Rik	-0.3313	4.75E-02
Sergef	-0.5571	1.67E-03	Pum3	-0.3311	1.98E-06
Smg5	-0.5568	6.63E-04	Sptbn2	-0.3304	1.78E-02
Greb1l	-0.5565	3.66E-04	Gm4924	-0.3301	1.96E-05
Ttc7b	-0.5561	5.58E-06	Ppp2r5a	-0.33	3.80E-03
Plcl2	-0.5559	2.28E-05	Cntfr	-0.3287	1.18E-02
Tars2	-0.5555	1.80E-03	Ccser2	-0.3285	2.64E-02
Gm15398	-0.5551	1.78E-02	Galnt18	-0.3284	9.63E-03
Samd5	-0.5482	1.16E-02	Hbp1	-0.3283	3.24E-02
Ldlr	-0.5433	4.88E-04	E130102H24Rik	-0.3267	2.45E-02
Pde4b	-0.5424	2.07E-05	Prpf4b	-0.326	3.65E-04
L3mbtl1	-0.5397	4.66E-03	Gm48956	-0.3256	1.10E-02
Abca2	-0.5381	3.72E-04	Scn1a	-0.3246	2.64E-03
Osbpl10	-0.5378	2.74E-03	Tmem131	-0.3237	3.65E-02
Bsn	-0.5375	2.29E-04	Tatdn1	-0.3233	1.19E-03
Atxn2l	-0.5337	2.03E-03	Ptpn3	-0.3231	2.98E-02
Sbf1	-0.533	1.94E-02	Donson	-0.3228	3.93E-03
Pcsk5	-0.5312	8.64E-03	Nrg1	-0.3227	2.22E-02
Lgi1	-0.5309	1.20E-03	Il1rapl1	-0.3227	1.02E-02
Atp1b3	-0.5299	3.13E-02	Nit1	-0.3224	2.67E-02
Chuk	-0.5293	6.15E-06	Fndc3b	-0.3223	1.06E-04

Continued on next page

Table 21 – continued from previous page

Gene	log_2 FC	p-value	Gene	log_2 FC	p-value
Gm44686	-0.5292	9.47E-03	Lmo7	-0.3222	2.10E-02
Abhd2	-0.5282	6.20E-04	Cyth3	-0.3211	4.65E-02
Scube1	-0.5279	2.02E-02	Rnf13	-0.321	3.33E-03
Sycp2	-0.5265	1.24E-02	Cadps2	-0.3207	1.32E-03
Usp24	-0.5259	2.40E-07			

8.6 SIGNIFICANTLY UPREGULATED GENES IN INACTIVE INDUCED NEURONS

Table 22: Significantly upregulated genes in inactive induced neurons compared to active induced neurons ordered by descending log_2 FC

Gene	log_2 FC	p-value	Gene	log_2 FC	p-value
Kcnc3	1.5668	3.01E-03	Hook2	0.4577	1.72E-02
Zfp64	0.9448	1.69E-04	Lmtk3	0.4431	4.65E-03
Actr1a	0.9336	4.41E-03	Ei24	0.436	4.91E-02
Cradd	0.9282	2.91E-02	Ctnnal1	0.4356	4.22E-02
Pou2f2	0.8675	7.92E-03	Ankhd1	0.4273	4.88E-04
Svop	0.7839	2.28E-03	Kcnq1ot1	0.4192	1.97E-02
mt-Nd2	0.7743	1.21E-02	Rev3l	0.4154	1.96E-03
Ppig	0.7416	2.62E-03	Arhgef12	0.4129	6.65E-03
Dpm1	0.732	1.52E-02	Cacna1a	0.4084	1.24E-02
Gnl2	0.719	1.88E-02	Cox16	0.4042	1.31E-02
Fbxo41	0.6891	5.17E-03	Terf1	0.3967	2.57E-04
Ccdc88c	0.6596	2.04E-02	Anks1b	0.3906	1.42E-02
Tnpo3	0.651	1.53E-02	Bod1l	0.3895	2.19E-02
Mar 02	0.6407	2.18E-02	Ulk2	0.3892	8.73E-03
Adar	0.6311	7.23E-03	Cep250	0.3872	6.76E-03
Chd3	0.6229	1.38E-02	Rxylt1	0.3795	4.44E-02
Mthfd2l	0.5906	2.96E-02	1600020E01Rik	0.3784	3.55E-04
Pkn2	0.5568	2.74E-02	Mgll	0.3781	1.14E-02
Rtf1	0.552	1.30E-02	Fam214a	0.3666	4.23E-02
Ddx50	0.552	1.24E-02	Opa1	0.3654	4.30E-02
Usp14	0.5457	1.39E-02	Nav2	0.3626	3.90E-02
Phc2	0.5427	2.60E-02	Dennd5b	0.3599	6.36E-03
Gnb1	0.5325	1.24E-02	Soga1	0.3591	4.69E-02
Dleu2	0.5235	7.32E-03	Nexmif	0.356	1.78E-02
Sec62	0.5169	1.38E-02	Pnisr	0.3514	3.62E-02

Continued on next page

Table 22 – continued from previous page

Gene	log_2 FC	p-value	Gene	log_2 FC	p-value
Eif5b	0.5137	8.39E-07	Pde4dip	0.3511	2.52E-02
Cers5	0.5094	2.37E-02	Fbxl20	0.3497	3.33E-02
Amph	0.5064	1.92E-02	Rgs6	0.3487	5.88E-03
Marf1	0.5019	4.12E-02	Cntn5	0.3462	4.51E-02
4732471J01Rik	0.4957	4.54E-02	Tpr	0.3456	1.56E-02
Epha4	0.4951	7.24E-03	Gps2	0.3448	4.12E-02
Hivep3	0.4912	1.90E-02	Ddx6	0.3446	3.18E-02
Prpf4b	0.4843	1.97E-03	Map7	0.3388	4.73E-02
Caln1	0.4782	3.17E-02	Tnks2	0.3381	2.87E-02
Nmt1	0.4743	1.03E-07	Prickle2	0.3339	1.66E-02
Polr2a	0.4694	7.30E-04	Ahi1	0.3338	4.47E-02
Ift88	0.4648	2.10E-02	Rnf169	0.3331	2.21E-03
Cdk11b	0.4641	2.88E-02	Atrx	0.3321	2.64E-02
Metap1d	0.4598	3.16E-03	Ash1l	0.3274	1.88E-02
9330159F19Rik	0.4588	2.35E-02			

8.7 SIGNIFICANTLY DOWNREGULATED GENES IN INACTIVE INDUCED NEURONS

Table 23: Significantly downregulated genes in inactive induced neurons compared to active induced neurons ordered by descending log_2 FC

Gene	log_2 FC	p-value	Gene	log_2 FC	p-value
8430422H06Rik	-9.5999	3.43E-16	Gphn	-0.7244	1.47E-05
Gm33125	-7.7648	4.40E-05	Nrbp2	-0.7238	0.034064
2210408F21Rik	-6.0074	1.34E-07	Gm20275	-0.7174	0.011658
Mapk14	-5.3694	6.27E-17	Gm50368	-0.7111	0.035928
Sema3c	-4.9532	1.99E-11	Mpdz	-0.7063	0.03132
6330562C20Rik	-4.9437	1.80E-06	Nol10	-0.6958	0.019687
Asxl3	-4.5589	1.17E-13	Hnrnph1	-0.6953	1.72E-05
Adgrg6	-4.285	3.68E-06	3110021N24Rik	-0.6881	0.047597
Grik1	-4.2629	1.05E-06	Srbd1	-0.6874	0.00013
Rpgrip1	-4.0708	3.60E-06	Galnt13	-0.6849	2.11E-10
Pde1c	-3.828	1.02E-12	Taco1	-0.6825	0.007986
Mrpl15	-3.7562	4.86E-08	Mir124a-1hg	-0.6748	0.03495
Cntnap2	-3.5894	9.50E-11	Pak1	-0.6685	0.016189
Chl1	-3.4456	4.11E-25	Gm31706	-0.6668	0.032107
Lrp1b	-3.3459	1.34E-15	Mbip	-0.6628	0.016189

Continued on next page

Table 23 – continued from previous page

Gene	log_2 FC	p-value	Gene	log_2 FC	p-value
Sil1	-2.7187	5.41E-11	Pmpca	-0.6529	0.026428
Fli1	-2.6559	0.002246	Igf2r	-0.6478	0.005788
Adk	-2.5453	1.44E-10	Cdyl	-0.6465	2.67E-07
Arhgef4	-2.4155	2.87E-07	Tmeff2	-0.642	0.002184
St18	-2.2432	0.00033	Macrod1	-0.6346	0.001371
AY036118	-2.1284	1.95E-26	Oxr1	-0.6319	0.016753
Il1rapl2	-2.0094	2.57E-06	Rps6ka3	-0.6319	0.007986
Gm15594	-1.9939	4.63E-08	Gm11867	-0.628	0.01855
Cmss1	-1.9618	1.92E-16	Clmp	-0.6145	0.043887
Tsix	-1.9391	1.52E-24	Casp3	-0.6068	0.011449
Cadps2	-1.8926	2.42E-09	Ube3a	-0.6011	0.002578
Gm6994	-1.6856	0.001115	5330438D12Rik	-0.5994	0.040009
Gm26917	-1.681	2.15E-23	Parp8	-0.5887	0.0117
Kat7	-1.5164	2.77E-13	Galnt11	-0.5883	0.013936
Daam2	-1.4966	0.015451	Bmpr2	-0.5753	0.000201
Igf2bp3	-1.4717	2.43E-12	Thrb	-0.5725	0.017859
Gm42439	-1.4612	1.69E-05	Ncor2	-0.5697	8.26E-05
Ctnna3	-1.4183	9.04E-12	Agrn	-0.5672	0.034891
Slc24a5	-1.3892	0.000258	Fam110b	-0.5557	0.046222
Epha7	-1.3669	2.06E-10	9630028H03Rik	-0.5543	0.046561
Fem1b	-1.3501	0.007385	Zfp871	-0.5404	0.018361
Sorbs2os	-1.34	0.000593	Zfand5	-0.536	0.034891
E130114P18Rik	-1.3205	0.00776	Rapgef4	-0.533	1.34E-15
Gm48765	-1.2765	1.63E-10	Trim44	-0.5289	0.020207
Svil	-1.2651	6.35E-09	Rsrp1	-0.5261	0.009015
Camk1d	-1.2082	3.83E-09	Ddx17	-0.525	0.00566
Lars2	-1.1925	1.30E-06	Purg	-0.5237	0.035989
Flna	-1.1914	6.05E-05	Epo	-0.5087	0.032019
Hnrnpa1	-1.1905	0.000997	Cblb	-0.5044	0.034279
Stard7	-1.127	7.20E-13	Cpsf6	-0.5039	0.035989
Gm26749	-1.1142	0.004784	Clk4	-0.5001	0.007899
Gm48742	-1.1023	0.002842	Tenm1	-0.4994	0.032743
Gm38102	-1.0813	0.011206	Ccnh	-0.4951	0.045365
Mef2c	-1.0456	0.008291	Sgsm3	-0.4826	0.046218
Kcnq1	-1.0302	0.000508	Prkg1	-0.4787	6.05E-05
Gm48228	-1.0258	0.012235	Fgfr1	-0.4782	0.029703
Gm26672	-0.9995	0.002495	Fam171a1	-0.4731	1.24E-14
Lipe	-0.9961	0.004845	Pdcd10	-0.4644	0.003755
Gria4	-0.9791	3.77E-09	Ddx39b	-0.4643	0.049704

Continued on next page

Table 23 – continued from previous page

Gene	log_2 FC	p-value	Gene	log_2 FC	p-value
Plekhg1	-0.9751	0.000571	Fer	-0.4593	0.023454
Hexb	-0.9698	0.000164	Atp9b	-0.4527	1.72E-26
Gm48747	-0.9657	0.022678	Hnrnpa3	-0.4503	0.000355
Filip1l	-0.958	0.034891	Hsd17b12	-0.4452	0.039983
Fndc9	-0.9446	0.01094	Igf2bp2	-0.4411	0.007677
Cdk8	-0.9427	1.34E-06	Ccnl2	-0.4392	0.000544
Gm36975	-0.934	0.005826	Kcnd2	-0.4386	0.005485
Lgmn	-0.9187	0.036819	Epha6	-0.4211	9.99E-09
Peak1	-0.9028	0.000234	Fgfr2	-0.4133	0.015237
Orc4	-0.8918	0.001034	Prox1	-0.4129	0.009678
Gm49179	-0.8907	0.005577	Larp4	-0.4105	1.41E-09
9630014M24Rik	-0.8838	0.018081	Gm37240	-0.4018	0.00095
Shc3	-0.8819	0.004204	Prpf39	-0.4006	0.011244
Usp50	-0.8697	0.003261	Cdip1	-0.3991	0.020015
Col4a3bp	-0.8496	0.019226	Mapre2	-0.389	0.027229
Sema5a	-0.849	0.010954	Foxj3	-0.3883	0.001209
Lysmd4	-0.8404	0.025924	Prkag2	-0.3806	8.95E-15
Acly	-0.8309	0.014005	Ppip5k2	-0.3787	0.035505
Frmpd4	-0.8074	3.54E-08	Vps41	-0.377	0.01265
Zfhx2	-0.8038	0.001918	Gas5	-0.3745	0.026154
Srsf1	-0.8037	0.001518	Ppm1l	-0.3715	0.021888
Ppm1h	-0.7865	0.029221	Cuedc1	-0.3684	1.69E-05
Fgf1	-0.7689	0.03495	Wipf1	-0.3681	1.59E-05
Srsf5	-0.7649	0.004938	Hnrnpa2b1	-0.3667	0.038368
Herc3	-0.7513	0.021095	Cdk14	-0.3295	2.33E-10
Gm42418	-0.7499	0.001232	Prdm8	-0.3258	0.04759

8.8 RSTUDIO SESSION INFO

R version 4.0.3 (2020-10-10)
Platform: x86_64-pc-linux-gnu (64-bit)
Running under: Debian GNU/Linux 10 (buster)
Matrix products: default
BLAS: /usr/lib/x86_64-linux-gnu/blas/libblas.so.3.8.0
LAPACK: /usr/lib/x86_64-linux-gnu/lapack/liblapack.so.3.8.0

locale:

[1] LC_CTYPE=en_US.UTF-8	LC_NUMERIC=C
[3] LC_TIME=de_DE.UTF-8	LC_COLLATE=en_US.UTF-8
[5] LC_MONETARY=de_DE.UTF-8	LC_MESSAGES=en_US.UTF-8
[7] LC_PAPER=de_DE.UTF-8	LC_NAME=C
[9] LC_ADDRESS=C	LC_TELEPHONE=C
[10] LC_MEASUREMENT=de_DE.UTF-8	LC_IDENTIFICATION=C

attached base packages:

[1] parallel stats4 stats graphics grDevices utils datasets methods base

other attached packages:

[1] pheatmap_1.0.12	Seurat_4.0.2	loomR_0.2.1.9000
[4] R6_2.5.0	hdf5r_1.3.3	scmap_1.12.0
[7] scRNAseq_2.4.0	LoomExperiment_1.8.0	rtracklayer_1.50.0
[10] rhdf5_2.34.0	SingleCellExperiment_1.12.0	SeuratObject_4.0.1
[13] Biobase_2.50.0	GenomicRanges_1.42.0	GenomeInfoDb_1.26.7
[16] IRanges_2.24.1	S4Vectors_0.28.1	BiocGenerics_0.36.1
[19] MatrixGenerics_1.2.1	matrixStats_0.58.0	SummarizedExperiment_1.20.0

loaded via a namespace (and not attached):

[1] utf8_1.2.1
[4] RSQLite_2.2.7
[7] grid_4.0.3
[10] munsell_0.5.0
[13] future_1.21.0
[16] rstudioapi_0.13
[19] listenv_0.8.0
[22] bit64_4.0.5
[25] generics_0.1.0
[28] randomForest_4.6-14
[31] rhdf5filters_1.2.1
[34] DelayedArray_0.16.3
[37] scales_1.1.1
[40] globals_0.14.0
[43] rlang_0.4.11
[46] spatstat.geom_2.1-0
[49] reshape2_1.4.4
[52] httpuv_1.6.1
[55] ellipsis_0.3.2
[58] proxy_0.4-25
[61] plyr_1.8.6
[64] purrr_0.3.4
[67] rpart_4.1-15
[70] pbapply_1.4-3
[73] zoo_1.8-9
[76] tinytex_0.31
[79] scattermore_0.7
[82] ProtGenerics_1.22.0
[85] patchwork_1.1.1
[88] XML_3.99-0.6
[91] biomaRt_2.46.3
[94] crayon_1.4.1
[97] later_1.2.0
[100] voxhunt_0.9.2
[103] MASS_7.3-53
[106] igraph_1.2.6
[109] plotly_4.9.3
[112] XVector_0.30.0
[115] sctransform_0.3.2
[118] Biostrings_2.58.0
[121] googleVis_0.6.10
[124] Rsamtools_2.6.0
[127] jsonlite_1.7.2
[130] askpass_1.1
[133] lattice_0.20-41
[136] survival_3.2-7
[139] png_0.1-7
[142] class_7.3-19
[145] blob_1.2.1
[148] dplyr_1.0.6
[151] future.apply_1.7.0
reticulate_1.20
AnnotationDbi_1.52.0
BiocParallel_1.24.1
codetools_0.2-18
miniUI_0.1.1.1
ROCR_1.0-11
GenomeInfoDbData_1.2.4
parallelly_1.25.0
xfun_0.23
AnnotationFilter_1.14.0
spatstat.utils_2.1-0
assertthat_0.2.1
gtable_0.3.0
goftest_1.2-2
splines_4.0.3
BiocManager_1.30.15
abind_1.4-5
tools_4.0.3
spatstat.core_2.1-2
ggridges_0.5.3
progress_1.2.2
RCurl_1.98-1.2
openssl_1.4.4
viridis_0.6.1
ggrepel_0.9.1
magrittr_2.0.1
lmtest_0.9-38
fitdistrplus_1.1-3
mime_0.10
gridExtra_2.3
tibble_3.1.2
htmltools_0.5.1.1
tidyr_1.1.3
ExperimentHub_1.16.1
rappdirs_0.3.3
pkgconfig_2.0.3
spatstat.sparse_2.0-0
stringr_1.4.0
RcppAnnoy_0.0.18
leiden_0.3.8
curl_4.3.1
nlme_3.1-152
Rhdf5lib_1.12.1
fansi_0.4.2
fastmap_1.1.0
interactiveDisplayBase_1.28.0
BiocVersion_3.12.0
stringi_1.6.2
AnnotationHub_2.22.1
irlba_2.3.3
tidyselect_1.1.1
htmlwidgets_1.5.3
Rtsne_0.15
ica_1.0-2
colorspace_2.0-1
tensor_1.5
polyclip_1.10-0
vctrs_0.3.8
BiocFileCache_1.14.0
bitops_1.0-7
cachem_1.0.5
promises_1.2.0.1
egg_0.4.5
ensembldb_2.14.1
lazyeval_0.2.2
yaml_2.2.1
GenomicFeatures_1.42.3
ggplot2_3.3.3
RColorBrewer_1.1-2
Rcpp_1.0.7
zlibbioc_1.36.0
prettyunits_1.1.1
deldir_0.2-10
cowplot_1.1.1
cluster_2.1.0
data.table_1.14.0
RANN_2.6.1
hms_1.1.0
xtable_1.8-4
compiler_4.0.3
KernSmooth_2.23-20
mgcv_1.8-33
DBI_1.1.1
dbplyr_2.1.1
Matrix_1.3-3
GenomicAlignments_1.26.0
xml2_1.3.2
digest_0.6.27
spatstat.data_2.1-0
uwot_0.1.10
shiny_1.6.0
lifecycle_1.0.0
viridisLite_0.4.0
pillar_1.6.1
httr_1.4.2
glue_1.4.2
bit_4.0.4
HDF5Array_1.18.1
memoise_2.0.0
e1071_1.7-7

8.9 PYTHON REQUIREMENTS

absl-py==0.11.0
aiohttp==3.7.4.post0
alabaster @ file:///home/ktietz/src/ci/alabaster_1611921544520/work
anndata==0.7.5
arboreto==0.1.6
argh==0.26.2
astroid @ file:///tmp/build/80754af9/astroid_1592495912941/work
astunparse==1.6.3
async-generator @ file:///home/ktietz/src/ci/async_generator_1611927993394/work
async-timeout==3.0.1
atomicwrites==1.4.0
attrs @ file:///tmp/build/80754af9/attrs_1620827162558/work
autopep8 @ file:///tmp/build/80754af9/autopep8_1615918855173/work
Babel @ file:///tmp/build/80754af9/babel_1620871417480/work
backcall @ file:///home/ktietz/src/ci/backcall_1611930011877/work
Editable install with no version control (batchglm==0.7.4)
-e /home/administrator/anaconda3/envs/spyder/lib/python3.8/site-packages
bleach @ file:///tmp/build/80754af9/bleach_1612211392645/work
bokeh @ file:///home/conda/feedstock_root/build_artifacts/bokeh_1620738354090/work
boltons==21.0.0
brotlipy==0.7.0
cachetools==4.2.1
certifi==2021.5.30
cffi @ file:///tmp/build/80754af9/cffi_1613246945912/work
chardet @ file:///tmp/build/80754af9/chardet_1607706746162/work
click @ file:///home/conda/feedstock_root/build_artifacts/click_1621503718520/work
cloudpickle @ file:///tmp/build/80754af9/cloudpickle_1598884132938/work
cryptography @ file:///tmp/build/80754af9/cryptography_1616769286105/work
ctxcore==0.1.1
cycler==0.10.0
cytoolz==0.11.0
dask @ file:///tmp/build/80754af9/dask-core_1624381970968/work
decorator @ file:///tmp/build/80754af9/decorator_1621259047763/work
defusedxml @ file:///tmp/build/80754af9/defusedxml_1615228127516/work
Deprecated==1.2.11
diff-match-patch @ file:///tmp/build/80754af9/diff-match-patch_1594828741838/work

```
# Editable install with no version control (diffxpy==0.7.4)
-e /home/administrator/anaconda3/envs/spyder/lib/python3.8/site-packages
dill==0.3.4
distributed @ file:///tmp/build/80754af9/distributed_1624589265858/work
dm-tree==0.1.5
docutils @ file:///tmp/build/80754af9/docutils_1620827984873/work
entrypoints==0.3
fa2==0.3.5
flake8 @ file:///tmp/build/80754af9/flake8_1615834841867/work
flatbuffers==1.12
fonttools==4.28.5
frozendict==2.0.2
fsspec @ file:///home/conda/feedstock_root/build_artifacts/fsspec_1623091113353/work
future==0.18.2
gast==0.3.3
get-version==2.1
google-auth==1.26.0
google-auth-oauthlib==0.4.2
google-pasta==0.2.0
graphtools==1.5.2
grpcio==1.32.0
h5py==2.10.0
HeapDict==1.0.1
idna @ file:///home/linux1/recipes/ci/idna_1610986105248/work
imagesize @ file:///home/ktietz/src/ci/imagesize_1611921604382/work
importlib-metadata @ file:///tmp/build/80754af9/importlib-metadata_1617874469820/work
interlap==0.2.7
intervaltree @ file:///tmp/build/80754af9/intervaltree_1598376443606/work
ipykernel @ file:///tmp/build/80754af9/ipykernel_1596207638929/work/dist/ipykernel-5.3.4-py3-none-
any.whl
ipython @ file:///tmp/build/80754af9/ipython_1617120885885/work
ipython-genutils @ file:///tmp/build/80754af9/ipython_genutils_1606773439826/work
isort @ file:///tmp/build/80754af9/isort_1624300337312/work
jedi @ file:///tmp/build/80754af9/jedi_1592841866100/work
jeepney @ file:///tmp/build/80754af9/jeepney_1606148855031/work
Jinja2 @ file:///tmp/build/80754af9/jinja2_1624781299557/work
joblib @ file:///tmp/build/80754af9/joblib_1613502643832/work
jsonschema @ file:///tmp/build/80754af9/jsonschema_1602607155483/work
```

jupyter-client @ file:///tmp/build/80754af9/jupyter_client_1616770841739/work
jupyter-core @ file:///tmp/build/80754af9/jupyter_core_1612213311222/work
jupyterlab-pygments @ file:///tmp/build/80754af9/jupyterlab_pygments_1601490720602/work
Keras-Preprocessing==1.1.2
keyring @ file:///tmp/build/80754af9/keyring_1621524402652/work
kiwisolver @ file:///tmp/build/80754af9/kiwisolver_1612282420641/work
lazy-object-proxy @ file:///tmp/build/80754af9/lazy-object-proxy_1607707356794/work
legacy-api-wrap==1.2
leidenalg @ file:///home/conda/feedstock_root/build_artifacts/leidenalg_1600924055570/work
llvmlite==0.34.0
locket==0.2.1
loompy==3.0.6
magic-impute==2.0.4
Markdown==3.3.3
MarkupSafe @ file:///tmp/build/80754af9/markupsafe_1621528148836/work
matplotlib==3.3.2
mccabe==0.6.1
mistune==0.8.4
mkl-fft==1.3.0
mkl-random==1.1.1
mkl-service==2.3.0
msgpack @ file:///tmp/build/80754af9/msgpack-python_1612287151062/work
multidict==5.1.0
multiprocessing-on-dill==3.5.0a4
natsort==7.1.0
nbclient @ file:///tmp/build/80754af9/nbclient_1614364831625/work
nbconvert @ file:///tmp/build/80754af9/nbconvert_1624479060632/work
nbformat @ file:///tmp/build/80754af9/nbformat_1617383369282/work
nest-asyncio @ file:///tmp/build/80754af9/nest-asyncio_1613680548246/work
networkx==2.5
numba==0.51.2
numexpr==2.7.1
numpy==1.19.2
numpy-groupies==0.9.13
numpydoc @ file:///tmp/build/80754af9/numpydoc_1605117425582/work
oauthlib==3.1.0
olefile==0.46
opt-einsum==3.3.0

packaging @ file:///tmp/build/80754af9/packaging_1611952188834/work
pandas==1.1.4
pandocfilters @ file:///tmp/build/80754af9/pandocfilters_1605120460739/work
parso==0.7.0
partd @ file:///home/conda/feedstock_root/build_artifacts/partd_1617910651905/work
pathtools==0.1.2
patsy==0.5.1
pexpect @ file:///tmp/build/80754af9/pexpect_1605563209008/work
pickleshare @ file:///tmp/build/80754af9/pickleshare_1606932040724/work
Pillow @ file:///tmp/build/80754af9/pillow_1617383569452/work
pluggy @ file:///tmp/build/80754af9/pluggy_1615976321666/work
prompt-toolkit @ file:///tmp/build/80754af9/prompt-toolkit_1616415428029/work
protobuf==3.14.0
psutil @ file:///tmp/build/80754af9/psutil_1612298023621/work
pyarrow==0.16.0
pyasn1==0.4.8
pyasn1-modules==0.2.8
pycairo==1.19.1
pycodestyle @ file:///home/ktietz/src/ci_mi/pycodestyle_1612807597675/work
pycparser @ file:///tmp/build/80754af9/pycparser_1594388511720/work
pydocstyle @ file:///tmp/build/80754af9/pydocstyle_1621600989141/work
pyflakes @ file:///home/ktietz/src/ci_ipy2/pyflakes_1612551159640/work
Pygments @ file:///tmp/build/80754af9/pygments_1621606182707/work
PyGSP==0.5.1
pylint @ file:///tmp/build/80754af9/pylint_1598623985952/work
pyOpenSSL @ file:///tmp/build/80754af9/pyopenssl_1608057966937/work
pyparsing @ file:///home/linux1/recipes/ci/pyparsing_1610983426697/work
pyrsistent @ file:///tmp/build/80754af9/pyrsistent_1600141720057/work
pyscenic==0.11.2
PySocks @ file:///tmp/build/80754af9/pysocks_1605305779399/work
python-dateutil @ file:///home/ktietz/src/ci/python-dateutil_1611928101742/work
python-igraph==0.7.1.post7
python-jsonrpc-server @ file:///tmp/build/80754af9/python-jsonrpc-server_1600278539111/work
python-language-server @ file:///tmp/build/80754af9/python-language-server_1600454544709/work
python-louvain==0.14
pytz @ file:///tmp/build/80754af9/pytz_1612215392582/work
PyWavelets==1.1.1
pyxdg @ file:///tmp/build/80754af9/pyxdg_1603822279816/work

PyYAML==5.4.1
pyzmq==20.0.0
QDarkStyle==2.8.1
QtAwesome @ file:///tmp/build/80754af9/qtawesome_1615991616277/work
qtconsole @ file:///tmp/build/80754af9/qtconsole_1623278325812/work
QtPy==1.9.0
requests @ file:///tmp/build/80754af9/requests_1608241421344/work
requests-oauthlib==1.3.0
rope @ file:///tmp/build/80754af9/rope_1623703006312/work
rsa==4.7
Rtree @ file:///tmp/build/80754af9/rtree_1618420845272/work
scanpy==1.6.0
scikit-image==0.14.2
scikit-learn==1.0.2
scikit-misc==0.1.3
scipy==1.4.1
scopeloompy @ git+https://github.com/aertslab/SCopeLoomPy.git@30d7a55758c883a093396924l4e13905492c222f
scprep==1.0.13
scvelo==0.2.3
seaborn==0.11.0
SecretStorage @ file:///tmp/build/80754af9/secretstorage_1614022784285/work
setuptools-scm==4.1.2
sinfo==0.3.1
sip==4.19.13
six @ file:///tmp/build/80754af9/six_1623709665295/work
snowballstemmer @ file:///tmp/build/80754af9/snowballstemmer_1611258885636/work
sortedcontainers @ file:///tmp/build/80754af9/sortedcontainers_1623949099177/work
sparse==0.11.2
Sphinx @ file:///tmp/build/80754af9/sphinx_1623884544367/work
sphinxcontrib-applehelp @ file:///home/ktietz/src/ci/sphinxcontrib-applehelp_1611920841464/work
sphinxcontrib-devhelp @ file:///home/ktietz/src/ci/sphinxcontrib-devhelp_1611920923094/work
sphinxcontrib-htmlhelp @ file:///tmp/build/80754af9/sphinxcontrib-htmlhelp_1623945626792/work
sphinxcontrib-jsmath @ file:///home/ktietz/src/ci/sphinxcontrib-jsmath_1611920942228/work
sphinxcontrib-qthelp @ file:///home/ktietz/src/ci/sphinxcontrib-qthelp_1611921055322/work
sphinxcontrib-serializinghtml @ file:///tmp/build/80754af9/sphinxcontrib-serializinghtml_1624451540180/work
spyder @ file:///tmp/build/80754af9/spyder_1599056981321/work
spyder-kernels @ file:///tmp/build/80754af9/spyder-kernels_1599056754858/work
statsmodels==0.12.1

stdlib-list==0.8.0
tables==3.6.1
tasklogger==1.0.0
tb-nightly==2.5.0a20210211
tblib @ file:///home/conda/feedstock_root/build_artifacts/tblib_1616261298899/work
tensorboard==2.4.1
tensorboard-data-server==0.3.0
tensorboard-plugin-wit==1.8.0
tensorflow==2.4.1
tensorflow-estimator==2.4.0
tensorflow-probability==0.12.1
termcolor==1.1.0
testpath @ file:///tmp/build/80754af9/testpath_1624638946665/work
tf-estimator-nightly==2.5.0.dev2021021101
tf-nightly==2.5.0.dev20210211
tfp-nightly==0.13.0.dev20210211
threadpoolctl @ file:///tmp/tmp9twdgx9k/threadpoolctl-2.1.0-py3-none-any.whl
toml @ file:///tmp/build/80754af9/toml_1616166611790/work
toolz @ file:///home/conda/feedstock_root/build_artifacts/toolz_1600973991856/work
tornado @ file:///tmp/build/80754af9/tornado_1606942300299/work
tqdm==4.54.0
traitlets @ file:///home/ktietz/src/ci/traitlets_1611929699868/work
typing-extensions @ file:///home/conda/feedstock_root/build_artifacts/typing_extensions_1622748266870/work
ujson @ file:///tmp/build/80754af9/ujson_1611259522456/work
umap-learn==0.4.6
urllib3 @ file:///tmp/build/80754af9/urllib3_1615837158687/work
watchdog @ file:///tmp/build/80754af9/watchdog_1620778207800/work
wcwidth @ file:///tmp/build/80754af9/wcwidth_1593447189090/work
webencodings==0.5.1
Werkzeug==1.0.1
wrapt==1.12.1
wurlitzer @ file:///tmp/build/80754af9/wurlitzer_1617224664226/work
yapf @ file:///tmp/build/80754af9/yapf_1615749224965/work
yarl==1.6.3
zict==2.0.0
zipp @ file:///tmp/build/80754af9/zipp_1615904174917/work

9

CURRICULUM VITÆ

CV removed due to data protection.

CV removed due to data protection.